UNIVERSITY OF CYPRUS

DEPARTMENT OF ELECTRICAL AND
COMPUTER ENGINEERING

DISTRIBUTED MONITORING AND CONTROL FOR SMART BUILDINGS: A MODEL-BASED FAULT DIAGNOSIS AND ACCOMMODATION FRAMEWORK

DOCTOR OF PHILOSOPHY DISSERTATION

PANAYIOTIS M. PAPADOPOULOS

2020

Department of Electrical and Computer Engineering

Distributed Monitoring and Control for Smart Buildings: A Model-Based Fault Diagnosis and Accommodation Framework

Panayiotis M. Papadopoulos

A Dissertation

Submitted in Partial Fulfillment of the

Requirements for the Degree of

Doctor of Philosophy

at the University of Cyprus

April, 2020

APPROVAL PAGE

Panayiotis M. Papadopoulos

Distributed Monitoring and Control for Smart Buildings: A Model-Based Fault Diagnosis and Accommodation Framework

The present Doctorate Dissertation was submitted in partial fulfillment of the requirements for the Degree of Doctor of Philosophy in the Department of Electrical and Computer Engineering, and was approved on April 30, 2020 by the members of the Examination Committee.

Committee Chair _____
Prof. Christos G. Panayiotou

Research Supervisor _____
Prof. Marios M. Polycarpou

Committee Member _____
Assistant Prof. Stelios Timotheou

Committee Member _____
Assistant Prof. Vasiliki Reppa

Committee Member _____
Prof. Petros A. Ioannou

DECLARATION OF DOCTORAL CANDIDATE

The present Doctorate Dissertation was submitted in partial fulfillment of the requirements for the Degree of Doctor of Philosophy of the University of Cyprus. It is a product of original work of my own, unless otherwise mentioned through references, notes, or any other statements.

Panayiotis M. Papadopoulos

.....

Abstract

Smart buildings are called the buildings which are enhanced with advanced algorithms that can derive decisions and take actions to improve energy efficiency and to maintain indoor comfortable conditions for the occupants. The heating, ventilation and air-conditioning (HVAC) system is essential for human comfort which is directly related to the productivity and health of occupants. However, the operation of an HVAC system comes at the cost of a huge amount of energy, almost half of the energy consumed by the building, while the building sector accounts up to 40% of the global energy consumption. Due to the uninterrupted operation of an HVAC system, components of its electromechanical equipment may fail and consequently this can lead to an undesirable increase of the energy consumption and to the violation of the indoor comfortable conditions. An HVAC system is a large-scale, complex system with many interconnected subsystems comprised of several electromechanical components and numerous building zones, thus the monitoring and control of HVAC systems can be a remarkably challenging task.

Producing the digital twin of the building and formulating its equipment as a set of interconnected subsystems, enables the design of agents to effectively control and monitor the underlying subsystems in a distributed fashion. This thesis presents several intelligent, model-based algorithms for distributed monitoring and control of complex HVAC systems that offer scalability, improved performance and robustness. Online, distributed monitoring algorithms can observe the behavior of the HVAC system and offer diagnosis capabilities in real-time that can inform the operating and maintenance staff about the presence, location, type and characteristics of faults (e.g. their severity and magnitude). The development of online distributed fault accommodation algorithms can alleviate the effects of faults without interrupting the operation of the HVAC systems, avoiding the excess waste of energy and the discomfort conditions for occupants, while ensuring their stable operation. Finally, for compensating the effects of modeling uncertainty and unknown disturbances as a result of occupancy, equipment, openings of doors and HVAC equipment degradation, a distributed adaptive control approach is presented, that can increase tracking performance and reduce energy consumption, during the healthy operation of the HVAC system.

Περίληψη

'Εξυπνα κτίρια ονομάζονται τα κτίρια τα οποία είναι ενισχυμένα με προηγμένους αλγόριθμους που μπορούν να λαμβάνουν αποφάσεις και μέτρα για τη βελτίωση της ενεργειακής απόδοσης και τη διατήρηση των εσωτερικών άνετων συνθηκών για τα άτομα που βρίσκονται ή διαμένουν σε αυτό. Το σύστημα θέρμανσης, εξαερισμού και κλιματισμού (HVAC) είναι απαραίτητο για την δημιουργία άνετων συνθηκών οι οποίες σχετίζονται άμεσα με την παραγωγικότητα και την υγεία των ατόμων που βρίσκονται ή διαμένουν σε αυτό. Ωστόσο, η λειτουργία του συστήματος HVAC απαιτεί ένα τεράστιο ποσό ενέργειας - σχεδόν τη μισή ενέργεια που καταναλώνεται από το κτίριο, ενώ ο τομέας των κτιρίων αντιπροσωπεύει έως και το 40% της παγκόσμιας κατανάλωσης ενέργειας. Λόγω της αδιάλειπτης λειτουργίας του συστήματος HVAC, τα στοιχεία του ηλεκτρομηχανολογικού του εξοπλισμού ενδέχεται να αποτύχουν και συνεπώς αυτό μπορεί να οδηγήσει σε ανεπιθύμητη αύξηση της κατανάλωσης ενέργειας και στην παραβίαση των άνετων συνθηκών εντός του κτιρίου. Το σύστημα HVAC είναι ένα πολύπλοκο σύστημα, μεγάλης κλίμακας, με πολλά διασυνδεδεμένα υποσυστήματα που αποτελούνται από ηλεκτρομηχανικά εξαρτήματα και πολυάριθμες οικοδομικές ζώνες (δωμάτια), επομένως η παρακολούθηση/επίβλεψη και ο έλεγχος των συστημάτων HVAC μπορεί να είναι ένα αρκετά δύσκολο έργο.

Η δημιουργία του ψηφιακού αντίγραφου του κτιρίου και η διαμόρφωση του εξοπλισμού του ως ένα σύνολο διασυνδεδεμένων υποσυστημάτων, επιτρέπει τον σχεδιασμό αλγορίθμων ικανών να ελέγχουν και να παρακολουθούν αποτελεσματικά τα επιβλεπόμενα υποσυστήματα με κατανεμημένο τρόπο. Αυτή η διδακτορική μελέτη παρουσιάζει διάφορους έξυπνους αλγορίθμους οι οποίοι είναι βασισμένοι στο μαθηματικό μοντέλο του συστήματος, προσφέρουν κατανεμημένη παρακολούθηση και έλεγχο των σύνθετων συστημάτων HVAC. Λογω της κατανεμημένης τους αρχιτεκτονικής, οι έξυπνοι αλγόριθμοι προσφέρουν δυνατότητα κλιμάκωσης, βελτιωμένη απόδοση και ευρωστία. Οι αλγόριθμοι παρακολούθησης παρέχουν παρατήρηση σε πραγματικό χρόνο της διαδικασίας του συστήματος HVAC και άμεση διάγνωση ανωμαλιών (δηλ. σφαλμάτων). Επιπλέον, η ανάπτυξη ευφυών, κατανεμημένων αλγορίθμων για διάγνωση σφαλμάτων μπορεί να υποστηρίξει το προσωπικό λειτουργίας και συντήρησης του κτιρίου, αποκαλύπτοντας την τοποθεσία, τον τύπο και τα χαρακτηριστικά των σφαλμάτων όπως για παράδειγμα η σοβαρότητα και το μέγεθος τους σφάλματος. Η ανάπτυξη κατανεμημένων αλγορίθμων ελέγχου με ανοχή στα σφάλματα μπορεί να μετριάσει τις επιπτώσεις των

σφαλμάτων χωρίς διακοπή της λειτουργίας των συστημάτων HVAC, αποφεύγοντας την υπερβολική σπατάλη ενέργειας και τις συνθήκες δυσφορίας για τα άτομα που βρίσκονται ή διαμένουν σε αυτό, εξασφαλίζοντας παράλληλα τη ευσταθή του λειτουργία. Τέλος, για την αντιστάθμιση των επιπτώσεων της αβεβαιότητας του μαθηματικού μοντέλου και των άγνωστων διαταραχών ως αποτέλεσμα του άγνωστου αριθμού των ατόμων που βρίσκονται σε αυτό, του εξοπλισμού ή συσκευών που βρίσκονται σε λειτουργία, των ανοιγμάτων των θυρών και παραθύρων, και της υποβάθμισης του εξοπλισμού HVAC, παρουσιάζεται ένας κατανεμημένος προσαρμοστικός έλεγχος που μπορεί να βελτιώσει την απόδοση ελέγχου και να μειώσει την κατανάλωση ενέργειας κατά την υγιή λειτουργία του συστήματος HVAC.

Acknowledgments

All these years of my doctoral studies have been full of emotions, with lots of ups and downs, tough and joyful moments. All the obstacles that I came across and the mistakes I've made, amend my character and personality with critical mind, patience and persistence to achieve all the goals I've determined. Every single day had its own role in this long trip. All the accomplishments achieved during my doctoral studies would not be feasible without the support and guidance for all the people encompassing me, therefore I owe them a huge thank you.

First of all, I would like to gratefully thank my research supervisor Prof. Marios Polycarpou who trusted and gave me the opportunity to study and work on his side. There were many dilemmas that I couldn't resolve without his bright scientific view and knowledge. Moreover, he gave me the opportunity to join the family of KIOS Research and Innovation Center of Excellence, where I've made a lot of collaborators, friends and family who I would like to thank as well.

In the very first day I joined KIOS, during my masters degree, I've met Assist. Prof. Vasiliki Reppa, who advised me and shaped my methodological thinking during all these years. Without her supervision and guidance it will not be possible to accomplish this doctoral degree. Also, during her Marie Curie program at Paris, France, she gave me the opportunity to join CentraleSupélec for a month, where besides the short visit, its was a very productive period.

I would like to thank Prof. Christos Panayiotou for his guidance and for his scientific insights. Moreover, I would like to thank all my committee members, and especially Prof. Petros Ioannou and Assist. Prof. Stelios Timotheou for all the useful feedback and contributions on this doctoral thesis.

During my doctoral studies, KIOS CoE and University of Cyprus gave me the opportunity to participate in the Erasmus program, where I've joined the Imperial College London for one semester. There, I had the opportunity to enrich my theoretical skills and to work in an international and inspiring environment.

Special thanks to Prof. Elias Kyriakides for the collaboration and for agreeing to serve as a member of my doctoral committee. Unfortunately, we've lost him too soon and I did not have the fortune to work with him for a longer time. I admired his humbleness, presence of mind, professionalism and his passion for research.

I would like to gratefully thank my closest colaborators and friends Stelios Vrachimis, Alexis

Kyriacou, Dr. Lenos Hadjidemetriou and Georgios Lymperopoulos for their regular intellectual and psychological support during all these years.

The multilevel support of my parents Marios and Evaggelia, and my parents-in-law Savvas and Sophia is uncountable. Specially, I would like to warmly thank and dedicate this thesis to my wife, Michaela, who has been on my side literally and figuratively, and shared all my happy and difficult moments.

Publications

Journal publications

1. V. Reppa, P. Papadopoulos, M. M. Polycarpou, and C. G. Panayiotou, "A Distributed Architecture for HVAC Sensor Fault Detection and Isolation", IEEE Transactions on Control Systems Technology, vol. 23, no. 4, pp. 1323–1337, Jul. 2015.
2. P. M. Papadopoulos, L. Hadjidemetriou, E. Kyriakides, and M. M. Polycarpou, "Robust Fault Detection, Isolation, and Accommodation of Current Sensors in Grid Side Converters," IEEE Transactions on Industry Applications, vol. 53, no. 3, pp. 2852–2861, May 2017.
3. P. M. Papadopoulos, V. Reppa, M. M. Polycarpou, and C. G. Panayiotou, "Scalable Distributed Sensor Fault Diagnosis for Smart Buildings", IEEE/CAA Journal of Automatica Sinica, vol. 7, no. 4, pp. 638–655, May 2020.

Journal publications (under review)

1. P. M. Papadopoulos, G. Lymperopoulos, M. M. Polycarpou and P. Ioannou, "Distributed Diagnosis of Sensor and Actuator Faults in Air Handling Units for Multi-zone Buildings", Energy and Buildings, (under review).
2. G. Lymperopoulos, P. M. Papadopoulos, P. Ioannou and M. M. Polycarpou, "Distributed Adaptive Control of Fan Coil Units for Multi-Zone Buildings: A Cascade Control Approach", IEEE Transactions on Control Systems Technology, (under review).

Conference proceedings

1. V. Reppa, P. Papadopoulos, M. M. Polycarpou, and C. G. Panayiotou, "Distributed detection and isolation of sensor faults in HVAC systems," in Proceedings of the Mediterranean Conference on Control and Automation (MED), 2013, pp. 401–406.
2. V. Reppa, P. Papadopoulos, M. M. Polycarpou, and C. G. Panayiotou, "A distributed virtual sensor scheme for smart buildings based on adaptive approximation," in Proceedings of the International Joint Conference on Neural Networks, 2014, pp. 99–106.
3. P. M. Papadopoulos, V. Reppa, M. M. Polycarpou, and C. G. Panayiotou, "Distributed Adaptive Estimation Scheme for Isolation of Sensor Faults in Multi-zone HVAC Systems," in Pro-

ceedings of the 9th IFAC Symposium on Fault Detection, Supervision and Safety for Technical Processes (SAFEPROCESS), 2015, pp. 1146–1151.

4. P. M. Papadopoulos, V. Reppa, M. M. Polycarpou, and C. G. Panayiotou, "Distributed adaptive sensor fault tolerant control for smart buildings," in Proceedings of the IEEE Conference on Decision and Control (CDC), 2015, pp. 3143–3148.
5. P. M. Papadopoulos, V. Reppa, M. M. Polycarpou, and C. G. Panayiotou, "Distributed Diagnosis of Actuator and Sensor Faults in HVAC Systems," in Proceeding of the IFAC World Congress, 2017, vol. 50, no. 1, pp. 4209–4215.
6. P. M. Papadopoulos, V. Reppa, M. M. Polycarpou, and C. G. Panayiotou, "Distributed Design of Sensor Fault-Tolerant Control for Preserving Comfortable Indoor Conditions in Buildings," in Proceedings of the 10th IFAC Symposium on Fault Detection, Supervision and Safety for Technical Processes (SAFEPROCESS), 2018, pp. 688–695.
7. P. M. Papadopoulos, V. Reppa, M. M. Polycarpou, and C. G. Panayiotou, "Distributed Sensor Fault Accommodation of Multi-Zone HVAC Systems," in Proceedings of the IEEE Conference on Decision and Control (CDC), 2018, pp. 7296–7301
8. G. Lymperopoulos, P. M. Papadopoulos, P. Ioannou and M. M. Polycarpou, "Distributed Adaptive Control of Air Handling Units for Interconnected Building Zones," in Proceedings of the American Control Conference (ACC), 2020, (accepted) pp. xx–xx
9. P. M. Papadopoulos, G. Lymperopoulos, M. M. Polycarpou and P. Ioannou, "Model-Based Fault Detection and Localization Algorithm for Air Handling Units in Large-Scale Buildings," in Proceedings of Indoor Air, 2020, (accepted) pp. xx–xx

Contents

List of Figures

List of Tables

Chapter 1

Introduction

Most of our world depends on machines and devices. In transportation, we use cars, buses, trams, trains, and planes to commute. In energy systems, we use machines such as gas/oil generators, photovoltaics, wind and hydroelectric turbines to produce electricity. In industry, we use large manufacturing machines to produce goods in a massive way. Information and computer technology (ICT) systems are comprised of devices such as servers, communication networks, personal computers, smart phones that help us store, process and share large amounts of data. In buildings, we install devices such as heating, ventilation and air-conditioning (HVAC) systems, lights, etc. to regulate indoor environmental conditions such as thermal comfort, air quality, luminosity, etc.

Due to the swift technological development in the fields of wireless communication and computerized technology, sensor networks can be easily installed in a variety of systems. Applying sensors in all the aforementioned machines gives the ability to *monitor* the system and furthermore to employ *automatic control*. Control systems contain hardware and software that allows to compute automatically control decision (control inputs) based on the sensed information (output) of the system. This can remove the human operator from the process and with proper control design, control systems can improve the efficiency of the corresponding system. Sensors can provide more exact information about the physical properties of systems. In some cases, sensors can be used to detect anomalies that can occur either in the process or the actuating part of the underlying plant. However, sensors are also prone to malfunction and that raises the dilemma between faulty measurements or faulty equipment. Since in control systems sensors are used to obtain control decision, the presence of faults can disorient the behaviour of the controlled system, that can lead to waste of energy, loss of equipment, accidents, etc.

Residential and commercial buildings, compared to the aforementioned sectors (i.e., industry, transportation, ICT) consume a huge amount of energy – almost half of the total world energy consumption [96]. *Smart buildings*, are called the buildings which are enhanced with intelligent equipment (i.e., devices with embedded reasoning) that can monitor and control the building equipment

to enhance security, efficiency, robustness and indoor comfort for the occupants. Heating, Ventilation and Air-Conditioning (HVAC) system is one of the most important systems in buildings since it is responsible for human comfort and it encounters a highest amount of a building's energy. Due to the uninterrupted operation of the HVAC system, components of the electromechanical equipment and sensors may fail and consequently this can lead to an increase of energy consumption and to the violation of the indoor comfort conditions.

This thesis proposes a range of distributed model-based, on-line monitoring and control methodologies for (i) *fault diagnosis* (i.e., detection, isolation and identification of faults) that provide information to the buildings' maintenance and operating staff about the presence, location, type and characteristics of faults, (ii) *fault accommodation* that offers alleviation and compensation of fault's effects that have a direct impact to the operation of the building equipment, and (iii) *adaptive control* for rejecting unknown disturbances that can affect the indoor environmental conditions in large-scale buildings for the efficient operation of the building equipment. Throughout the thesis, the performance of the proposed monitoring and control methodologies is examined using analytical and simulation results.

This chapter introduces the reader to the topic of this doctoral thesis. The first part of this chapter (Section 1.1) gives the motivation of designing and applying the proposed distributed model-based monitoring and control algorithms for the building equipment. The second part (Section 1.2) gives a wide overview about the aforementioned building systems. The state-of-the-art on the monitoring and control methods is presented in Section 1.4. Section 1.7 gives the outline of this doctoral thesis.

1.1 Motivation

According to the National Human Activity Pattern Survey (NHAPS), an average person in USA spends 86.9% of his/her life indoors [75]. Therefore, it is essential for the occupants of a building to feel comfortable in terms of thermal conditions, air quality, lighting, entertainment, etc. Indoor comfort is crucial for human health and productivity [6]. In recent years, there has been significant research focus and technological activity in the development of *smart buildings*, which have emerged based on a need to monitor and control the indoor living conditions and health of the occupants, as well as the energy consumption of large-scale buildings. The concept of smart buildings was initially motivated by a need to increase the energy efficiency of buildings [145], and reliability of a building's equipment [27], while decreasing the risk of safety-critical conditions [24], [117]. Studies operated by the International Energy Agency (IEA) and Eurostat, for the year 2004, showed that the building sector in USA and European Union reported around 37–40% of the total energy consumption, compared to remainder sectors (i.e., industry and transportation) [112]. Besides the status of 2004, the outlook of buildings' energy use has an increasing trend for both residential and non-residential build-

ings, in both developed and non-developed countries. In order to increase energy efficiency and cost effectiveness, improve comfort, productivity and safety, and enhance robustness and reliability, smart buildings incorporate embedded intelligence based on information and computer technology, aiming at autonomously adapting the evolving building environment [25]. Specifically, smart buildings constitute a cyber-physical system that incorporates a range of hardware sensing and actuation devices, combined with smart software. This combination enables the coordination and scheduling of actions for handling the dynamic and uncertain environment of a building yield from unpredictable loads and events, occupancy, weather, etc.

Health, living quality and productivity highly depend on the indoor conditions related to humidity, temperature, quality of air and many more. These factors are closely related to the operation of the Heating, Ventilation and Air-conditioning (HVAC) system. Therefore, the HVAC system is one of the most critical and essential components of a building with respect to both comfort and energy consumption, since it accounts for a large percentage of the energy consumed by the building, reaching 40% of the total energy in commercial buildings and 30% in non-commercial buildings [112]. Even if the energy efficiency of buildings can be increased either by applying sophisticated control approaches or by improving the building structure (by using protection to reduce thermal permeability, or blocking thermal bridges and air intrusion, etc.), the operation of the HVAC system still has the key role energy consumption and in maintaining indoor comfort. For this reason, a variety of optimal control algorithms for coordination and scheduling of the HVAC system have been designed to improve the occupants' thermal comfort and to increase the energy savings of a building. However, HVAC systems are complex machines that consist of a huge number of interconnected components that operate almost 24/7, and therefore this intermitted operation can inevitably cause faults or failures on the electrical and mechanical equipment (such as sensors, wires, fans, valves, pumps) of the HVAC system. Faults may intensify the energy consumption and create discomfort conditions for occupants. Particularly, the occurrence of faults in HVAC systems can cause performance degradation and improper control, which was estimated to cause an increase of 15% to 30% of a building's energy consumption, according to the Electrical and Mechanical Services Department of Hong Kong [41].

1.2 Overview of HVAC Systems

HVAC system is a large-scale, complex system with many interconnected subsystems comprised of several electromechanical components and a number of building zones. HVAC systems with *heating* operation consist of devices such as boilers, heat pumps, heating coils, etc., while HVAC systems with *cooling* operation are composed of cooling towers, chillers, cooling coils, etc. Especially, HVAC systems installed in commercial buildings, which are difficult to be naturally ventilated [42], are equipped with *ventilation* provision (i.e., fans, supply/return ducts, mixing boxes, exhaust ducts, filters, etc.)

that provides the indoor spaces with clean fresh air, removes and filters the contaminated air (i.e., air concentration levels with sulfur dioxide (by-product of the burning of fossil fuels), particles (PM 10), particles (PM 2.5), CO, Oxidants (ozone), Nitrogen dioxide, etc. [12]). There are several types of heat exchange systems for the building zones such as:

- Heating radiators [11, 61, 103, 104]
- Air Handling Units (AHU) units that are distinguished into:
  - AHUs with Constant-Air-Volume (CAV) units, called also Fan-Coil Units (FCU) [172–174]
  - AHUs with Variable-Air-Volume (VAV) units [56, 83, 87, 106, 146, 148, 153, 180],
- Underfloor heating and cooling systems [14, 43, 57, 71, 114, 121]
- UnderFloor-Air-Distribution (UFAD) systems [7, 161].

Heating radiator systems are the most popular central-heating emitters. Hot water (approximately between 75 to 80^{o}C) passes through the pipes of the coil/radiator and this makes the surface temperature of the coil/radiator bigger than the indoor air temperature. Therefore, through convection, the air in the thermal zone/room is heated.

In Underfloor heating systems, low-temperature water (e.g., 35–40^{o}C) is circulated through a network of pipes concealed below the floor tiles. Heat diffusion into the room is primarily a result of radiation and allows users to obtain uniform temperature distribution in the conditioned zone.

AHU HVAC systems are commonly installed in large-scale buildings since they can provide both heating and cooling in multiple zones. Mainly an AHU is comprised of a fan, heating coil, cooling coil, mixing box and a filter. The mixing box is used to maintain appropriate humidity and amount of ventilation air in each conditioned space and thus good quality of the indoor air can be ensured. An AHU can use both fresh air and returned air from the underlying air-conditioned room, where the percentage of fresh air and returned air is regulated by the mixing box in order to achieve a trade off between the energy waste and indoor air quality. As it is illustrated in Fig. 1.1, two common types of AHU systems exist, equipped with either: (i) constant-air-volume (CAV) units, also called fan-coil Units (FCU) or (ii) variable-air-volume (VAV) units. The main difference between these two systems is that a VAV system adjusts the air flow according to the variation of a building load condition, using either a supply fan equipped with variable frequency drive (VFD) or a VAV box in which a dumper adjusts the amount of air supplied to the room. The CAV/FCU system supplies constant air flow to a conditioned zone and by adjusting the water flow through the coils regulates the room air temperature [170].

UnderFloor-Air-Distribution (UFAD) systems have a similar process with the Air Handling Units (AHU) units systems. The main difference is that in UFAD systems the air is supplied from the floor while in AHU systems the air is supplied from the roof. UFAD systems are more effective in the heating operation since the cold air is denser than the hot air and due to the buoyancy of fluids, the

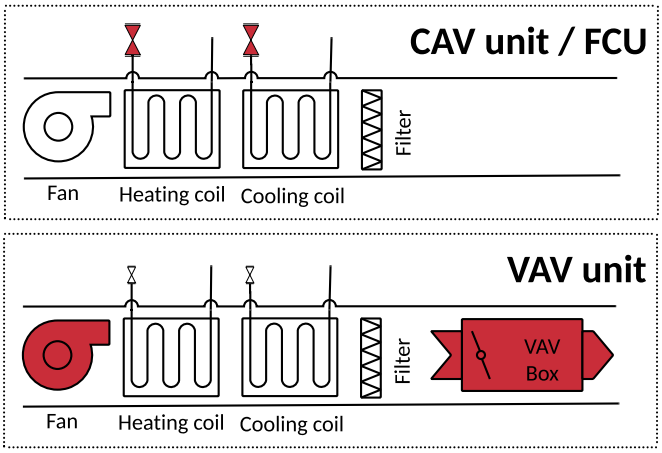

Figure 1.1: Types of air handling units (AHUs). The difference between constant-air-volume (CAV) units (also mentioned as fan-coil units(FCUs)) and variable-air-volume (VAV) units.

hot air coming from the floor can be mixed more easily with the cold air in the room. On the other hand, AHU systems are more effective in the cooling mode.

All the aforementioned heat exchange systems are supplied with a heating or cooling load from a central HVAC system such as heating units, cooling units, heat pumps or geothermal systems. Geothermal systems [18, 32, 50, 136, 140, 160, 164] can supply the heat exchanges with either heating or cooling load since they take into advantage the temperature difference of the ambient temperature (surface air temperature) that changes according to the environmental conditions compared to the geothermal reservoirs that have constant temperature. Using pipes, a stored liquid passes into a certain depth level that allows to change its thermal conditions and then it is pumped into a storage above the surface of the ground in order to be distributed in a heat exchange system (e.g., Underfloor heating system, AHU system, radiator, etc.). At the moment geothermal systems are not so popular due to the high installation cost and long term payback that makes their cost inefficient.

Heating units are composed of components such as burners, boilers, condensers, storage tanks, while the cooling units are composed of components such as chillers and cooling towers. Note that either the heating unit or the cooling unit is active at each time. The market direction on the central HVAC systems is on the heat pump systems due to their high energy efficiency rates. Besides the energy aspect, heat pump systems can switch from heating to cooling mode and also a special case of heat pump systems i.e., 4-pipe heat pump system can supply the heat exchange systems with heating and cooling load at the same time. This functionality is effective for large-scale buildings (e.g., malls, hotels, hospitals, schools, campuses) that may have heating and cooling requirements simultaneously. Fig. 1.2 presents a schematic diagram that gives an illustration of types of HVAC systems that can be applied in a building. Specifically, it consists of a central-heating radiator system, Air-Handling Units (AHUs), a heating unit, a cooling unit, and an underflow heating system.

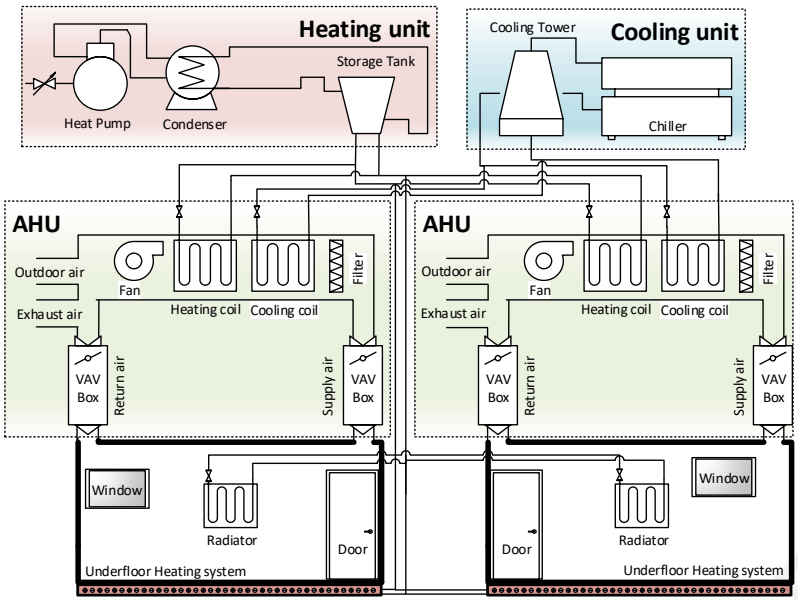

Figure 1.2: Schematic diagram of a generic HVAC system consists of heating unit, cooling unit and Air-Handling Units (AHU), Variable-Air Volume (VAV) boxes, wall-mounted radiators and underfloor heating system for each room.

1.3 Overview of Faults in HVAC Systems

As it is has been reviewed in Section 1.2, HVAC systems are complex electromechanical systems with huge number of components. Due to the uninterrupted operation of the equipment of HVAC systems, various types of faults can occur. One way to categorize the types of faults can be based on the component that is affected. For instance, faults can be categorized into: (i) sensor faults (measuring for example temperature, humidity, CO_2, motion) [130], (ii) actuator faults (i.e., valve, fan, tube, damper, compressor, motor, etc), (iii) process faults (i.e., open window, open external door, etc), (iv) communication fault (i.e., wire break, message loss, network partitioning, omission/gap, timing faults, completely arbitrary faults) [28, 36, 101]. Moreover, faults can also be categorized according to the type of the fault; fouling or failure of equipment, offset, control fault, performance degradation, stuck fault [33]. Faults can occur at different levels: component, subsystem, system, or even building level. A fault at any of these levels can further affect the operations of many other related components, and therefore, makes it difficult to understand the relationship between causes and effects and to quantify the overall impacts on the whole building energy performance. For example, the degradation of fans may affect the air side of the system by reducing the supply airflow or increasing fan power. It may also affect the heat transfer performance of coils and its energy consumption, thus further affecting the water side performance of the system. Secondly, the operational faults may present diverse impacts on different aspects of the building performance. For instance, a positive offset of the thermostat (i.e., the zone air temperature reading is higher than the actual value) can generate different influence on both the energy consumption and thermal comfort during different seasonal periods. During the

heating seasons, it reduces the heating energy consumption by maintaining the room temperature at lower levels, but, meanwhile, it deteriorates the indoor thermal comfort conditions. During the cooling seasons, energy consumption increases, and over-cooling may present. Investigations of these diverse impacts are essential to understand overall fault impacts. Thirdly, one particular fault may present very different operational characteristics and needs to be handled with a different approach. Taking the temperature sensor offset as an example, it can be: (1) a static (stuck at a value) fault, if the offset is a constant value throughout the analysis period, (2) an abrupt fault, if the offset arises suddenly during the analysis period and stays at a constant level after occurrence, (3) a degradation (incipient) fault, if the sensor offset drifts over time. In a similar way, actuator faults in HVAC systems represent leakages at the static equipment (i.e., pipes, tubes) or when the equipment with moving parts (i.e., valves, fans, dampers, compressors, motors) has stacked (at a point or at zero) or degraded. [176].

1.4 State-of-the-art

This section introduces the state-of-the-art on the topic of this doctoral thesis. The state-of-the-art is divided into three sections that consists of the literature review on: (i) the control methods, (ii) the fault diagnosis methods and (iii) fault accommodation methods that either are currently applied in the industry of building systems or are the outcome of the research and innovation in the area of smart building.

1.4.1 State-of-the-art on HVAC Control

Several researchers have proposed a large number of control designs to improve both tracking performance and energy efficiency of HVAC systems. According to [4] and [20], the control methods for HVAC systems can be classified into:

- *classical control* (i.e., on/off, PID [47]),
- *hard control* (i.e., gain scheduling PID, nonlinear control [10, 60, 63, 100, 141], robust control [9, 151], optimal control [62, 123, 154], adaptive control [26, 171], model predictive control (MPC) [8, 49, 52, 93]),
- *soft control* (i.e., fuzzy logic, neural network control) [48, 85],
- *hybrid control* (adaptive fuzzy, adaptive neuro, fuzzy PID, etc.) [13, 48, 122, 175], and
- *other control techniques* such as direct feedback linear control, pulse modulation adaptive control, pattern recognition adaptive control, reinforcement learning control, etc.

Taking into account the consecutive way that AHU components (i.e., mixing box, fan, heating coil and cooling coil) are connected, *cascade control* may be used. Cascade control is a specialized control architecture formed by inner and outer feedback loops. Several researchers have developed cascade control schemes, the majority of which aim to control the supply air temperature by regulating the

water valve of coils [55, 116, 181], while only one of them proposed a cascade design for controlling the zone's air temperature using a genetic algorithm [66].

In addition to exploiting the cascade topology of AHUs, the control design should overcome the challenges that emerge due to the large scale of buildings, and alleviate the computational complexity of traditional centralized control schemes as well as avoid single points of failure. With the recent advances in the area of Internet-of-Things (IoT), a distributed control design may not suffer from the disadvantages of centralized schemes, but instead can reduce communication requirements and improve scalability. Therefore, in the last decade the majority of publications on HVAC control propose a distributed design [15–17, 59, 77, 78, 89, 90, 110, 111, 120, 139, 159, 178]. Most of the aforementioned distributed control algorithms propose MPC design [15, 16, 77, 78, 89, 110, 111, 139, 159] that offers an optimal solution, but without considering the effects of modeling uncertainty (i.e., occupancy, equipment, openings of doors), unknown disturbances and HVAC equipment degradation. On the other hand, there are only few works that propose distributed control algorithms with on-line learning [26, 90, 91, 120].

1.4.2 State-of-the-art on HVAC Fault Diagnosis

The reliability of HVAC equipment (i.e., valves, fans, dampers, pumps) and sensor data (such as measurement of air/water/refrigerant temperature and flow) is crucial for the performance of the aforementioned control algorithms. Due to the intermittent operation of HVAC systems, failures or faults in actuators or/and sensors are inevitable to occur, causing unsatisfactory indoor thermal conditions and a waste of energy, estimated between 15% to 30% of building's energy use [45, 133]. A *failure* (i.e., a permanent interruption of a system's ability to perform a required function) is more likely to be diagnosed or even be observed from staff or occupants. Alternatively, a *fault* (i.e., an undetermined deviation of at least one characteristic property or parameter of the system from the acceptable, usual or standard condition) is difficult or even impossible to be diagnosed without the use of fault diagnosis (FD) algorithms.

Due to the aforementioned arguments, fault diagnosis (FD) that studies the detection, isolation and identification of faults, has gained great attention in the area of building systems [72]. Currently, the majority of HVAC monitoring systems in the industry uses *ruled-based* algorithms to diagnose anomalies during the operation of HVAC systems, due to their simplicity. The rules are formed by comparing sensor data or relations of sensor data with predefined constant thresholds obtained by experts (usually also called expert systems). Some examples of ruled-based fault diagnosis schemes for HVAC systems are: (i) the performance assessment rules that identify the mode of operation using specific relationships of measured information [138, 165] and (ii) the cause-effect graphs where the various operation modes of the system (both healthy and faulty modes) are represented as discrete events [134, 179]. The main weaknesses of rule-based FD methods are that they are very specific to

the system, can fail beyond the boundaries of the expertise incorporated in them, and are difficult to update [72].

State-of-the-art FD algorithms can be divided into two categories; *data-driven*/*data-mining* and *model-based* FD algorithms. The former category includes mainly traditional computational intelligence algorithms that originate from machine learning and pattern recognition field. Most of the data-driven methods require historical data (i.e., database of sensor data) for training the fault decision rules. Amongst the popular data-driven methods are: Principal Component Analysis (PCA) [157], [38], Support Vector Machines (SVM) [79], [19,84,102], Neural Networks (NN) [39,152], Genetic Algorithms (GA) [106,156], Fuzzy logic models [87,88], etc.

Model-based FD methods can be classified according to the type of model, that is; *statistical* and *state-space* models. Statistical models use data to identify a simple model such as: autoregressive model with exogenous inputs (ARX) [168], autoregressive moving average model with exogenous inputs (ARMAX) [150,167], fast fourier transform (FFT) [166]. The statistical models try to predict the output of the system during the operation using techniques such as average error (AE) of residuals. Statistical analysis employs simplistic models that require a training interval to obtain the corresponding model parameters and the state of the system (e.g., temperature). The state is represented as a random variable that is a linear combination of its previous values. In order to obtain a valid prediction of the system's state using statistical models, an adequate training and knowledge of the initial state of the system are required. The latter subcategory corresponds to the state-estimation models that perform online learning of the state based on the real time data of the system. Some examples of FD algorithms based on state-estimation models are Kalman filtering [23,143] and observer-based estimation schemes [149]. However, state-estimation techniques allow the utilization of nonlinear representations of the system dynamics that give a more realistic behavior of the heat transfer processes, compared to the aforementioned methods that employ an approximated model. The availability of analytical models, describing the behavior of quantities such as temperature, air flow, pressure in the building environment or in the HVAC system, is challenging because of the: (i) possibly unknown heat gains caused by equipment, solar effects, the occupants' presence, equipment degradation, opening of doors, (ii) large number of physically interconnected building zones, and (iii) complexity of the electromechanical part of the HVAC system. However, recently established European legislative framework about energy performance of buildings directive, includes the issuing of buildings' energy performance certificates that emerge the development of a building's energy model. Energy models incorporate the thermal properties of a building's envelope (e.g. structure, material values) and energy efficiency of a building's equipment (such as heating and cooling systems), making less demanding the modeling procedure of a building's thermal model.

Model-based FDI algorithms can be applied without necessitating any training period compared to data-driven methods that cannot guarantee the robustness of the decision outcome (i.e., detection,

isolation), since the decision highly depends on the training set. Data-driven methods commonly use a fixed, pre-designed detection threshold calculated using a training set [30,38,144,157]. Hence, false alarms may trigger in the presence of an event that was not contained in the training set. Further, in respect to the fault isolation procedure, data-driven methods necessitate historical data of faulty situations (that are, in most of the cases, difficult to be obtained) to build the isolation logic, while there is no such requirement for model-based methods. Data-driven methods commonly require rich information collected by, most likely, a large number of sensors in order to be efficient. The performance of model-based methods is independent of the number of sensors. Usually, large-scale buildings are equipped with a significant number of sensor devices in order to improve the monitoring and control of multi-zone HVAC systems. As a consequence, multiple sensor faults are likely to occur. In the case of data-diven FD methods, the isolation process of multiple sensor faults becomes cumbersome since it necessitates the collection of a large amount of data of past system operation under the occurrence of various multiple sensor faults. Past data are commonly used to create a database of faulty cases, to which new data are compared. Another issue that data-diven FD methods may have to deal with is their scalability. Date-driven methods need to be trained specifically for the corresponding building system, and if the building structure is altered, then these methods should be trained again. The new training period might be quite long in terms of collecting more data of the new system operation.

In large-scale buildings, the utilization of a global model describing the entire building system can be prohibitive for the design of a model-based FD technique. Exploiting the distributed topology of the building system, every FD agent can be designed to monitor a single building zone and to execute the fault isolation process locally, while taking into account faults that affect part of the building system and not the entire system [130]. This strategy is effective for handling the problem of the occurrence of multiple homogeneous or heterogeneous faults [109,129]. The distributed architecture can be scalable in the case that the building structure may alter, since a new FD agent dedicated to the new building part can be augmented following a plug-and-play strategy [132]. With the spatially distributed deployment of the FD agents, there is no central point for executing the FD process that corresponds to a 'single point of failure'. This is especially important in safety-critical buildings such as hospitals, schools and other public buildings.

Most works in the literature of model-based FD address the problem of fault diagnosis for single-zone HVAC systems [84,106,158]. Only a few of them deal with fault diagnosis in multi-zone HVAC systems assuming that the zones are separated [54,144] whereas there is no work that considers heat transfer between zones. Previous works on model-based FD algorithms emphasize on diagnosing (i.e., detect, isolation and identification) of faults affecting sensor measuring the zone's air temperature. However, sensors placed in the electromechanical equipment (such as the coil's water temperature sensors, supply air temperature sensors) and actuators (such as flow valves) can also be affected by faults. This raises concerns about the performance of the existing fault diagnosis algorithms.

1.4.3 State-of-the-art on HVAC Fault Accommodation

The recovery of faulty situations in HVAC systems can be achieved by shutting down the operation of the system in order to replace the faulty equipment or devices, which however is inconvenient and possibly ineffective from the viewpoint of energy consumption. The operation of the HVAC system in the period between the diagnosis and the replacement of the faulty equipment can also be energy inefficient and can cause discomfort to occupants. Alternatively, fault-tolerant control (FTC) schemes can compensate fault effects in control systems by deploying the appropriate remedial actions to preserve its nominal operation under faulty situations using the outcome of a fault detection and isolation mechanism. FTC schemes are classified into (i) fault accommodation and (ii) control reconfiguration [22]. Fault accommodation accounts for adjusting the parameters of the controllers to compensate the effects of faults, while for performing control reconfiguration the inputs and outputs of the controller are changed to reduce the effect of faults. Moreover, FTC methods can be distinguished into two categories; *passive* and *active* FTC. In passive FTC, the control law remains the same in both healthy and faulty conditions. Specifically, in passive FTC, faults are treated as uncertainties to the system's parameters leading this approach to be conservative since this design can obtain small levels of control performance. Alternatively, in active FTC, the nominal control law, which is designed based on the nominal dynamics of the system (i.e., in healthy conditions), can be replaced by an admissible control law right after the fault is diagnosed (i.e., detected and isolated). The role of control reconfiguration is to compensate any effect which can be caused by the fault occurrence. The implementation of a FTC in HVAC systems will preserve its operation close to the nominal point, which eventually will prevent needless waste of energy and uncomfortable conditions. As analyzed in the previous section for the FD methodologies, FTC schemes can be distinguished based on the methodology to data-driven [58, 67, 70, 87, 94, 95, 152, 163] and model-based [35, 137, 146]. Recently, there is an effort to facilitate optimization and model predictive control methodologies to compensate the effects of faults in HVAC systems [21, 68, 98, 99]. However, only model based FTC methodologies can analyze rigorously the closed-loop stability properties of the overall system. In order to learn the fault characteristics, data-driven methodologies require a huge amount of data, while on the other hand model-based methodologies need an analytical model that characterizes the behavior of the system. An efficient approach for ensuring the proper operation of HVAC systems under sensor fault conditions is the employment of AFTC schemes based on virtual sensors. The design of virtual sensors relies on developing mathematical models of the process implemented in software, which are used to reconstruct, estimate or predict the faulty or missing measurements [82]. In HVAC systems, which are typically highly complex, spatially distributed and with a large number of interconnected components, the utilization of model-based virtual sensors provides a more appealing approach compared to physical redundancy. Using the physical sensors approach implies additional cost for installation and

maintenance, while, if they are not added to the system during the initial HVAC installation, especially in the electromechanical part, invasive actions by specialized personnel are required. This may delay the initialization of the proper HVAC operation after the fault isolation or even risk a serious damage of the electromechanical part when accessing the system.Several researchers have investigated the design of virtual sensor schemes, combining information from healthy sensors with static or dynamic analytical models, such as observers, aiming at reconstructing/estimating the output of a faulty sensor or correcting the faulty output using the estimation of the sensor fault [65, 131, 142, 162]. In HVAC systems, there is a significant research activity in designing virtual sensors following a data-driven modeling approach with the goal of predicting the output of a faulty sensor [152], [58], [80]. However, these methods require a large amount of data collected under various normal operating conditions for synthesizing the virtual sensor models. An alternative approach to the design of virtual sensors for HVAC systems relies on the use of static models based on first-principles (see [82] and the references therein). This type of virtual sensors is more appropriate for monitoring or fault identification than for feedback control. There are very few virtual sensor schemes based on correcting the faulty output using the sensor fault estimation [46], while to the authors' best knowledge, no work has yet been developed on distributed virtual sensor schemes.

Taking into account the interconnected characteristics of HVAC systems, the early diagnosis and accommodation of faults is critical, since local fault effects may propagate from a local subsystem to neighboring subsystems either through the physical interconnections or through the distributed control scheme. In many practical applications involving large-scale buildings distributed FTC schemes are more effective since by handling the occurrence of faults locally and exchanging information between neighboring subsystems and local control agents, the delay in fault diagnosis and estimation can be reduced, facilitating the early compensation of faults effects. Nevertheless, there are currently no distributed FTC schemes for HVAC systems in the literature.

1.5 Objectives of the Thesis

Taking into consideration the state-of-the art presented in Section 1.4, this section presents the main objectives of this doctoral thesis. This thesis proposes a framework of distributed, model-based methodologies to monitor and control the HVAC system in large-scale buildings. The monitoring part involves the development of distributed fault diagnosis methodologies that provide detection, isolation and identification of unknown faults, while the distributed control part involves: (i) the design of distributed fault accommodation methods that can alleviate the effects of faults that can affect the operation of the HVAC system, causing inefficiencies and uncomfortable conditions and (ii) the design of a distributed adaptive control approach to compensate the effects of unknown disturbances and modeling uncertainties of the HVAC system under healthy conditions. Specifically, this research

focuses on the following objectives:

- *Utilization of realistic HVAC models*: The utilization of realistic HVAC models that capture the complexity, the variety of electromechanical systems and the nonlinear behavior of the actual HVAC system that will enable the design of algorithms able to effectively monitor and control the HVAC systems.
- *HVAC system partitioning*: The partitioning of the HVAC model dynamics into a network of interconnected subsystems will allow the design of effective distributed monitoring and control algorithms.
- *Distributed Diagnosis*: The development of distributed model-based agents that can consider the physical interactions between the underlying HVAC subsystems, aim to *detect* i.e., capture the presence of faults , to *isolate* i.e., reveal the location of the fault, and to *identify* i.e., determine the type (sensor or actuator) or and/or the magnitude of the fault in the presence of modeling uncertainties and measurement noise that may cause false alarms to the diagnosis algorithm.
- *Effective Diagnosis*: The proposed distributed fault diagnosis methods should provide improved performance characteristics compared to the state-of-the-art diagnosis algorithms for HVAC systems with respect to detectability, isolability, robustness and scalability.
- *Distributed Accommodation*: To develop stable distributed fault accommodation algorithms that can compensate the effects caused by the occurrence of sensor faults in real-time, without interrupting the operation of the HVAC system.
- *Distributed Adaptive Control*: To design a distributed adaptive control algorithm that is able to effectively regulate and maintain air temperature in all thermal zones of the building at a desired temperature that is defined by the users of each zone. The control algorithm will be able to compensate the effects cause due to parameter changes, modeling uncertainties and unknown disturbances, while the existing HVAC control methodologies do not offer robustness to those effects.

1.6 Contributions of the Thesis

This section demonstrates the contributions of this doctoral thesis with respect to the state-of-the-art of monitoring and control methodologies for smart buildings. The contributions are summarized below according to the following points.

1. By utilizing representative and realistic HVAC models, and by formulating them as a set of physically interconnected subsystems, it provides a framework that captures the complexity and nonlinearity of large-scale, multi-zone HVAC systems with strong physical interconnections between electromechanical equipment and underlying zones and between adjacent zones (connected through walls and doors), where the state-of-the-art monitoring and control algo-

rithms study linear HVAC models where physical interconnections are not considered.

2. Design a distributed diagnosis architecture for sensor and actuator faults that enhances scalability, diagnosability (i.e., detectability, isolability) and robustness in the presence of measurement noise and modeling uncertainties. The proposed distributed fault diagnosis architecture aims to dramatically reduce the maintenance time for the building operators and consequently, this can decrease the energy waste and the uncomfortable conditions that can be caused in the buildings until the recovery of the HVAC system. This can be achieved since the proposed distributed diagnosis algorithms, that are designed considering the physical interconnections of the HVAC system, lead to the design of less conservative, online diagnosis thresholds, with improved detectabilty and diagnosability. Furthermore, the distributed architecture allows a scalable diagnosis algorithm which can be modified with minor effort, while the existing centralized diagnosis algorithms are lacking scalability.
3. Develop a scalable, stable, distributed sensor fault accommodation algorithms that are capable in real-time (without interrupting the operation of the system) to prevent the increase of energy consumption and preserve indoor comfortable conditions, that can have a indirect impact to their productivity and health of occupants. Existing fault accommodation algorithms for HVAC systems emphasize on data-driven and model predictive control accommodation algorithms that are lacking of tracking performance and stability guarantees.
4. Develop a distributed adaptive control algorithm which can enhance the control performance of the HVAC system by providing stable temperature regulation in building thermal zones in the presence of modeling uncertainty and unknown disturbances. The adaptive control algorithm offers an online tuning of the control gains. The adaptive control gains are updated online using a local adaptive law that takes into account the interconnection between the HVAC zones and the electromechanical equipment. The appropriate selection of the learning rate offers improved tracking performance with reduced energy use in comparison with the existing HVAC control methodologies.

1.7 Outline of the Thesis

The thesis is organized in eleven chapters. The diagram in Fig. 1.3 illustrates the outline of the thesis.

Chapter 2 indicated with a gray box in Fig. 1.3, presents the mathematical modeling of HVAC systems using three models that named as (i) variable-air-volume (VAV) HVAC model, (ii) fan-coil unit (FCU) HVAC model and (iii) air handling unit (AHU) HVAC model. VAV HVAC model describes the temperature dynamics of a multi-zone HVAC system with a cooling operation of which the zones are thermally isolated i.e., the heat transfer between thermal zones is not modeled, while the interaction of zones and the electromechanical systems is modeled. VAV HVAC model describes the temperature

dynamics of a multi-zone HVAC system with a heating operation of which the zones are thermally connected i.e., the heat transfer between thermal zones through wall and doors is modeled. Note that the dynamic terms that describe the heat transfer between doors is described with nonlinear terms. The AHU HVAC model describes the temperature dynamics of a multi-zone HVAC system with both heating and cooling operation. Heat transfer between thermal zones, the AHU and the thermal zones and between the component of the AHU are included in the model.

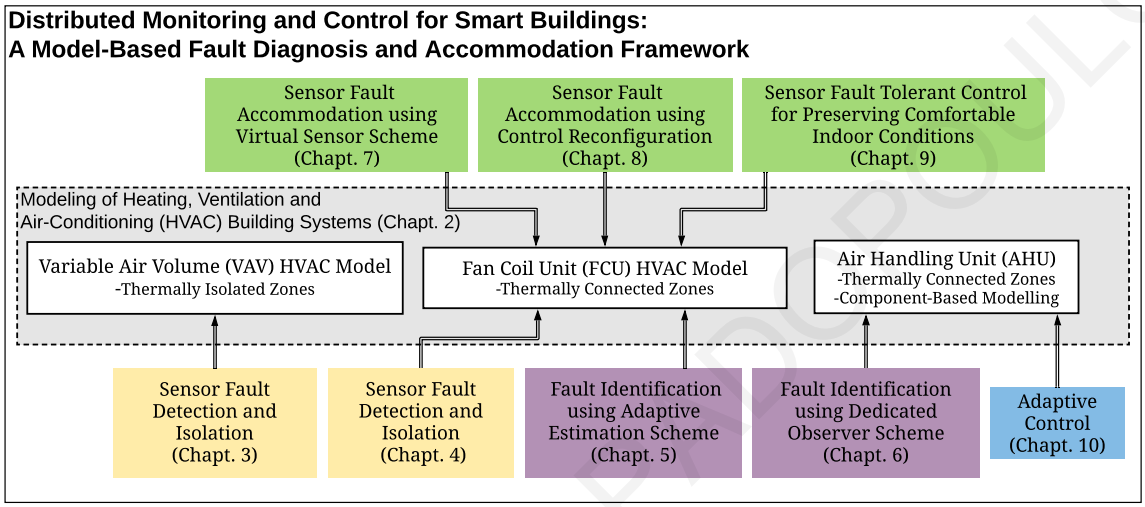

Figure 1.3: Thesis Outline

Chapter 3 and 4, indicated with a yellow box in Fig. 1.3, correspond to distributed detection and isolation of sensor faults in HVAC systems. Specifically, Chapter 3 presents the design of a distributed detection and isolation architecture for sensor faults in VAV HVAC systems, while Chapter 4 presents the design of a distributed detection and isolation architecture for sensor faults in FCU HVAC systems.

Chapter 5 and 6, indicated with a purple box in Fig. 1.3, correspond to distributed identification of faults in HVAC systems. Specifically, Chapter 5 presents the design of a distributed fault identification methods that uses adaptive estimation schemes to distinguish between sensor and actuator faults in FCU HVAC systems. Chapter 6 presents the design of a distributed fault identification approach that is based on dedicated observers detect, isolate and identify between sensor and actuator faults in AHU HVAC systems.

Chapter 7, 8 and 9, indicated with a green box in Fig. 1.3, correspond to distributed accommodation of sensor faults in HVAC systems. Specifically, Chapter 7 presents the design of a distributed sensor fault accommodation algorithm using a virtual sensor scheme. Chapter 8 presents the design of a distributed sensor fault accommodation algorithm using a control reconfiguration. Chapter 9 presents the design of a distributed sensor fault tolerant control algorithm for preserving comfortable indoor conditions.

Chapter 10 indicated with a blue box in Fig. 1.3, corresponds to distributed adaptive control of

AHU HVAC systems. The distributed adaptive control design aims to regulate the air temperature in thermal zones in the presence of modeling uncertainty, unknown disturbances using theoretical tool from robust adaptive control theory.

Chapter 11 summarize the main contributions of the thesis and presents the impact of applying the proposed methodologies to Smart Buildings. Furthermore, the future research steps are given as well.

Chapter 2

Modeling of HVAC Building Systems

Modeling of HVAC systems is one important aspect in model-based approaches. In general, any system can be modeled with *infinite dimensional state-space* models described by partial differential equations (PDEs) and *finite-dimensional state-space* models that are described by ordinary differential equations (ODEs).

The infinite dimensional state-space models for HVAC systems are formulated with computational fluid dynamics (CFD) that uses numerical analysis and data structures to analyze and solve problems that involve fluid flows. Specifically, CFD analysis numerically solves the discrete form of the Navier-Stokes equations (i.e., equation of conservation of mass, momentum and energy) and species concentrations. While the CFD method can provide a detailed description of the spatial distribution and evolution of air pressure, velocity, temperature, humidity, concentration of substances and air turbulence, it is also associated with a high computational overhead. Therefore, it is mainly used for the simulation of only a single HVAC component or a couple of rooms at a time. Its modeling accuracy depends on the correct representation of the boundary conditions, the discretization method and the level of transient characteristics. On the other hand, finite-dimensional state-space models for HVAC systems depend on mass and energy conservation equations based on the following assumptions: i) the air temperature and velocity have uniform behavior throughout a zone ii) the transient and spatial effects are neglected at the components which exchange air iii) at the exterior and interior surface of the zones, supply/return ducts, etc., the heat transfer is modeled using constant heat transfer coefficients iv) the heat transfer at the water storage tanks with the ambient is modeled using a single constant heat transfer coefficient for all surfaces, and v) the axial mixing of water is neglected and vi) the water temperature is constant across the cross section of the tubes.

Finite-dimensional state-space models that describe the HVAC system's behavior can be classified based on HVAC system's operation (i.e., heating models, cooling models, heating and cooling models, ventilation), and HVAC system's structure (i.e., single-zone (operated by a single unit), multi-zone (operated by multi-unit system)). Besides the electrical and mechanical equipment, described above,

it is important to note that the most essential part of the HVAC system is the conditioned zones, where the size of zones (i.e., volume), thermal characteristics (e.g., thermal transfer coefficients) of external and internal walls, adjacent doors, etc., can change the indoor thermal conditions and consequently the energy consumption of the building. A thermal zone is defined as the building area, the climate of which is controlled by the HVAC electromechanical system [113].

A typical building may consist of multiple interconnected thermal zones. Zone temperature can be affected by neighboring zones directly due to convection if there are internal openings, such as open doors, or indirectly due to conduction from walls. The interaction between zones may change drastically due to human activity. Opening of a door between two zones of different temperature may cause air flow from the zone that has higher temperature to the other and, subsequently, heat exchange due to convection [86]. Heat gains produced by the equipment apart from the HVAC sytem, occupancy, solar heat gains produce by glazing and open/closed doors or windows are typically unknown, time-varying and difficult to measure. In addition, degradation affects significantly heat transfer properties of materials, changing heat transfer coefficients as well as thermal capacities [40]. As temperature changes, air density fluctuates as well.

This Chapter deals with the formulation of the mathematical, finite-dimensional state-space models that characterizing the behaviour of different types of multi-zone Heating, Ventilation and Air-Conditioning (HVAC) systems. Additionally, this Chapter proposes the configuration of HVAC system's dynamics as a network of physically interconnected subsystems. Partitioning the system into a network of interconnected subsystems enhances the design of distributed algorithms of control and monitoring of large-scale, multi-zone HVAC systems.

2.1 Preliminaries

Notation	
k	discrete time
t	continuous time
$\mathbb{R}$	field of the real numbers
$x \in \mathbb{R}$	a scalar variable
$\mathbf{x} \in \mathbb{R}^n$	a vector
$\mathbf{A} \in \mathbb{R}^{n \times n}$	a matrix
$\|\|\mathbf{x}(k)\|\|$	the Euclidean (l_2) vector norm in $\mathbb{R}^n$ at each time k, for any vector $\mathbf{x} \in \mathbb{R}^n$
$\mathbf{x} \in l_\infty$	means that $\|\|\mathbf{x}\|\|_\infty = \sup_{k \geq 0} \|\mathbf{x}(k)\|$ exists
$\lambda(A)$	the eigenvalues of matrix $\mathbf{A}$
$\lambda_{\max}(\mathbf{A})$	the maximum eigenvalue of matrix $\mathbf{A}$

2.2 Network Configuration

The main step for employing the proposed distributed, model-based fault diagnosis, fault accommodation and control methodologies is to formulate the multi-zone HVAC system as a network of interconnected, nonlinear subsystems, where every local subsystem Σ is described by

$$\Sigma: \quad \dot{\mathbf{x}}(t) = \mathbf{A}\mathbf{x}(t) + \gamma(\mathbf{x}(t), \mathbf{u}(t)) + h(\mathbf{x}(t), \mathbf{u}(t), \mathbf{z}(t), \mathbf{u}_z(t)) + \mathbf{d}(t) + \eta(\mathbf{x}(t), \mathbf{u}(t), \mathbf{u}_z(t), \mathbf{z}(t), t), \quad (2.1)$$

where $\mathbf{x} \in \mathbb{R}^n$, $\mathbf{u} \in \mathbb{R}^\ell$ are the state and input vector of the local subsystem, respectively, while $\mathbf{z} \in \mathbb{R}^p$ and $\mathbf{u}_z \in \mathbb{R}^{\ell_z}$ are the interconnection state and interconnection input vector, containing the states and inputs of the neighboring (interconnected) subsystems. The constant matrix $\mathbf{A} \in \mathbb{R}^{n \times n}$ is the linearized part of the state equation and $\gamma : \mathbb{R}^n \times \mathbb{R}^\ell \mapsto \mathbb{R}^n$ represents the known nonlinear dynamics. The term $\mathbf{A}\mathbf{x} + \gamma(\mathbf{x}, \mathbf{u})$ represents the known local dynamics, while $h : \mathbb{R}^n \times \mathbb{R}^\ell \times \mathbb{R}^{\ell_z} \times \mathbb{R}^p \mapsto \mathbb{R}^n$ represents the known interconnection dynamics. The $\mathbf{d} : \mathbb{R} \mapsto \mathbb{R}^n$ represents the known exogenous inputs and last term $\eta : \mathbb{R}^n \times \mathbb{R}^\ell \times \mathbb{R}^{\ell_z} \times \mathbb{R}^p \times \mathbb{R} \mapsto \mathbb{R}^n$ denotes the modeling uncertainty of the local subsystem, representing various sources of uncertainty such as system unknown disturbances such heat sources that are unmeasured or not modeled, linearization error, uncertainty in the model's parameters, etc. The input vector $\mathbf{u}$ is generated by a local feedback controller based a desired reference input. An example of a network of two interconnected subsystems $\Sigma^{(1)}$ and $\Sigma^{(2)}$ is described by

$$\begin{aligned}\Sigma^{(1)}: \quad \dot{\mathbf{x}}^{(1)}(t) &= \mathbf{A}^{(1)}\mathbf{x}^{(1)}(t) + \gamma^{(1)}(\mathbf{x}^{(1)}(t), \mathbf{u}^{(1)}(t)) + h^{(1)}(\mathbf{x}^{(1)}(t), \mathbf{u}^{(1)}(t), \mathbf{z}^{(1)}(t), \mathbf{u}_z^{(1)}(t)) \\ &\quad + \mathbf{d}^{(1)}(t) + \eta^{(1)}(\mathbf{x}^{(1)}(t), \mathbf{u}^{(1)}(t), \mathbf{u}_z^{(1)}(t), \mathbf{z}^{(1)}(t), t), \quad (2.2)\end{aligned}$$

$$\begin{aligned}\Sigma^{(2)}: \quad \dot{\mathbf{x}}^{(2)}(t) &= \mathbf{A}^{(2)}\mathbf{x}^{(2)}(t) + \gamma^{(2)}(\mathbf{x}^{(2)}(t), \mathbf{u}^{(2)}(t)) + h^{(2)}(\mathbf{x}^{(2)}(t), \mathbf{u}^{(2)}(t), \mathbf{z}^{(2)}(t), \mathbf{u}_z^{(2)}(t)) \\ &\quad + \mathbf{d}^{(2)}(t) + \eta^{(2)}(\mathbf{x}^{(2)}(t), \mathbf{u}^{(2)}(t), \mathbf{u}_z^{(2)}(t), \mathbf{z}^{(2)}(t), t), \quad (2.3)\end{aligned}$$

where $\mathbf{z}^{(1)} = \mathbf{x}^{(2)}$, $\mathbf{z}^{(2)} = \mathbf{x}^{(1)}$, $\mathbf{u}_z^{(1)} = \mathbf{u}^{(2)}$ and $\mathbf{u}_z^{(2)} = \mathbf{u}^{(1)}$. Fig. 2.1 shows the schematic diagram of the network of two interconnected subsystems as it is described in (2.2)–(2.3).

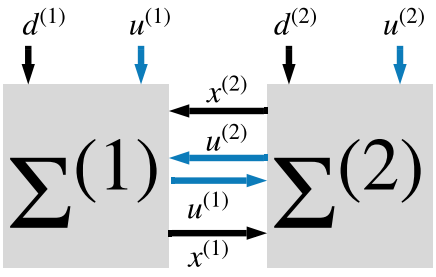

Figure 2.1: Schematic diagram of a network of two interconnected subsystems.

The following sections present the modeling of three types of multi-zone HVAC systems that facilitate either variable-air-volume (VAV) units or fan-coil units (FCUs), or a detailed air handling units (AHUs), that are the most common HVAC systems installed in commercial, large-scale buildings.

Besides, VAVs and FCUs fall under the category of AHUs, are modelled in individually. The main distinction between these two types of HVAC systems is that VAV units regulate the flow of (hot or cold) air entering the zone using an air dumper while, a FCU regulates the flow of (hot or cold) water passing through the coil using a water valve.

2.3 Modeling of Variable Air Volume (VAV) Systems

Consider a HVAC system equipped with Variable Air Volume (VAV) units, which consists of N separated zones (e.g. dormitory rooms, classrooms) and the electromechanical part with a cooling operation. The basic components of the electromechanical part of the HVAC, shown in Fig. 2.2 are the cooling coil, the chiller and the chilled water tank, the fan, the supply and return ducts and the variable air volume (VAV) boxes. The cooling coil is connected to the chiller through the chiller water tank, which regulates the water inserted to the cooling coil. The control inputs to the HVAC system are the air flow rate to each of the N zones (controlled through the fan and the VAV boxes) and the chilled water mass flow rate (controlled by a 3-way valve). By controlling these inputs, the objective is to achieve the desired temperature in each building zone (for occupants' comfort) and in the cooling coil (for energy efficiency). The humidity and indoor air quality are not controlled. The temperature dynamics in each zone, cooling coil and chiller water tank can be modeled based on the fundamental mass and energy conservation equations under the assumptions presented in [146, 148].

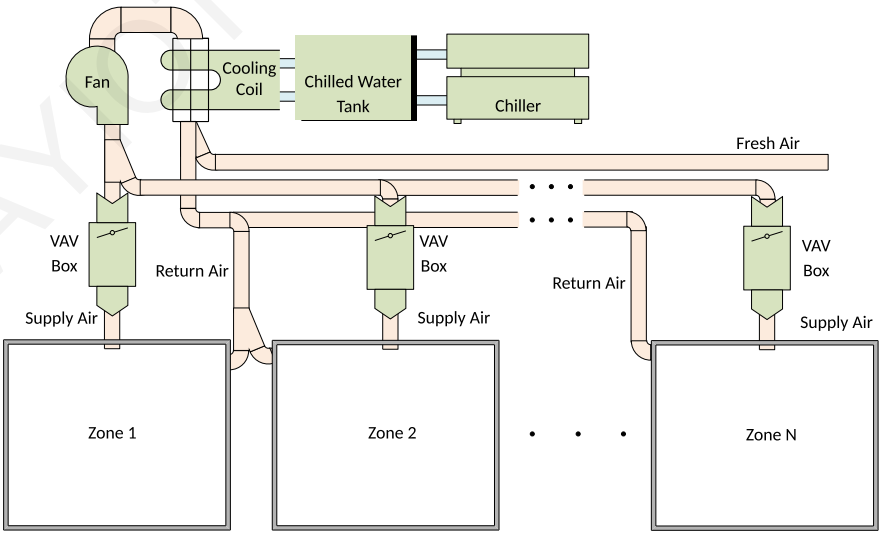

Figure 2.2: Schematic diagram of a multi-zone VAV HVAC system with N separated zones and cooling operation.

The temperature dynamic equations of the N-zone HVAC system are described by

$$M_{z_i} C_v \frac{dT_{z_i}(t)}{dt} = \rho_a C_{pa}(T_{ao}(t) - T_{z_i}(t))u^{(i)}(t) + U_{z_i} A_{z_i}(T_{amb} - T_{z_i}(t)) + \widetilde{T}_{z_i}(t), \tag{2.4}$$

$$\begin{aligned} M_{cc} C_v \frac{dT_{ao}(t)}{dt} &= \rho_a C_{pa} \left(\frac{1}{N} \sum_{i=1}^{N} T_{z_i}(t) - T_{ao}(t) \right) \sum_{i=1}^{N} u^{(i)}(t) \\ &\quad + U_{cc} A_{cc} \left(T_{amb} - \left(T_{ao}(t) + \frac{1}{N} \sum_{i=1}^{N} T_{z_i}(t) \right) \right) \\ &\quad + Q_w \rho_w C_{pw}(T_t(t) - T_{wo}) + \rho_a (h_{fg} - C_{pa}) w_z \sum_{i=1}^{N} u^{(i)}(t) \\ &\quad - \rho_a (h_{fg} - C_{pa}) w_{ao} \sum_{i=1}^{N} u^e_{(i)}(t), \end{aligned} \tag{2.5}$$

$$M_t C_v \frac{dT_t(t)}{dt} = Q_w \rho_w C_{pw}(T_{wo} - T_t(t)) + U_t A_t(T_{amb} - T_t(t)) + \frac{15000}{V_t \rho_w C_{pw}} u^e(t), \tag{2.6}$$

where T_{z_i} (°C) is the temperature of the i-th zone, $i \in \{1, \ldots, N\}$, T_{ao} (°C) is the output air temperature from cooling coil and T_t (°C) is the temperature of the water in the chiller storage tank. The variable $u^{(i)}$ (m^3/ sec) is the volumetric flow rate of air entering into the i-th zone and u^e (m^3/ sec) is the chilled water mass flow rate. The value $\widetilde{T}_{z_i}(t)$ (°C/sec) represents the rate of internal heat change, due to occupants, appliances, solar gains from the i-th zone. For the purposes of this paper, it is assumed that the ambient temperature T_{amb} (°C) is constant and known.

The remainder constant parameters of the HVAC system are the heat mass capacitance corresponding to the i-th zone M_{z_i} (kg), specific heat at constant volume C_v (J/kg K), the overall heat transfer coefficients of the I-th zone, the cooling coil and the chilled water tank U_{z_i}, U_{cc} and U_t (W/m^2 K), respectively, the density of air and water ρ_a and ρ_w (kg/m^3), respectively, the area of the I-th zone, the cooling coil and the chilled water tank A_{z_i}, A_{cc} and A_t (m^2), respectively, the specific heat at constant pressure of air and water C_{pa} and C_{pw} (J/kg K), respectively, the latent heat of water h_{fg} (J/kg), the temperature of output water T_{wo} (°C) and the humidity factors w_z, w_{ao} [148].

In each of the N zones, there exist a sensor measuring the zone temperature T_{z_i}, while two sensors are available in the electromechanical part of the HVAC, measuring the temperature of the air exiting the cooling coil T_{ao} and the temperature of the chilled water in the tank T_t. The control inputs to the N-zone HVAC system are the volumetric flow rate of air $u^{(i)}$ to each zone and the chilled water mass flow rate to the storage tank u^e, generated by distributed feedback controllers based on some reference signals.

VAV HVAC system Network Configuration

The N-zone HVAC system equipped with VAV units can be regarded as a network of $N+1$ interconnected, nonlinear subsystems that correspond to the electromechanical part, comprised of the cooling coil and chiller water tank, and the N building zones and it is illustrated in Fig. 2.3b. Let us define

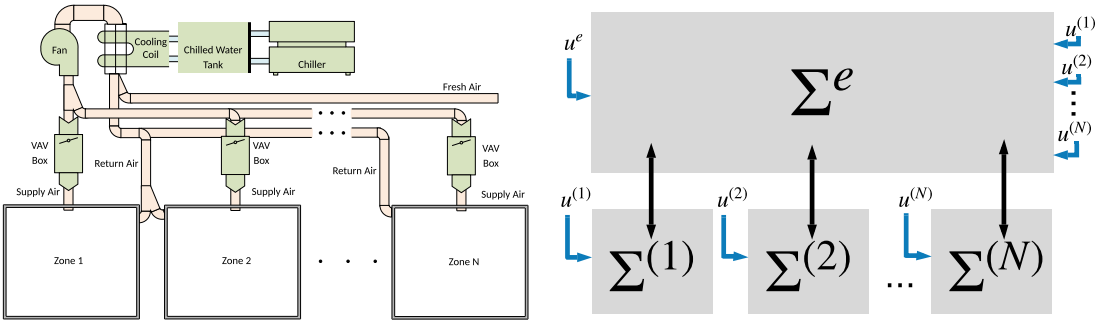

(a) Diagram of a multi-zone VAV HVAC system

(b) Diagram of interconnected subsystems

Figure 2.3: Network configuration for the multi-zone VAV HVAC system.

$\mathbf{T}^e = \left[T_1^e, T_2^e\right]^\top = [T_{ao}, T_t]^\top$, where T_{ao} (°C) is the output air temperature from the cooling coil and T_t (°C) is the temperature of the water in the chiller storage tank, $\mathbf{T}_z = [T_{z_1}, \ldots, T_{z_N}]^\top$, where T_{z_i} (°C) is the temperature of the i-th zone, $\mathbf{u} = \left[u^{(1)}, \ldots, u^{(N)}\right]^\top$, where $u^{(i)}$ (m^3/sec) is the volumetric flow rate of air entering into the i-th zone and u^e (m^3/sec) is the chilled water mass flow rate. By expressing the temperature dynamic equations of the multi-zone HVAC system equipped with VAV units given in (2.4)–(2.6) in the form of (2.1) such that $\mathbf{x} \equiv \mathbf{T}_e$, $u \equiv u^e$, $\mathbf{z} \equiv \mathbf{T}_z$, $\mathbf{u}_z \equiv u$, the subsystem that corresponds to the electromechanical part, denoted by Σ^e, can be expressed as:

$$\Sigma^e: \quad \dot{\mathbf{T}}^e(t) = \mathbf{A}^e\mathbf{T}^e(t) + \gamma^e(u^e(t)) + h^e(\mathbf{T}^e(t), \mathbf{T}_z(t), \mathbf{u}(t)) + \eta^e(t). \tag{2.7}$$

where

$$\mathbf{A}^e = \begin{bmatrix} -\frac{U_{cc}A_{cc}}{M_{cc}C_v} & \frac{Q_w\rho_wC_{pw}}{M_{cc}C_v} \\ 0 & -\frac{Q_w\rho_wC_{pw}+U_tA_t}{V_t\rho_wC_{pw}} \end{bmatrix} \tag{2.8}$$

$$\gamma^e(u^e) = \begin{bmatrix} \frac{U_{cc}A_{cc}}{M_{cc}C_v}T_{amb} - \frac{Q_w\rho_wC_{pw}}{M_{cc}C_v}T_{wo} \\ \frac{U_tA_t}{V_t\rho_wC_{pw}}T_{amb} + \frac{Q_w\rho_wC_{pw}}{V_t\rho_wC_{pw}}T_{wo} \end{bmatrix} + \begin{bmatrix} 0 \\ \frac{15000}{V_t\rho_wC_{pw}} \end{bmatrix} u^e, \tag{2.9}$$

$$h^e(T_1^e, \mathbf{T}_z, \mathbf{u}) = \begin{bmatrix} h_1^e(T_1^e, \mathbf{T}_z, \mathbf{u}) \\ 0 \end{bmatrix} \tag{2.10}$$

$$\begin{aligned} h_1^e(T_1^e, \mathbf{T}_z, \mathbf{u}) = &\left(\frac{\rho_aC_{pa}}{M_{cc}C_v}\sum_{I=1}^{N}u^{(i)} - \frac{U_{cc}A_{cc}}{M_{cc}C_v}\right)\frac{1}{N}\sum_{i=1}^{N}T_{z_i} \\ &+ \frac{\rho_a}{M_{cc}C_v}\left((h_{fg} - C_{pa})(w_z - w_{ao}) - C_{pa}T_1^e\right)\sum_{i=1}^{N}u^{(i)}. \end{aligned} \tag{2.11}$$

It is noted that the first two terms of (2.7) represent the local dynamics of Σ^e, while h^e characterizes the interconnection dynamics between Σ^e and $\left\{\Sigma^{(1)}, \ldots, \Sigma^{(N)}\right\}$, where $\Sigma^{(i)}$ corresponds to the temperature dynamics of air in the i-th zone for all $i \in \{1, \ldots, N\}$. By expressing the air temperature dynamic equation writing (2.4) in the form of (2.1) with $x \equiv T_{z_i}$, $u \equiv u^{(i)}$, $z \equiv T_1^e$, $u_z = 0$, the

subsystem of the i-th zone can be expressed as:

$$\Sigma^{(i)}: \quad \dot{T}_{z_i}(t) = A^{(i)}T_{z_i}(t) + \gamma^{(i)}(T_{z_i}(t), u^{(i)}(t)) + h^{(i)}(T_1^e(t), u^{(i)}(t)) + \eta^{(i)}(t). \tag{2.12}$$

where $A^{(i)} = -\frac{U_{z_I}A_{z_i}}{M_{z_i}C_v}$, $\eta^{(i)}(t) = \frac{1}{M_{z_i}C_v}\widetilde{T}_{z_i}(t)$ and

$$\gamma^{(i)}(T_{z_i}(t), u^{(i)}(t)) = -\frac{\rho_a C_{pa}}{M_{z_i}C_v}T_{z_i}(t)u^{(i)}(t) + \frac{U_{z_i}A_{z_i}}{M_{z_i}C_v}T_{amb}(t), \tag{2.13}$$

$$h^{(i)}(T_1^e(t), u^{(i)}(t)) = \frac{\rho_a C_{pa}}{M_{z_i}C_v}T_1^e(t)u^{(i)}(t). \tag{2.14}$$

Again, the first two terms $A^{(i)}T_{z_i}$ and $\gamma^{(i)}(T_{z_i}, u^e_{(i)})$ correspond to the local dynamics of $\Sigma^e_{(i)}$, while $h^{(i)}$ represents the interconnection dynamics between $\Sigma^e_{(i)}$ and Σ^e. The terms η^e and $\eta^{(i)}$ denote the modeling uncertainties of subsystems Σ^e and $\Sigma^e_{(i)}$, respectively. The inputs of subsystems Σ^e and $\Sigma^e_{(i)}$ can be affected by actuator faults modeled as

$$u^e(t) = c^e(t) + f_a^e(t), \tag{2.15}$$

$$u^{(i)}(t) = c^{(i)}(t) + f_a^{(i)}(t), \tag{2.16}$$

where f_a^e is the actuator bias fault that may affect the valve regulating the chilled water mass flow rate and $f_a^{(i)}$ is the actuator bias fault that may affect the air damper that regulates the volumetric flow rate of air entering into the i-th zone. The signals c^e and $c^{(i)}$ are the controller outputs generated using a feedback control scheme based on some (differentiable) desired reference signals y_r^e and $y_r^{(i)}$ for the states T^e and T_{z_i}, respectively.

The i-th subsystem $\Sigma^{(i)}$, $i \in \{1, \ldots, N\}$, is monitored using a temperature sensor, denoted by $\mathcal{S}^{(i)}$, characterized by the output $y^{(i)} \in \mathbb{R}$; i.e.,

$$\mathcal{S}^{(i)}: \qquad y^{(i)}(t) = T_{z_i}(t) + n^{(i)}(t) + f^{(i)}(t), \tag{2.17}$$

where $n^{(i)} \in \mathbb{R}$ denotes the noise corrupting the measurements $y^{(i)}$ of sensor $\mathcal{S}^e_{(i)}$ and $f^{(i)} \in \mathbb{R}$ represents the possible sensor fault. The nonlinear subsystem Σ^e is monitored using a sensor set $\mathcal{S}^e$ that includes two temperature sensors $\mathcal{S}^e\{1\}$ and $\mathcal{S}^e\{2\}$, characterized by

$$\mathcal{S}^e\{1\}: \qquad y_1^e(t) = T_1^e(t) + n_1^e(t) + f_1^e(t) \tag{2.18}$$

$$\mathcal{S}^e\{2\}: \qquad y_2^e(t) = T_2^e(t) + n_2^e(t) + f_2^e(t), \tag{2.19}$$

where $y_j^e \in \mathbb{R}$ is the sensor output, $n_j^e \in \mathbb{R}$ denotes the noise corrupting the measurements of sensor $\mathcal{S}^e\{j\}$ and $f_j^e \in \mathbb{R}$ represents the possible sensor fault.

2.4 Modeling of Fan Coil Unit (FCU) Systems

This Chapter presents the modeling of a multi-zone HVAC system with fan-coil units (FCUs), which is an extended version of the model presented in [172, 173] using terms from [161]. The electromechanical part of the system consists of a hot water unit e.g. heat pump, condenser, storage tank hot

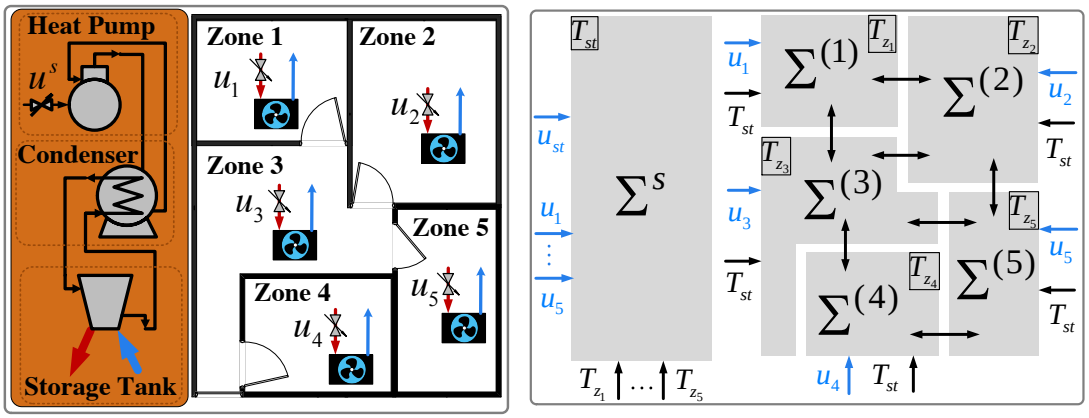

(a) Multi-zone FCU HVAC system.

(b) Subsystems network.

Figure 2.4: Network configuration for the multi-zone FCU HVAC system.

water from the storage tank is circulated in the fan-coil units located in the plenum of each zone and then returns back to the storage tank. This approach concerns the modeling of multi-zone HVAC system with heating operation, although the same structure of the HVAC system can be used also for cooling operation by replacing the heat pump with a chiller. The water temperature in the storage tank is described by the thermal-mass balance equation expressed as

$$\frac{dT_{st}(t)}{dt} = \frac{U_{st,max}}{C_{st}} P_s(T_{st}(t)) u^s(t) - \frac{a_{st}}{C_{st}}(T_{st}(t) - T_{pl}(t)) + \frac{a_{sz}}{C_{st}} \sum_{i \in \mathcal{N}} u^{(i)}(t) U_{i,max}(T_{z_i}(t) - T_{st}(t)) + \frac{a_{st}}{C_{st}} \widetilde{T}_{st}(t) \tag{2.20}$$

where

$$P_s(T_{st}(t)) = \begin{cases} 1 + (P_{max} - 1)\left(1 - \frac{T_{st}(t) - T_o(t)}{\Delta T_{max}}\right), & \Delta T(t) \leq \Delta T_{max} \\ 1, & \Delta T(t) > \Delta T_{max} \end{cases} \tag{2.21}$$

and $T_{st}(t)$ (^{o}C) is the temperature of the water in the storage tank, $T_{z_i}(t)$ (^{o}C) is the *i-th* zone air temperature with $i \in \mathcal{N}$, $\mathcal{N} = \{1, \ldots, N\}$, where N is the number of zones. The known variables $T_{pl}(t)$ (^{o}C) and $T_o(t)$ (^{o}C) are the plenum (duct) temperature and the the source heat temperature of the heat pump, respectively. $P_s(T_{st}(t))$ represents the performance coefficient of the heat pump, $\widetilde{T}_{st}(t)$ (^{o}C) denotes the disturbances affecting the water temperature dynamics due to e.g. defective thermal insulation of the storage tank, P_{max} is the rated maximum value of $P_s(T_{st}(t))$, and ΔT_{max} (^{o}C) is the maximum temperature difference for the heat pump. The parameter $u^{(i)}(t)$ is the mass flow rate of hot water flowing in the coil of *i-th* zone and $u^s(t)$ is the normalized energy in the heat pump. The constant C_{st} (kJ/^{o}C) is the heat capacity of the storage tank, $U_{i,max}$ (kg/h) is the maximum mass flow rate of hot water through the coil placed at the *i-th* zone, and $U_{st,max}$ (kJ/h) is the heat pump rated capacity. The coefficients a_{sz} and a_{st} (kJ/kg ^{o}C) refer to as the effectiveness of the heating coil and the heat loss coefficient of storage tank from exterior surfaces, respectively.

The *i-th* zone temperature dynamics can be described as

$$\frac{dT_{z_i}(t)}{dt} = \frac{U_{i,max}a_{sz}}{C_{z_i}}(T_{st}(t) - T_{z_i}(t))u_{(i)}(t) - \frac{a_{z_i}}{C_{z_i}}(T_{z_i}(t) - T_{amb}(t)) - \frac{hA_{w_i}}{C_{z_i}}(T_{i1}(t) - T_{z_i}(t)) - \frac{1}{C_{z_i}}\sum_{j\in\mathcal{K}_i} a_{z_{i,j}}(T_{z_i}(t) - T_{z_j}(t)) + \frac{a_{z_i}}{C_{z_i}}\widetilde{T}_{z_i}(t) + \frac{\rho_{air}C_p\sqrt{2(C_p - C_v)}}{C_{z_i}} \times \left(\sum_{j\in\mathcal{K}_i} sgn(T_{z_j}(t) - T_{z_i}(t))A_{d_{i,j}} \max(T_{z_i}(t), T_{z_j}(t))\sqrt{\left|T_{z_j}(t) - T_{z_i}(t)\right|}\right), \quad (2.22)$$

where $T_{i1}(t)$ (^{o}C) is the known temperature of the surface node of the mass wall in the *i-th* zone, $T_{amb}(t)$ (^{o}C) is the known ambient temperature, $\widetilde{T}_{z_i}(t)$ (^{o}C) is the temperature dynamics of the *i-th* zone due to presence of appliances, occupants, lights, h (W/m^2 ^{o}C) is the heat transfer coefficient due to the presence of walls, A_{w_i} (m^2) is the surface area of the mass wall, and C_{z_i} (kJ/^{o}C) is the air heat capacity of the *i-th* zone. The coefficient a_{z_i} (kJ/h ^{o}C) corresponds to the heat loss coefficient of the *i-th* zone, and $a_{z_{i,j}}$ (kJ/h ^{o}C) is the inter-zone heat loss coefficient between *i-th* and *j-th* zone due to the presence of walls, $A_{d_{i,j}}$ (m^2) is area of the door connecting *i-th* and *j-th* zone with $j \in \mathcal{K}_i$, $\mathcal{K}_i = \{j : a_{z_{ij}} \neq 0\}$. It is noted that $\mathcal{K}_i$ is the set that consists of the indices of zones that are interconnected with the *i-th* zone.

FCU Network Architecture

Similarly, as we saw in the previous section, the thermal dynamics of the multi-zone HVAC system with fan-coil units (FCUs) presented in the previous Section can be characterized as a network of $N + 1$ interconnected subsystems denoted by Σ^s, $\Sigma_s^{(1)}$,...,$\Sigma_s^{(N)}$, where Σ^s represents the temperature dynamics of the storage tank, and $\Sigma_{(i)}^s$, $i \in \mathcal{N}$, represents the temperature dynamics of the i-th building zone. The subsystem Σ^s can be expressed as

$$\Sigma^s : \quad \dot{T}_{st}(t) = A^s T_{st}(t) + \gamma^s(T_{st}(t), u^s(t)) + h^s(T_{st}(t), \mathbf{T}_z(t), \mathbf{u}(t)) + d^s\left(T_{pl}(t)\right) + \eta^s(t), \quad (2.23)$$

where $T_{st} \in \mathbb{R}$ ((^{o}C) the temperature of the water in the storage tank) represents the local state of subsystem Σ^s and $u^s \in \mathbb{R}$ (the normalized energy in the heat pump) denotes the local control input of subsystem Σ^s. The terms γ^s and h^s describe the nonlinear local and interconnection dynamics of subsystem Σ^s, respectively. The term d^s collects uncontrollable but known exogenous inputs affecting the local subsystem Σ^s, while the term η^s models unknown inputs affecting the water temperature dynamics of the storage tank. The vector $\mathbf{T}_z \triangleq [T_{z_1}, \ldots, T_{z_N}]$ is the interconnection vector that includes the states of neighbouring subsystems (temperatures of all building zones), where T_{z_i} is the air temperature of the interconnected building zone i (i.e. state of subsystem $\Sigma^{(i)}$), and $\mathbf{u} \triangleq \left[u^{(1)}, \ldots, u^{(N)}\right]$, where $u_{(i)}^s$ is the mass flow rate of hot water flowing in the coil of i-th zone and represents the control

input of subsystem $\Sigma^{(i)}$, and are defined as:

$$\gamma^s(T_{st}(t), u^s(t)) = g^s(T_{st}(t))u^s(t) = \frac{U_{st,max}}{C_{st}} P_s(T_{st})u^s(t), \tag{2.24}$$

$$h^s(T_{st}(t), \mathbf{T}_z(t), \mathbf{u}(t)) = \frac{a_{sz}}{C_{st}} \sum_{i\in\{1,\dots,N\}} U_{i,max}(T_{st}(t) - T_{z_i}(t))u^{(i)}(t). \tag{2.25}$$

Note that the term γ^s can be simplified into the bilinear term $g^s(T_{st})u^s$ (see (2.24)). The constant A^s is defined as $A^s = -\frac{a_{st}}{C_{st}}$ and $\eta^s(T_{pl}) = \frac{a_{st}}{C_{st}} T_{pl}$. The defined function u_e^s collects all the dynamics of T_{st}.

Each subsystem $\Sigma^{(i)}$ for all $i \in \mathcal{N}$, is interconnected with subsystems Σ^s and $\Sigma^{(j)}$, $j \in \mathcal{K}_i$ (where $\mathcal{K}_i$ consists of the indices of zones that are physically interconnected with the i-th zone), described by

$$\Sigma_{(i)}^s : \dot{T}_{z_i}(t) = A^{(i)}T_{z_i}(t) + \gamma^{(i)}(T_{st}(t), T_{z_i}(t), u^{(i)}(t)) + h^{(i)}(T_{z_i}(t), \mathbf{T}_{\mathcal{K}_i}(t)) + d^{(i)}(T_{i1}(t), T_{amb}(t)) + \eta^{(i)}(t) \tag{2.26}$$

where $\mathbf{T}_{\mathcal{K}_i}(t) = \left[T_{z_j}(t) : j \in \mathcal{K}_i\right]^\top$, $\mathbf{T}_{\mathcal{K}_i}$ denotes a column vector of length card$(\mathcal{K}_i)$, where each element corresponds to the state T_{z_j} of the neighboring subsystem $\Sigma^{(j)}$, $j \in \mathcal{K}_i$. The term $d^{(i)}$ collects the known exogenous inptus that affect the local subsystem $\Sigma^{(i)}$, while the term $\eta^{(i)}$ models the unknown modeling uncertainies of subsystem $\Sigma^{(i)}$, and $A^{(i)}$ collects the linear terms. The terms $\gamma^{(i)}$ and $h^{(i)}$ respectively denote the local and interconnection nonlinear dynamics of the subsystem $\Sigma^{(i)}$. , i.e.,

$$\gamma^{(i)}(T_{st}(t), T_{z_i}(t)u^{(i)}(t)) = g^{(i)}(T_{st}(t), T_{z_i}(t))u^{(i)}(t) = \sigma^{(i)}(T_{st}(t) - T_{z_i}(t))u^{(i)}(t), \tag{2.27}$$

$$h^{(i)}(T_{z_i}(t), \mathbf{T}_{\mathcal{K}_i}(t)) = \frac{1}{C_{z_i}} \sum_{j\in\mathcal{K}_i} a_{z_{i,j}} T_{z_j}(t) + p^{(i)}\left(\sum_{j\in\mathcal{K}_i} sgn(T_{z_j}(t) - T_{z_i}(t)) A_{d_{i,j}} \max(T_{z_i}(t), T_{z_j}(t)) \sqrt{\left|T_{z_j}(t) - T_{z_i}(t)\right|} \right), \tag{2.28}$$

with $\sigma^{(i)} = \frac{U_{i,max}a_{sz}}{C_{z_i}}$, $p^{(i)} = \frac{\rho_{air}C_p\sqrt{2(C_p - C_v)}}{C_{z_i}}$, and $d^{(i)}(T_{i1}, T_{amb}) = \frac{a_{z_i}}{C_{z_i}} T_{i1} - \frac{hA_{w_i}}{C_{z_i}} T_{amb}$. The inputs of subsystems Σ^s and $\Sigma^{(i)}$ can be affected by actuator faults modelled as

$$u^s(t) = c^s(t) + f_a^s(t), \tag{2.29}$$

$$u^{(i)}(t) = c^{(i)}(t) + f_a^{(i)}(t), \tag{2.30}$$

where f_a^s is the actuator bias fault that may affect the valve regulating the normalized energy in the heat pump and $f_a^{(i)}$ is the actuator bias fault that may affect the valve regulating the flow of water in fan-coil unit of the i-th zone. The system inputs u^s and $u^{(i)}$ satisfy $u^s(t) = sat(c^s(t))$, $u^{(i)}(t) = sat(c^{(i)}(t))$ where $sat(.)$ is defined as

$$sat(u(t)) = \begin{cases} 0, & u(t) < 0 \\ u(t), & u(t) \in [0, 1] \\ 1, & u(t) > 1 \end{cases}, \tag{2.31}$$

where c^s and $c^{(i)}$ are the controller outputs generated using a feedback control scheme based on some (differentiable) desired reference signals y_r^s and $y_r^{(i)}$ for the states T_{st} and T_{z_i}, respectively. An example of the network configuration of a 5-zone HVAC system is given in Fig. 2.4b. The black arrows denote the shared states between the subsystems due to physical interconnections between the zones as well as between the storage tank and the zones. Note that the saturation in (2.31) is an outcome of known physical constraints of the system, e.g. valves. The water temperature of Σ^s (storage tank) is measured by the sensor $\mathcal{S}^s$, i.e.

$$\mathcal{S}^s : y^s(t) = T_{st}(t) + n^s(t) + f^s(t), \tag{2.32}$$

where $y^s \in \mathbb{R}$ is the sensor output, $n^s \in \mathbb{R}$ is the measurement noise and $f^s \in \mathbb{R}$ denotes a permanent bias sensor fault, while the output of the sensor $\mathcal{S}^{(i)}$ used to measure the air temperature of subsystem $\Sigma^{(i)}$ is expressed as

$$\mathcal{S}^{(i)} : y^{(i)}(t) = T_{z_i}(t) + n^{(i)}(t) + f^{(i)}(t), \tag{2.33}$$

where $y^{(i)} \in \mathbb{R}$ is the sensor output and $n^{(i)} \in \mathbb{R}$ is the measurement noise. The signal $f^{(i)} \in \mathbb{R}$ denotes a permanent bias sensor fault [130].

2.5 Modeling of Air Handling Unit (AHU) Systems

This section provides a detailed description of the structure and modeling of multi-zone HVAC systems. Such systems are composed of building zones, Air Handling Units (AHUs) and thermal storage units, which are analyzed in the following subsections. The basic structure of such systems is demonstrated in Fig. 2.5. It should be noted that the model presented next considers constant flux, air is assumed to be fully mixed, air distribution is uniform and there are not pressure losses across the zones and AHUs. Table 2.1 shows the nomenclature of this model.

2.5.1 Zone Model

A thermal zone is defined as the building area, the climate of which is controlled by an AHU. A typical building may consist of multiple interconnected thermal zones. We consider the following dynamical model of the air temperature for the i^{th} zone of a building with N thermal zones, with $i \in \mathcal{N} = \{1, \ldots, N\}$ [3, 5, 147]:

$$\rho_{\text{a}} V_{\text{z}_i} C_{\text{z}_i} \frac{dT_{\text{z}_i}(t)}{dt} = \dot{m}_{\text{sa}_i} C_{\text{pa}} \left(T_{\text{sa}_i}(t) - T_{\text{z}_i}(t)\right) + \sum_{j \in \mathcal{N}_i} a_{i,j} \left(T_{\text{z}_j}(t) - T_{\text{z}_i}(t)\right) + a_{\text{z}_i} \left(T_{\text{amb}}(t) - T_{\text{z}_i}(t)\right) + Q_i(t). \tag{2.34}$$

where T_{z_i} (^{o}C) is the air temperature of the i^{th} zone, T_{sa_i} (^{o}C) is the supply air temperature in the i^{th} zone, T_{amb} (^{o}C) is the outdoor ambient air temperature and T_{z_j} (^{o}C) is the air temperature of j^{th}

Table 2.1: Nomenclature

Symbol	Definition	Symbol	Definition
ρ_{a}	Air density (kg/m^3)	W	Power (W)
$a_{i,j}$	Inter-zone coefficient ($W/^{\circ}C$)	Q	Heat gain (W)
a_{z_i}	External wall coefficient ($W/^{\circ}C$)	T_s	Sampling time (s)
U	Conduction heat transfer coefficient of coil ($W/m^2{}^{\circ}C$)	T	Temperature ($^{\circ}C$)
A	Area of coil (m^2)	t	time (s)
C	Specific heat capacity ($J/kg\,^{\circ}C$)	f	fault function
$\dot{m}$	Mass flow rate (kg/s)	n	sensor noise
$\mathrm{f_r}$	Fan's power fraction		
N	Total number of zones	V	Volume (m^3)
$\mathcal{N}_i$	Indices of neighboring zones of i^{th} zone		
amb	Ambient	st	Storage tank
c	Coil	wm	Water and metal
f	Fan	hp	Heat pump
i, j	Zone number	z	Zone
m	Mixing box	Superscript	Definition
o	Outside air	d	Discrete version
pa	Constant pressure air	ref	Reference signal
pw	Constant pressure water	*	Nominal value
sa	Supply air	Accent	Use
hc	Heating coil	$\sim$	Design constant
cc	Cooling coil		

neighboring zone for all $j \in \mathcal{N}_i$ where $\mathcal{N}_i$ contains the indices of the neighboring zones of the i^{th} zone. The mass flow rate of the air supplied into the zone from the air handling unit is represented by $\dot{m}_{\mathrm{sa_i}}$ (kg/s). As shown in (2.34), for a constant air mass flow rate $\dot{m}_{\mathrm{sa_i}}$, the air temperature of a zone can be regulated T_{z_i} by the supply air temperature T_{sa_i} and is affected by the temperature of neighboring zones T_{z_j} for all $j \in \mathcal{N}_i$, ambient temperature T_{amb}, and heat gain Q_i that may be a result of human activity, electrical equipment, lights, radiation, or other heat sources. The constant parameter ρ_{a} (kg/m^3) represents the air density, $V_{\mathrm{z_i}}$ (m^3) is the zone volume, $C_{\mathrm{z_i}}$ ($J/kg\,^{\circ}C$) represents the zone thermal capacitance, C_{pa} ($J/kg\,^{\circ}C$) is the air specific heat capacity in constant pressure, $a_{\mathrm{z_i}}$ ($W/^{\circ}C$) is the external wall heat transfer coefficient and ($W/^{\circ}C$) corresponds to the inter zone heat transfer coefficient.

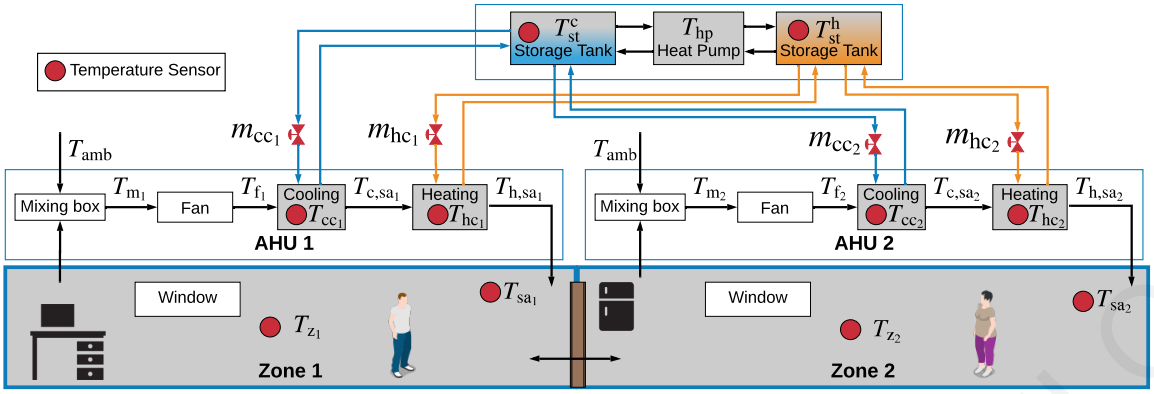

Figure 2.5: Schematic diagram of a multi-zone AHU HVAC system. Gray boxes indicate components with dynamic behavior.

2.5.2 Air Handling Unit Model

A typical Air Handling Unit (AHU) is used for regulating the climate conditions i.e., temperature, humidity and quality of air in a thermal zone. AHUs consists of a mixing box, a fan, a cooling coil and a heating coil [147], as shown in Fig. 2.5.

The mixing box and the fan have a static behavior and hence can be modeled with algebraic equations. The mixing box combines return air from the zone with outside air in order to guarantee circulation of fresh air in the zone and avoid the concentration of contaminants. The air temperature in the mixing box T_{m_i} (^{o}C) of the i^{th} AHU is modeled as follows:

$$T_{\mathrm{m}_i}(t) = \frac{\dot{m}_{\mathrm{o}_i} T_{\mathrm{amb}}(t) + (\dot{m}_{\mathrm{sa}_i} - \dot{m}_{\mathrm{o}_i})\, T_{\mathrm{z}_i}(t)}{\dot{m}_{\mathrm{sa}_i}}. \tag{2.35}$$

where $\dot{m}_{\mathrm{o}_i}$ (kg/s) is the air mass flow rate from the ambient. The fan regulates the air flow rate inside the AHU, receiving air from the mixing box and passing it to the coils. During its operation, the air temperature leaving the fan $T_{\mathrm{f_i}}$ (^{o}C) in the i^{th} AHU increases as follows:

$$T_{\mathrm{f}_i}(t) = \frac{W_{\mathrm{f}_i} \mathrm{f_r}}{\dot{m}_{\mathrm{sa}_i} C_{\mathrm{pa}}} + T_{\mathrm{m}_i}(t). \tag{2.36}$$

where $W_{\mathrm{f_i}}$ (W) is the maximum power of the fan and f is fan's power fraction.

The heating and cooling coils regulate the temperature of air that is supplied to the zone. The heating coil receives hot water from a hot water storage tank and transfers thermal energy to the air that passes through the coil, while the cooling coil receives cold water from a cold water storage and absorbs thermal energy from the air that passes through it. Depending on the needs of the zone for heating or cooling, only one of the two coils may be operating at a specific moment. Coils have a dynamic behavior which is characterized by the temperature change of the water and air that pass through them. Whether they are cooling or heating coils, their dynamics follow a similar formulation.

Thus, the air that passes through the cooling coil and heating coil is given by

$$\begin{cases} C_{\mathrm{sa}_i}\frac{\mathrm{d}T_{\mathrm{c,sa}_i}(t)}{\mathrm{d}t} = (\mathrm{UA})_{\mathrm{cc}_i}\left(T_{\mathrm{cc}_i}(t) - T_{\mathrm{c,sa}_i}(t)\right) - \dot{m}_{\mathrm{sa}_i}C_{\mathrm{pa}}\left(T_{\mathrm{c,sa}_i}(t) - T_{\mathrm{f}_i}(t)\right), \\ C_{\mathrm{sa}_i}\frac{\mathrm{d}T_{\mathrm{h,sa}_i}(t)}{\mathrm{d}t} = (\mathrm{UA})_{\mathrm{hc}_i}\left(T_{\mathrm{hc}_i}(t) - T_{\mathrm{h,sa}_i}(t)\right) - \dot{m}_{\mathrm{sa}_i}C_{\mathrm{pa}}\left(T_{\mathrm{h,sa}_i}(t) - T_{\mathrm{c,sa}_i}(t)\right). \end{cases} \tag{2.37}$$

Due to the orientation of the heating and the cooling coil as we can notice from Fig. 2.5, the air that pass through the cooling coil is affected by the air temperature leaving the fan T_{f_i} (^{o}C) while the air temperature of the heating coil is affected from the temperature of the air that pass through the cooling coil $T_{\mathrm{c,sa}_i}$ (^{o}C). This process affects the temperature of the water that passes through the cooling coil and heating coil as follows:

$$C_{\mathrm{wm}_i}\frac{\mathrm{d}T_{\mathrm{cc}_i}(t)}{\mathrm{d}t} = \dot{m}_{\mathrm{cc}_i}(t)C_{\mathrm{pw}}\left(T^{\mathrm{c}}_{\mathrm{st}}(t) - T_{\mathrm{cc}_i}(t)\right) - (\mathrm{UA})_{\mathrm{cc}_i}\left(T_{\mathrm{cc}_i}(t) - T_{\mathrm{sa}_i}(t)\right), \tag{2.38}$$

$$C_{\mathrm{wm}_i}\frac{\mathrm{d}T_{\mathrm{hc}_i}(t)}{\mathrm{d}t} = \dot{m}_{\mathrm{hc}_i}(t)C_{\mathrm{pw}}\left(T^{\mathrm{h}}_{\mathrm{st}}(t) - T_{\mathrm{hc}_i}(t)\right) - (\mathrm{UA})_{\mathrm{hc}_i}\left(T_{\mathrm{hc}_i}(t) - T_{\mathrm{sa}_i}(t)\right), \tag{2.39}$$

where C_{sa_i} ($J/kg\,^{\circ}$C) is the thermal capacitance of the coil and $(\mathrm{UA})_{\mathrm{c}_i}$ ($W/^{\circ}$C) is the overall conduction heat transfer coefficient of the coil, C_{pw} ($J/kg\,^{\circ}$C) is the water specific heat capacity in constant pressure, C_{wm_i} ($J/kg\,^{\circ}$C) is the thermal capacitance in the water metal point of the coil, $T^{\mathrm{c}}_{\mathrm{st}}$ (^{o}C), $T^{\mathrm{h}}_{\mathrm{st}}$ (^{o}C) represents the temperature of water that arrives to the coil from the chilled water storage tank and the heated water storage tank, respectively as it is illustrated in Fig. 2.5. Specifically, a four-pipe heat pump has the ability to supply with heated and chilled water the chilled water storage tank and the hot water storage tank, respectively. This kind of HVAC systems can facilitate heating and cooling simultaneously to increase control performance in large-scale buildings where zones can have different thermal loads [69].

AHU Network Architecture

In the next part is presented the . The zone dynamics given in (2.34) can be re-written in the following compact form:

$$\frac{dT_{\mathrm{z}_i}}{dt} = A_{\mathrm{z}_i}T_{\mathrm{z}_i}(t) + B_{\mathrm{z}_i}\left[T_{\mathrm{sa}_i}(t) + \sum_{j\in N_i}\frac{a_{i,j}}{\dot{m}_{\mathrm{sa}_i}C_{\mathrm{pa}}}T_{\mathrm{z}_j}(t) + \frac{a_{\mathrm{z}_i}}{\dot{m}_{\mathrm{sa}_i}C_{\mathrm{pa}}}T_{\mathrm{amb}}(t) + \frac{Q_i(t)}{\dot{m}_{\mathrm{sa}_i}C_{\mathrm{pa}}}\right], \tag{2.40}$$

where

$$A_{\mathrm{z}_i} = -\frac{\dot{m}_{\mathrm{sa}_i}C_{\mathrm{pa}} + \sum_{j\in N_i}a_{i,j} + a_{\mathrm{z}_i}}{\rho_{\mathrm{a}}V_{\mathrm{z}_i}C_{\mathrm{z}_i}}, \tag{2.41}$$

$$B_{\mathrm{z}_i} = \frac{\dot{m}_{\mathrm{sa}_i}C_{\mathrm{pa}}}{\rho_{\mathrm{a}}V_{\mathrm{z}_i}C_{\mathrm{z}_i}}. \tag{2.42}$$

Using sampling time T_s, we can write the discrete version of the zone dynamics, which will be useful for the observer design, as follows:

$$\Sigma^{(i)}_{\mathrm{z}}: \quad T_{\mathrm{z}_i}(k+1) = A^{\mathrm{d}}_{\mathrm{z}_i}T_{\mathrm{z}_i}(k) + B^{\mathrm{d}}_{\mathrm{z}_i}\left[T_{\mathrm{sa}_i}(k) + \sum_{j\in N_i}\frac{a_{i,j}}{\dot{m}_{\mathrm{sa}_i}C_{\mathrm{pa}}}T_{\mathrm{z}_j}(k) + \frac{a_{\mathrm{z}_i}}{\dot{m}_{\mathrm{sa}_i}C_{\mathrm{pa}}}T_{\mathrm{amb}}(k) + \frac{Q_i(k)}{\dot{m}_{\mathrm{sa}_i}C_{\mathrm{pa}}}\right], \tag{2.43}$$

where

$$t = kT_s,\;\; A_{z_i}^{\mathrm{d}} = e^{A_{z_i}T_s},\;\; B_{z_i}^{\mathrm{d}} = \frac{A_{z_i}^{\mathrm{d}} - 1}{A_{z_i}} B_{z_i}. \tag{2.44}$$

In order to design a proper observer that can estimate the temperature of supply air, which is produced by the AHU, we re-write the supply air dynamics of (2.37) in the following compact form:

$$\frac{\mathrm{d}\mathbf{T}_{\mathrm{sa}_i}}{\mathrm{d}t} = \mathbf{A}_{\mathrm{sa}_i}\mathbf{T}_{\mathrm{sa}_i}(t) + \mathbf{B}_{\mathrm{sa}_i}\left(\mathbf{T}_{\mathrm{c}_i}(k) + \mathbf{G}_{\mathrm{f,sa}_i} + \mathbf{G}_{\mathrm{amb,sa}_i}T_{\mathrm{amb}}(t) + \mathbf{G}_{\mathrm{ma,sa}_i}T_{\mathrm{z}_i}(t)\right), \tag{2.45}$$

with $\mathbf{T}_{\mathrm{sa}_i}(t) = \begin{bmatrix} T_{\mathrm{c,sa}_i}(t) \\ T_{\mathrm{h,sa}_i}(t) \end{bmatrix}$, $\mathbf{T}_{\mathrm{c}_i}(t) = \begin{bmatrix} T_{\mathrm{cc}_i}(t) \\ T_{\mathrm{hc}_i}(t) \end{bmatrix}$, where

$$\mathbf{A}_{\mathrm{sa}_i} = \begin{bmatrix} -\frac{\left((\mathrm{UA})_{\mathrm{cc}_i} + \dot{m}_{\mathrm{sa}_i}C_{\mathrm{pa}}\right)}{C_{\mathrm{sa}_i}} & 0 \\ \frac{\dot{m}_{\mathrm{sa}_i}C_{\mathrm{pa}}}{C_{\mathrm{sa}_i}} & -\frac{\left((\mathrm{UA})_{\mathrm{hc}_i} + \dot{m}_{\mathrm{sa}_i}C_{\mathrm{pa}}\right)}{C_{\mathrm{sa}_i}} \end{bmatrix},\;\; \mathbf{B}_{\mathrm{sa}_i} = \begin{bmatrix} \frac{(\mathrm{UA})_{\mathrm{cc}_i}}{C_{\mathrm{sa}_i}} & 0 \\ 0 & \frac{(\mathrm{UA})_{\mathrm{hc}_i}}{C_{\mathrm{sa}_i}} \end{bmatrix}, \tag{2.46}$$

$$\mathbf{G}_{\mathrm{f,sa}_i} = \begin{bmatrix} \frac{W_{\mathrm{fan}_i}f}{(\mathrm{UA})_{\mathrm{cc}_i}} & 0 \end{bmatrix}^{\top},\;\; \mathbf{G}_{\mathrm{amb,sa}_i} = \begin{bmatrix} \frac{C_{\mathrm{pa}}m_{\mathrm{o}_i}}{(\mathrm{UA})_{\mathrm{cc}_i}} & 0 \end{bmatrix}^{\top},\;\; \mathbf{G}_{\mathrm{ma,sa}_i} = \begin{bmatrix} \frac{C_{\mathrm{pa}}\left(m_{\mathrm{sa}_i} - m_{\mathrm{o}_i}\right)}{(\mathrm{UA})_{\mathrm{cc}_i}} & 0 \end{bmatrix}^{\top}. \tag{2.47}$$

Using sampling time T_s, we can write the discrete version of the supply air dynamics, which will be useful for the implementation of the fault diagnosis algorithm, as follows:

$$\Sigma_{\mathrm{sa}}^{(i)}:\;\; \mathbf{T}_{\mathrm{sa}_i}(k+1) = \mathbf{A}_{\mathrm{sa}_i}^{\mathrm{d}}\mathbf{T}_{\mathrm{sa}_i}(k) + \mathbf{B}_{\mathrm{sa}_i}^{\mathrm{d}}\left(\mathbf{T}_{\mathrm{c}_i}(k) + \mathbf{G}_{\mathrm{f,sa}_i} + \mathbf{G}_{\mathrm{amb,sa}_i}T_{\mathrm{amb}}(z) + \mathbf{G}_{\mathrm{ma,sa}_i}T_{\mathrm{z}_i}(z)\right), \tag{2.48}$$

where

$$t = kT_s,\;\; \mathbf{A}_{\mathrm{sa}_i}^{\mathrm{d}} = e^{\mathbf{A}_{\mathrm{sa}_i}T_s},\;\; \mathbf{B}_{\mathrm{sa}_i}^{\mathrm{d}} = \frac{\mathbf{A}_{\mathrm{sa}_i}^{\mathrm{d}} - \mathbf{I}}{\mathbf{A}_{\mathrm{sa}_i}}\mathbf{B}_{\mathrm{sa}_i}. \tag{2.49}$$

This section presents the design of the estimator of cooling coil's water temperature. According to (2.38) the water temperature depends on the air temperature leaving the cooling coil that is not measured. In order to address the issue of the unavailable measurements, we can combine the air side of the cooling coil dynamics given in (2.37) with the water side dynamics of the cooling coil given in (2.38) that leads to the following compact form

$$\frac{\mathrm{d}\mathbf{T}_{\mathrm{sc}_i}}{\mathrm{d}t} = \mathbf{A}_{\mathrm{sc}_i}\mathbf{T}_{\mathrm{sc}_i}(t) + \mathbf{B}_{\mathrm{sc}}\left(\mathbf{C}^{\top}\left(T_{\mathrm{st}}^{\mathrm{c}}(t) - \mathbf{C}\mathbf{T}_{\mathrm{sc}_i}(t)\right)u_{\mathrm{cc_i}}(t) + \mathbf{G}_{\mathrm{f,sc}_i} + \mathbf{G}_{\mathrm{amb,sc}_i}T_{\mathrm{amb}}(t) + \mathbf{G}_{\mathrm{ma,sc}_i}T_{\mathrm{z}_i}(t)\right), \tag{2.50}$$

with $\mathbf{T}_{\mathrm{sc}_i}(t) = \begin{bmatrix} T_{\mathrm{c,sa}_i}(t) \\ T_{\mathrm{cc}_i}(t) \end{bmatrix}$ and $u_{\mathrm{cc_i}}(t) = \dot{m}_{\mathrm{cc_i}}(t)$, where

$$\mathbf{A}_{\mathrm{sc}_i} = \begin{bmatrix} -\frac{\left((\mathrm{UA})_{\mathrm{cc}_i} + \dot{m}_{\mathrm{sa}_i}C_{\mathrm{pa}}\right)}{C_{\mathrm{sa}_i}} & \frac{(\mathrm{UA})_{\mathrm{cc}_i}}{C_{\mathrm{sa}_i}} \\ \frac{(\mathrm{UA})_{\mathrm{cc}_i}}{C_{\mathrm{wm}_i}} & -\frac{(\mathrm{UA})_{\mathrm{cc}_i}}{C_{\mathrm{wm}_i}} \end{bmatrix},\;\; \mathbf{B}_{\mathrm{sc}_i} = \begin{bmatrix} 1 & 0 \\ 0 & \frac{C_{\mathrm{pw}}}{C_{\mathrm{wm}_i}} \end{bmatrix},\;\; \mathbf{C} = \begin{bmatrix} 0 & 1 \end{bmatrix}, \tag{2.51}$$

$$\mathbf{G}_{\mathrm{f,sc}_i} = \begin{bmatrix} \frac{W_{\mathrm{fan}_i}\mathrm{f_r}}{C_{\mathrm{sa}_i}} & 0 \end{bmatrix}^{\top},\;\; \mathbf{G}_{\mathrm{amb,sc}_i} = \begin{bmatrix} \frac{C_{\mathrm{pa}}m_{\mathrm{o}_i}}{C_{\mathrm{sa}_i}} & 0 \end{bmatrix}^{\top},\;\; \mathbf{G}_{\mathrm{ma,sc}_i} = \begin{bmatrix} \frac{C_{\mathrm{pa}}\left(m_{\mathrm{sa}_i} - m_{\mathrm{o}_i}\right)}{C_{\mathrm{sa}_i}} & 0 \end{bmatrix}^{\top}. \tag{2.52}$$

Using sampling time T_s, we can write the discrete version of the air and water dynamics of the cooling coil, which will be useful for the implementation of the fault diagnosis algorithm, as follows:

$$\Sigma_{\text{sc}}^{(i)}: \quad \mathbf{T}_{\text{sc}_i}(k+1) = \mathbf{A}_{\text{sc}_i}^{\text{d}}\mathbf{T}_{\text{sc}_i}(k) + \mathbf{B}_{\text{sc}_i}^{\text{d}}\Bigg(\mathbf{C}^{\top}\Big(T_{\text{st}}^{\text{c}}(k) - \mathbf{C}\mathbf{T}_{\text{sc}_i}(k)\Big)u_{\text{cc}_i}(k) + \mathbf{G}_{\text{f,sc}_i} + \mathbf{G}_{\text{amb,sc}_i}T_{\text{amb}}(k) + \mathbf{G}_{\text{ma,sc}_i}T_{\text{z}_i}(k)\Bigg) \tag{2.53}$$

where

$$t = kT_s, \quad \mathbf{A}_{\text{sc}_i}^{\text{d}} = e^{\mathbf{A}_{\text{sc}_i}T_s}, \quad \mathbf{B}_{\text{sc}_i}^{\text{d}} = \frac{\mathbf{A}_{\text{sc}_i}^{\text{d}} - 1}{\mathbf{A}_{\text{sc}_i}}\mathbf{B}_{\text{sc}_i}. \tag{2.54}$$

As it is presented in (2.39) , heating coil's water temperature dynamics depend on the air temperature that pass through the heating coil $T_{\text{h,sa}_i}(t)$ that is measured by the sensor given in (2.62). Now the air side of the heating coil is depends on the air temperature leaving the cooling coil $T_{\text{c,sa}_i}(t)$ that is not measured. Thus, we combined the air and water side of both cooling and heating coil in order to derive the following compact form

$$\frac{\text{d}\mathbf{T}_{\text{sh}_i}}{\text{d}t} = \mathbf{A}_{\text{sh}_i}\mathbf{T}_{\text{sh}_i}(t) + \mathbf{B}_{\text{sh}_i}\Bigg(\mathbf{C}_{\text{sc}}^{\top}\Big(T_{\text{st}}^{\text{c}}(t) - \mathbf{C}_{\text{sc}}\mathbf{T}_{\text{sh}_i}(t)\Big)u_{\text{cc}_i}(t) + \mathbf{C}_{\text{sh}}^{\top}\Big(T_{\text{st}}^{\text{h}}(t) - \mathbf{C}_{\text{sh}}\mathbf{T}_{\text{sh}_i}(t)\Big)u_{\text{hc}_i}(t) + \mathbf{G}_{\text{f,sh}_i} + \mathbf{G}_{\text{amb,sh}_i}T_{\text{amb}}(t) + \mathbf{G}_{\text{ma,sh}_i}T_{\text{z}_i}(t)\Bigg), \tag{2.55}$$

with $\mathbf{T}_{\text{sh}_i}(k) = \begin{bmatrix} T_{\text{c,sa}_i}(k) & T_{\text{cc}_i}(k) & T_{\text{h,sa}_i}(k) & T_{\text{hc}_i}(k) \end{bmatrix}^{\top}$ and $u_{\text{hc}_i}(t) = \dot{m}_{\text{hc}_i}(t)$, where

$$\mathbf{A}_{\text{sh}_i} = \begin{bmatrix} -\frac{\left((\text{UA})_{\text{cc}_i} + \dot{m}_{\text{sa}_i}C_{\text{pa}}\right)}{C_{\text{sa}_i}} & \frac{(\text{UA})_{\text{cc}_i}}{C_{\text{sa}_i}} & 0 & 0 \\ \frac{(\text{UA})_{\text{cc}_i}}{C_{\text{wm}_i}} & -\frac{(\text{UA})_{\text{cc}_i}}{C_{\text{wm}_i}} & 0 & 0 \\ \frac{\dot{m}_{\text{sa}_i}C_{\text{pa}}}{C_{\text{sa}_i}} & 0 & -\frac{\left((\text{UA})_{\text{hc}_i} + \dot{m}_{\text{sa}_i}C_{\text{pa}}\right)}{C_{\text{sa}_i}} & \frac{(\text{UA})_{\text{hc}_i}}{C_{\text{sa}_i}} \\ 0 & 0 & -\frac{(\text{UA})_{\text{hc}_i}}{C_{\text{wm}_i}} & \frac{(\text{UA})_{\text{hc}_i}}{C_{\text{wm}_i}} \end{bmatrix}, \quad \mathbf{B}_{\text{sh}_i} = \begin{bmatrix} 1 & 0 & 0 & 0 \\ 0 & \frac{C_{\text{pw}}}{C_{\text{wm}_i}} & 0 & 0 \\ 0 & 0 & 0 & 0 \\ 0 & 0 & 0 & \frac{C_{\text{pw}}}{C_{\text{wm}_i}} \end{bmatrix}, \tag{2.56}$$

$$\mathbf{C}_{\text{sc}} = \begin{bmatrix} 0 & 1 & 0 & 0 \end{bmatrix}, \quad \mathbf{C}_{\text{sh}} = \begin{bmatrix} 0 & 0 & 0 & 1 \end{bmatrix}, \quad \mathbf{G}_{\text{f,sh}_i} = \begin{bmatrix} \frac{W_{\text{fan}_i}f}{C_{\text{sa}_i}} & 0 & 0 & 0 \end{bmatrix}^{\top}, \tag{2.57}$$

$$\mathbf{G}_{\text{amb,sh}_i} = \begin{bmatrix} \frac{C_{\text{pa}}m_{\text{o}_i}}{C_{\text{sa}_i}} & 0 & 0 & 0 \end{bmatrix}^{\top}, \quad \mathbf{G}_{\text{ma,sh}_i} = \begin{bmatrix} \frac{C_{\text{pa}}\left(m_{\text{sa}_i} - m_{\text{o}_i}\right)}{C_{\text{sa}_i}} & 0 & 0 & 0 \end{bmatrix}^{\top}. \tag{2.58}$$

Using sampling time T_s, we can write the discrete version of the air and water dynamics of the heating coil, which will be useful for the implementation of the fault diagnosis algorithm, as follows:

$$\Sigma_{\text{sh}}^{(i)}: \quad \mathbf{T}_{\text{sh}_i}(k+1) = \mathbf{A}_{\text{sh}_i}^{\text{d}}\mathbf{T}_{\text{sh}_i}(k) + \mathbf{B}_{\text{sh}_i}^{\text{d}}\Bigg(\mathbf{C}_{\text{sc}}^{\top}\Big(T_{\text{st}}^{\text{c}}(k) - \mathbf{C}_{\text{sc}_i}\mathbf{T}_{\text{sh}_i}(k)\Big)\dot{m}_{\text{cc}_i}(k) + \mathbf{C}_{\text{sh}}^{\top}\Big(T_{\text{st}}^{\text{h}}(k) - \mathbf{C}_{\text{sh}_i}\mathbf{T}_{\text{sh}_i}(k)\Big)\dot{m}_{\text{hc}_i}(k) + \mathbf{G}_{\text{f,sh}_i} + \mathbf{G}_{\text{amb,sh}_i}T_{\text{amb}}(k) + \mathbf{G}_{\text{ma,sh}_i}T_{\text{z}_i}(k)\Bigg) \tag{2.59}$$

where

$$t = kT_s, \quad \mathbf{A}^{\mathrm{d}}_{\mathrm{sh}_i} = e^{\mathbf{A}_{\mathrm{sh}_i} T_s}, \quad \mathbf{B}^{\mathrm{d}}_{\mathrm{sh}_i} = \frac{\mathbf{A}^{\mathrm{d}}_{\mathrm{sh}_i} - 1}{\mathbf{A}_{\mathrm{sh}_i}} \mathbf{B}_{\mathrm{sh}_i}. \tag{2.60}$$

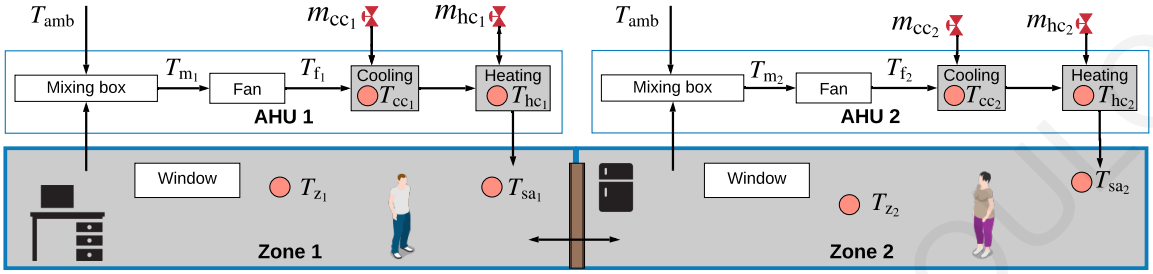

(a) Multi-zone FCU HVAC system.

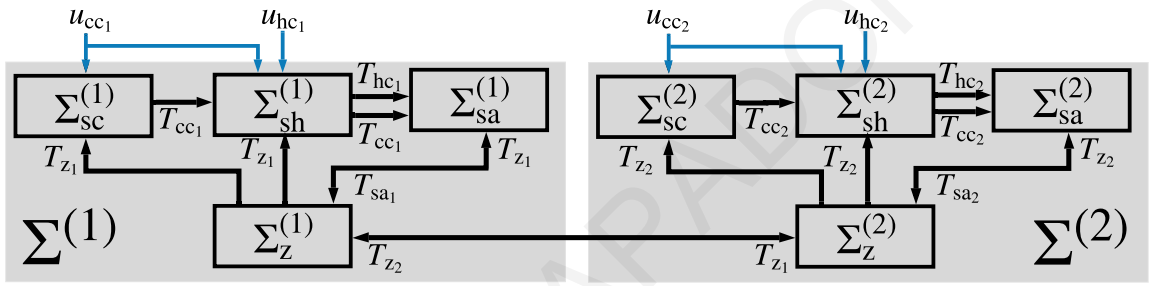

(b) Subsystems network.

Figure 2.6: Network configuration of the a multi-zone AHU HVAC system.

The available sensor measurements for each AHU that are

$$y_{\mathrm{z}_i}(t) = T_{\mathrm{z}_i}(t) + n_{\mathrm{z}_i}(t) + f_{\mathrm{z}_i}(t), \tag{2.61}$$

$$y_{\mathrm{sa}_i}(t) = \mathbf{C} \begin{bmatrix} T_{\mathrm{c,sa}_i}(t) \\ T_{\mathrm{h,sa}_i}(t) \end{bmatrix} + n_{\mathrm{sa}_i}(t) + f_{\mathrm{sa}_i}(t), \tag{2.62}$$

$$y_{\mathrm{cc}_i}(t) = T_{\mathrm{cc}_i}(t) + n_{\mathrm{cc}_i}(t) + f_{\mathrm{cc}_i}(t), \tag{2.63}$$

$$y_{\mathrm{hc}_i}(t) = T_{\mathrm{hc}_i}(t) + n_{\mathrm{hc}_i}(t) + f_{\mathrm{hc}_i}(t), \tag{2.64}$$

with $\mathbf{C} = \begin{bmatrix} 0 & 1 \end{bmatrix}$, where y_{z_i} is the measurement of the ith zone air temperature T_{z_i}, y_{z_j} is the measurement air temperature of neighboring zone T_{z_j} $j \in N_i$, y_{sa_i} is the measurement of the supply air temperature T_{sa_i} and y_{cc_i}, y_{hc_i} are the measurements of water temperature in cooling coil T_{cc_i} and heating coil T_{cc_i}, respectively. The terms n_{z_i} n_{sa_i}, n_{cc_i}, n_{hc_i} represent the noise corrupting the measurements and f_{z_i}, f_{sa_i} f_{cc_i}, f_{hc_i} are the corresponding sensor faults. Moreover, faults can occurred in the actuation devices of the AHU that corresponds the mechanical valves that regulate the water mass flow rate of the cold/hot water that pass through the cooling and heating coils, respectively. The

water mass flow rate in cooling and heating coil valves can be represented by

$$u_{\mathrm{cc}_i}(t) = c_{\mathrm{cc}_i}(t) + f^m_{\mathrm{cc}_i}(t), \tag{2.65}$$

$$u_{\mathrm{hc}_i}(t) = c_{\mathrm{hc}_i}(t) + f^m_{\mathrm{hc}_i}(t), \tag{2.66}$$

where $u_{\mathrm{cc}_i} = \dot{m}_{\mathrm{cc}_i}$ and $u_{\mathrm{cc}_i}\dot{m}_{\mathrm{hc}_i}$ are actual water flow rate of the cooling and heating coils, respectively, c_{cc_i} and c_{hc_i} are the control inputs and $f^m_{\mathrm{cc}_i}$ and $f^m_{\mathrm{hc}_i}$ are the actuator faults that can affect the valves of cooling coil and heating coil, respectively. Note that due to the physical limitations of valves the actual water mass flow rate of both coils is bounded; i.e., $u_{\mathrm{cc}_i}(t) \in [0, u_{\mathrm{cc}_{\mathrm{max},i}}]$ and $u_{\mathrm{hc}_i}(t) \in [0, u_{\mathrm{hc}_{\mathrm{max},i}}]$ for all $i \in \mathcal{N}$.

Remark: For the purposes of this work the measurements of heated and chilled water temperature in the storage tank $T^{\mathrm{h}}_{\mathrm{st}}$ and $T^{\mathrm{c}}_{\mathrm{st}}$, respectively and ambient air temperature T_{amb} are considered known and healthy.

2.6 Fault Modeling

Faults in HVAC systems can affect the HVAC system's equipment, i.e., actuators (such as valves, dumpers, fans) and sensor devices (measuring water and air temperature) in several points in the electromechanical equipment and zones of a large-scale HVAC system. As it is discussed in the Chapter 1.3, faults can have various behaviors in time domain. In this doctoral thesis emphasize on two types of faults; *offset* faults and *performance degradation* faults. The remainder fault types, i.e., fouling, failures, control and stuck faults, can be detected more easily either from the building operators or from the existing ruled-based Buildings Management Systems (BMS) diagnostics. On the other hand, offset and performance degradation is difficult to be observed/notice or diagnosed. Therefore, at this point, the different fault models used to emulate the behavior of the fault function f are introduced, for the faults presented in (2.15), (2.16), (2.29), (5.2), (2.65), (2.66) for the actuator faults and (2.17), (2.18), (2.19), (2.32), (2.61)–(2.64) for the sensor faults. A fault in continuous time can be represented by

$$f(t) = \beta(t - t_f)\phi(t - t_f), \tag{2.67}$$

where β is the time profile and ϕ is the (unknown) function of the fault that occurs at the (unknown) time instant t_f. The time profile of the fault is modeled as $\beta(t) = 0$ for $t < t_f$ and $\beta(t) = 1 - e^{-\alpha t}$ for $t \geq t_f$, where α is the (unknown) evolution rate of the fault. In the case of offset (abrupt) faults, the time profile of the fault is modeled by letting $\alpha \to \infty$, while $\alpha \to 0$ describes an incipient fault that evolves gradually and corresponds to performance degradation fault. Similarly, in discrete time, a fault can be represented by

$$f(k) = \beta(k - k_f)\phi(k - k_f), \tag{2.68}$$

where β is the time profile and ϕ is the (unknown) function of the fault that occurs at the (unknown) time instant k_f. The time profile of the fault is modeled as $\beta(k) = 0$ for $k < k_f$ and $\beta(k) = 1 - \gamma^k$ for $k \geq k_f$, where γ is the (unknown) evolution rate of the fault. In the case of offset (abrupt faults), the time profile of the fault is modeled by letting $\gamma \to 0$, while $\gamma \to 1$ describes an incipient fault that evolves gradually and corresponds to performance degradation fault.

The unknown function of the fault $\phi(.)$ can be equal to a constant value that corresponds to bias fault, while $\phi(.)$ can be a percentage of the measured quantity for a sensor fault and a percentage of the control input for an actuator fault that correspond to a multiplicative fault such as:

$$\phi(t) = \phi_o T(t), \tag{2.69}$$

$$\phi(t) = \phi_o c(t), \tag{2.70}$$

where T is the measured temperature, c is the control input computed by the controller, and $0 < \phi_o < 1$ is the ratio of the multiplicative fault.

The fault patterns can be either single (i.e, occurrence of one fault) or multiple (i.e., more than one fault). Multiple faults can be simultaneous faults i.e., occur at the same time and consecutive i.e., in different time instances. Moreover, in practice, there maybe more than one sensor covering a single zone (especially large zones) compared to the actuators in the electromechanical part of the HVAC system that are unique. In this case, the multiple measurements can be combined by averaging or using advanced sensor fusion methods, while the proposed monitoring and control methodologies can still be applied.

The following Chapters present the outcomes of this doctoral thesis that is a package of intelligent algorithms for distributed monitoring and control that aim to ensure the reliable and efficient operation of the large-scale HVAC systems.

Chapter 3

Distributed Sensor Fault Detection and Isolation Architecture for VAV HVAC systems

3.1 Introduction

The majority of the sensor fault detection and isolation (SFDI) methods developed so far are based on a centralized approach, or have focused on the diagnosis of faults in one of the HVAC subsystems, e.g. chiller, AHU, VAV, considering each subsystem separately [81, 105, 155], thus the physical interconnection of the equipment is neglected. HVAC systems are highly complex, nonlinear systems, typically comprised of multiple interconnected subsystems, especially in the case of large-scale buildings, such as hospitals, shopping malls, business centers, airports, universities and many more. Thus, a centralized approach for fault diagnosis may be less suitable compared to a non-centralized approach, since it is characterized by: (i) increased computational complexity of the FDI algorithms, since centralized architectures are tailored to handle (multiple) faults globally, (ii) increased communication requirements due to the transmission of information to a central point, (iii) vulnerability to security threats, because the central cyber core in which the SFDI algorithm resides is a single-point of failure, and (iv) reduced potential of scalability in case of system expansion (e.g. building a new ward in a hospital), due to the utilization of a global physical model or black-box. Moreover, treating the occurrence of faults in a HVAC subsystem separately may be less efficient, since the propagation of faults in a distributed control architecture is neglected.

3.2 Objective

The main objective of Chapter is the design and analysis of a distributed, model-based method for detecting and isolating multiple sensor faults affecting a multi-zone HVAC systems. Based on the nonlinear HVAC model presented in Chapter 2.3, we develop a distributed SFDI methodology exploiting the spatial distribution of the HVAC system; i.e., modeling the HVAC system as a set of $N+1$ interconnected nonlinear subsystems Σ, that correspond to the N zones and the electromechanical part as illustrated in Fig. 3.1a. For each nonlinear subsystem, we design a dedicated local sensor fault diagnosis (LSFD) agent, which is responsible for detecting and isolating the presence of sensor faults in a distributed manner. To this end, each LSFD agent uses the input and output measurements of its underlying subsystem, as well as the sensor measurements or reference signals of its neighboring subsystems. The sensor fault detection decision logic implemented in the agents relies on checking whether certain analytical redundancy relations (ARRs) are satisfied. The ARRs are formulated using estimation-based residuals and adaptive thresholds, taking into account bounded modeling uncertainties and measurement noise. The distributed isolation of multiple faulty sensors in the HVAC system is carried out using a diagnostic reasoning-based decision logic applied to a sensor fault signature matrix. The performance of the proposed methodology is analyzed with respect to sensor fault detectability and isolability [115], characterizing under certain conditions the class of sensor faults that can be detected and isolated.

The added value of this particular case study is the design of a distributed isolation decision logic and its application to multi-zone HVAC systems that are inherently distributed systems, where the interconnected subsystems are characterized by heterogeneous nonlinear dynamics, as well as the analysis of the different ways that local and propagated sensor faults may affect each subsystem. Moreover, the utilization of adaptive thresholds ensures the robustness of the proposed method against modeling uncertainties and measurement noise, excluding false alarms that are not only annoying to the occupants but also deceptive in emergency situations.

3.3 Design of the Sensor Fault Diagnosis Algorithm

The design of the proposed distributed SFDI technique is realized as follows. Taking into account the $N+1$ subsystems, defined through (2.7) and (2.12), the first step is to design a local sensor fault diagnosis (LSFD) agent for each of the interconnected subsystems; i.e. the agent $\mathcal{M}^e$ dedicated to subsystem Σ^e and the agent $\mathcal{M}^{(I)}$ dedicated to subsystem $\Sigma^{(I)}$, $I \in \{1,\ldots,N\}$ [124–126]. Each LSFD agent has access to the input and output data of the underlying subsystem, while it may exchange information with some agents. The exchanged information is associated with the form of the physical and input interconnections. Particularly, the agent $\mathcal{M}^e$ that monitors the electromechanical part transmits the measurements of $S^e\{1\}$ to each agent $\mathcal{M}^{(I)}$, while it uses a priori known temperature reference

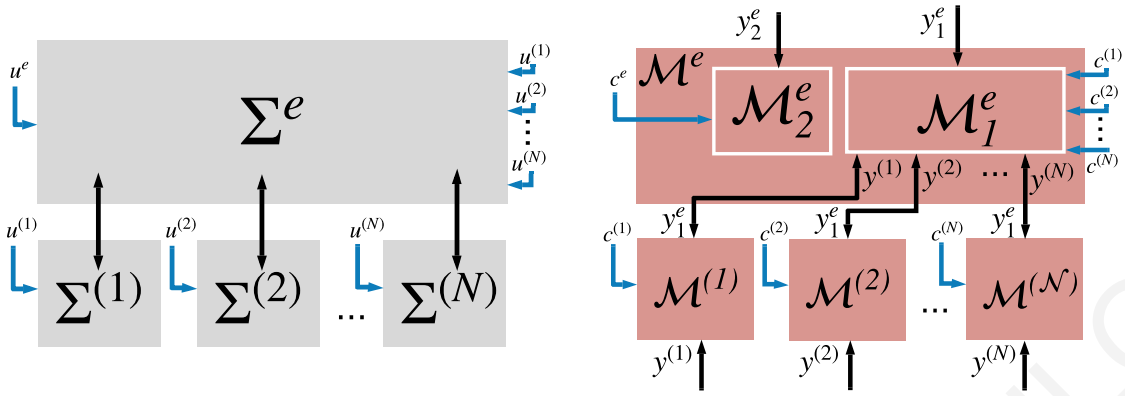

(a) Subsystems of the VAV HVAC system

(b) Agents of the VAV HVAC system

Figure 3.1: Distributed Sensor Fault Detection and Isolation Architecture of the VAV HVAC system.

signals of $\Sigma^{(I)}$, $I \in \{1, \ldots, N\}$ from the agent $\mathcal{M}^{(I)}$ [29].

The task of $\mathcal{M}^e$ is to detect and isolate sensor faults affecting $\mathcal{S}^e\{1\}$ and $\mathcal{S}^e\{2\}$. Assuming the occurrence of multiple sensor faults, two modules are designed in the agent $\mathcal{M}^e$ such that the j-th module, denoted by $\mathcal{M}^e_j$ is dedicated to the sensor $\mathcal{S}^e\{j\}$, $j = 1, 2$, and is responsible for isolating a sensor fault that affects $\mathcal{S}^e\{j\}$. The task of $\mathcal{M}^{(I)}$ is to isolate sensor faults in $\mathcal{S}^{(I)}$. However, each agent $\mathcal{M}^{(I)}$ uses the sensor information y^e_1 transmitted from $\mathcal{M}^e$, which may be faulty, thus affecting the decision of $\mathcal{M}^{(I)}$; i.e., the agent $\mathcal{M}^{(I)}$ may not be able to distinguish between sensor faults in both $\mathcal{S}^{(I)}$ and $\mathcal{S}^e\{1\}$. Therefore, the decision of the agent $\mathcal{M}^e$ is transmitted to $\mathcal{M}^{(I)}$ upon request, after the time instant that $\mathcal{M}^{(I)}$ detects the presence of sensor faults [124]. The decision logic implemented in $\mathcal{M}^e_1$, $\mathcal{M}^e_2$ and $\mathcal{M}^{(I)}$, $I \in \{1, \ldots, N\}$ relies on checking whether analytical redundancy relations (ARRs) are satisfied, while every ARR is formulated using estimator-based residuals and adaptive thresholds. Taking into account (2.1), the structure of every estimator, designed for each agent/module, has the following general representation:

$$\dot{\hat{x}}(t) = Ax(t) + \gamma(y(t), u(t)) + h(y(t), u(t), u_z(t), z'(t)) + L\left(y(t) - C\hat{x}(t)\right) \tag{3.1}$$

where $\hat{x} \in \mathbb{R}^n$ is the estimation of x (with $\hat{x}(0) = 0$) using the measurements $y \in \mathbb{R}^m$, L is the gain matrix chosen such that the matrix $A - LC$ is stable and $z' \in \mathbb{R}^p$ is comprised of a priori known reference signals or measurements of the interconnection variables z. The sensor output is described by $y(t) = Cx(t) + d(t) + f(t)$, where $C \in \mathbb{R}^{m \times n}$ is the output matrix, while d and f are the noise and fault vector respectively, corrupting the sensor measurements. The estimator (3.1) is a special case of the Lipschitz observer designed in [126] and [124], satisfying the corresponding assumptions, while the stability of the estimator (3.1) is ensured if the pair (A, C) is observable.

3.3.1 Residual Generation

The first stage of decision-making process conducted by the LSFD agents is the generation of residu-

als. Residuals are features that portray the status of the monitoring subsystem. Any unusual changes in these features may imply the presence of faults. In this work, residuals represent the deviations of the sensor data (observed behavior) from the estimated sensor outputs (expected behavior).

The nonlinear estimation model of the module $\mathcal{M}_1^e$ is selected as in (3.1) with $y \equiv y_1^e$, $A \equiv A^e$ $\gamma \equiv \gamma^e$, $h \equiv h^e$ and defining $\widehat{T}_1^e \equiv \hat{x}$; i.e.,

$$\dot{\widehat{T}}_1^e(t) = A^e \widehat{T}_1^e(t) + \gamma^e(\chi(t)) + h^e(y_1^e(t), T_r(t), Q_a(t)) + L_1^e \left(y_1^e(t) - C_1^e \widehat{T}_1^e(t)\right), \tag{3.2}$$

where $\widehat{T}_1^e \in \mathbb{R}^2$ is the estimation of T^e (using the measurements y_1^e), with initial conditions $\widehat{T}_1^e(0) = [0,0]^\top$, $L_1^e \in \mathbb{R}^{2\times 1}$ is the estimator gain matrix, chosen such that $A_{L_1}^e = A^e - L_1^e C_1^e$ is stable, $C_1^e = [1,0]$ and $T_r(t) = [T_{r_1}(t), \ldots, T_{r_N}(t)]^\top$, where $T_r(t)$ includes the a priori known reference signals of subsystem $\Sigma^{(I)}$, $I \in \{1, \ldots, N\}$.

The residual generated by the module $\mathcal{M}_1^e$, is denoted by $\varepsilon_{y_1}^e \in \mathbb{R}$ and is defined as

$$\varepsilon_{y_1}^e(t) = y_1^e(t) - C_1^e \widehat{T}_1^e(t). \tag{3.3}$$

Let us define the state estimation error $\varepsilon_{T_1}^e(t) = T^e(t) - \widehat{T}_1^e(t)$; given (2.7), (2.18) and (3.2), the residual $\varepsilon_{y_1}^e$ under healthy conditions can be re-written as:

$$\begin{aligned}\varepsilon_{y_1}^e(t) &= C_1^e e^{A_{L_1}^e t} \varepsilon_{T_1}^e(0) + d_1^e(t) \\ &+ \int_0^t C_1^e e^{A_{L_1}^e (t-\tau)} \Big(h^e(T_1^e(\tau), T_z(\tau), Q_a(\tau)) - h^e(y_1^e(\tau), T_r(\tau), Q_a(\tau)) - L_1^e d_1^e(\tau) \Big) d\tau,\end{aligned} \tag{3.4}$$

where y_1^e is the sensor measurement defined in (2.18). According to (3.3) and (3.4), the residual $\varepsilon_{y_1}^e$ is affected only by a possible fault in the sensor $\mathcal{S}^e\{1\}$.

The estimator in the module $\mathcal{M}_2^e$ is structured as in (3.1) with $y \equiv y_2^e$, $A \equiv A_{22}^e$, $\gamma \equiv \gamma_2^e$ (γ_2^e is the second element of γ^e), $h \equiv 0$ and defining $\widehat{T}_2^e \equiv \hat{x}$; i.e.,

$$\dot{\widehat{T}}_2^e(t) = A_{22}^e \widehat{T}_2^e(t) + \gamma_2^e(\chi(t)) + L_2^e \left(y_2^e(t) - \widehat{T}_2^e(t)\right) \tag{3.5}$$

where $\widehat{T}_2^e \in \mathbb{R}$ is the estimation of T_2^e, with initial conditions $\widehat{T}_2^e(0) = 0$, A_{22}^e is the element $\{2,2\}$ of the matrix A^e given in (2.8) and $L_2^e \in \mathbb{R}$ is the estimator gain chosen such $A_{L_2}^e = A_{22}^e - L_2^e$ is stable.

The residual generated by the module $\mathcal{M}_2^e$, denoted by $\varepsilon_{y_2}^e \in \mathbb{R}$, is expressed as:

$$\varepsilon_{y_2}^e(t) = y_2^e(t) - \widehat{T}_2^e(t). \tag{3.6}$$

where y_2^e is the sensor measurement described by (2.19). Let us define the state estimation error as $\varepsilon_{T_2}^e(t) = T_2^e(t) - \widehat{T}_2^e(t)$; given (2.7), (2.19) and (3.5), the residual $\varepsilon_{y_2}^e$ under healthy conditions is re-written as:

$$\varepsilon_{y_2}^e(t) = e^{A_{L_2}^e t} \varepsilon_{T_2}^e(0) + d_2^e(t) - \int_0^t e^{A_{L_2}^e (t-\tau)} L_2^e d_2^e(\tau) d\tau. \tag{3.7}$$

According to (3.6), (3.7), the residual $\varepsilon^e_{y_2}$ is affected only by a possible fault in the sensor $\mathcal{S}^e\{2\}$.

The nonlinear estimator implemented in the agent $\mathcal{M}^{(I)}$, $I \in \{1,\dots,N\}$ is structured as in (3.1) with $y \equiv y^{(I)}$, $A \equiv A^{(I)}$, $\gamma \equiv \gamma^{(I)}$, $h \equiv h^{(I)}$ and defining $\widehat{T}_{z_I} \equiv \hat{x}$; i.e.,

$$\dot{\widehat{T}}_{z_I}(t) = A^{(I)}\widehat{T}_{z_I}(t) + \gamma^{(I)}(y^{(I)}(t), Q_{a_I}(t)) + h^{(I)}(y^e_1(t), Q_{a_I}(t)) + L^{(I)}\left(y^{(I)}(t) - \widehat{T}_{z_I}(t)\right), \tag{3.8}$$

where $\widehat{T}_{z_I} \in \mathbb{R}$ is the estimation of T_{z_I}, $I \in \{1,\dots,N\}$, with initial conditions $\widehat{T}^{(I)}(0) = 0$ and $L^{(I)} \in \mathbb{R}$ is the estimator gain, chosen such that $A^{(I)}_L = A^{(I)} - L^{(I)}$ is stable; i.e. $L^{(I)} > A^{(I)}$.

The residual generated by the agent $\mathcal{M}^{(I)}$, $I \in \{1,\dots,N\}$, is denoted by $\varepsilon^{(I)}_y \in \mathbb{R}$ and is described by

$$\varepsilon^{(I)}_y(t) = y^{(I)}(t) - \widehat{T}_{z_I}(t), \tag{3.9}$$

Taking into account (2.12), (2.17) and (3.8), the residual $\varepsilon^{(I)}_y$, $I \in \{1,\dots,N\}$ under healthy conditions can be expressed as:

$$\varepsilon^{(I)}_y(t) = e^{A^{(I)}_L t}\varepsilon^{(I)}_x(0) + d^{(I)}(t) + \int_0^t e^{A^{(I)}_L(t-\tau)}\Bigg(\eta^{(I)}(\tau) - L^{(I)}d^{(I)}(\tau) + \gamma^{(I)}(T_{z_I}(\tau), Q_{a_I}(\tau))$$

$$- \gamma^{(I)}(y^{(I)}(\tau), Q_{a_I}(\tau)) + h^{(I)}(T^e_1(\tau), Q_{a_I}(\tau)) - h^{(I)}(y^e_1(\tau), Q_{a_I}(\tau))\Bigg)d\tau, \tag{3.10}$$

where $y^{(I)}$ and y^e_1 are sensor measurements described by (2.17) and (2.18), respectively. Based on (3.9) and (3.10), the residual $\varepsilon^{(I)}_y$ is affected by possible faults in either sensor $\mathcal{S}^e\{1\}$ or sensor $\mathcal{S}^{(I)}$.

3.3.2 Computation of Adaptive Thresholds

Due to the presence of disturbances and sensor measurement noise, the observed behavior is typically not identical to the expected behavior even during the healthy operation of the sensors in the building zones and electromechanical part. For this reason, the residuals are compared to thresholds that are designed to bound the residuals under healthy conditions, ensuring the robustness of the agents $\mathcal{M}^e$ and $\mathcal{M}^{(I)}$, for all I, with respect to various sources of uncertainties. The adaptive thresholds designed in this work are time-varying functions of measured or computable signals. The adaptive nature of the thresholds can contribute in reducing the conservativeness in the decision making compared to fixed thresholds. The adaptive thresholds are computed taking into account the following assumption.

Assumption 1. The modeling uncertainty of $\Sigma^{(I)}$, $I \in \{1,\dots,N\}$ and the measurement noise of each sensor $\mathcal{S}^{(I)}$ and $\mathcal{S}^e\{j\}$, $j = 1,2$ are unknown but uniformly bounded; i.e., $\left|\eta^{(I)}(t)\right| \le \bar{\eta}^{(I)}$, $\left|d^{(I)}(t)\right| \le \bar{d}^{(I)}$ and $\left|d^e_j(t)\right| \le \bar{d}^e_j$, where $\bar{\eta}^{(I)}$, $\bar{d}^{(I)}_j$, $\bar{d}^e_j$ are known constant bounds.

The bound $\bar{\eta}^{(I)}$ is commonly used for distinguishing between disturbances and faults [51], while the noise bounds $\bar{d}^{(I)}$ and $\bar{d}^e_j$ correspond to a practical representation of the available knowledge for

the sensor noise that is typically provided in a given operation range by sensor manufacturers. It is noted that in the case that time varying bounds $\overline{\eta}^{(I)}(t)$, $\overline{d}^{(I)}(t)$ and $\overline{d}^{e}_{j}(t)$ are available, this information can be incorporated into the following procedure without significant difficulties.

The adaptive threshold implemented in the module $\mathcal{M}^{e}_{j}$, denoted by $\overline{\varepsilon}^{e}_{y_j}(t)$, $j = 1, 2$, is computed such that

$$|\varepsilon^{e}_{y_j}(t)| \leq \overline{\varepsilon}^{e}_{y_j}(t), \tag{3.11}$$

where $\varepsilon^{e}_{y_j}(t)$ is the residual defined in (3.3) and (3.6). Taking into account Assumption 1 and that there exists a known bound $\overline{T}^{e}$ such that $|T^{e}(0)| \leq \overline{T}^{e}$, and positive constants ρ^{e}_{1}, ξ^{e}_{1} such that $|C^{e}_{1}e^{A^{e}_{L_1}t}| \leq \rho^{e}_{1}e^{-\xi^{e}_{1}t}$ for all t, the adaptive threshold is obtained taking into account (3.4) under healthy conditions ($f^{e}_{1}(t) = 0$) and Assumption 1; i.e.,

$$\overline{\varepsilon}^{e}_{y_1}(t) = \rho^{e}_{1}e^{-\xi^{e}_{1}t}\overline{T}^{e} + \overline{d}^{e}_{1} + \int_{0}^{t} \rho^{e}_{1}e^{-\xi^{e}_{1}(t-\tau)}\left(\left|L^{e}_{1}\right|\overline{d}^{e}_{1} + \overline{h}^{e}(\tau)\right)d\tau, \tag{3.12}$$

where $\overline{h}^{e}(t)$ is computed such that $\left|h^{e}(T^{e}_{1}(t), T_z(t), Q_a(t)) - h^{e}(y^{e}_{1}(t), T_r(t), Q_a(t))\right| \leq \overline{h}^{e}(t)$; i.e.,

$$\overline{h}^{e}(t) = \left|\frac{\rho_a C_{pa}}{M_{cc}C_v}\sum_{I=1}^{N} Q_{a_I}(t) - \frac{U_{cc}A_{cc}}{M_{cc}C_v}\right|\frac{1}{N}\sum_{I=1}^{N}\overline{T}_I + \frac{\rho_a C_{pa}}{M_{cc}C_v}\overline{d}^{e}_{1}\left|\sum_{I=1}^{N} Q_{a_I}(t)\right|, \tag{3.13}$$

where $\overline{T}_I$, is a known constant bound such that $\left|T_{z_I}(t) - T_{r_I}(t)\right| \leq \overline{T}_I$, for all t.

Taking into account (3.7), the adaptive threshold $\overline{\varepsilon}^{e}_{y_2}$, implemented in the module $\mathcal{M}^{e}_{2}$, is described by

$$\overline{\varepsilon}^{e}_{y_2}(t) = \rho^{e}_{2}e^{-\xi^{e}_{2}t}\overline{T}^{e}_{2} + \overline{d}^{e}_{2} + \int_{0}^{t} \rho^{e}_{2}e^{-\xi^{e}_{2}(t-\tau)}\left|L^{e}_{2}\right|\overline{d}^{e}_{2}d\tau, \tag{3.14}$$

where $\overline{T}^{e}_{2}$ is a known bound such that $|T^{e}_{2}(0)| \leq \overline{T}^{e}_{2}$, and ρ^{e}_{2}, ξ^{e}_{2} are positive constants such that $|e^{A^{e}_{L_2}t}| \leq \rho^{e}_{2}e^{-\xi^{e}_{2}t}$ for all t.

The adaptive threshold implemented in the agent $\mathcal{M}^{(I)}$, denoted by $\overline{\varepsilon}^{(I)}_{y}(t)$, $I \in \{1, \ldots, N\}$, is computed such that

$$|\varepsilon^{(I)}_{y}(t)| \leq \overline{\varepsilon}^{(I)}_{y}(t), \tag{3.15}$$

where $\varepsilon^{(I)}_{y}(t)$ is the residual under healthy conditions ($f^{(I)} = 0$, $I \in \{1, \ldots, N\}$ and $f^{e}_{1} = 0$) defined in (3.10). Hence, the adaptive threshold $\overline{\varepsilon}^{(I)}_{y}(t)$ is described by:

$$\overline{\varepsilon}^{(I)}_{y}(t) = \rho^{(I)}e^{-\xi^{(I)}t}\overline{T}_{z_I} + \overline{d}^{(I)} + \int_{0}^{t} \rho^{(I)}e^{-\xi^{(I)}(t-\tau)}\left(\overline{\eta}^{(I)} + \left|L^{(I)}\right|\overline{d}^{(I)} + \frac{\rho_a C_{pa}}{M_{z_I}C_v}\left(\overline{d}^{(I)} + \overline{d}^{e}_{1}\right)\left|Q_{a_I}(\tau)\right|\right)d\tau, \tag{3.16}$$

where $\overline{T}_{z_I}$ is a known bound such that $|T_{z_I}(0)| \leq \overline{T}_{z_I}$, $\rho^{(I)}$, $\xi^{(I)}$ are positive constants such that $|e^{A^{(I)}_{L}t}| \leq \rho^{(I)}e^{-\xi^{(I)}t}$ for all t, and

$$\left|\gamma^{(I)}(T_{z_I}, Q_{a_I}) - \gamma^{(I)}(y^{(I)}, Q_{a_I})\right| \leq \frac{\rho_a C_{pa}}{M_{z_I}C_v}\left|Q_{a_I}\right|\overline{d}^{(I)}, \tag{3.17}$$

$$\left|h^{(I)}(T^{e}_{1}, Q_{a_I}) - h^{(I)}(y^{e}_{1}, Q_{a_I})\right| \leq \frac{\rho_a C_{pa}}{M_{z_I}C_v}\left|Q_{a_I}\right|\overline{d}^{e}_{1}. \tag{3.18}$$

It is noted that the adaptive thresholds defined in (3.12), (3.14) and (3.16) can be implemented using straightforward linear filtering techniques:

$$\overline{\varepsilon}^e_{y_1} = \rho^e_1 e^{-\xi^e_1 t}\overline{T}^e_1 + \overline{d}^e_1 + H^e_1(s)\left[\left|L^e_1\right|\overline{d}^e_1 + \overline{h}^e(t)\right], \tag{3.19}$$

$$\overline{\varepsilon}^e_{y_2} = \rho^e_2 e^{-\xi^e_2 t}\overline{T}^e_2 + \overline{d}^e_2 + H^e_2(s)\left|L^e_2\right|\overline{d}^e_2, \tag{3.20}$$

$$\overline{\varepsilon}^{(I)}_y = \rho^{(I)} e^{-\xi^{(I)} t}\overline{T}_{z_I} + \overline{d}^{(I)} + H_I(s)\left(\overline{\eta}^{(I)} + \left|L^{(I)}\right|\overline{d}^{(I)}\right) + H_I(s)\left[\frac{\rho_a C_{pa}}{M_{z_I} C_v}\left(\overline{d}^{(I)} + \overline{d}^e_1\right)\left|Q_{a_I}(t)\right|\right], \tag{3.21}$$

where $H^{(I)}(s) = \frac{\rho^{(I)}}{s+\xi^{(I)}}$, $I \in \{1,\ldots,N\}$, $H^e_1(s) = \frac{\rho^e_1}{s+\xi^e_1}$, $H^e_2(s) = \frac{\rho^e_2}{s+\xi^e_2}$ are stable, first-order filters. Note that for any signal $z(t)$, the notation $H(s)[z(t)]$ denotes the output of the filter $H(s)$ with $z(t)$ as input, while s is the Laplace operator.

3.3.3 Distributed SFDI Decision Logic

This section presents the decision making process realized by the agent $\mathcal{M}^e$ and its modules $\mathcal{M}^e_1$ and $\mathcal{M}^e_2$, and the agent $\mathcal{M}^{(I)}, I \in \{1,\ldots,N\}$ for detecting and isolating multiple sensor faults in a distributed manner. The decision logic relies on checking the satisfaction of a set of analytical redundancy relations (ARRs) [22, 34, 118]. In this work, the ARRs are dynamical constraints, formulated using the residuals and adaptive thresholds.

Sensor Fault Detection

The decision logic implemented in the modules $\mathcal{M}^e_1$ and $\mathcal{M}^e_2$, which are included in the agent $\mathcal{M}^e$, is based on the following ARRs:

$$\mathcal{E}^e_j: \quad \left|\varepsilon^e_{y_j}(t)\right| - \overline{\varepsilon}^e_{y_j}(t) \le 0, \ j = 1,2 \tag{3.22}$$

where $\varepsilon^e_{y_1}$, $\varepsilon^e_{y_2}$ and $\overline{\varepsilon}^e_{y_1}$, $\overline{\varepsilon}^e_{y_2}$ are defined in (3.4), (3.7) and (3.12), (3.14), respectively. Under healthy conditions, the inequality (3.22) is always true, implying that the ARRs $\mathcal{E}^e_1$ and $\mathcal{E}^e_2$ are always satisfied. The module $\mathcal{M}^e_j$ infers the presence of sensor fault f^e_j, $j = 1,2$, when $\mathcal{E}^e_j$ defined in (3.22) is violated. The decision of the module $\mathcal{M}^e_j$, $j = 1,2$ can be described by the following boolean function

$$D^e_j(t) = \begin{cases} 0, & \text{if } t < t^e_{D_j} \\ 1, & \text{if } t \ge t^e_{D_j} \end{cases} \tag{3.23}$$

$$t^e_{D_j} = \min_t\{t : |\varepsilon^e_{y_j}(t)| - \overline{\varepsilon}^e_{y_j}(t) > 0\} \tag{3.24}$$

where $t^e_{D_j}$ is the time instant of detection. When $D^e_j(t) = 1$, the module $\mathcal{M}^e_j$, $j = 1,2$ detects the sensor fault f^e_j. Note that as long as $D^e_j(t) = 0$ either there is no sensor fault affecting $\mathcal{S}^e\{j\}$ or sensor fault f^e_j has occurred, but has not been detected by the module $\mathcal{M}^e_j$ until the time instant $t^e_{D_j}$. If $D^e_j(t) = 1$, this implies that the sensor fault f^e_j is guaranteed to affect $\mathcal{S}^e\{j\}$.

The sensor fault detection decision logic of the agent $\mathcal{M}^{(I)}, I \in \{1,\dots,N\}$ is based on the following ARR

$$\mathcal{E}^{(I)}: \quad \left|\varepsilon_y^{(I)}(t)\right| - \overline{\varepsilon}_y^{(I)}(t) \leq 0,\ I \in \{1,\dots,N\}, \tag{3.25}$$

where $\varepsilon_y^{(I)}$ and $\overline{\varepsilon}_y^{(I)}$ are defined in (3.10) and (3.16), respectively. Under healthy conditions the ARR $\mathcal{E}^{(I)}$, $I \in \{1,\dots,N\}$ is always satisfied. If $\mathcal{E}^{(I)}$ is violated, then this implies that a sensor fault has occurred in either $\mathcal{S}^{(I)}$ or $\mathcal{S}^e\{1\}$ or both of them. The decision of $\mathcal{M}^{(I)}$ on the presence of sensor faults $f^{(I)}$ or f_1^e is represented by a boolean function, defined as

$$D^{(I,1)}(t) = \begin{cases} 0, & \text{if } t < t_D^{(I)} \\ 1, & \text{if } t \geq t_D^{(I)} \end{cases} \tag{3.26}$$

$$t_D^{(I)} = \min_t \{t : |\varepsilon_y^{(I)}(t)| - \overline{\varepsilon}_y^{(I)}(t) > 0\} \tag{3.27}$$

where $t_D^{(I)}$ is the time of detection for agent $\mathcal{M}^{(I)}$. When $D^{(I,1)}(t) = 1$ the agent $\mathcal{M}^{(I)}, I \in \{1,\dots,N\}$ infers that either f_1^e or $f^{(I)}$ or both, have occurred. As long as $D^{(I,1)}(t) = 0$ either there is no sensor fault in both $\mathcal{S}^{(I)}$ and $\mathcal{S}^e\{1\}$ or sensor faults have occurred, but have not been detected by the agent $\mathcal{M}^{(I)}$ until the time instant $t_D^{(I)}$. If $D^{(I,1)}(t) = 1$, then it is ensured that at least one of $\mathcal{S}^{(I)}$ and $\mathcal{S}^e\{1\}$ is faulty.

Sensor Fault Isolation

In the context of smart buildings, it is important not only to be able to detect the occurrence of sensor faults but also to be able to isolate the location of the fault as soon as possible. The agent $\mathcal{M}^e$ can isolate multiple sensor faults in the sensor set $\mathcal{S}^e$ by comparing the observed pattern of sensor faults, defined as $D^e(t) = \left[D_1^e(t), D_2^e(t)\right]^\top$ to the columns of the sensor fault signature matrix F^e, presented in Table 3.1. The rows of F^e correspond to the ARRs $\mathcal{E}_1^e$ and $\mathcal{E}_2^e$, while the columns correspond the three possible combinations of sensor faults that occur in $\mathcal{S}^e$, i.e. $\mathcal{F}_1^e = \left\{f_1^e\right\}$, $\mathcal{F}_2^e = \left\{f_2^e\right\}$ and $\mathcal{F}_3^e = \left\{f_1^e, f_2^e\right\}$. The j-th theoretical pattern of the matrix F^e is defined as $F_j^e = \left[F_{1j}^e, F_{2j}^e\right]^\top$, $j = 1,2,3$, where $F_{qj}^e = 1$ if at least one sensor fault of the combination $\mathcal{F}_j^e$ is involved in the ARR $\mathcal{E}_q^e$, and $F_{qj}^e = 0$ otherwise. Based on the sensor fault signature matrix presented in Table 3.1, all possible sensor fault combinations are isolable by the agent $\mathcal{M}^e$, since there are three distinct theoretical patterns.

Table 3.1: Sensor fault signature matrix F^e ($\mathcal{F}_1^e = \left\{f_1^e\right\}$, $\mathcal{F}_2^e = \left\{f_2^e\right\}$ and $\mathcal{F}_3^e = \left\{f_1^e, f_2^e\right\}$).

	$\mathcal{F}_1^e$	$\mathcal{F}_2^e$	$\mathcal{F}_3^e$
$\mathcal{E}_1^e$	1	0	1
$\mathcal{E}_2^e$	0	1	1

Assuming the occurrence of multiple sensor faults, the decision of the agent $\mathcal{M}^{(I)}$ is combined with the decision of the agent $\mathcal{M}^e$. Specifically, when $\mathcal{M}^{(I)}$ detects the presence of sensor faults

$(D^{(I,1)}(t) = 1)$, it requests from $\mathcal{M}^e$ to transmit its decision D_1^e on whether the sensor $\mathcal{S}^e\{1\}$ is faulty in order to isolate the sensor faults. The reason for the combinatorial process of the decisions is that the agent $\mathcal{M}^{(I)}$ uses the measurements of sensor $\mathcal{S}_1^e$ for the generation of the residual and adaptive threshold as well as the formulation of the ARR $\mathcal{E}^{(I)}$. Hence, the distributed sensor fault isolation is conducted by comparing the observed pattern of sensor faults, defined as $D^{(I)}(t) = \left[D^{(I,1)}(t), D_1^e(t)\right]^\top$ to the columns of the sensor fault signature matrix $F^{(I)}$, $I \in \{1, \ldots, N\}$, presented in Table 3.2. The rows of $F^{(I)}$ correspond to the ARRs $\mathcal{E}^{(I)}$ and $\mathcal{E}_1^e$, while the columns correspond the three possible combinations of sensor fault occurrence, i.e. $\mathcal{F}_1^{(I)} = \left\{f^{(I)}\right\}$, $\mathcal{F}_2^{(I)} = \left\{f_1^e\right\}$ and $\mathcal{F}_3^{(I)} = \left\{f^{(I)}, f_1^e\right\}$.

Table 3.2: Sensor fault signature matrix $F^{(I)}$ ($\mathcal{F}_1^{(I)} = \left\{f^{(I)}\right\}$, $\mathcal{F}_2^{(I)} = \left\{f_1^e\right\}$ and $\mathcal{F}_3^{(I)} = \left\{f^{(I)}, f_1^e\right\}$).

	$\mathcal{F}_1^{(I)}$	$\mathcal{F}_2^{(I)}$	$\mathcal{F}_3^{(I)}$
$\mathcal{E}^{(I)}$	1	*	1
$\mathcal{E}_1^e$	0	1	1

The j-th column of the matrix $F^{(I)}$ corresponds to the j-th theoretical pattern of sensor faults, defined as $F_j^{(I)} = \left[F_{1j}^{(I)}, F_{2j}^{(I)}\right]^\top$, $j = 1, 2, 3$ where: (i) $F_{qj}^{(I)} = 1$, if the sensor fault combination $\mathcal{F}_j^{(I)}$ contains at least one sensor fault that can provoke the violation of (or else, is involved in) the ARR of the q-th row, $q = 1, 2$ (ii) $F_{qj}^{(I)} = 0$, if none of the sensor faults of the combination $\mathcal{F}_j^{(I)}$is involved in the ARR of the q-th row, $q = 1, 2$ (iii) $F_{qj}^{(I)} = *$, if none of the sensor faults of the combination $\mathcal{F}_j^{(I)}$ may affect the sensor set $\mathcal{S}^{(I)}$, but all of them are involved in the ARR of the q-th row, $q = 1, 2$. Particularly, the semantics of $F_{21}^{(I)} = *$ implies that the sensor fault f_1^e can explain why $\mathcal{E}^{(I)}$ is violated, but $\mathcal{E}^{(I)}$ may be less sensitive to f_1^e than $f^{(I)}$, so it may be satisfied although f_1^e has occurred. This is based on the fact that the effects of the faulty transmitted information y_1^e on the residual $\varepsilon_y^{(I)}$ and adaptive threshold $\bar{\varepsilon}_y^{(I)}$, used in the formulation of $\mathcal{E}^{(I)}$, depend on the type of interconnection dynamics $h^{(I)}$, defined in (2.14). The sensitivity of ARRs to sensor faults is analyzed next.

For isolating multiple sensor faults, the agents $\mathcal{M}^e$ and $\mathcal{M}^{(I)}$ check the consistency between the observed patterns $D^e(t)$ and $D^{(I)}(t)$ and the theoretical patterns F^e and $F^{(I)}$, respectively. As long as $D^e(t) = [0, 0]^\top$ and $D^{(I)}(t) = [0, 0]^\top$, no consistency check is realized; otherwise, the result of the consistency test is the determination of the sensor fault diagnosis set, which contains the diagnosed sensor fault combinations. Specifically, the agent $\mathcal{M}^e$ isolates sensor faults in the electromechanical part of HVAC based on the diagnosis set $\mathcal{D}_s^e(t)$, defined as

$$\mathcal{D}_s^e(t) = \left\{\mathcal{F}_{c_i}^e : i \in \mathcal{I}_{\mathcal{D}}^e(t)\right\}, \tag{3.28}$$

where $\mathcal{I}_{\mathcal{D}}^e(t) = \left\{i : F_i^e = D^e(t),\ i \in \{1, 2, 3\}\right\}$. The decision of the agent $\mathcal{M}^{(I)}$, $I \in \{1, \ldots, N\}$, relies on the diagnosis set $\mathcal{D}_s^{(I)}(t)$, defined as

$$\mathcal{D}_s^{(I)}(t) = \left\{\mathcal{F}_{c_i}^{(I)} : i \in \mathcal{I}_{\mathcal{D}}^{(I)}(t)\right\}, \tag{3.29}$$

where $\mathcal{I}_{\mathcal{D}}^{(I)}(t) = \left\{i : F_i^{(I)} = D^{(I)}(t),\ i \in \{1,2,3\}\right\}$. It is noted that $F_{21}^{(I)} = *$ is consistent to either 0 or 1

Remark: The proposed sensor fault diagnosis methodology has been developed by applying a dedicated scheme with multiple observers, where each observer of an agent/module is driven by a single sensor (like in $\mathcal{M}_1^e$ and $\mathcal{M}_2^e$) or a set of one local sensor and one sensor in the neighboring subsystem (as the observer in $\mathcal{M}^{(I)}$ for all I). The isolation decision logic relies on the fact that the agents/modules are characterized by (i) robustness, i.e the agents are insensitive to modeling uncertainties and measurement noise under healthy conditions, and (ii) structural fault sensitivity, implying that the agents/modules are sensitive to subsets of sensor faults. Particularly, the agent $\mathcal{M}^{(I)}$ is designed to be structurally sensitive to sensor faults $f^{(I)}$ and f_1^e, while the modules $\mathcal{M}_1^e$ and $\mathcal{M}_2^e$ are sensitive to sensor faults f_1^e and f_2^e, respectively. The residuals are generated using an observer driven by a set of sensors, while the adaptive thresholds are designed to bound the residual under healthy conditions. Therefore, when the magnitude of a residual exceeds the corresponding adaptive threshold, this sensor set is isolated as faulty. An alternative decision logic for isolating sensor faults is to infer that there are faults in a specific sensor set, when the magnitudes of all residuals generated by the observer, which is not driven by this sensor set, do not exceed the corresponding thresholds [37]. This decision logic is applied to a generalized scheme of multiple observers or an unknown input observer (UIO) scheme [76, 135]. In the case of multiple sensor faults, the number of observers in a dedicated scheme may be less than the number of observers in a generalized or UIO scheme.

3.4 Performance Analysis

The objective of this section is to analyze the performance of the proposed distributed SFDI methodology with respect to the sensor fault detectability and isolability of the agents $\mathcal{M}^e$ and $\mathcal{M}^{(I)}$, $I \in \{1,\ldots,N\}$. Specifically, certain conditions are derived, under which we characterize the class of sensor faults affecting $\mathcal{S}^e, \mathcal{S}^{(I)}, I \in \{1,\ldots,N\}$ that can be detected and isolated. It is important to note that the class of detectable/isolable sensor faults satisfying these conditions are obtained under *worst-case assumptions*, in the sense that they are valid for any modeling uncertainty and measurement noise satisfying Assumption 1. It is noted that in practice, the modeling uncertainty and measurement noise may not reach the limit (worst-case) of Assumption 1.

3.4.1 Electromechanical Sensor Fault Isolability Conditions

The conditions for guaranteeing the isolation of sensor faults f_1^e and f_2^e by the modules $\mathcal{M}_1^e$ and $\mathcal{M}_2^e$, respectively, are stated in the following Lemma.

Lemma 1. *Consider that the sensor faults f_1^e and f_2^e occur at the time instants $t_{f_1}^e$ and $t_{f_2}^e$, respectively.*

(a) *The occurrence of a fault in the temperature sensor of the cooling coil* $\mathcal{S}^e\{1\}$ *is guaranteed to be isolated under worst-case conditions, if there exists a time instant* $t^* > t^e_{f_1}$ *such that the sensor fault* f^e_1 *satisfies the condition*

$$\left| f^e_1(t^*) - \int_{t^e_{f_1}}^{t^*} C^e_1 e^{A^e_{L_1}(t^*-\tau)} \left(L^e_1 f^e_1(\tau) + \begin{bmatrix} \frac{\rho_a C_{pa}}{M_{cc} C_v} \left(\sum_{I=1}^{N} Q_{a_I}(\tau) \right) f^e_1(\tau) \\ 0 \end{bmatrix} \right) d\tau \right| > 2\bar{\varepsilon}^e_{y_1}(t^*), \quad (3.30)$$

where $\bar{\varepsilon}^e_{y_1}(t)$ *is the adaptive threshold, generated by the module* $\mathcal{M}^e_1$.

(b) *The occurrence of a fault in the temperature sensor of the chilled water tank* $\mathcal{S}^e\{2\}$ *is guaranteed to be isolated under worst-case conditions, if there exists a time instant* $t^* > t^e_{f_2}$ *such that the sensor fault* f^e_2 *satisfies the condition*

$$\left| f^e_2(t^*) - \int_{t^e_{f_2}}^{t^*} e^{A^e_{L_2}(t^*-\tau)} L^e_2 f^e_2(\tau) d\tau \right| > 2\bar{\varepsilon}^e_{y_2}(t^*), \quad (3.31)$$

where $\bar{\varepsilon}^e_{y_2}(t)$ *is the adaptive threshold, generated by the module* $\mathcal{M}^e_2$.

Proof. (a) Assume that no fault affects $\mathcal{S}^e\{1\}$, i.e. $f^e_1 = 0$; then using (2.7) and (3.2), the state estimation error of the module $\mathcal{M}^e_1$ satisfies

$$\varepsilon^e_{T_1}(t) = e^{A^e_{L_1} t} \varepsilon^e_{T_1}(0) + \int_0^t e^{A^e_{L_1}(t-\tau)} \Big(h^e(T^e_1(\tau), T_z(\tau), Q_a(\tau)) - h^e(T^e_1(\tau) + d^e_1(\tau), T_r(\tau), Q_a(\tau)) - L^e_1 d^e_1(\tau) \Big) d\tau. \quad (3.32)$$

For $t \geq t^e_{f_1}$, the residual $\varepsilon^e_{y_1}$ is described by:

$$\varepsilon^e_{y_1}(t) = C^e_1 e^{A^e_{L_1}\left(t - t^e_{f_1}\right)} \varepsilon^e_{T_1}(t^e_{f_1}) + d^e_1(t) + f^e_1(t) + \int_{t^e_{f_1}}^{t} C^e_1 e^{A^e_{L_1}(t-\tau)} \Bigg(- L^e_1 d^e_1(\tau) - L^e_1 f^e_1(\tau) + h^e(T^e_1(\tau), T_z(\tau), Q_a(\tau)) - h^e(T^e_1(\tau) + d^e_1(\tau) + f^e_1(\tau), T_r(\tau), Q_a(\tau)) \Bigg) d\tau. \quad (3.33)$$

By adding and subtracting the integral $\int_{t^e_{f_1}}^{t} C^e_1 e^{A^e_{L_1}(t-\tau)} h^e(T^e_1(\tau) + d^e_1(\tau), T_r(\tau), Q_a(\tau)) d\tau$, and using (3.32), we obtain

$$\varepsilon^e_{y_1}(t) = \varepsilon^e_{y_{1H}}(t) + \varepsilon^e_{y_{1F}}(t), \quad (3.34)$$

where $\varepsilon^e_{y_{1H}}(t)$ equals to the residual under healthy conditions described by (3.4) and $\varepsilon^e_{y_{1F}}(t)$ describes the effects of sensor fault f^e_1 on the residual $\varepsilon^e_{y_1}$, defined as:

$$\varepsilon^e_{y_{1F}}(t) = \int_{t^e_{f_1}}^{t} C^e_1 e^{A^e_{L_1}(t-\tau)} \Big(h^e(T^e_1(\tau) + d^e_1(\tau), T_r(\tau), Q_a(\tau)) - h^e(T^e_1(\tau) + d^e_1(\tau) + f^e_1(\tau), T_r(\tau), Q_a(\tau)) \Big) d\tau + f^e_1(t) - \int_{t^e_{f_1}}^{t} C^e_1 e^{A^e_{L_1}(t-\tau)} L^e_1 f^e_1(\tau) d\tau. \quad (3.35)$$

Taking into account (3.11) and (3.34), it yields

$$\left|\varepsilon^e_{y_1}(t)\right| \geq \left|\varepsilon^e_{y_{1F}}(t)\right| - \left|\varepsilon^e_{y_{1H}}(t)\right| \geq \left|\varepsilon^e_{y_{1F}}(t)\right| - \overline{\varepsilon}^e_{y_1}(t). \tag{3.36}$$

If there exists a time instant t^* such that the effects of sensor fault f^e_1 on the residual $\varepsilon^e_{y_1}$ satisfy the condition $\left|\varepsilon^e_{y_{1F}}(t^*)\right| > 2\overline{\varepsilon}^e_{y_1}(t^*)$, i.e. satisfy (3.30), then, based on (3.36), this implies that $\left|\varepsilon^e_{y_1}(t^*)\right| > \overline{\varepsilon}^e_{y_1}(t^*)$ and the violation of the ARR $\mathcal{E}^e_1$. Thus, sensor fault f^e_1 is guaranteed to be isolated by the module $\mathcal{M}^e_1$.

(b) Assume that no fault affects $\mathcal{S}^e\{2\}$, i.e. $f^e_2 = 0$; using (2.7) and (3.5), the state estimation error of the module $\mathcal{M}^e_2$ is

$$\varepsilon^e_{T_2}(t) = e^{A^e_{L_2} t}\varepsilon^e_{T_2}(0) - \int_0^t e^{A^e_{L_2}(t-\tau)} L^e_2 d^e_2(\tau) d\tau. \tag{3.37}$$

For $t \geq t^e_{f_2}$, the residual $\varepsilon^e_{y_2}$ is expressed as:

$$\varepsilon^e_{y_2}(t) = e^{A^e_{L_2}\left(t-t^e_{f_2}\right)}\varepsilon^e_{T_2}(t^e_{f_2}) + d^e_2(t) + f^e_2(t) - \int_{t^e_{f_2}}^t e^{A^e_{L_2}(t-\tau)} L^e_2\left(f^e_2(\tau) + d^e_2(\tau)\right) d\tau. \tag{3.38}$$

By replacing $\varepsilon^e_{T_2}(t^e_{f_2})$ using (3.37), we have

$$\varepsilon^e_{y_2}(t) = \varepsilon^e_{y_{2H}}(t) + \varepsilon^e_{y_{2F}}(t), \tag{3.39}$$

where $\varepsilon^e_{y_{2H}}(t)$ equals to the residual under healthy conditions described by (3.7) and $\varepsilon^e_{y_{2F}}(t)$ describes the effects of sensor fault f^e_2 on the residual $\varepsilon^e_{y_2}$, defined as:

$$\varepsilon^e_{y_{2F}}(t) = f^e_2(t) - \int_{t^e_{f_2}}^t e^{A^e_{L_2}(t-\tau)} L^e_2 f^e_2(\tau) d\tau \tag{3.40}$$

Following the same procedure described in (3.36), if there exists a time instant t^* such that the effects of sensor fault f^e_2 on the residual $\varepsilon^e_{y_2}$ satisfy the condition $\left|\varepsilon^e_{y_{2F}}(t^*)\right| > 2\overline{\varepsilon}^e_{y_2}(t^*)$, i.e., (3.31) is valid, then it is implied that $\left|\varepsilon^e_{y_2}(t^*)\right| > \overline{\varepsilon}^e_{y_2}(t^*)$ and the ARR $\mathcal{E}^e_2$ is violated. Thus, sensor fault f^e_2 is guaranteed to be isolated by the module $\mathcal{M}^e_2$. □

In general, conditions (3.30) and (3.31) can be regarded as a figure of merit, characterizing the ability of $\mathcal{M}^e_1$ and $\mathcal{M}^e_2$ to capture the occurrence of sensor fault f^e_1 and f^e_2, respectively. Based on these conditions, we can define the minimum magnitude of sensor fault f^e_1 and f^e_2 that are isolable by the module $\mathcal{M}^e_1$ and $\mathcal{M}^e_2$, respectively. Particularly, if f^e_1 is constant, i.e. $f^e_1 = \theta^e_1$, and at some time instant t^*, the constant sensor fault θ^e_1 satisfies

$$\left|\theta^e_1\right| > \frac{2\overline{\varepsilon}^e_{y_1}(t^*)}{|w(t^*)|} \tag{3.41}$$

where

$$w(t) = 1 - \int_{t^e_{f_1}}^{t^*} C^e_1 e^{A^e_{L_1}(t^*-\tau)}\left(L^{(l)} + \begin{bmatrix} \frac{\rho_a C_{pa}}{M_{cc} C_v} \sum_{I=1}^{N} Q_{a_I}(\tau) \\ 0 \end{bmatrix}\right) d\tau \tag{3.42}$$

given that $w(t^*) \neq 0$, the module $\mathcal{M}_1^e$ is guaranteed to isolate sensor fault f_1^e. Similarly, if f_2^e is constant, i.e. $f_2^e = \theta_2^e$, and at some time instant t^*, the constant sensor fault θ_2^e satisfies

$$\left|\theta_2^e\right| > \frac{2\overline{\varepsilon}_{y_2}^e(t^*)}{\left|1 - \frac{L_2^e}{A_{L_2}^e}\left(1 - e^{A_{L_2}^e(t^* - t_{f_2}^e)}\right)\right|}, \tag{3.43}$$

given that $\left|1 - \frac{L_2^e}{A_{L_2}^e}\left(1 - e^{A_{L_2}^e(t^* - t_{f_2}^e)}\right)\right| \neq 0$, the module $\mathcal{M}_2^e$ is guaranteed to isolate sensor fault f_2^e.

Taking into account (3.41) and (3.43), we can characterize the minimum isolable magnitude of sensor fault θ_j^e, $j = 1, 2$, with respect to the bound of sensor noise $\overline{d}_j^e$, and the selected design parameters used for the implementation of the estimator in the module $\mathcal{M}_j^e$ (e.g. L_j^e) and the adaptive thresholds (ρ_j^e, ξ_j^e).

3.4.2 Building Zone Sensor Fault Detectability and Isolability Conditions

The conditions for ensuring the detection/isolation of $f^{(I)}$ and f_1^e by the agent $\mathcal{M}^{(I)}$, are stated in the following Lemma.

Lemma 2. *Consider that the sensor faults f_1^e and $f^{(I)}$ occur at the time instants $t_{f_1}^e$ and $t_f^{(I)}$, respectively.*

(a) *Let $t_f^{(I)} < t_{f_1}^e$; the occurrence of a fault in the temperature sensor of the I-th zone $\mathcal{S}^{(I)}$ is guaranteed to be isolated under worst-case conditions, if there exists a time instant $t^* \in [t_f^{(I)}, t_{f_1}^e)$ such that the sensor fault $f^{(I)}$ satisfies the condition*

$$\left| f^{(I)}(t^*) - \int_{t_f^{(I)}}^{t^*} e^{A_L^{(I)}(t^* - \tau)}\left(L^{(I)} f^{(I)}(\tau) - \frac{\rho_a C_{pa}}{M_{z_I} C_v} Q_{a_I}(\tau) f^{(I)}(\tau)\right) d\tau \right| > 2\overline{\varepsilon}_y^{(I)}(t^*). \tag{3.44}$$

(b) *Let $t_{f_1}^e < t_f^{(I)}$; the occurrence of a fault in the temperature sensor of the cooling coil $\mathcal{S}^e\{1\}$ is guaranteed to be detected under worst-case conditions, if there exists a time instant $t^* \in [t_{f_1}^e, t_f^{(I)})$ such that the sensor fault f_1^e satisfies the condition*

$$\left| \int_{t_{f_1}^e}^{t^*} e^{A_L^{(I)}(t^* - \tau)} \frac{\rho_a C_{pa}}{M_{z_I} C_v} Q_{a_I}(\tau) f_1^e(\tau) d\tau \right| > 2\overline{\varepsilon}_y^{(I)}(t^*), \tag{3.45}$$

where $\overline{\varepsilon}_y^{(I)}(t)$ is the adaptive threshold, generated by the agent $\mathcal{M}^{(I)}$.

(c) *The occurrence of faults in the temperature sensors $\mathcal{S}^{(I)}$ and $\mathcal{S}^e\{1\}$ is guaranteed to be detected under worst-case conditions, if there exists a time instant $t^* \geq \max(t_f^{(I)}, t_{f_1}^e)$ such that the sensor fault $f^{(I)}$ satisfies the condition*

$$\left| f^{(I)}(t^*) - \int_{t_{f_1}^e}^{t^*} e^{A_L^{(I)}(t^* - \tau)} \frac{\rho_a C_{pa}}{M_{z_I} C_v} Q_{a_I}(\tau) f_1^e(\tau) d\tau \right.$$

$$\left. - \int_{t_f^{(I)}}^{t^*} e^{A_L^{(I)}(t^* - \tau)}\left(L^{(I)} f^{(I)}(\tau) - \frac{\rho_a C_{pa}}{M_{z_I} C_v} Q_{a_I}(\tau) f^{(I)}(\tau)\right) d\tau \right| > 2\overline{\varepsilon}_y^{(I)}(t^*), \tag{3.46}$$

Proof. (a) Assume that no fault affects $\mathcal{S}^{(I)}$, $I \in \{1,\dots,N\}$, and $\mathcal{S}^{e}\{1\}$, i.e. $f^{(I)} = f_1^e = 0$; based on (2.12) and (3.8), the state estimation error of the agent $\mathcal{M}^{(I)}$ is

$$\varepsilon_T^{(I)}(t) = e^{A_L^{(I)}t}\varepsilon_T^{(I)}(0) + \int_0^t e^{A_L^{(I)}(t-\tau)}\Bigg(\eta^{(I)}(\tau) - L^{(I)}d^{(I)}(\tau) + \gamma^{(I)}(T_{z_I}(\tau), Q_{a_I}(\tau)) + h^{(I)}(T_1^e(\tau), Q_{a_I}(\tau))$$

$$- \gamma^{(I)}(T_{z_I}(\tau) + d^{(I)}(\tau), Q_{a_I}(\tau)) - h^{(I)}(T_1^e(\tau) + d_1^e(\tau), Q_{a_I}(\tau))\Bigg)d\tau. \tag{3.47}$$

For $t \geq t_f^{(I)}$, the residual $\varepsilon_y^{(I)}$ is expressed as:

$$\varepsilon_y^{(I)}(t) = e^{A_L^{(I)}\left(t-t_f^{(I)}\right)}\varepsilon_T^{(I)}(t_f^{(I)}) + d^{(I)}(t) + f^{(I)}(t) + \int_{t_f^{(I)}}^t e^{A_L^{(I)}(t-\tau)}\Bigg(\eta^{(I)}(\tau) - L^{(I)}d^{(I)}(\tau)$$

$$- L^{(I)}f^{(I)}(\tau) + \gamma^{(I)}(T_{z_I}(\tau), Q_{a_I}(\tau)) + h^{(I)}(T_1^e(\tau), Q_{a_I}(\tau))$$

$$- \gamma^{(I)}(T_{z_I}(\tau) + d^{(I)}(\tau) + f^{(I)}(\tau), Q_{a_I}(\tau)) - h^{(I)}(T_1^e(\tau) + d_1^e(\tau), Q_{a_I}(\tau))\Bigg)d\tau. \tag{3.48}$$

After some algebraic manipulation and using (3.47) leads to

$$\varepsilon_y^{(I)}(t) = \varepsilon_{y_H}^{(I)}(t) + \varepsilon_{y_F}^{(I)}(t), \tag{3.49}$$

where $\varepsilon_{y_H}^{(I)}(t)$ corresponds to the residual under healthy conditions described by (3.10) and $\varepsilon_{y_F}^{(I)}(t)$ describes the effects of sensor fault $f^{(I)}$ on the residual $\varepsilon_y^{(I)}$, defined as:

$$\varepsilon_{y_F}^{(I)}(t) = f^{(I)}(t) - \int_{t_f^{(I)}}^t e^{A_L^{(I)}(t-\tau)}\left(L^{(I)}f^{(I)}(\tau) - \frac{\rho_a C_{pa}}{M_{z_I}C_v}Q_{a_I}(\tau)f^{(I)}(\tau)\right)d\tau. \tag{3.50}$$

Taking into account (3.15) and (3.49), it yields

$$\left|\varepsilon_y^{(I)}(t)\right| \geq \left|\varepsilon_{y_F}^{(I)}(t)\right| - \left|\varepsilon_{y_H}^{(I)}(t)\right| \geq \left|\varepsilon_{y_F}^{(I)}(t)\right| - \bar{\varepsilon}_y^{(I)}(t). \tag{3.51}$$

If there exists a time instant t^* such that the effects of sensor fault $f^{(I)}$ on the residual $\varepsilon_y^{(I)}$ satisfy the condition $\left|\varepsilon_{y_F}^{(I)}(t^*)\right| > 2\bar{\varepsilon}_y^{(I)}(t^*)$, implying that (3.44) is valid, then, using (3.51), this entails that $\left|\varepsilon_y^{(I)}(t^*)\right| > \bar{\varepsilon}_y^{(I)}(t^*)$, leading to the isolation of sensor fault $f^{(I)}$.

(b) Part (b) of Lemma 2 can be proved in a similar way to part (a).

(c) For $t \geq t_{f_1}^e > t_f^{(I)}$, the residual $\varepsilon_y^{(I)}$ is expressed as:

$$\varepsilon_y^{(I)}(t) = e^{A_L^{(I)}\left(t-t_{f_1}^e\right)}\varepsilon_x^{(I)}(t_{f_1}^e) + d^{(I)}(t) + f^{(I)}(t) + \int_{t_{f_1}^e}^t e^{A_L^{(I)}(t-\tau)}\Bigg(\eta^{(I)}(\tau) - L^{(I)}d^{(I)}(\tau)$$

$$- L^{(I)}f^{(I)}(\tau) + \gamma^{(I)}(T_{z_I}(\tau), Q_{a_I}(\tau)) - \gamma^{(I)}(T_{z_I}(\tau) + d^{(I)}(\tau) + f^{(I)}(\tau), Q_{a_I}(\tau))$$

$$+ h^{(I)}(T_1^e(\tau), Q_{a_I}(\tau)) - h^{(I)}(T_1^e(\tau) + d_1^e(\tau) + f_1^e(\tau), Q_{a_I}(\tau))\Bigg)d\tau. \tag{3.52}$$

The term $\varepsilon_x^{(I)}(t_{f_1}^e)$ is determined through the following equation

$$\varepsilon_T^{(I)}(t) = e^{A_L^{(I)}\left(t-t_f^{(I)}\right)}\varepsilon_T^{(I)}(t_f^{(I)}) + \int_{t_f^{(I)}}^{t} e^{A_L^{(I)}(t-\tau)}\Bigg(\eta^{(I)}(\tau) - L^{(I)}d^{(I)}(\tau) - L^{(I)}f^{(I)}(\tau) + \gamma^{(I)}(T_{z_I}(\tau), Q_{a_I}(\tau))$$
$$- \gamma^{(I)}(T_{z_I}(\tau) + d^{(I)}(\tau) + f^{(I)}(\tau), Q_{a_I}(\tau))$$
$$+ h^{(I)}(T_1^e(\tau), Q_{a_I}(\tau)) - h^{(I)}(T_1^e(\tau) + d_1^e(\tau), Q_{a_I}(\tau))\Bigg)d\tau. \tag{3.53}$$

Using (3.47) and (3.53) and after some algebraic manipulation, the effects of sensor faults $f^{(I)}$ and f_1^e for $t \geq t_{f_1}^e > t_f^{(I)}$ are described as:

$$\varepsilon_{y_F}^{(I)}(t) = f^{(I)}(t) - \int_{t_{f_1}^e}^{t} e^{A_L^{(I)}(t-\tau)}\frac{\rho_a C_{pa}}{M_{z_I}C_v}Q_{a_I}(\tau)f_1^e(\tau)d\tau - \int_{t_f^{(I)}}^{t} e^{A_L^{(I)}(t^*-\tau)}\Bigg(L^{(I)}f^{(I)}(\tau)$$
$$- \frac{\rho_a C_{pa}}{M_{z_I}C_v}Q_{a_I}(\tau)f^{(I)}(\tau)\Bigg)d\tau. \tag{3.54}$$

If there exists a time instant t^* such that the effects of sensor fault $f^{(I)}$ on the residual $\varepsilon_y^{(I)}$ satisfy the condition $\left|\varepsilon_{y_F}^{(I)}(t^*)\right| > 2\bar{\varepsilon}_y^{(I)}(t^*)$, implying that (3.46) is valid, then, using (3.51) and (3.54), it is implied that $\left|\varepsilon_y^{(I)}(t^*)\right| > \bar{\varepsilon}_y^{(I)}(t^*)$, leading to the detection of sensor faults $f^{(I)}$ and f_1^e. Following the same procedure, it can be proved that (3.46) is also valid for $t \geq t_f^{(I)} > t_{f_1}^e$. □

Using Lemma (2), we may characterize the class of sensor faults $f^{(I)}$ and f_1^e that are detectable/isolable by the agent $\mathcal{M}^{(I)}$ with respect to the bounds of modeling uncertainty and measurement noise, as well as the selected design parameters used for the implementation of the estimator of $\mathcal{M}^{(I)}$ (e.g. $L^{(I)}$) and the adaptive thresholds $(\rho^{(I)}, \xi^{(I)})$. During the design, we can simulate various types of faults, i.e. various fault functions and profiles, which may affect a single sensor, and seek the minimum fault magnitude that satisfies the sensor fault detectability/isolability conditions. This analysis can be performed off-line for calibrating the design parameters before the real-time implementation of the proposed agents.

Comparing (3.44) to (3.45), we may infer that sensor fault $f^{(I)}$ affects the residual of $\mathcal{M}^{(I)}$ in a different way than sensor fault f_1^e in the sense that the effects of $f^{(I)}$ are function of $f^{(I)}$ and its filtered version that depends on $L^{(I)}$, while the effects of f_1^e are the filtered version of f_1^e that depends on the interconnection function $h^{(I)}$ only (defined in (2.14). The fact that sensor fault f_1^e may affect $\mathcal{E}^{(I)}$ in a different way than $f^{(I)}$ is exploited in the design of the sensor fault signature matrix $F^{(I)}$, $I = 1, 2$, by differentiating $F_{11}^{(I)}$ from $F_{12}^{(I)}$. Based on (3.44) to (3.45) and assuming constant sensor faults, we may determine the minimum magnitude of sensor fault $f^{(I)}$ and f_1^e that are detectable/isolable by the agent $\mathcal{M}^{(I)}$ in a similar way as in (3.41) and (3.43).

For the modules $\mathcal{M}_1^e$ and $\mathcal{M}_2^e$ of the agent $\mathcal{M}^e$, the detectability analysis is equivalent to the isolability analysis, since each module is dedicated to monitor the status of a single sensor, leading to the sensor fault signature matrix presented in Table 3.1. Thus, in Lemma 4.1 we characterize the minimum effects of sensor faults $f_1^e(t)$ and $f_2^e(t)$ that will be isolable by the modules $\mathcal{M}_1^e$ and $\mathcal{M}_2^e$, respectively, by provoking the violation of $\mathcal{E}_1^e$ and $\mathcal{E}_2^e$, respectively. In the case of the agent $\mathcal{M}^{(I)}$, we distinguish the case of a single sensor fault occurrence and the occurrence of two sensor faults. In the first case, we characterize the minimum effects of a local sensor fault ($f^{(I)}$) or a propagated sensor fault (f_1^e) that are guaranteed to be isolable (i.e. provoke the violation of the ARR $\mathcal{E}^{(I)}$) by the agent $\mathcal{M}^{(I)}$ in conjunction with the sensor fault signature matrix presented in Table II. In the second case, we characterize the minimum effects of both local and propagated sensor faults that are guaranteed to provoke the violation of the ARR $\mathcal{E}^{(I)}$.

3.5 Simulation Results

The objective of this section is to illustrate the application of the proposed distributed SFDI method applied to the class of HVAC systems described in Chapter 2 consisting of eight zones ($N = 8$) [148]. The operation of the HVAC system is simulated based on equations (2.7)-(2.14). The dimensions of each zone are 3.5m × 1.75m × 2m. The parameters used for the simulation of Σ^e described by (2.7)-(2.11) are: $\frac{U_{cc}A_{cc}}{M_{cc}C_v}$=0.02815, $\frac{Q_w\rho_w C_{pw}}{M_{cc}C_v}$=1.2084 and $\frac{Q_w\rho_w C_{pw}+U_tA_t}{V_t\rho_w C_{pw}}$=0.0007, T_{wo}=5, $\frac{U_{cc}A_{cc}}{M_{cc}C_v}$=0.02815, $\frac{U_tA_t}{V_t\rho_w C_{pw}}$=5.4566×10^{-4}, $\frac{Q_w\rho_w C_{pw}}{V_t\rho_w C_{pw}}$=1.544×10^{-5} and $\frac{15000}{V_t\rho_w C_{pw}}$ = 0.006. The function h^e is defined using the parameters $\frac{\rho_a C_{pa}}{M_{cc}C_v}$=3.932, $\frac{U_{cc}A_{cc}}{M_{cc}C_v}$=0.02815 and $\frac{\rho_a}{M_{cc}C_v}((h_{fg} - C_{pa})(w_z - w_{ao})$=0.0005. The parameters used for the simulation of the subsystem $\Sigma^{(I)}$ $I \in \{1,\ldots,8\}$ given in (2.12)-(2.14) are: $A^{(I)} = -0.0006$, $\frac{\rho_a C_{pa}}{M_{z_I}C_v} = 0.1144$, $\frac{U_{z_I}A_{z_I}}{M_{z_I}C_v} = 0.0006$, $T_{amb} = 35$. The modeling uncertainty $\eta^{(I)}(t)$ is simulated as $\eta^{(I)}(t)$=5%$Y^{(I)}$sin$(2\pi\nu t)$, $\nu = 10$ and the noise of each sensor is uniformly distributed, bounded by $\bar{d}^{(j)} = 3\%Y^{(j)}$ and $\bar{d}_j^e = 3\%Y_j^e$, $j = 1, 2$, where $Y^{(I)}, Y_j^e$, are the steady state values of $y^{(I)}, y_j^e$, respectively, under healthy conditions; i.e., controlling the temperatures of each building zone and the electromechanical part and assuming no uncertainty, the steady state values are defined when the temperatures converge to the desired reference signals. Here, $Y_1^e = 10$, $Y_2^e = 4$ and $Y^{(I)} = 24$ for all I.

Eight feedback linearization controllers [74] were implemented, where each controller is responsible for keeping the temperature of each zone at 24°C. A backstepping controller [44] was applied for maintaining the temperature of the output air of the cooling coil at 10°C. It is noted that every zone temperature controller uses the measurements of the temperature of the cooling coil, while the controller of the electromechanical part uses the a priori known set points of the temperature of the zones, as well as the air flow rate (control input) of every zone. Based on Section 3.3, we design nine agents, one for the electromechanical part and eight for the zones, while the agent of the electromechanical

part consists of two modules. The estimators of the agents are structured as in (3.2), (3.5) and (3.8) with estimator gains: $L^{(I)}=3$, $I \in \{1,\ldots,8\}$, $L_1^e=[4.97, 5.16]^\top$ and $L_2^e=3$. The adaptive thresholds of the agents, defined in (3.12), (3.14) and (3.16), are designed using the following parameters: ρ_1^e=1, ξ_1^e=4, ρ_2^e=1, ξ_2^e=3 $\rho^{(I)}=1$ and $\xi^{(I)}$=3.

We have considered two multiple sensor fault scenarios; in the *first scenario*, the sensors of the electromechanical subsystem and zones 3,4,5,6 are affected by faults, while in the *second scenario*, the sensors in all building zones become faulty. In all scenarios, the sensor faults are abrupt with time varying fault functions; i.e., $\phi_1^e(t) = 15\%Y_1^e + 0.5\sin(0.01t)$, $\phi_2^e(t) = 15\%Y_2^e + 0.5\sin(0.01t)$ and $\phi^{(I)}(t) = 15\%Y^{(I)} + 0.5\sin(0.01t)$, $I \in \{1,\ldots,8\}$. The time instants of occurrence of sensor faults are: $t_{f_1}^e = 2000$ sec, $t_{f_2}^e = 2500$ sec, $t_f^{(1)} = 3000$ sec, $t_f^{(2)} = 3500$ sec, $t_f^{(3)} = 4000$ sec, $t_f^{(4)} = 4500$ sec, $t_f^{(5)} = 5000$ sec, $t_f^{(6)} = 5500$ sec, $t_f^{(7)} = 6000$ sec and $t_f^{(8)} = 6500$ sec.

The results of the application of the distributed SFDI method to the HVAC system are illustrated in Fig. 3.2–3.5, with Fig. 3.2 and 3.4 presenting the results for the first sensor fault scenario, while Fig. 3.3 and 3.5 for the second scenario. Comparing the observed pattern, $D^e(t) = \left[D_1^e(t), D_2^e(t)\right]^\top$, where the temporal evolution of $D_1^e(t)$ and $D_2^e(t)$ is shown in Fig. 3.2a and 3.2b, respectively, to the columns of fault signature matrix F^e shown in Table 3.1, the agent $\mathcal{M}^e$ isolates the sensor faults initially in the cooling coil and then in the chilled water tank, based on the following diagnosis set: (i) $\mathcal{D}_s^e(t) = \{f_1^e\}$, since $D^e(t) = F_1^e$ for $t \in [2000, 2500)$, and (ii) $\mathcal{D}_s^e(t) = \{f_1^e, f_2^e\}$, since $D^e(t) = F_3^e$ for $t \geq 2500$.

It is noted that the effects of the sensor fault in the cooling coil on the residuals and thresholds of the eight agents that monitor the building zones are low and are not detectable by these agents (see Fig. 3.2c–3.2j). The distinct effects of local sensor fault ($f^{(I)}$) and propagated sensor fault (f_1^e), which are analyzed in Section 3.4.2, can be observed through the simulation results presented in Fig. 3.2c–3.2j. Based on Fig. 3.2c, 3.2d, 3.2i and 3.2j, the agents $\mathcal{M}^{(1)}$, $\mathcal{M}^{(2)}$, $\mathcal{M}^{(7)}$ and $\mathcal{M}^{(8)}$ do not detect the presence of the faulty temperature sensor in the cooling coil, although they use its measurements. These agents do not also detect the occurrence of sensor faults in the building zones 3,4,5 and 6, but this is due to the fact that every agent $\mathcal{M}^{(I)}$ is sensitive to faults $f^{(I)}$ and f_1^e and not to fault $f^{(Q)}$, $Q \neq I$.

Each of the agents $\mathcal{M}^{(3)}$, $\mathcal{M}^{(4)}$, $\mathcal{M}^{(5)}$ and $\mathcal{M}^{(6)}$ detects the presence of sensor faults just after the consecutive occurrence of the sensor fault in each monitoring building zone, as presented in Fig. 3.2e, 3.2f, 3.2g and 3.2h. Then, using the decision of $\mathcal{M}_1^e$, the agent $\mathcal{M}^{(I)}$ compares the observed pattern $D^{(I)}(t) = \left[D^{(I,1)}(t), D_1^e(t)\right]^\top$, $I \in \{3,4,5,6\}$, where the temporal evolution of D_1^e, $D^{(3,1)}$, $D^{(4,1)}$, $D^{(5,1)}$ and $D^{(6,1)}$ are presented in Fig. 3.2a, 3.2e, 3.2f, 3.2g and 3.2h to the columns of the sensor fault signature matrix $F^{(I)}$ shown in Table 3.2. Given that $D^{(I)}(t) = [1,1]^\top$ for all $I \in \{3,4,5,6\}$, the resultant diagnosis set is $\mathcal{D}^{(I)}(t) = \{\{f^{(I)}, f_1^e\}, f_1^e\}$. Based on this diagnosis outcome, the agent $\mathcal{M}^{(I)}$ for all $I \in \{3,4,5,6\}$ infers that the sensor $\mathcal{S}^{(I)}$ in the I-th building zone is *possibly* faulty, because it cannot conclude if only the sensor fault f_1^e has occurred, provoking the violation of $\mathcal{E}^{(I)}$ or both f_1^e and $f^{(I)}$ have occurred. On the other hand, in the second fault scenario, where the sensors of all

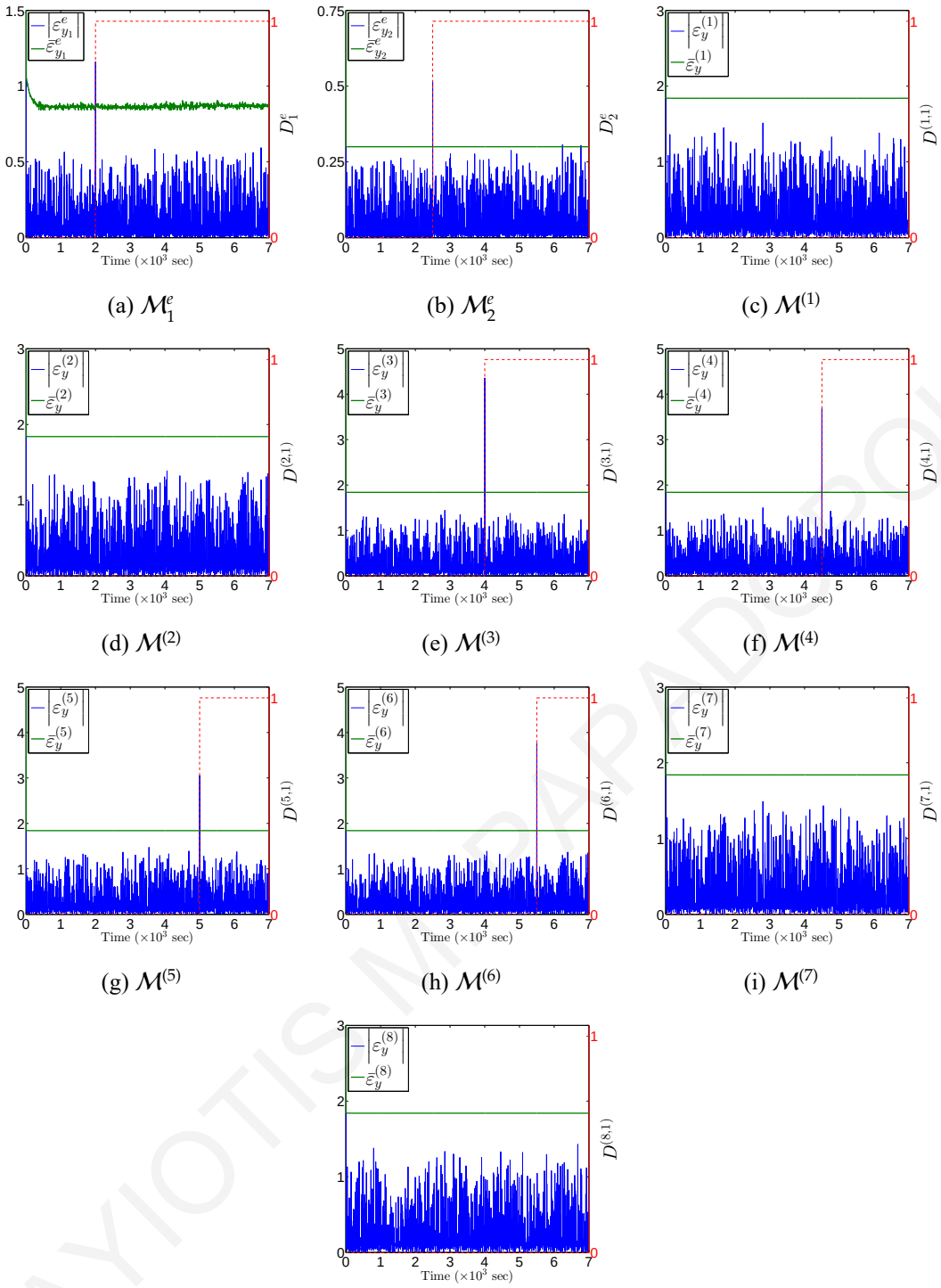

(a) $\mathcal{M}_1^e$ (b) $\mathcal{M}_2^e$ (c) $\mathcal{M}^{(1)}$

(d) $\mathcal{M}^{(2)}$ (e) $\mathcal{M}^{(3)}$ (f) $\mathcal{M}^{(4)}$

(g) $\mathcal{M}^{(5)}$ (h) $\mathcal{M}^{(6)}$ (i) $\mathcal{M}^{(7)}$

(j) $\mathcal{M}^{(8)}$

Figure 3.2: Decision making-process of $\mathcal{M}_1^e$, $\mathcal{M}_2^e$ and $\mathcal{M}^{(I)}$, $I \in \{1,\ldots,8\}$ for isolating multiple sensor faults that affect the electromechanical subsystem and building zones 3,4,5,6 consecutively. Every subfigure presents the temporal evolution of the magnitude of the residual (blue line) and the adaptive threshold (green line), as well as the boolean decision function (red dashed line).

building zones become faulty, but the temperature sensor of the cooling coil is healthy, the agent $\mathcal{M}^{(I)}$ not only detects the presence of sensor faults but also isolates the sensor fault in the I-th building zone. This is realized in conjunction with the decision of the module $\mathcal{M}_1^e$ (Fig. 3.2a). In other words,

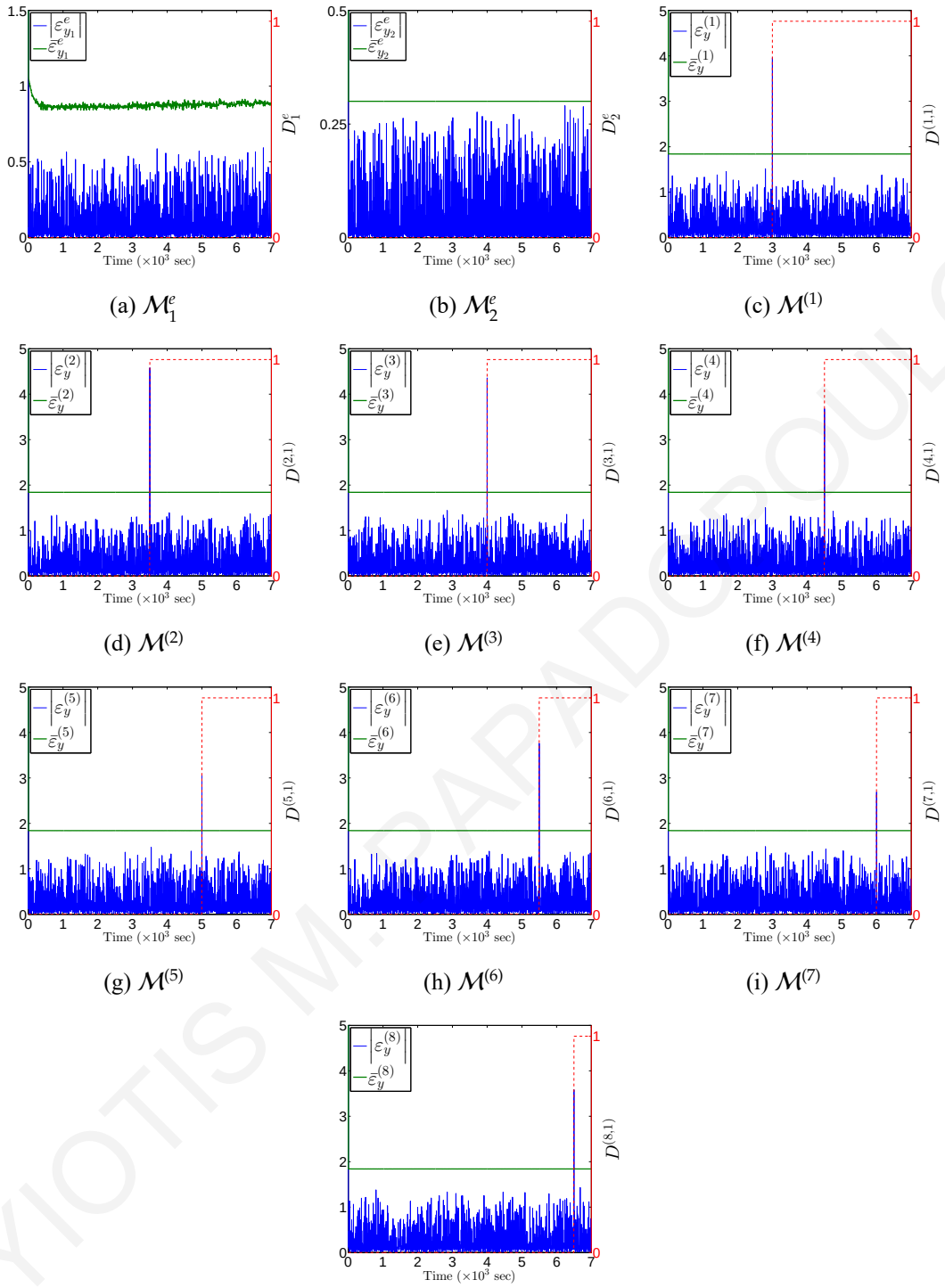

(a) $\mathcal{M}_1^e$ (b) $\mathcal{M}_2^e$ (c) $\mathcal{M}^{(1)}$

(d) $\mathcal{M}^{(2)}$ (e) $\mathcal{M}^{(3)}$ (f) $\mathcal{M}^{(4)}$

(g) $\mathcal{M}^{(5)}$ (h) $\mathcal{M}^{(6)}$ (i) $\mathcal{M}^{(7)}$

(j) $\mathcal{M}^{(8)}$

Figure 3.3: Decision making-process of $\mathcal{M}_1^e$, $\mathcal{M}_2^e$ and $\mathcal{M}^{(I)}$, $I \in \{1, \ldots, 8\}$ for isolating multiple sensor faults that affect all building zones consecutively. Every subfigure presents the temporal evolution of the magnitude of the residual (blue line) and the adaptive threshold (green line), as well as the boolean decision function (red dashed line).

all monitoring agents $\mathcal{M}^{(1)} - \mathcal{M}^{(8)}$ can isolate in a distributed manner the consecutive occurrence of multiple sensor faults in all zones (Fig. 3.3c–3.3j). Particularly, when the agent $\mathcal{M}^{(I)}$ detects sensor faults, the observed pattern equals to $D^{(I)}(t) = [1, 0]^\top$, which is consistent with the first column of

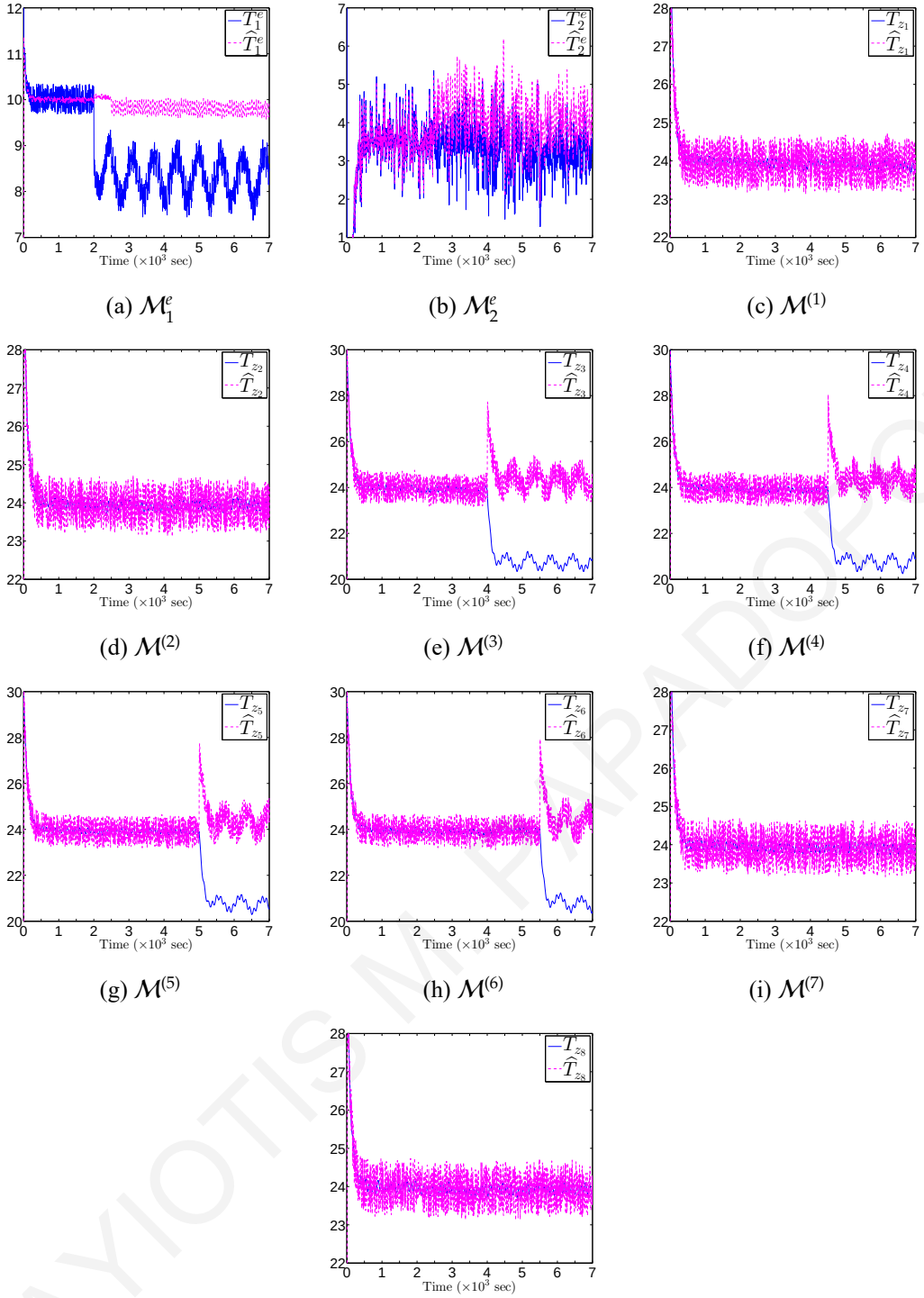

(a) $\mathcal{M}_1^e$ (b) $\mathcal{M}_2^e$ (c) $\mathcal{M}^{(1)}$

(d) $\mathcal{M}^{(2)}$ (e) $\mathcal{M}^{(3)}$ (f) $\mathcal{M}^{(4)}$

(g) $\mathcal{M}^{(5)}$ (h) $\mathcal{M}^{(6)}$ (i) $\mathcal{M}^{(7)}$

(j) $\mathcal{M}^{(8)}$

Figure 3.4: Temperature estimation models (magenta dashed line) of $\mathcal{M}_1^e$, $\mathcal{M}_2^e$ and $\mathcal{M}^{(I)}$, $I \in \{1,\ldots,8\}$ compared to actual temperatures (blue solid line) of the cooling coil, chilled water tank and building zones, under healthy conditions and consecutive occurrence of sensor faults in the electromechanical subsystem and building zones 3,4,5,6.

the sensor fault signature matrix $F^{(I)}$ shown in Table 3.2, leading to the diagnosis set $\mathcal{D}^{(I)}(t) = \{f^{(I)}\}$. By comparing the simulation results illustrated in Fig. 3.3c-3.3j to the simulation results in Fig. 3.2c-3.2j, it can be stated that the effects of the propagated sensor fault f_1^e on the residuals and adaptive

thresholds of $\mathcal{M}^{(1)} - \mathcal{M}^{(8)}$ are much lower than the effects of the local sensor faults. Therefore, in the first sensor fault scenario, we may infer that the occurrence of the local fault $f^{(I)}$ is more likely to have provoked the violation of $\mathcal{E}^{(I)}$, $I \in \{3,4,5,6\}$, than the occurrence of the propagated sensor fault f_1^e, and characterize the sensor $\mathcal{S}^{(I)}$ as faulty for all $I \in \{3,4,5,6\}$.

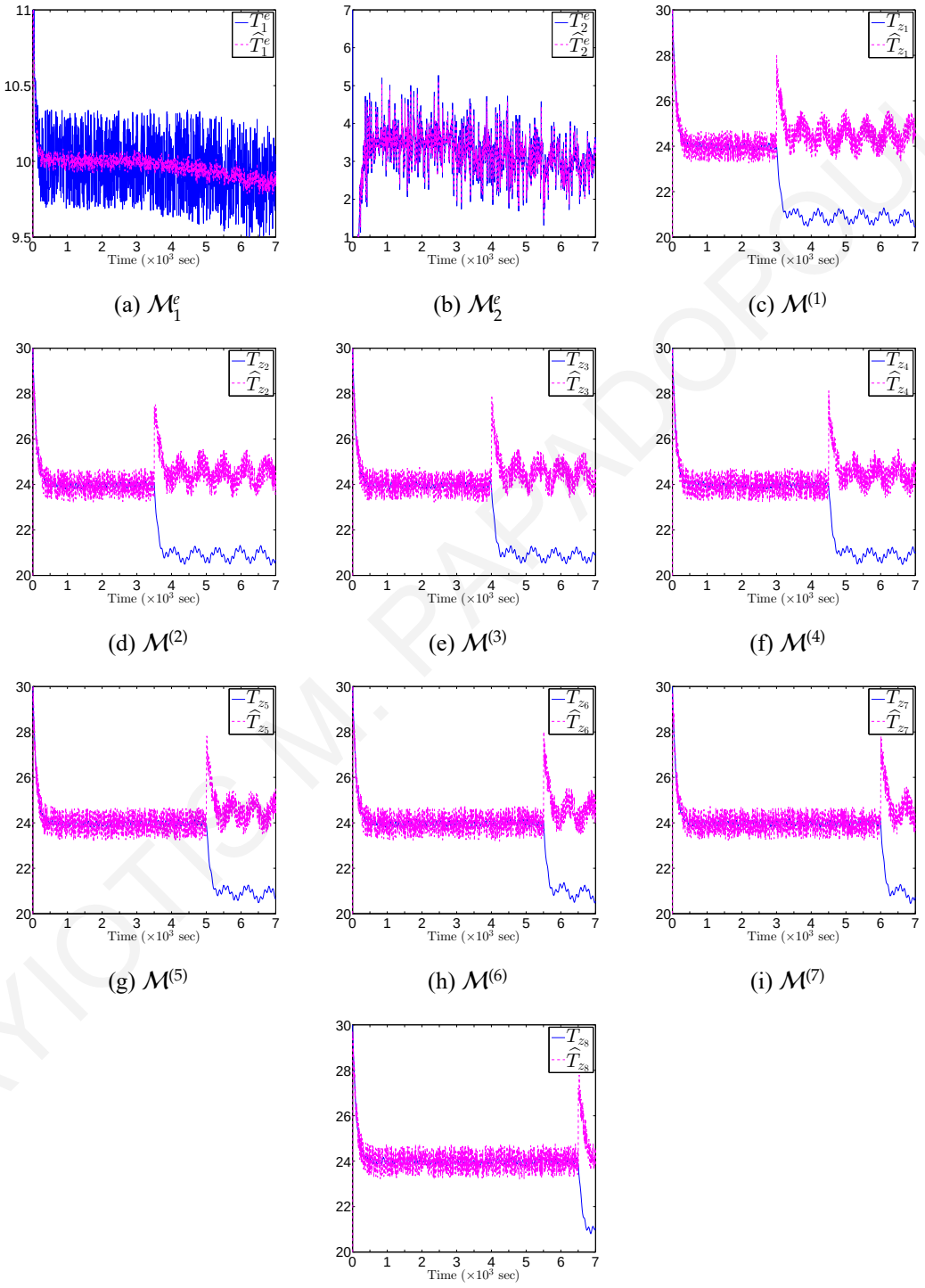

(a) $\mathcal{M}_1^e$ (b) $\mathcal{M}_2^e$ (c) $\mathcal{M}^{(1)}$

(d) $\mathcal{M}^{(2)}$ (e) $\mathcal{M}^{(3)}$ (f) $\mathcal{M}^{(4)}$

(g) $\mathcal{M}^{(5)}$ (h) $\mathcal{M}^{(6)}$ (i) $\mathcal{M}^{(7)}$

(j) $\mathcal{M}^{(8)}$

Figure 3.5: Temperature estimation models (magenta dashed line) of $\mathcal{M}_1^e$, $\mathcal{M}_2^e$ and $\mathcal{M}^{(I)}$, $I \in \{1,\ldots,8\}$ compared to actual temperatures (blue solid line) of the cooling coil, chilled water tank and building zones, under healthy conditions and consecutive occurrence of sensor faults in all building zones.

The effects of sensor faults on the actual temperature of the cooling coil, chilled water tank and all building zones, as well as the temperature estimations derived by the modules $\mathcal{M}_1^e$, $\mathcal{M}_2^e$ and agent $\mathcal{M}^{(I)}$, $I \in \{1,\ldots,8\}$ can be observed in Fig. 3.4 and 3.5. According to Fig. 3.4a, when the temperature sensor of the cooling coil becomes faulty, the backsteping controller perceives the positive fault variation in the sensor output as an increase in the temperature and generates chilled water flow rate aiming at decreasing the actual temperature of the cooling coil. Also, due to this sensor fault the estimation of the temperature in the cooling coil is 'faulty', i.e. different from the actual temperature. When the temperature sensor of the water tank becomes also faulty, based on Fig. 3.4a and 3.4b, the actual temperature in the chilled water tank is less influenced compared to the actual temperature of the cooling coil, while its estimation deviates from the actual temperature less than the estimation of the temperature in the cooling coil. The occurrence of the sensor faults in the cooling coil and the chilled water tank is not observable in the actual temperature of the zones and their estimations provided by the agents $\mathcal{M}^{(1)}-\mathcal{M}^{(8)}$. As expected, the actual temperature of the building zones and their estimations are directly affected by faults in their temperature sensors (Fig. 3.4e-3.4h and Fig. 3.5c-3.5j). Particularly, due to the positive variation in the output of the sensor in the I-th zone $I \in \{1,\ldots,8\}$, the feedback linearization controller generates air flow rate (control input) aiming at decreasing the temperature in the I-th zone. Also, in the second scenario, it can be observed that the actual temperatures of the cooling coil and chilled water tank are not affected considerably by the occurrence of multiple sensor faults in all building zones (Fig. 3.5a and 3.5b). By comparing the simulation results illustrated in Fig. 3.5c-3.5j to the simulation results in Fig. 3.4c-3.4j, we can observe that the effects of the propagated sensor fault f_1^e on the the actual temperature of all zones and the estimated temperature provided by $\mathcal{M}^{(1)}-\mathcal{M}^{(8)}$ are much lower than the effects of the local sensor faults.

3.6 Conclusions

In this chapter, a model-based, distributed architecture for multiple sensor fault detection and isolation (SFDI) in a multi-zone HVAC system is presented. The HVAC system was modeled as a set of interconnected subsystems. For each subsystem, we designed a local sensor fault diagnosis (LSFD) agent, where every agent was dedicated to each of the interconnected subsystems. The distributed isolation of multiple sensor faults was conducted by combining the decisions of the LSFD agents and applying a reasoning-based decision logic. The performance of the proposed methodology was analyzed with respect to sensor fault detectability and multiple sensor fault isolability, characterizing the class of detectable and isolable sensor faults. The proposed SFDI technique may contribute to the reduction of energy consumption in large-scale buildings, as well as provide a procedure for the condition-base maintenance, thus reducing unnecessary maintenance work. Moreover the distributed deployment of the LSFD agents enhances the reliability with respect to security threats, while it is

scalable for handling additional building zones in large-scale buildings. Simulation results illustrated the effectiveness of the proposed distributed SFDI methodology in isolating multiple sensor faults in a HVAC system with a eight thermally separated zones.

Chapter 4

Distributed Sensor Fault Detection and Isolation Architecture for FCU HVAC systems

4.1 Introduction

In Chapter 3, the design of a distributed approach for sensor fault detection and isolation in VAV HVAC systems is presented. However, the performance of the fault diagnosis methods in the previous chapter was evaluated in small-scale buildings and the performance was only examined in a HVAC system with separated zones where the heat transfer between zones (through walls and/or doors) was not considered in system's dynamics (see dynamics presented in Chapter 2.3). Modeling the heat transfer between zones leads to non-linear, non-Lispschitz dynamic terms that can create a more realistic model and thus less conservative fault detection thresholds. This can improve the detectability aspect of the algorithm since the modeling error is reduced and moreover can avert any false alarms caused by the event of an opened door. However, dealing with hard nonlinearities creates challenges with the design and analysis.

4.2 Objective

The main objective of this work is the design of a scalable distributed model-based method for diagnosing multiple sensor faults in large-scale HVAC systems, while taking into account interconnected building zones through walls and doors. Based on the topology of the HVAC system and the building zones, the overall system is divided into interconnected subsystems. A sensor set $\mathcal{S}^{(i)}$ collects the measurements of each subsystem. A local sensor fault diagnosis agent $\mathcal{M}^{(i)}$ is designed to monitor the corresponding sensor set $\mathcal{S}^{(i)}$ and to detect and isolate single and multiple sensor faults based on local

state estimation obtained using local information and information transmitted from its neighboring agents (e.g., control inputs, sensor measurements) as illustrated in Fig. 4.1. Each dedicated sensor fault diagnosis agent $\mathcal{M}^{(i)}$ is comprised of a distributed sensor fault detection module and a distributed sensor fault isolation module. The former is responsible for detecting the occurrence of sensor faults in the monitored subsystem and/or its neighboring interconnected subsystems. A local detection signal is generated by comparing the *residual* (that corresponds to the discrepancies between the output and the expected output) with the corresponding *adaptive threshold* (designed to bound the residual under healthy conditions). Based on the local state estimation, each agent can detect sensor faults affecting either the local or the neighbouring subsystems. The distributed sensor fault isolation module, which is activated based on the local detection decision, takes into consideration the connectivity (due to the exchange of information between the distributed diagnosis agents) in order to construct a fault signature matrix that can eliminate a number of possible sensor faults and under some conditions can pinpoint the exact location of sensor faults. The performance analysis of the proposed method is provided with respect to robustness, fault detectability and scalability, taking into account modeling uncertainties and strong physical interconnections between the building zones that can improve the fault detectability of the algorithm since the modeling error is reduced and moreover can avert false detection alarms caused by the event of an opened door. Finally, simulation results generated by the application of the proposed method to a large-scale HVAC building system show its effectiveness.

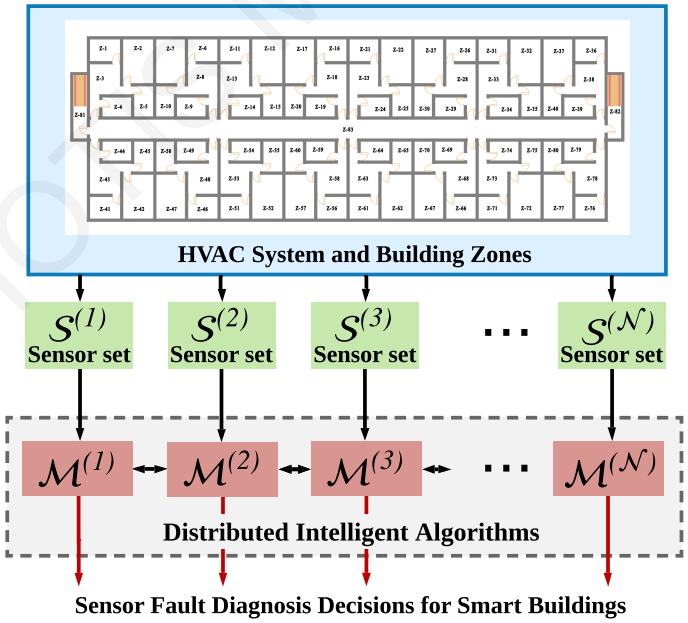

Figure 4.1: Subsystems of the FCU HVAC system.

4.3 Design of the Distributed Sensor Fault Diagnosis Algorithm

The objective of this work is to design a scalable distributed methodology for detecting the faulty operation of the temperature sensors in the multi-zone HVAC system and isolating the location of the faulty sensors. Faults may occur at an unknown time in one or more building zones or in the electromechanical part of HVAC. The proposed methodology is designed taking into account the following assumption.

Assumption 2. For all $t \geq 0$, the modeling uncertainties $r^s(t)$, $r^{(i)}(t)$ and measurement noise $n^s(t)$, $n^{(i)}(t)$ are uniformly bounded such that $|r^s(t)| \leq \bar{r}^s$, $\left|r^{(i)}(t)\right| \leq \bar{r}^{(i)}$ and $|n^s(t)| \leq \bar{n}^s$, $\left|n^{(i)}(t)\right| \leq \bar{n}^{(i)}$, for all $i \in \mathcal{N}$.

The above assumption characterizes known bounds on the modeling uncertainty and measurement noise, which are required in order to distinguish between the occurrence of sensor faults and the presence of modeling uncertainties and measurement noise.

Based on the network of $N + 1$ interconnected subsystems presented in Section 4.2a, a bank of distributed monitoring agents is developed. Fig. 4.2b illustrates the distributed structure of the sensor fault diagnosis agents (red boxes), dedicated to subsystem Σ^s (left) and to each subsystem $\Sigma^{(i)}$, $i \in \{1, \ldots, 5\}$ (right). Every distributed sensor fault diagnosis agent is composed by the following two modules:

- *Sensor fault detection module*: Using the available (local and shared) sensor measurements and control inputs, an estimator is designed based on the known nonlinear dynamics of its monitored subsystem. A residual, which corresponds to the deviation of the measured (observed) output of the monitored subsystem from the expected output, is generated on-line. Based on Assumption 2 and considering a healthy system, an adaptive threshold is designed to bound the residual at every time instant. Both the residual and the adaptive threshold are monitored on-line. The violation of the adaptive threshold indicates the presence of sensor faults and activates the sensor fault isolation module.
- *Sensor fault isolation module*: The local decision about the occurrence of sensor faults is processed in combination with the decisions of the neighboring agents, aiming at isolating multiple sensor faults.

4.3.1 Distributed Sensor Fault Detection Module

The design of the distributed sensor fault detection module includes the computation of residuals and adaptive thresholds, and the formulation of the sensor fault detection decision logic.

Residual generation The residual ε^s generated by the agent $\mathcal{M}^s$ is defined as,

$$\varepsilon^s(t) = y^s(t) - \hat{T}_{st}(t), \tag{4.1}$$

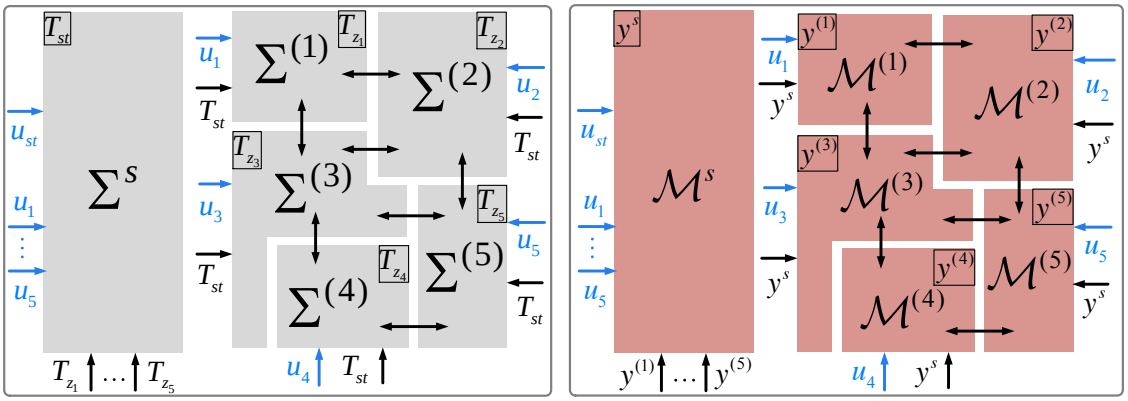

(a) Subsystems of the FCU HVAC system

(b) Agents of the FCU HVAC system

Figure 4.2: Distributed Sensor Fault Detection and Isolation Architecture for the FCU HVAC systems with thermally interconnected zones.

where

$$\dot{\hat{T}}_{st}(t) = (A^s - L^s)\,\hat{T}_{st}(t) + g^s(y^s(t))u_{st}(t) + h^s(y^s(t), y(t), u(t)) + \eta^s(T_{pl}(t)) + L^s y^s(t), \tag{4.2}$$

where $\hat{T}_{st}$ is the estimation of the state T_{st} with $\hat{T}_{st}(0) = 0$, $y(t) = \left[y^{(1)}, \ldots, y^{(N)}\right]^\top$, and L^s is the observer gain selected such that $(A^s - L^s)$ is negative. Let us define the estimation error as $\varepsilon_T^s(t) = T_{st}(t) - \hat{T}_{st}(t)$; then based on (2.23) and (4.2), ε_T^s satisfies

$$\dot{\varepsilon}_T^s(t) = (A^s - L^s)\varepsilon_T^s(t) + \widetilde{g}^s(t)u_{st}(t) + \widetilde{h}^s(t) + r^s(t) - L^s\left(n^s(t) + f^s(t)\right), \tag{4.3}$$

with $\widetilde{g}^s(t) \triangleq g^s(T_{st}(t)) - g^s(y^s(t))$, $\widetilde{h}^s(t) \triangleq h^s(T_{st}(t), T_z(t), u(t)) - h^s(y^s(t), y(t), u(t))$ and

$$\widetilde{g}^s = \frac{U_{st,max}}{C_{st}}\left(P_s(T_{st}) - P_s(y^s)\right), \tag{4.4}$$

$$\widetilde{h}^s = \frac{a_{sz}}{C_{st}} \sum_{i \in \mathcal{N}} U_{i,max}(n^{(i)} - n^s + f^{(i)} - f^s)u_i, \tag{4.5}$$

where P_s is defined in (2.21). Based on (2.32), the residual ε^s defined in (4.1) can be re-written as

$$\varepsilon^s(t) = \varepsilon_T^s(t) + n^s(t) + f^s(t). \tag{4.6}$$

Remark: Given (2.32), (5.1) and (4.3)-(4.5), it yields that ε^s can be affected by a fault in sensor $\mathcal{S}^s$ and/or any sensor fault in $\mathcal{S}^{(i)}$, $i \in \mathcal{N}$.

The residual $\varepsilon^{(i)}$ generated by the monitoring agent $\mathcal{M}^{(i)}$ i.e.,

$$\varepsilon^{(i)}(t) = y^{(i)}(t) - \hat{T}_{z_i}(t), \tag{4.7}$$

where

$$\dot{\hat{T}}_{z_i}(t) = \left(A^{(i)} - L^{(i)}\right)\hat{T}_{z_i}(t) + g^{(i)}(y^s(t), y^{(i)}(t))u_i(t) + \eta^{(i)}(T_{i1}(t), T_{amb}(t)) + h^{(i)}(y^{(i)}(t), y_{\mathcal{K}_i}(t)) + L^{(i)}y^{(i)}(t), \tag{4.8}$$

where $\hat{T}_{z_i}(0) = 0$, $\hat{T}_{z_i}$ is the estimation of the state T_{z_i} (*i-th* zone air temperature), $y_{\mathcal{K}_i}(t) = \left[y^{(j)} : j \in \mathcal{K}_i\right]$, and $L^{(i)}$ is the observer gain selected such that $\left(A^{(i)} - L^{(i)}\right)$ is negative for all $i \in \mathcal{N}$. Let us define the estimation error as $\varepsilon_T^{(i)}(t) = T_{z_i}(t) - \hat{T}_{z_i}(t)$; then $\varepsilon_T^{(i)}$ satisfies

$$\dot{\varepsilon}_T^{(i)}(t) = \left(A^{(i)} - L^{(i)}\right)\varepsilon_T^{(i)}(t) + \widetilde{g}^{(i)}(t)u_i(t) + \widetilde{h}^{(i)}(t) + r^{(i)}(t) - L^{(i)}\left(n^{(i)}(t) + f^{(i)}(t)\right), \tag{4.9}$$

where $\widetilde{g}^{(i)}(t) \triangleq g^{(i)}(T_{st}(t), T_{z_i}(t)) - g^{(i)}(y^s(t), y^{(i)}(t))$, $\widetilde{h}^{(i)}(t) \triangleq h^{(i)}(T_{z_i}(t), T_{\mathcal{K}_i}(t)) - h^{(i)}(y^{(i)}(t), y_{\mathcal{K}_i}(t))$ and

$$\widetilde{g}^{(i)} = \sigma^{(i)}\left(n^{(i)} - n^s + f^{(i)} - f^s\right), \tag{4.10}$$

$$\widetilde{h}^{(i)} = p^{(i)}\sum_{j\in\mathcal{K}_i} A_{d_{ij}}\left(\mu^{(i)}(T_{z_i}, T_{z_j}) - \mu^{(i)}(y^{(i)}, y^{(j)})\right) + \sum_{j\in\mathcal{K}_i}\frac{a_{z_{ij}}}{C_{z_i}}(n^{(j)} + f^{(j)}), \tag{4.11}$$

with

$$\mu^{(i)}(w_1, w_2) = \text{sgn}(w_2 - w_1)\max(w_1, w_2)\sqrt{|w_2 - w_1|}. \tag{4.12}$$

Based on (5.1), the residual $\varepsilon^{(i)}$ defined in (4.7) can be re-written as

$$\varepsilon^{(i)}(t) = \varepsilon_T^{(i)}(t) + n^{(i)}(t) + f^{(i)}(t). \tag{4.13}$$

Remark: Given (2.32), (5.1) and (4.9)-(9.13), it yields that the residual $\varepsilon^{(i)}$ can be affected by a sensor fault in $\mathcal{S}^{(i)}$ and/or any sensor fault in $\mathcal{S}^{(j)}$, $j \in \mathcal{K}_i$ (sensors of neighboring subsystems) and/or sensor faults in $\mathcal{S}^s$.

Adaptive threshold design: The adaptive threshold $\overline{\varepsilon}^s(t) \in \mathbb{R}$ associated with the agent $\mathcal{M}^s$ is designed to bound the residual under healthy conditions (all sensors are healthy), which is denoted by $\varepsilon_H^s(t)$. Particularly, $\varepsilon_H^s(t)$ is defined as

$$\varepsilon_H^s(t) = \varepsilon_{T,H}^s(t) + n^s(t), \tag{4.14}$$

where $\varepsilon_{T,H}^s(t)$ is the state estimation error under healthy conditions that satisfies (4.3)-(4.5) with $f^s(t) = 0$ and $f^{(i)}(t) = 0$ for all $i \in \mathcal{N}$ and $y^s(t) = y_H^s(t)$, where

$$y_H^s(t) = T_{st}(t) + n^s(t). \tag{4.15}$$

Let us define $\overline{\varepsilon}_H^s(t) \in \mathbb{R}$ the adaptive threshold such that

$$|\varepsilon_H^s(t)| \le |\varepsilon_{T,H}^s(t)| + \overline{n}^s \le \overline{\varepsilon}_H^s(t), \ \forall\, t. \tag{4.16}$$

By bounding the solution of (4.3) and using (4.16), it yields

$$\overline{\varepsilon}_H^s(t) = \overline{T}_{st}\rho^s e^{-\zeta^s t} + \overline{n}^s + \frac{\rho^s(1 - e^{-\zeta^s t})}{\zeta^s}(\overline{r}^s + |L^s|\,\overline{n}^s) + \int_0^t \rho^s e^{-\zeta^s(t-\tau)}\Bigg(\overline{g}^s(y_H^s(\tau))\,|u_{st}(\tau)| + \frac{a_{sz}}{C_{st}}\sum_{i\in\mathcal{N}} U_{i,max}(\overline{n}^{(i)} + \overline{n}^s)\,|u_i(\tau)|\Bigg)d\tau, \tag{4.17}$$

where $\overline{T}_{st}$ is a bound on the initial state estimation error such that $\left|\varepsilon_T^s(0)\right| \leq \overline{T}_{st}$, ρ^s, ζ^s are positive constants selected such that $\left|e^{(A^s-L^s)t}\right| \leq \rho^s e^{-\zeta^s t}$, for all t, and the function $\overline{g}^s(y_H^s)$ is defined in (4.20) and is designed to bound the difference $\widetilde{g}^s$ defined in (4.4) under healthy conditions. Given (2.21), $\widetilde{g}^s = \omega(P(T_{st}) - P(y^s))$ where $\omega = \frac{U_{st,max}}{C_{st}}$ and

$$P(T_{st}) = \begin{cases} (1 + \lambda\,(\kappa - T_{st}))\,, & T_{st}(t) \leq \kappa \\ 1, & T_{st} > \kappa \end{cases} \tag{4.18}$$

$$P(y_H^s) = \begin{cases} \left(1 + \lambda\left(\kappa - y_H^s\right)\right), & y_H^s \leq \kappa \\ 1, & y_H^s > \kappa \end{cases} \tag{4.19}$$

with $\lambda = \frac{(P_{max}-1)}{\Delta T_{max}}$ and $\kappa = \Delta T_{max} + T_o$. The variable T_{st} is unknown but belongs to a known interval; i.e. under healthy conditions ($f^s = 0$), (4.15) is valid, so based on Assumption 2, $T_{st} \in \left[y_H^s - \overline{n}^s, y_H^s + \overline{n}^s\right]$. Due to this inclusion, by applying interval arithmetic we have the following cases

1. if $y_H^s \leq \kappa - \overline{n}^s$, then $T_{st} \leq \kappa$ and $|\widetilde{g}^s| = |\omega\lambda(y_H^s - T_{st})| = |\omega\lambda n^s| \leq \omega\lambda\overline{n}^s$
2. if $y_H^s > \kappa + \overline{n}^s$, then $T_{st}(t) \leq \kappa$ and $|\widetilde{g}^s| = 0$

However if $y^s \in (\kappa - \overline{n}^s, \kappa + \overline{n}^s]$, T_{st} may satisfy either $T_{st} > \kappa$ or $T_{st} \leq \kappa$. Thus, we need to investigate the following cases:

3. if $y_H^s \in (\kappa, \kappa + \overline{n}^s]$ and $T_{st} \leq \kappa$, then $|\widetilde{g}^s| = |\omega\lambda(\kappa - T_{st})|$
4. if $y_H^s \in (\kappa, \kappa + \overline{n}^s]$ and $T_{st} > \kappa$, then $|\widetilde{g}^s| = 0$
5. if $y_H^s \in (\kappa - \overline{n}^s, \kappa]$ and $T_{st} \leq \kappa$, then $|\widetilde{g}^s| = |\omega\lambda(y_H^s - T_{st})| = |\omega\lambda n^s|$
6. if $y_H^s \in (\kappa - \overline{n}^s, \kappa]$ and $T_{st} > \kappa$ then $|\widetilde{g}^s| = \omega\lambda|\kappa - y_H^s|$.

Given that $T_{st} \in \left[y_H^s - \overline{n}^s, y_H^s + \overline{n}^s\right]$, it yields that $\omega\lambda|\kappa - T_{st}| \in \omega\lambda\left[|\kappa - y_H^s - \overline{n}^s|, |\kappa - y_H^s + \overline{n}^s|\right]$. Therefore, in cases 3 and 4 $|\widetilde{g}^s| \leq \max(|\kappa - y_H^s - \overline{n}^s|, |\kappa - y_H^s + \overline{n}^s|)$ irrespective of the exact value of T_{st}. In case 6, since $y_H^s \in (\kappa - \overline{n}^s, \kappa]$, then $\kappa - y_H^s > 0$ and $\kappa - y_H^s < \overline{n}^s$, we have $|\widetilde{g}^s| = \omega\lambda|\kappa - y_H^s| \leq \omega\lambda\overline{n}^s$. The following inclusion functions give the bound $\overline{g}^s$. So, in both cases 5 and 6, $|\widetilde{g}^s| \leq \omega\lambda\overline{n}^s$. In summary,

$$\overline{g}^s(y_H^s) = \begin{cases} 0 & , y_H^s > \kappa + \overline{n}^s \\ \omega\lambda \max\left(|\kappa - y_H^s - \overline{n}^s|,\right. & \\ \qquad \left.|\kappa - y_H^s + \overline{n}^s|\right) & , y_H^s(t) \in (\kappa, \kappa + \overline{n}^s] \\ \omega\lambda\overline{n}^s & , y_H^s \leq \kappa \end{cases}. \tag{4.20}$$

Similarly, the adaptive threshold $\overline{\varepsilon}^{(i)}(t) \in \mathbb{R}$ associated with the agent $\mathcal{M}^{(i)}$ is designed to bound $|\varepsilon_H^{(i)}(t)|$ that denotes the residual under healthy conditions, defined as

$$\varepsilon_H^{(i)}(t) = \varepsilon_{T,H}^{(i)}(t) + n^{(i)}(t), \tag{4.21}$$

where $\varepsilon_{T,H}^{(i)}(t)$ is the state estimation error under healthy conditions that satisfies (4.9)-(9.13) with

$f^s(t) = 0$, $f^{(i)}(t) = 0$ and $f^{(j)} = 0$ for all $j \in \mathcal{K}_i$ and $y^{(i)}(t) = y_H^{(i)}(t)$, where

$$y_H^{(i)}(t) = T_{z_i}(t) + n^{(i)}(t). \tag{4.22}$$

Let us define $\overline{\varepsilon}_H^{(i)}(t) \in \mathbb{R}$ the adaptive threshold under healthy conditions such that

$$|\varepsilon_H^{(i)}(t)| \leq |\varepsilon_{T,H}^{(i)}(t)| + \overline{n}^{(i)} \leq \overline{\varepsilon}_H^{(i)}(t), \ \forall\, t. \tag{4.23}$$

By bounding the solution of (4.9) and using (4.23), it yields

$$\begin{aligned}\overline{\varepsilon}_H^{(i)}(t) = \overline{T}_{z_i}\rho^{(i)}e^{-\zeta^{(i)}t} + \overline{n}^{(i)} + \frac{\rho^{(i)}(1-e^{-\zeta^{(i)}t})}{\zeta^{(i)}}\left(\left|L^{(i)}\right|\overline{n}^{(i)} + \overline{r}^{(i)} + \sum_{j\in\mathcal{K}_i}\frac{a_{z_{i,j}}}{C_{z_i}}\overline{n}^{(j)}\right)\\ + \int_0^t \rho^{(i)}e^{-\zeta^{(i)}(t-\tau)}\left(\sigma^{(i)}\overline{n}^{(i)}|u^{(i)}(\tau)| + \sigma^{(i)}\overline{n}^{s}|u^{(i)}(\tau)| + p^{(i)}\sum_{j\in\mathcal{K}_i}A_{d_{i,j}}\overline{\mu}^{(i)}(y_H^{(i)}(\tau), y_H^{(j)}(\tau))\right)d\tau,\end{aligned} \tag{4.24}$$

where $\overline{T}_{z_i}$ is a bound such that $|\varepsilon_T^s(0)| \leq \overline{T}_{z_i}$ and $\rho^{(i)}$, $\zeta^{(i)}$ are positive constants selected such that $|e^{(A^{(i)}-L^{(i)})t}| \leq \rho^{(i)}e^{-\zeta^{(i)}t}$, for all t. The function $\overline{\mu}^{(i)}$ is defined through (4.26)-(4.30) and (4.32)-(4.34) and is designed to bound the difference $\widetilde{\mu}^{(i)} = \mu^{(i)}(T_{z_i}, T_{z_j}) - \mu^{(i)}(y_H^{(i)}, y_H^{(j)})$ where $y_H^{(i)}$ and $y_H^{(j)}$ satisfy (4.22). Let us define

$$\mu^{(i)}(T_{z_i}(t), T_{z_j}(t)) = \chi_2(t)\chi_1(t) \tag{4.25}$$

where $\chi_1 = \sqrt{\left|T_{z_j} - T_{z_i}\right|}$ and $\chi_2 = \text{sgn}(T_{z_j} - T_{z_i})\max(T_{z_i}, T_{z_j})$. Based on Assumption 2 and (4.22), $T_{z_i} \in \left[y_H^{(i)} - \overline{n}^{(i)}, y_H^{(i)} + \overline{n}^{(i)}\right]$, for all $i \in \mathcal{N}$ Taking into account the monotonicity of χ_1 and applying interval arithmetic, we obtain

$$\chi_1 \in \left[\underline{\chi}_1^{(i)}, \overline{\chi}_1^{(i)}\right] \tag{4.26}$$

$$\left[\underline{\chi}_1^{(i)}, \overline{\chi}_1^{(i)}\right] = \begin{cases} \left[\sqrt{\alpha-\beta}, \sqrt{\alpha+\beta}\right], & \text{if } \alpha(t) > \beta \\ \left[\sqrt{|\alpha+\beta|}, \sqrt{|\alpha-\beta|}\right], & \text{if } \alpha(t) < -\beta \\ \left[0, \sqrt{\max\left(|\alpha-\beta|, |\alpha+\beta|\right)}\right], & \text{if } |\alpha(t)| \leq \beta \end{cases} \tag{4.27}$$

where $\alpha(t) = y_H^{(j)}(t) - y_H^{(i)}(t)$, $\beta = \overline{n}^{(j)} + \overline{n}^{(i)}$. Following the same procedure, we have

$$\chi_2 \in \left[\underline{\chi}_2^{(i)}, \overline{\chi}_2^{(i)}\right] \tag{4.28}$$

$$\left[\underline{\chi}_2^{(i)}, \overline{\chi}_2^{(i)}\right] = \begin{cases} \left[y_H^{(j)} - \overline{n}^{(j)}, y_H^{(j)} + \overline{n}^{(j)}\right], & \text{if } \alpha > \beta \\ \left[-y_H^{(i)} - \overline{n}^{(i)}, -y_H^{(i)} + \overline{n}^{(i)}\right], & \text{if } \alpha < -\beta \\ \left[\min(W), \max(W)\right], & \text{if } |\alpha| \leq \beta \end{cases} \tag{4.29}$$

$$W = \{-\min(w_1, w_2), -\max(w_1, w_2), \min(w_1, w_2), \max(w_1, w_2)\} \tag{4.30}$$

where $w_1 = y_H^{(j)}(t) + \overline{n}^{(j)}$ and $w_2 = y_H^{(i)}(t) + \overline{n}^{(i)}$. Based on (4.25), (4.26) and (4.28), it yields

$$\mu^{(i)}(T_{z_i}, T_{z_j}) \in [\underline{\chi}^{(i)}, \overline{\chi}^{(i)}] \tag{4.31}$$

with

$$\underline{\chi}^{(i)} = \min(\underline{\chi}_1^{(i)}\underline{\chi}_2^{(i)}, \underline{\chi}_1^{(i)}\overline{\chi}_2^{(i)}, \overline{\chi}_1^{(i)}\underline{\chi}_2^{(i)}, \overline{\chi}_1^{(i)}\overline{\chi}_2^{(i)}), \tag{4.32}$$

$$\overline{\chi}^{(i)} = \max(\underline{\chi}_1^{(i)}\underline{\chi}_2^{(i)}, \underline{\chi}_1^{(i)}\overline{\chi}_2^{(i)}, \overline{\chi}_1^{(i)}\underline{\chi}_2^{(i)}, \overline{\chi}_1^{(i)}\overline{\chi}_2^{(i)}). \tag{4.33}$$

Using (4.31) and applying interval arithmetic results in $\widetilde{\mu}^{(i)} \in \left[\underline{\chi}^{(i)} - v^{(i)}, \overline{\chi}^{(i)} - v^{(i)})\right]$ with $v^{(i)} = \mu^{(i)}(y_H^{(i)}, y_H^{(j)})$. The upper bound that satisfies $|\widetilde{\mu}^{(i)}| \leq \overline{\mu}^{(i)}(y_H^{(i)}, y_H^{(j)})$ is computed as

$$\overline{\mu}^{(i)}(y_H^{(i)}, y_H^{(j)}) = \max(|\underline{\chi}^{(i)} - v^{(i)}|, |\overline{\chi}^{(i)} - v^{(i)}|). \tag{4.34}$$

The adaptive thresholds $\overline{\varepsilon}^s(t)$ and $\overline{\varepsilon}^{(i)}(t)$ that are used for sensor fault detection are described by the following equations.

$$\begin{aligned}\overline{\varepsilon}^s(t) = {} & \overline{T}_{st}\rho^s e^{-\zeta^s t} + \overline{n}^s + \frac{\rho^s(1-e^{-\zeta^s t})}{\zeta^s}(\overline{r}^s + |L^s|\,\overline{n}^s) + \int_0^t \rho^s e^{-\zeta^s(t-\tau)}\Bigg(\overline{g}^s(y^s(\tau))\,|u_{st}(\tau)| \\ & + \frac{a_{sz}}{C_{st}}\sum_{i\in\mathcal{N}} U_{i,max}(\overline{n}^{(i)} + \overline{n}^s)\,|u_i(\tau)|\Bigg)d\tau \end{aligned} \tag{4.35}$$

$$\begin{aligned}\overline{\varepsilon}^{(i)}(t) = {} & \overline{T}_{z_i}\rho^{(i)} e^{-\zeta^{(i)} t} + \overline{n}^{(i)} + \frac{\rho^{(i)}(1-e^{-\zeta^{(i)} t})}{\zeta^{(i)}}\Bigg(\left|L^{(i)}\right|\overline{n}^{(i)} + \overline{r}^{(i)} + \sum_{j\in\mathcal{K}_i}\frac{a_{z_{i,j}}}{C_{z_i}}\overline{n}^{(j)}\Bigg) \\ & + \int_0^t \rho^{(i)} e^{-\zeta^{(i)}(t-\tau)}\Bigg(\sigma^{(i)}\overline{n}^{(i)}|u^{(i)}(\tau)| + \sigma^{(i)}\overline{n}^s|u^{(i)}(\tau)| + p^{(i)}\sum_{j\in\mathcal{K}_i} A_{d_{i,j}}\overline{\mu}^{(i)}(y^{(i)}(\tau), y^{(j)}(\tau))\Bigg)d\tau, \end{aligned} \tag{4.36}$$

where y^s and $y^{(i)}$ are described by (2.32) and (5.1), respectively. The implementation of $\overline{\varepsilon}^s(t)$ and $\overline{\varepsilon}^{(i)}(t)$ can be realized using linear filtering techniques; i.e. $\int_0^t \rho e^{-\zeta(t-\tau)}z(\tau)d\tau$ can be implemented as $\frac{\rho}{s+\zeta}[z(t)]$ that corresponds to the output of the stable, linear filter $\frac{\rho}{s+\zeta}$ with input $z(t)$.

Remark: Note that under the occurrence of sensor faults, $\overline{\varepsilon}^s(t)$ may be affected by a fault in sensor $\mathcal{S}^s$ and $\overline{\varepsilon}^{(i)}(t)$ may be affected by faults in sensor $\mathcal{S}^{(i)}$ and $\mathcal{S}^{(j)}$ for all $j \in \mathcal{K}_i$.

4.3.2 Sensor fault detection logic

The sensor fault detection process performed by the agents $\mathcal{M}^s$ and $\mathcal{M}^{(i)}$ is based on checking online whether the following analytical redundancy relations (ARR), denoted by $\mathcal{E}^s$ and $\mathcal{E}^{(i)}$, are satisfied

$$\mathcal{E}^s : |\varepsilon^s(t)| \leq \overline{\varepsilon}^s(t), \tag{4.37}$$

$$\mathcal{E}^{(i)} : \left|\varepsilon^{(i)}(t)\right| \leq \overline{\varepsilon}^{(i)}(t), \tag{4.38}$$

where ε^s and $\overline{\varepsilon}^s$ are defined in (4.1) and (4.35), while $\varepsilon^{(i)}$ and $\overline{\varepsilon}^{(i)}$ are given in (4.7) and (4.36). Hence, the boolean decision signal D^s (correspondingly $D^{(i)}$) indicates the violation of $\mathcal{E}^s$ (correspondingly of $\mathcal{E}^{(i)}$) such as D^s ($D^{(i)}$) i.e. when the threshold $\overline{\varepsilon}^s$ ($\overline{\varepsilon}^{(i)}$) is violated by the absolute value of the corresponding residual ε^s ($\varepsilon^{(i)}$, $i \in \mathcal{N}$).

4.3.3 Distributed Sensor Fault Isolation Module

When the detection decision signal D^s (correspondingly for $D^{(i)}$) becomes non-zero, the agent $\mathcal{M}^s$ (correspondingly for $\mathcal{M}^{(i)}$) initiates the fault isolation process, using local and neighboring detection decision signals.

The distributed isolation procedure applied by each agent involves the comparison of the observed pattern of sensor faults that may affect the neighborhood of the agent to a number of theoretical patterns, represented by the columns of a sensor fault signature matrix. In the case of the agent $\mathcal{M}^s$, the observed pattern of sensor faults, denoted by $\Phi^s(t) \in [0,1]^{N+1}$, where $[0,1]^{N+1}$ denotes a binary vector of $N+1$ length, defined as $\Phi^s(t) = [D^s, D^{(1)}, \ldots, D^{(N)}]$. Note that $D^{(i)}$ is transmitted to $\mathcal{M}^s$ by the agent $\mathcal{M}^{(i)}$ for all $i \in \mathcal{N}$. The sensor fault signature matrix F^s consists of $N+1$ rows, which correspond to the set of ARRs $\{\mathcal{E}^s, \mathcal{E}^{(1)}, ..., \mathcal{E}^{(N)}\}$, and $N_c = 2^{N+1} - 1$ columns that correspond to all possible sensor fault combinations that may affect the building zones and the storage tank, where the k-th combination is indicated by $\mathcal{F}^s_{c_k}$, $k \in \{1, \ldots, N_c\}$. The k-th column corresponds to the theoretical pattern, denoted by F^s_k and defined as $F^s_k = [F^s_{1k}, \ldots, F^s_{Nk}]^\top$.

In the case of agent $\mathcal{M}^{(i)}$, the observed pattern of sensor faults, denoted by $\Phi^{(i)}(t) \in [0,1]^{|\mathcal{K}_i|+2}$, is a vector made up of the detection decisions $D^s(t)$, $D^{(i)}(t)$ and $D^{(j)}(t)$ for all $j \in \mathcal{K}_i$. The sensor fault signature matrix consists of $|\mathcal{K}_i|+2$ rows, which correspond to the set of ARRs $\{\mathcal{E}^s, \mathcal{E}^{(i)}\} \bigcup_{j \in \mathcal{K}_i} \left\{\mathcal{E}^{(j)}\right\}$, and $N_c^{(i)} = 2^{|\mathcal{K}_i|+2} - 1$ columns that correspond to all possible sensor fault combinations that may affect the storage tank, the i-th building zone and its $|\mathcal{K}_i|$ neighboring zones. The k-th column corresponds to the theoretical pattern, denoted by $F^{(i)}_k$. For example, taking into account the 5-zone HVAC system shown in Fig. 4.2b, based on which the observed pattern of agent $\mathcal{M}^s$ is defined as $\Phi^s(t) = \left[D^s(t), D^{(1)}(t), D^{(2)}(t), D^{(3)}(t), D^{(4)}(t), D^{(5)}(t)\right]$. Moreover, the sensor fault signature matrix F^s of the agent $\mathcal{M}^s$ presented in Fig.4.2b, is comprised of 6 rows and 63 columns as shown Table 4.1, which illustrates a part of the sensor fault signature matrix F^s considering 6 single sensor faults, and one possible combination of two simultaneous sensor faults, $\{f^s, f^{(1)}\}$. The assignment $F^s_{22} = 1$ implies that $f^{(1)}$ necessarily discloses its occurrence by provoking the violation of $\mathcal{E}^{(1)}$, while $F^s_{12} = *$ implies that $f^{(1)}$ may justify the violation of $\mathcal{E}^s$, but $\mathcal{E}^s$ may be satisfied in spite of the occurrence of the sensor fault $f^{(1)}$. Otherwise, $F^s_{15} = 0$, since $f^{(5)}$ is not involved in $\mathcal{E}^{(1)}$ [130].

The sensor fault isolation process of the agent $\mathcal{M}^{(4)}$ presented in Fig. 4.2b consists of the observed pattern $\Phi^{(4)} = \left[D^s, D^{(4)}, D^{(3)}, D^{(5)}\right]$ and the sensor fault signature matrix $F^{(4)}$ comprised of 4 rows that corresponds to ARRs $\{\mathcal{E}^s, \mathcal{E}^{(4)}, \mathcal{E}^{(3)}, \mathcal{E}^{(5)}\}$ and 15 columns. Table 4.2 illustrates a part of $F^{(4)}$ considering 4 single sensor faults and 3 possible combinations of simultaneous sensor faults (i.e., $\{f^s, f^{(4)}\}$, $\{f^s, f^{(3)}\}$ and $\{f^s, f^{(5)}\}$).

Remark: The sensor fault isolation process of the agent $\mathcal{M}^{(4)}$ is realized in the neighborhood of $\mathcal{M}^{(4)}$ (see Fig.4.2b) since the sensor faults $f^{(1)}$ and $f^{(2)}$ do not affect the residual generation of $\mathcal{M}^{(4)}$ (see

Table 4.1: Part of the sensor fault signature matrix of the agent $\mathcal{M}^s$ showing in Fig. 4.2b

	f^s	$f^{(1)}$	$f^{(2)}$	$f^{(3)}$	$f^{(4)}$	$f^{(5)}$	$\{f^s, f^{(1)}\}$
$\mathcal{E}^s$	1	*	*	*	*	*	1
$\mathcal{E}^{(1)}$	*	1	*	*	0	0	1
$\mathcal{E}^{(2)}$	*	*	1	*	0	*	*
$\mathcal{E}^{(3)}$	*	*	*	1	*	*	*
$\mathcal{E}^{(4)}$	*	0	0	*	1	*	*
$\mathcal{E}^{(5)}$	*	0	*	*	*	1	*

Section (20)-(24) with $\mathcal{K}_4 = \{3, 5\}$).

Table 4.2: Part of the sensor fault signature matrix of the agent $\mathcal{M}^{(4)}$ showing in Fig. 4.2b

	f^s	$f^{(4)}$	$f^{(3)}$	$f^{(5)}$	$\{f^s, f^{(4)}\}$	$\{f^s, f^{(3)}\}$	$\{f^s, f^{(5)}\}$
$\mathcal{E}^s$	1	*	*	*	1	1	1
$\mathcal{E}^{(4)}$	*	1	*	*	1	*	*
$\mathcal{E}^{(3)}$	*	*	1	*	*	1	*
$\mathcal{E}^{(5)}$	*	*	*	1	*	*	1

The outcome of the online comparison of the observed fault pattern Φ^s to the N_c theoretical fault patterns F_k^s, $k \in \{1, \ldots, N_c\}$, and the observed pattern $\Phi^{(i)}$ to the $N_c^{(i)}$ theoretical patterns $F_q^{(i)}$, $q \in \{1, \ldots, N_c^{(i)}\}$ is the diagnosis sets $\Upsilon^s(t)$ and $\Upsilon^{(i)}(t)$, which are determined as

$$\Upsilon^s(t) = \left\{\mathcal{F}_{c_i}^s : i \in \mathcal{I}_\Upsilon^s(t)\right\} \ , \Upsilon^{(i)}(t) = \left\{\mathcal{F}_{c_i}^{(i)} : i \in \mathcal{I}_\Upsilon^{(i)}(t)\right\}, \tag{4.39}$$

with $\mathcal{I}_\Upsilon^s(t) = \left\{k : F_k^s = \Phi^s(t),\ k \in \{1, \ldots, N_c\}\right\}$ and $\mathcal{I}_\Upsilon^{(i)}(t) = \left\{k : F_k^{(i)} = \Phi^{(i)}(t),\ k \in \{1, \ldots, N_c^{(i)}\}\right\}$. The diagnosis sets contains all the possible fault combinations.

4.4 Performance Analysis

In this section we study the performance of the proposed sensor fault diagnosis architecture with respect to robustness (i.e., the ability to avoid false alarms in the presence of modeling uncertainty and measurement noise), detectability (i.e., the ability to detect faults in the presence of modeling uncertainty and measurement noise) and scalability (i.e., the ability to be easily modified in the case of increasing the number of zones).

4.4.1 Robustness analysis

The property of robustness refers to the ability of the agents $\mathcal{M}^s$ and $\mathcal{M}^{(i)}$, $i \in \mathcal{N}$ to avoid false alarms in the presence of the modeling uncertainties r^s, $r^{(i)}$ and measurement noise n^s, $n^{(i)}$, in the absence of either local and propagated sensor fault. The robustness is accomplished by guaranteeing that the ARRs $\mathcal{E}^s$ and $\mathcal{E}^{(i)}$, respectively defined in (4.37) and (4.38), are satisfied, i.e. the magnitude of the residual remains below the adaptive threshold, under healthy conditions.

Lemma 3. *If there are no faults affecting the sensor in the storage tank and all the sensors in the building zones, the ARR $\mathcal{E}^s$ is guaranteed to be satisfied and the agent $\mathcal{M}^s$ does not raise any false alarm in the presence of the modeling uncertainty r^s and measurement noise n^s and $n^{(i)}$ for all $i \in \mathcal{N}$.*

Proof. If $f^s(t) = 0$ and $f^{(i)}(t) = 0$ for all $i \in \mathcal{N}$ then the residual $\varepsilon^s(t)$ is equal to $\varepsilon^s_H(t)$ defined in (4.14) and the adaptive threshold $\overline{\varepsilon}^s(t)$ is equal to $\overline{\varepsilon}^s_H(t)$ defined in (4.17). Therefore, (4.16) is valid and the ARR $\mathcal{E}^s$ defined in (4.37) is guaranteed to be satisfied. The robustness property is guaranteed based on the design of the fault diagnosis architecture. □

Lemma 4. *If there are no faults affecting the sensors in the storage tank and the building zone i, as well as the $|\mathcal{K}_i|$ sensors in the neighboring building zones, the ARR $\mathcal{E}^{(i)}$ is guaranteed to be satisfied and the agent $\mathcal{M}^{(i)}$ does not raise any false alarm in the presence of the modeling uncertainty $r^{(i)}$ and measurement noise n^s and $n^{(i)}$ for all $i \in \{\mathcal{K}_i \cup \{i\}\}$.*

Proof. If $f^s(t) = 0$ and $f^{(i)}(t) = 0$ for all $i \in \{\mathcal{K}_i \cup \{i\}\}$ then the residual $\varepsilon^{(i)}(t)$ is equal to $\varepsilon^{(i)}_H(t)$ defined in (4.21) and the adaptive threshold $\overline{\varepsilon}^{(i)}(t)$ is equal to $\overline{\varepsilon}^{(i)}_H(t)$ defined in (4.24). Therefore, (4.23) is valid and the ARR $\mathcal{E}^{(i)}$ defined in (4.38) is guaranteed to be satisfied. □

4.4.2 Detectability analysis

This section contains the analysis on the detectability of the proposed distributed sensor fault diagnosis architecture where we analyze the ability of the agents to detect local and propagated sensor faults. Specifically, certain conditions are derived, under which we characterize the class of faults affecting the sensors in (2.32) and (5.1) that can be detected. It is important to note that the class of detectable sensor faults satisfying these conditions is obtained under worst-case assumptions, in the sense that they are valid for any modeling uncertainty and measurement noise satisfying Assumption 2. The analysis is divided into two parts; the sensor fault detectability analysis of agent $\mathcal{M}^s$ and the sensor fault detectability analysis of agent $\mathcal{M}^{(i)}$, $i \in \mathcal{N}$.

Sensor Fault Detectability of agent $\mathcal{M}^s$

The residual ε^s described by (4.1) (or (4.6)) and the corresponding adaptive threshold $\overline{\varepsilon}^s$ of (4.35) are sensitive to any fault that may occur in the sensor of the storage tank (local sensor fault) at the time

instant t_f^s, or in the sensors of the building zones (propagated sensor faults) that may occur at the time instances $t_f^{(i)}$, $i \in \mathcal{N}$. Under faulty conditions, ε^s and $\overline{\varepsilon}^s$ can be expressed as

$$\varepsilon^s(t) = \varepsilon_H^s(t) + \varepsilon_F^s(t), \tag{4.40}$$

$$\overline{\varepsilon}^s(t) = \overline{\varepsilon}_H^s(t) + \overline{\varepsilon}_F^s(t), \tag{4.41}$$

where ε_H^s (defined in (4.6)) and $\overline{\varepsilon}_H^s$ (defined in (4.17)) are the healthy parts of ε^s and $\overline{\varepsilon}^s$, respectively, and ε_F^s and $\overline{\varepsilon}_F^s$ are the faulty parts of ε^s and $\overline{\varepsilon}^s$, respectively, which include the effects of faults [130]. Given (4.16), (4.40) and (4.41), sensor faults are guaranteed to be detected if there exists a $t^\star$ such that

$$\left|\varepsilon_F^s(t^\star)\right| - \overline{\varepsilon}_F^s(t^\star) > 2\overline{\varepsilon}_H^s(t^\star). \tag{4.42}$$

Condition (4.42) guarantees the violation of ARR $\mathcal{E}^s$ given in (4.37). The sensor fault effects ε_F^s and $\overline{\varepsilon}_F^s$ can be characterized taking into account the occurrence of:

- a local sensor fault $f^s(t)$ for $t \in [t_f^s, \min_{i\in\mathcal{N}}\{\mathrm{t}_f^{(i)}\})$,
- propagated sensor faults $f^{(i)}(t)$ for $t \in [\min_{i\in\mathcal{N}}\{\mathrm{t}_f^{(i)}\}, t_f^s)$ with $\max_{i\in\mathcal{N}}\{\mathrm{t}_f^{(i)}\} < t_f^s$
- both local $f^s(t)$ and propagated sensor faults $f^{(i)}(t)$ for $t \geq \max(t_f^s, \max_{i\in\mathcal{N}}\{\mathrm{t}_f^{(i)}\})$.

Lemma 5. *A sensor fault f^s affecting the temperature sensor $\mathcal{S}^s$ at the time instant t_f^s is guaranteed to be detected by $\mathcal{M}^s$, if there exists a time instant $t^\star \in (t_f^s, \min_{i\in\mathcal{N}}\{\mathrm{t}_f^{(i)}\})$ such that,*

$$2\overline{\varepsilon}_H^s(t^\star) < \left| f^s(t^\star) + \int_{t_f^s}^{t^\star} e^{(A^s-L^s)(t^\star-\tau)} \left(- L^s f^s(\tau) + \frac{U_{st,max}}{C_{st}} \left(P_s(y_H^s(\tau)) - P_s(y_H^s(\tau) + f^s(\tau))\right) u_{st}(\tau) \right.\right.$$
$$\left.\left. - \frac{a_{sz}}{C_{st}} \sum_{j\in\mathcal{N}} U_{i,max} u_i(\tau) f^s(\tau) \right) d\tau \right| - \int_{t_f^s}^{t^\star} \rho^s e^{-\zeta^s(t-\tau)} \left(\left(\overline{g}^s(y_H^s(\tau) + f^s(\tau)) - \overline{g}^s(y_H^s(\tau))\right) |u_{st}(\tau)| \right) d\tau, \tag{4.43}$$

where y_H^s is defined in (4.15).

Proof. Under healthy conditions the residual ε^s equals to ε_H^s defined in (4.14), where the state estimation error under healthy conditions $\varepsilon_{T,H}^s$ corresponds to the solution of (4.3), taking into account that $f^s(t) = 0$ and $f^{(i)}(t) = 0$ for all $i \in \mathcal{N}$ and $y^s(t) = y_H^s(t)$ where y_H^s is defined in (4.15); i.e.,

$$\varepsilon_{T,H}^s(t) = \varepsilon_{T,H}^s(0) e^{(A^s-L^s)t} + \int_0^t e^{(A^s-L^s)(t-\tau)} \left(r^s(\tau) + \frac{U_{st,max}}{C_{st}} \left(P_s(T_{st}(\tau)) - P_s(y_H^s(\tau))\right) u_{st}(\tau) \right.$$
$$\left. - L^s n^s(\tau) + \frac{a_{sz}}{C_{st}} \sum_{i\in\mathcal{N}} U_{i,max}(n^{(i)}(\tau) - n^s(\tau)) u^{(i)}(\tau) \right) d\tau. \tag{4.44}$$

where $\varepsilon_{T,H}^s(0) = \varepsilon_T^s(0)$. Assuming local sensor fault ($f^s(t) \neq 0$ and $f^{(i)}(t) = 0$ for all $i \in \mathcal{N}$), the state estimation error is given by the solution of (4.3) for $t \geq t_f^s$; i.e.,

$$\varepsilon_T^s(t) = \varepsilon_T^s(t_f^s) e^{(A^s-L^s)\left(t-t_f^s\right)} + \int_{t_f^s}^t e^{(A^s-L^s)(t-\tau)} \left(r^s(\tau) + \frac{U_{st,max}}{C_{st}} \left(P_s(T_{st}(\tau)) - P_s(y_H^s(\tau) + f^s(\tau))\right) u_{st}(\tau) \right.$$
$$\left. + \frac{a_{sz}}{C_{st}} \sum_{i\in\mathcal{N}} U_{i,max}(n^{(i)}(\tau) - n^s(\tau) - f^s(\tau)) u_i(\tau) - L^s n^s(\tau) - L^s f^s(\tau) \right) d\tau. \tag{4.45}$$

Based on the sensor output 2.32 and the fault model (2.67), $\varepsilon_T^s(t_f^s) = \varepsilon_{T,H}^s(t_f^s)$. By using (4.44) for $t = t_f^s$ in (4.45) it yields

$$\varepsilon_T^s(t) = \varepsilon_{T,H}^s(t) + \int_{t_f^s}^{t} e^{(A^s - L^s)(t-\tau)} \Bigg(- L^s f^s(\tau) + \frac{U_{st,max}}{C_{st}} \left(P_s(y_H^s(\tau)) - P_s(y_H^s(\tau) + f^s(\tau)) \right) u_{st}(\tau) - \frac{a_{sz}}{C_{st}} \sum_{i \in \mathcal{N}} U_{i,max} f^s(\tau) u_i(\tau) \Bigg) d\tau. \tag{4.46}$$

Combining (4.6), (4.14) and (4.40) result in

$$\varepsilon_F^s(t) = \varepsilon^s(t) - \varepsilon_H^s(t) = \varepsilon_T^s(t) - \varepsilon_{T,H}^s(t) + f^s(t) \tag{4.47}$$

By introducing (4.46) in (4.47), we obtain

$$\varepsilon_F^s(t) = f^s(t) + \int_{t_f^s}^{t} e^{(A^s - L^s)(t-\tau)} \Bigg(- L^s f^s(\tau) + \frac{U_{st,max}}{C_{st}} \left(P_s(y_H^s(\tau)) - P_s(y_H^s(\tau) + f^s(\tau)) \right) u_{st}(\tau) - \frac{a_{sz}}{C_{st}} \sum_{i \in \mathcal{N}} U_{i,max} f^s(\tau) u_i(\tau) \Bigg) d\tau. \tag{4.48}$$

The effects of sensor faults on the adaptive threshold can be determined using (4.17), (4.35) and (4.41) as

$$\overline{\varepsilon}_F^s(t) = \overline{\varepsilon}^s(t) - \overline{\varepsilon}_H^s(t) = \int_0^t \rho^s e^{-\zeta^s(t-\tau)} \left(\overline{g}^s(y_H^s(\tau) + f^s(\tau)) - \overline{g}^s(y_H^s(\tau)) \right) |u_{st}(\tau)| \, d\tau. \tag{4.49}$$

Based on the sensor output 2.32 and the fault model (2.67), $f^s(t) = 0$ for $t < t_f^s$ implying that $\int_0^{t_f^s} \rho^s e^{-\zeta^s(t-\tau)} \left(\overline{g}^s(y_H^s(\tau) + f^s(\tau)) - \overline{g}^s(y_H^s(\tau)) \right) |u_{st}(\tau)| \, d\tau = 0$. Thus (4.49) becomes

$$\overline{\varepsilon}_F^s(t) = \int_{t_f^s}^{t} \rho^s e^{-\zeta^s(t-\tau)} (\overline{g}^s(y_H^s(\tau) + f^s(\tau)) - \overline{g}^s(y_H^s(\tau))) \, |u_{st}(\tau)| \, d\tau. \tag{4.50}$$

Introducing (4.48) and (4.50) in (4.42) leads to (4.43). □

The conditions for guaranteeing the detection of (possibly multiple) propagated faults that affect the sensors located in the building zones by the agent $\mathcal{M}^s$ is analyzed in Lemma 6. It is worth noting that the propagated sensor faults $f^{(i)}$ can affect the residual ε^s defined through (4.3)-(4.5) and not the adaptive thresholds $\overline{\varepsilon}^s(t)$ defined in (4.35).

Lemma 6. *Sensor faults $f^{(i)}$ affecting the temperature sensors $\mathcal{S}^{(i)}$ in the building zones at the time instances $t_f^{(i)}$ are guaranteed to be detected by $\mathcal{M}^s$, if there exists a time instant $t^\star \in (\min_{i \in \mathcal{N}} \{t_f^{(i)}\}, t_f^s)$ with $\max_{i \in \mathcal{N}} \{t_f^{(i)}\} < t_f^s$ such that,*

$$2\overline{\varepsilon}_H^s(t^\star) < \left| \frac{a_{sz}}{C_{st}} \sum_{i \in \mathcal{N}} \int_{t_f^{(i)}}^{t^\star} e^{(A^s - L^s)(t^\star - \tau)} U_{i,max} f^{(i)}(\tau) u_i(\tau) d\tau \right|. \tag{4.51}$$

Proof. Under healthy conditions the residual ε^s equals to ε_H^s defined in (4.14), where the state estimation error under healthy conditions $\varepsilon_{T,H}^s$ is defined in (4.44). Let us consider two propagated sensor

faults in e.g. zone 1 and zone 2, where sensor fault $f^{(1)}$ occurs at $t_f^{(1)}$ and sensor fault $f^{(2)}$ occurs at $t_f^{(2)}$ with $t_f^{(1)} < t_f^{(2)}$. Based on the state estimation error dynamics given in (4.3), $\varepsilon_T^s(t)$ for $t \in [t_f^{(1)}, t_f^{(2)})$ is given by

$$\varepsilon_T^s(t) = \varepsilon_T^s(t_f^{(1)}) e^{(A^s - L^s)\left(t - t_f^{(1)}\right)} + \int_{t_f^{(1)}}^{t} e^{(A^s - L^s)(t-\tau)} \Bigg(r^s(\tau) + \frac{U_{st,max}}{C_{st}} \left(P_s(T_{st}(\tau)) - P_s(y_H^s(\tau)) \right) u_{st}(\tau) - L^s n^s(\tau) + \frac{a_{sz}}{C_{st}} \sum_{i \in \mathcal{N}} U_{i,max} (n^{(i)}(\tau) - n^s(\tau)) u_i(\tau) + \frac{a_{sz}}{C_{st}} U_{1,max} f^{(1)}(\tau) u_1(\tau) \Bigg) d\tau, \tag{4.52}$$

while for $t \geq t_f^{(2)}$ $\varepsilon_T^s(t)$ is expressed as

$$\varepsilon_T^s(t) = \varepsilon_T^s(t_f^{(2)}) e^{(A^s - L^s)\left(t - t_f^{(2)}\right)} + \int_{t_f^{(2)}}^{t} e^{(A^s - L^s)(t-\tau)} \Bigg(r^s(\tau) + \frac{U_{st,max}}{C_{st}} \left(P_s(T_{st}(\tau)) - P_s(y_H^s(\tau)) \right) u_{st}(\tau) + \frac{a_{sz}}{C_{st}} \sum_{i \in \mathcal{N}} U_{i,max} (n^{(i)}(\tau) - n^s(\tau)) u_i(\tau) - L^s n^s(\tau) + \frac{a_{sz}}{C_{st}} (U_{1,max} f^{(1)}(\tau) u_1(\tau) + U_{2,max} f^{(2)}(\tau) u_2(\tau)) \Bigg) d\tau. \tag{4.53}$$

By using (4.44) for $t = t_f^{(2)}$ in (4.52), and then using (4.52) for $t = t_f^{(2)}$ in (4.53) it yields

$$\varepsilon_T^s(t) = \varepsilon_{T,H}^s(t) + \frac{a_{sz}}{C_{st}} \Bigg(\int_{t_f^{(1)}}^{t} e^{(A^s - L^s)(t-\tau)} U_{1,max} f^{(1)}(\tau) u_1(\tau) d\tau + \int_{t_f^{(2)}}^{t} e^{(A^s - L^s)(t-\tau)} U_{2,max} f^{(2)}(\tau) u_2(\tau) d\tau \Bigg). \tag{4.54}$$

Equation (4.54) is also valid in the case that $t_f^{(2)} < t_f^{(1)}$. If we perform the same mathematical manipulations, we can obtain that the state estimation error $\varepsilon_T^s(t)$ for $t \in (\min_{i \in \mathcal{N}} \{t_f^{(i)}\}, t_f^s)$ with $\max_{i \in \mathcal{N}} \{t_f^{(i)}\} < t_f^s$ is described by

$$\varepsilon_T^s(t) = \varepsilon_{T,H}^s(t) + \frac{a_{sz}}{C_{st}} \sum_{i \in \mathcal{N}} \int_{t_f^{(i)}}^{t} e^{(A^s - L^s)(t-\tau)} U_{i,max} f^{(i)}(\tau) u_i(\tau) d\tau. \tag{4.55}$$

By combining (4.47) with $f^s = 0$ and (4.55), the effects of propagated sensor faults on the residual are described by

$$\varepsilon_F^s(t) = \frac{a_{sz}}{C_{st}} \sum_{i \in \mathcal{N}} \int_{t_f^{(i)}}^{t} e^{(A^s - L^s)(t-\tau)} U_{i,max} f^{(i)}(\tau) u_i(\tau) d\tau. \tag{4.56}$$

Using (4.56) in (4.42) and given that $\overline{\varepsilon}_F^s(t) = 0$ leads to (4.51). □

Lemma 7. *The sensor faults f^s and $f^{(i)}$ that occur at the time instants t_f^s and $t_f^{(i)}$, respectively are*

guaranteed to be detected by $\mathcal{M}^s$, if there exist a time instant $t^\star \geq \max(t_f^s, \max_{i\in\mathcal{N}}\{\mathrm{t}_f^{(i)}\})$ such that,

$$2\overline{\varepsilon}_H^s(t^\star) < \Bigg| f^s(t^\star) + \int_{\max(t_f^s, \max_{i\in\mathcal{N}}\{\mathrm{t}_f^{(i)}\})}^{t^\star} e^{(A^s-L^s)(t^\star-\tau)} \Bigg(-L^s f^s(\tau) + \frac{U_{st,max}\,(P_{max}-1)}{C_{st}\Delta T_{max}} u_{st}(\tau) f^s(\tau) + \frac{a_{sz}}{C_{st}} \sum_{j\in\mathcal{N}} U_{i,max} u_i(\tau) \left(f^{(i)}(\tau) - f^s(\tau) \right) \Bigg) d\tau \Bigg| - \int_{\max(t_f^s, \max_{i\in\mathcal{N}}\{\mathrm{t}_f^{(i)}\})}^{t^\star} \rho^s e^{-\zeta^s(t-\tau)} \Bigg(\left(\overline{g}^s(y_H^s(\tau) + f^s(\tau)) - \overline{g}^s(y_H^s(\tau)) \right) |u_{st}(\tau)| \Bigg) d\tau. \tag{4.57}$$

The proof of Lemma 7 is not provided, but it can be obtained similarly as in Lemmas 5–6. Lemma 5–7 provide certain conditions that characterize analytically the class of local and propagated sensor faults that are guaranteed to be detectable by the agent $\mathcal{M}^s$.

Sensor Fault Detectability Analysis of agent $\mathcal{M}^{(i)}$

The residual $\varepsilon^{(i)}$ given in (4.7) (or (4.13)) and the corresponding adaptive threshold $\overline{\varepsilon}^{(i)}$ of (4.36) are sensitive to any faults that may occur in the building zone i (local sensor fault) at the time instant $t_f^{(i)}$, or in the sensor of the storage tank at the time instant t_f^s, or in the $|\mathcal{K}_i|$ neighboring zones (propagated sensor faults) that may occur at the time instances $t_f^{(j)}$, $j \in \mathcal{K}_i$. Under faulty conditions, $\varepsilon^{(i)}$ and $\overline{\varepsilon}^{(i)}$ can be expressed as

$$\varepsilon^{(i)}(t) = \varepsilon_H^{(i)}(t) + \varepsilon_F^{(i)}(t), \tag{4.58}$$

$$\overline{\varepsilon}^{(i)}(t) = \overline{\varepsilon}_H^{(i)}(t) + \overline{\varepsilon}_F^{(i)}(t), \tag{4.59}$$

where $\varepsilon_H^{(i)}$ (defined in (4.13)) and $\overline{\varepsilon}_H^{(i)}$ (defined in (4.21)) are the healthy parts of $\varepsilon^{(i)}$ and $\overline{\varepsilon}^{(i)}$, respectively, and $\varepsilon_F^{(i)}$ and $\overline{\varepsilon}_F^{(i)}$ are the faulty parts of $\varepsilon^{(i)}$ and $\overline{\varepsilon}^{(i)}$, which include the effects of faults. Given (4.23), (4.58) and (4.59), sensor faults are guaranteed to be detected if there exists a time instant $t^\star$ such that

$$\left| \varepsilon_F^{(i)}(t^\star) \right| - \overline{\varepsilon}_F^{(i)}(t^\star) > 2\overline{\varepsilon}_H^{(i)}(t^\star). \tag{4.60}$$

Condition (4.60) guarantees the violation of ARR $\mathcal{E}^{(i)}$ given in (4.38). The sensor fault effects $\varepsilon_F^{(i)}$ and $\overline{\varepsilon}_F^{(i)}$ can be characterized taking into account the occurrence of:

- a local sensor fault $f^{(i)}(t)$ for $t \in [t_f^{(i)}, \min(\min_{j\in\mathcal{K}_i}\{\mathrm{t}_f^{(i)}\}, t_f^s))$,
- propagated sensor faults $f^{(j)}(t)$ for $t \in [\min_{j\in\mathcal{K}_i}\{\mathrm{t}_f^{(i)}\}, t_f^s)$ with $\max(\max_{j\in\mathcal{K}_i}\{\mathrm{t}_f^{(j)}\}, t_f^s) < t_f^{(i)}$
- both local $f^{(i)}(t)$ and propagated sensor faults $f^s(t)$, $f^{(j)}(t)$ for $t \geq \max(t_f^{(j)}, t_f^s, \max_{i\in\mathcal{N}}\{\mathrm{t}_f^{(i)}\})$.

The proofs of the following Lemmas 8–10 are not given, but they can be obtained similarly as the proofs of Lemmas 5–6.

Lemma 8. *The sensor fault $f^{(i)}$ affecting the temperature sensor $\mathcal{S}^{(i)}$ at the time instant $t_f^{(i)}$ is guaranteed to be detected by $\mathcal{M}^{(i)}$ under worst-case conditions, if there exist a time instant $t^\star \in [t_f^{(i)}, \min(\min_{j\in\mathcal{K}_i}\{\mathrm{t}_f^{(i)}\}, t_f^s))$ such that,*

$$2\overline{\varepsilon}_H^{(i)}(t^\star) < \Bigg| f^{(i)}(t^\star) + \int_{t_f^{(i)}}^{t^\star} e^{(A^{(i)}-L^{(i)})(t-\tau)}\Bigg(\sigma^{(i)} f^{(i)}(\tau)u_i(\tau) + p^{(i)}\sum_{j\in\mathcal{K}_i} A_{d_{ij}}\Big(\mu^{(i)}(y_H^{(i)}(\tau), y_H^{(j)}(\tau))$$
$$-\mu^{(i)}(y_H^{(i)}(\tau) + f^{(i)}(\tau), y_H^{(j)}(\tau))\Big) - L^{(i)} f^{(i)}(\tau)\Bigg)d\tau\Bigg|$$
$$- \int_{t_f^{(i)}}^{t^\star} \rho^{(i)} e^{-\zeta^{(i)}(t-\tau)} p^{(i)} \sum_{j\in\mathcal{K}_i} A_{d_{i,j}} \times \Big(\overline{\mu}^{(i)}(y_H^{(i)}(\tau) + f^{(i)}(\tau), y_H^{(j)}(\tau)) - \overline{\mu}^{(i)}(y_H^{(i)}(\tau), y_H^{(j)}(\tau))\Big)d\tau.$$

Lemma 9. *The sensor faults f^s and $f^{(j)}$ occur at the time instants t_f^s and $t_f^{(j)}$, respectively, are guaranteed to be detected by $\mathcal{M}^{(i)}$ under worst-case conditions, if there exist a time instant $t^\star \in [\min_{j\in\mathcal{K}_i}\{\mathrm{t}_f^{(i)}\}, t_f^s)$ with $\max(\max_{j\in\mathcal{K}_i}\{\mathrm{t}_f^{(j)}\}, t_f^s) < t_f^{(i)}$ such that,*

$$2\overline{\varepsilon}_H^{(i)}(t^\star) < \Bigg| \int_{\min_{j\in\mathcal{K}_i}\{\mathrm{t}_f^{(i)}\}}^{t^\star} e^{(A^{(i)}-L^{(i)})(t-\tau)}\Bigg(- \sigma^{(i)} f^s(\tau)u_i(\tau) + p^{(i)}\sum_{j\in\mathcal{K}_i} A_{d_{ij}}\Big(\mu^{(i)}(y_H^{(i)}(\tau), y_H^{(j)}(\tau))$$
$$-\mu^{(i)}(y_H^{(i)}(\tau), y_H^{(j)}(\tau) + f^{(j)}(\tau))\Big)$$
$$+ \sum_{j\in\mathcal{K}_i}\frac{a_{z_{ij}}}{C_{z_i}} f^{(j)}(\tau)\Bigg)d\tau\Bigg| - \int_{\min_{j\in\mathcal{K}_i}\{\mathrm{t}_f^{(i)}\}}^{t^\star} \rho^{(i)} e^{-\zeta^{(i)}(t-\tau)} p^{(i)}$$
$$\times \sum_{j\in\mathcal{K}_i} A_{d_{i,j}}\Big(\overline{\mu}^{(i)}(y_H^{(i)}(\tau), y_H^{(j)}(\tau) + f^{(j)}(\tau)) - \overline{\mu}^{(i)}(y_H^{(i)}(\tau), y_H^{(j)}(\tau))\Big)d\tau.$$

Lemma 10. *The sensor faults $f^{(i)}$, f^s and $f^{(j)}$ occur at the time instants $t_f^{(i)}$, t_f^s and $t_f^{(j)}$, respectively, are guaranteed to be detected by $\mathcal{M}^{(i)}$ under worst-case conditions, if there exist a time instant $t^\star \geq \max(t_f^{(j)}, t_f^s, \max_{i\in\mathcal{N}}\{\mathrm{t}_f^{(i)}\})$ such that,*

$$2\overline{\varepsilon}_H^{(i)}(t^\star) < \Bigg| f^{(i)}(t^\star) + \int_{\max(t_f^{(j)}, t_f^s, \max_{i\in\mathcal{N}}\{\mathrm{t}_f^{(i)}\})}^{t^\star} e^{(A^{(i)}-L^{(i)})(t-\tau)} \times \Bigg(\sigma^{(i)}(f^{(i)}(\tau) - f^s(\tau))u_i(\tau) + p^{(i)}\sum_{j\in\mathcal{K}_i} A_{d_{ij}}$$
$$\times\Big(\mu^{(i)}(y_H^{(i)}(\tau), y_H^{(j)}(\tau)) - \mu^{(i)}(y_H^{(i)}(\tau) + f^{(i)}(\tau), y_H^{(j)}(\tau) + f^{(j)}(\tau))\Big)$$
$$+ \sum_{j\in\mathcal{K}_i}\frac{a_{z_{ij}}}{C_{z_i}} f^{(j)}(\tau) - L^{(i)} f^{(i)}(\tau)\Bigg)d\tau\Bigg| - \int_{\max(t_f^{(j)}, t_f^s, \max_{i\in\mathcal{N}}\{\mathrm{t}_f^{(i)}\})}^{t^\star} \rho^{(i)} e^{-\zeta^{(i)}(t-\tau)}$$
$$\times p^{(i)}\sum_{j\in\mathcal{K}_i} A_{d_{i,j}}\Big(\overline{\mu}^{(i)}(y_H^{(i)}(\tau) + f^{(i)}(\tau), y_H^{(j)}(\tau) + f^{(j)}(\tau)) - \overline{\mu}^{(i)}(y_H^{(i)}(\tau), y_H^{(j)}(\tau))\Big)d\tau.$$

Lemmas 8–10 provide certain conditions that characterize analytically the class of local and propagated sensor faults that are guaranteed to be detectable by the agent $\mathcal{M}^{(i)}$.

Remark: The detectability conditions obtained in Lemmas 5–7 and 8–10, give an indication of the class of local and propagated sensor faults that are guaranteed to be detectable by the agents $\mathcal{M}^s$ and $\mathcal{M}^{(i)}$, respectively, based on the system's available parameters and proposed algorithm's design parameters. However, due to the non-linear and switching terms in systems' dynamics, the aforementioned conditions depend on real-time signals; thus, obtaining off-line predefined, fixed conditions is not possible.

The above issue can be addressed by creating a Monte-Carlo analysis, examining the detectability performance by varying the sensor noise, modeling uncertainty and observer design parameters (see simulation-based analysis presented in the Section 7.4.)

4.4.3 Scalability analysis

This subsection provides a discussion on the scalability of the proposed distributed sensor fault diagnosis technique in the case that the multi-zone HVAC system is enlarged with respect to the number of building zones. For example, a new building zone may be constructed, whose temperature is monitored by a sensor and controlled by a fan-coil unit. In the following analysis we consider the aforementioned example. A similar discussion can be considered for the case that some buildings zones are removed.

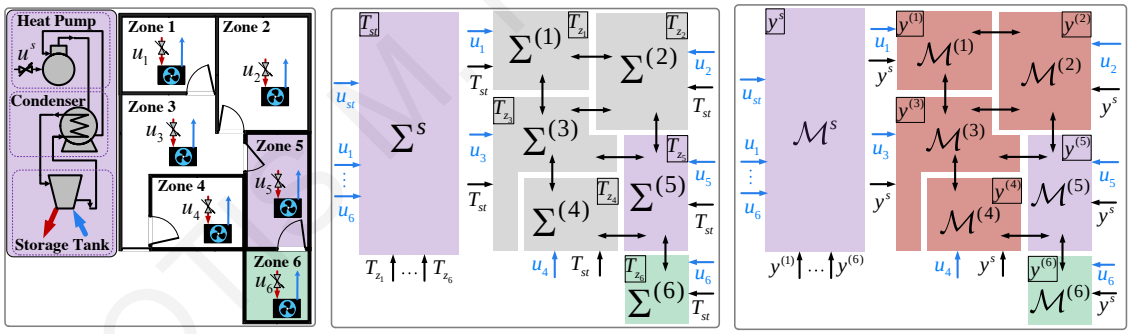

(a) (b) (c)

Figure 4.3: Reconfiguration of the distributed sensor fault diagnosis architecture for the enlarged HVAC system. The 6-th zone (green floor) is added to (a) which is connected to the 5-st zone. In (b) and (c) the reconfiguration of the network of interconnected subsystems and the reconfiguration of the sensor fault diagnosis agents are presented, respectively. Green color denotes the added components/subsystems/agents while the purple color denotes the modified components/subsystems/agents.

Consider that a 6-th zone is constructed next to the 5-th zone of the HVAC system shown in Fig. 4.3a, while there is a door (and walls) connecting the two zones. The 6-th zone is comprised of a temperature sensor and a fan-coil unit connected to the central electromechanical part. Given the architectural/thermal parameters and the manufacturing properties of the fan-coil unit installed in the new zone, the subsystem $\Sigma^{(6)}$ (green box in Fig. 4.3b) is defined according to (2.26) with $i = 6$

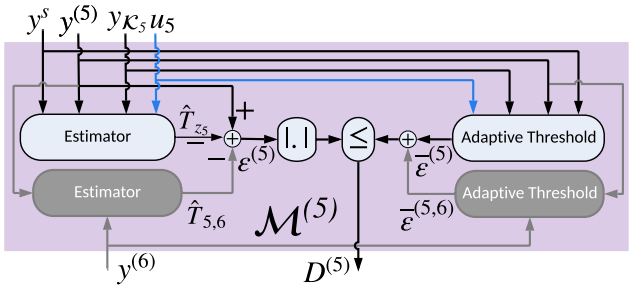

Figure 4.4: Reconfigured agent $\mathcal{M}^{(5)}$. The gray boxes and arrows denote the plugin blocks and signals added to the existing agent $\mathcal{M}^{(5)}$ at $t \geq t_{en}$, with $y_{\mathcal{K}_5} = \{y^{(2)}, y^{(3)}, y^{(4)}\}$.

and $\mathcal{K}_6 = \{5\}$. The equations in Table 4.3 describe the modification of the existing HVAC model according to the physical variation of the HVAC system for $t < t_{en}$, where t_{en} is the time at which the HVAC system is enlarged. Note that χ^s and $\chi^{(5)}$ collect the dynamic terms of the electromechanical part and the 5-th zone, respectively. The agent $\mathcal{M}^{(6)}$ is designed based on (4.7), (4.8), (4.36) and

Table 4.3: Model variations after the enlargement of the HVAC system.

Σ^s	$\dot{T}_{st} = \chi^s(T_{st}, T_z, u) + \frac{a_{sz}}{C_{st}} U_{6,max}(T_{st} - T_{z_6})u_6$
$\Sigma^{(5)}, \mathcal{K}_5 = \{2,3,4\}$	$\dot{T}_{z_5} = \chi^{(5)}(T_{z_5}, T_{st}, T_{\mathcal{K}_5}, u_5) + \frac{1}{C_{z_1}} a_{z_{5,6}} T_{z_6} + p^{(5)} A_{d_{5,6}} \mu^{(5)}(T_{z_5}, T_{z_6})$

Table 4.4: Design plug-in blocks to the Sensor Fault Diagnosis scheme.

$\mathcal{M}^s$	$\mathcal{E}^s: \ \lvert\varepsilon^s\rvert \leq \overline{\varepsilon}^s + \overline{\varepsilon}^{s(6)}$
	$\varepsilon^s = y^s - \hat{T}_{st} - \hat{T}_{st(6)}$
	$\dot{\hat{T}}_{st(6)} = (A^s - L^s)\hat{T}_{st(6)} + \frac{a_{sz}}{C_{st}} U_{6,max}(y^s - y^{(6)})u_6,$
	$\hat{T}_{st(6)}(t_{en}) = 0$
	$\overline{\varepsilon}^{s(6)} = \int_{t_e}^{t} \rho^s e^{-\zeta^s(t-\tau)} \frac{a_{sz}}{C_{st}} U_{6,max}(\overline{n}^s + \overline{n}^{(6)}) \lvert u_6(\tau)\rvert$
$\mathcal{M}^{(5)}$	$\mathcal{E}^{(5)}: \ \left\lvert\varepsilon^{(5)}\right\rvert \leq \overline{\varepsilon}^{(5)} + \overline{\varepsilon}^{(5,6)}$
	$\varepsilon^{(5)} = y^{(5)} - \hat{T}_{z_5} - \hat{T}_{5,6}$
	$\dot{\hat{T}}_{5,6} = \left(A^{(5)} - L^{(5)}\right)\hat{T}_{5,6} + \frac{1}{C_{z_5}} a_{z_{5,6}} y^{(6)} + p^{(5)} A_{d_{5,6}} \mu^{(5)}(y^{(5)}, y^{(6)}),$
	$\hat{T}_{5,6}(t_{en}) = 0$
	$\overline{\varepsilon}^{(5,6)} = \int_{t_e}^{t} \rho^{(5)} e^{-\zeta^{(5)}(t-\tau)} p^{(5)} A_{d_{5,6}} \overline{\mu}^{(5)}(y^{(5)}, y^{(6)}) + \frac{\rho^{(5)}(1-e^{-\zeta^{(5)}t})}{\zeta^{(5)}} \frac{a_{z_{5,6}}}{C_{z_5}} \overline{n}^{(6)}$

(4.38). Only the agents $\mathcal{M}^s$ and $\mathcal{M}^{(5)}$, presented with purple boxes in Fig. 4.3c, should be modified

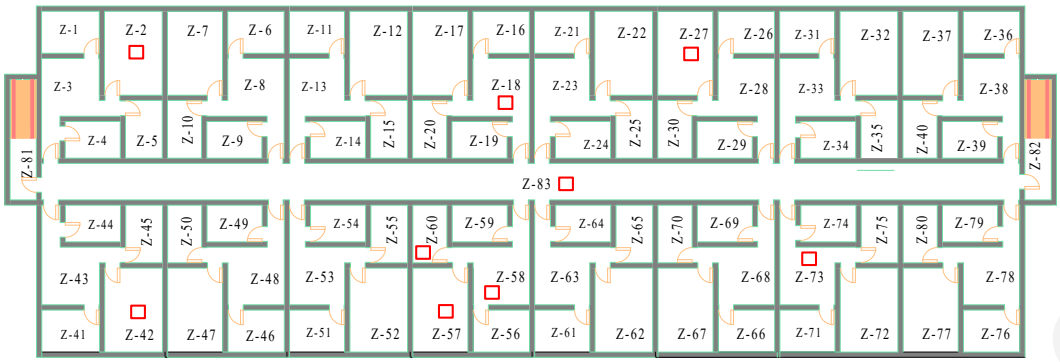

Figure 4.5: Down-view of a 83-zone building. Red squared boxes denote the zones with the faulty sensors.

Table 4.5: Design parameters of the 83-zone HVAC system: zones 1–5 (1^{st} apartment), 81 (left stair hall) and 83 (corridor).

Parameter	Value	Unit
$\{C_{st}, C_{z_1}, C_{z_2}, C_{z_3}, C_{z_4}, C_{z_5}, C_{z_{81}}, C_{z_{83}}\}$	{ 8370, 29.96, 57.71, 54.38, 26.63, 26.63, 3819, 30557 }	kJ/ ^{o}C
$\{U_{1,max}, U_{2,max}, U_{3,max}, U_{4,max}, U_{5,max}, U_{81,max}, U_{83,max}\}$	{ 3700, 7125.9, 6714.8, 3700, 3700, 7400, 59200 }	kg/h
$\{a_{z_1}, a_{z_2}, a_{z_3}, a_{z_4}, a_{z_5}, a_{z_{81}}, a_{z_{83}}\}$	740	kJ/h ^{o}C
$\{a_{z_{1,2}}, a_{z_{1,3}}, a_{z_{2,3}}, a_{z_{2,5}}, a_{z_{3,4}}, a_{z_{3,5}}\}$	50	kJ/h^{o}C
$\{A_{w_1}, A_{w_2}, A_{w_3}, A_{w_4}, A_{w_5}, A_{w_{81}}, A_{w_{83}}\}$	{ 31.21, 43.69, 54.09, 29.72, 29.72, 45.74, 297.24 }	m^2
$\{A_{d_{1,3}}, A_{d_{2,3}}, A_{d_{3,4}}, A_{d_{3,5}}, A_{d_{3,81}}, A_{d_{81,83}}\}$	1.951	m^2

based on a plugin process shown in Table 4.4. The existing estimator and adaptive threshold of these agents ($\mathcal{M}^s$ and $\mathcal{M}^{(5)}$) are not modified but some new plug-in blocks are added. For agent $\mathcal{M}^{(5)}$, the plug-in blocks are illustrated with gray color in Fig. 4.4. This allows to scale the sensor fault diagnosis scheme even without re-designing any agents of the 5-th zone HVAC system. The scalability property, which is possible due to the distributed monitoring architecture of the proposed scheme, is important in large-scale systems since it allows the evolution of the HVAC with additional zones without having to redesign the overall system.

4.5 Simulation Results

The objective of this Section is the evaluation of the proposed distributed fault diagnosis method applied to a large-scale building. Let us consider a 83-zone HVAC system whose down-view is presented in Fig. 4.5. Table 4.5 provides a list of parameters for the 83-zone HVAC system. As shown in Fig. 4.5 the building consists of 16 apartments (5-zones each), 2 stair halls and 1 corridor. The structural properties of each apartment are the same, hence the Table 4.5 contains the parameters of one apartment (i.e., zone 1–5), one stair hall (i.e., zone 81) and the corridor (i.e., zone 83). The remainder parameters of the 83-zone HVAC system are: $a_{st} = 12$ kJ/kg^{o}C, $a_{sz} = 0.6$ kJ/kg^{o}C, $U_{st,max} = 27.36 \times 10^5$ kJ/^{o}C, $P_{max} = 3.5$, $\Delta T_{max} = 45$ ^{o}C, $h = 8.26$ W/m^{2o}C, $T_{pl} = 20$ ^{o}C, $T_o = 5$ ^{o}C, $T_{amb} = 5$ ^{o}C and $T_{i1} = 10$ ^{o}C, $i \in \{1, \ldots, 83\}$. Moreover, the specific heat capacity of air at constant pressure is

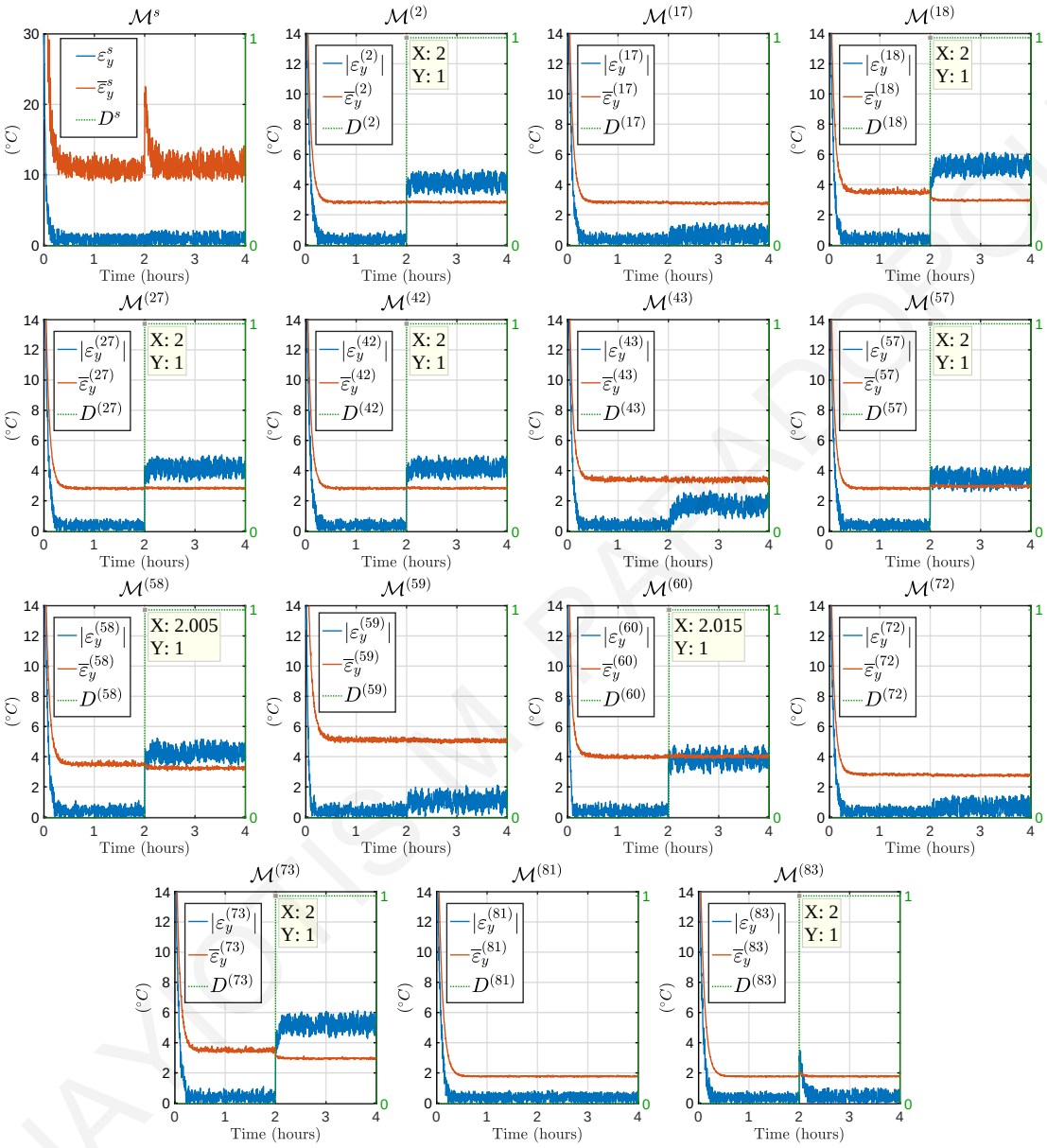

Figure 4.6: ARRs of agents $\mathcal{M}^s$ and $\mathcal{M}^{(j)}$, $j \in M$. The residuals ε^s and $\varepsilon^{(j)}$ (blue line), adaptive thresholds $\overline{\varepsilon}^s$ and $\overline{\varepsilon}^{(j)}$ (red line) and boolean decision signals D^s and $D^{(j)}$ (green dotted line) for $j \in M$ are presented.

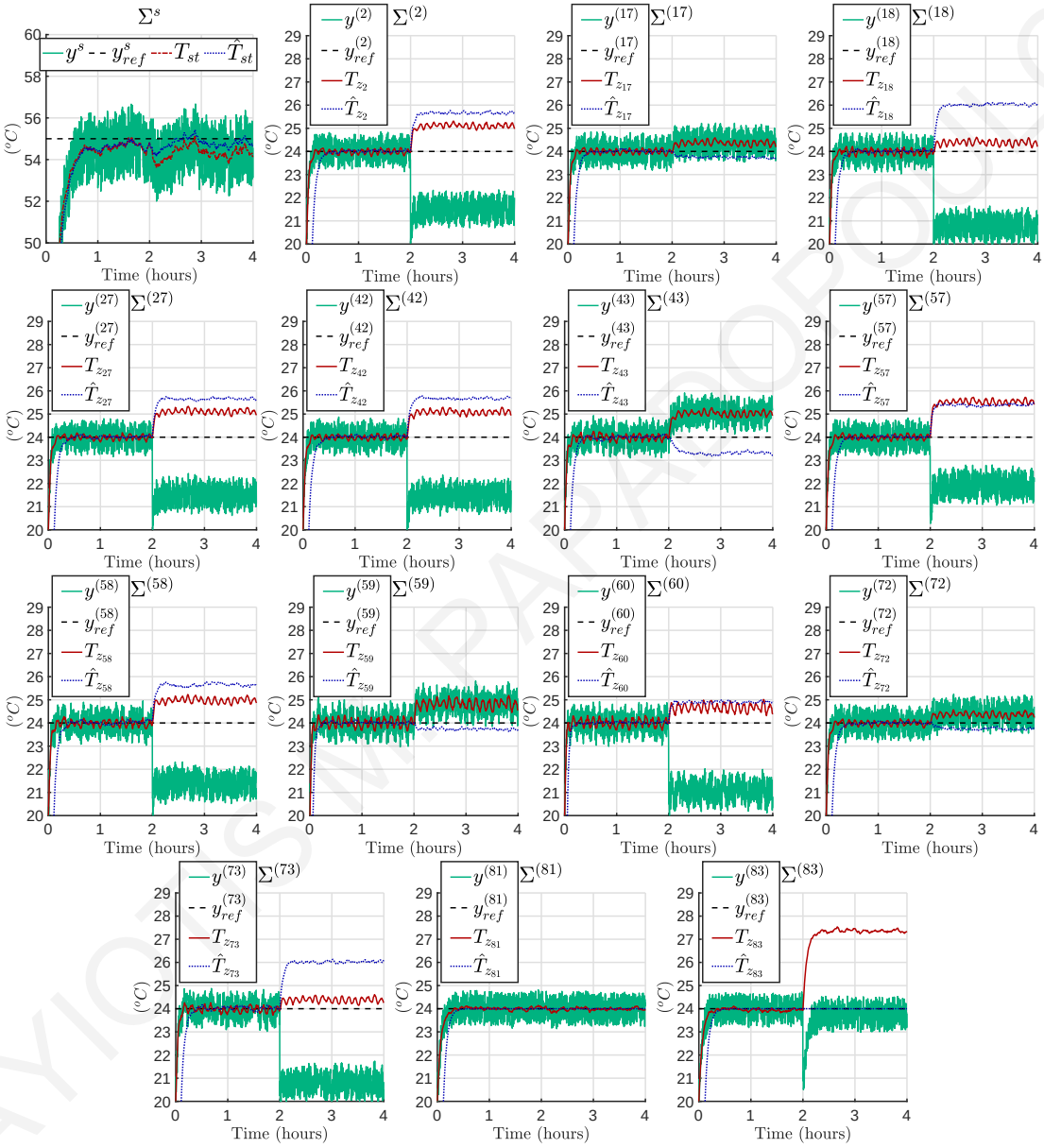

Figure 4.7: Temperature responses for subsystems Σ^s and $\Sigma^{(j)}$ for all $j \in M$. The temperature reference points y^s_{ref}, $y^{(j)}_{ref}$ (black dashed line), the sensor measurements y^s, $y^{(j)}$ (green solid line), the temperatures T_{st}, T_{z_j} (red dashed-doted line) and the estimations $\hat{T}_{st}$, $\hat{T}_{z_j}$ (blue dotted line) of subsystems Σ^s and $\Sigma^{(j)}$ for all $j \in M$.

$C_p = 1.004$ kJ/kgK, the specific heat capacity of air at constant volume is $C_v = 0.717$ kJ/kgK, and the air density is $\rho_{air} = 1.225$ kg/m^3. The modeling uncertainty associated with each subsystem is modeled as $r^s(t) = 5\%T_{pl}\sin(0.1t)$ ^{o}C and $r^{(i)}(t) = 5\%T_{amb}\sin(0.1t)$ ^{o}C, $i \in \{1,\ldots,83\}$. For simulation purposes, the noise corrupting the sensor output is simulated by a uniform random variable with $n^s(t) = [-3\%y^s_{ref}, 3\%y^s_{ref}]$ and $n^{(i)}(t) = [-3\%y^{(i)}_{ref}, 3\%y^{(i)}_{ref}]$, where y^s_{ref} and $y^{(i)}_{ref}$ are the set points of temperatures selected as $y^s_{ref} = 55$ ^{o}C and $y^{(i)}_{ref} = 24$ ^{o}C, $i \in \mathcal{N} = \{1,\ldots,83\}$. The design parameters of the fault diagnosis methodology are selected as follows: $L^s = 5$, $\rho^s = 1$, $\zeta^s = 40$, $L^{(i)} = 5$, for all $i \in \mathcal{N}$, $\rho^{(j)} = 1.1$, $\zeta^{(j)} = 22$, $j \in D = \{i|5i, i \in \{1,\ldots,16\}\}$, $\zeta^{(j)} = 15$, $j \in \mathcal{N} \setminus \{D \cup \{81,82,83\}\}$ and $L^{(81)} = L^{(82)} = L^{(83)} = 15$, $\rho^{(81)} = \rho^{(82)} = \rho^{(83)} = 1.1$, $\zeta^{(81)} = \zeta^{(82)} = \zeta^{(83)} = 12$. The 83-zone HVAC system is simulated for 4 hours with initial conditions $T_{st}(0) = 30$ ^{o}C and $T_{z_i}(0) = 22$ ^{o}C, $i \in \{1,\ldots,83\}$ and a single fault scenario is executed with multiple simultaneous sensor faults such as $f^{(j)}(t^{(j)}_f) = -15\%y^{(j)}_{ref}$ at $t^{(j)} = 2h$, $j \in \mathcal{J} = \{2,18,27,42,57,58,60,73,83\}$, where $\mathcal{J}$ contains the indices of the faulty temperature sensors. The zones with the faulty sensors are indicated with a red square in Fig. 4.5.

In Fig. 4.6 the ARRs of the sensor fault diagnosis agents $\mathcal{M}^s$ and $\mathcal{M}^{(j)}$, $j \in M$, are presented, where M is the set of indices given by

$$M = \{2,17,18,27,42,43,57,58,59,60,72,73,81,83\}.$$

Note that due to space limitation we have not included the results of all 83 agents. Specifically, each plot of Fig. 4.6 contains the residuals ε^s, $\varepsilon^{(j)}$, the adaptive thresholds $\bar{\varepsilon}^s$, $\bar{\varepsilon}^{(j)}$ and the decision detection signals D^s, $D^{(j)}$, $j \in M$. Note that sensor fault diagnosis agents $\mathcal{M}^{(2)}$, $\mathcal{M}^{(18)}$, $\mathcal{M}^{(27)}$, $\mathcal{M}^{(42)}$, $\mathcal{M}^{(57)}$, $\mathcal{M}^{(58)}$, $\mathcal{M}^{(60)}$, $\mathcal{M}^{(73)}$ and $\mathcal{M}^{(83)}$ detected the corresponding local sensor faults, while the remainder agents $\mathcal{M}^s$ and $\mathcal{M}^{(j)}$, $j \in \mathcal{N} \setminus \mathcal{J}$ do not detect any sensor fault. From Fig. 4.6 it can be noticed that the adaptive threshold in (4.35) is affected by the local sensor faults, while the adaptive thresholds in (4.36) are affected by both local and neighboring sensor faults.

Every agent that detects sensor fault activates the isolation process (see Section 4.3.3). For example, for the sensor fault isolation process executed by the agent $\mathcal{M}^{(60)}$ the sensor fault signature matrix $F^{(60)}$ is designed and a part of it is presented in Table 4.6. The observed pattern $\Phi^{(60)}$ at $t = 2.015$ h is

$$\begin{aligned}\Phi^{(60)}(2.015) =& [D^s, D^{(60)}, D^{(55)}, D^{(57)}, D^{(58)}, D^{(59)}, D^{(83)}]\\ =& [0,1,0,1,1,0,1],\end{aligned} \tag{4.61}$$

and is compared to all theoretical patterns given by the columns of the sensor fault signature matrix $F^{(60)}$ and the agent $\mathcal{M}^{(60)}$ contracts the diagnosis set $\Upsilon^{(60)}$

$$\begin{aligned}\Upsilon^{(60)} =& \{f^{(60)}, f^{(58)}, f^{(60,57)}, f^{(60,78)}, f^{(60,83)}, f^{(57,58)}, f^{(57,83)}, f^{(58,83)}, f^{(60,57,58)}, f^{(60,57,83)},\\ & f^{(60,58,83)}, f^{(57,58,83)}, f^{(60,57,58,83)}\},\end{aligned} \tag{4.62}$$

where $f^{(i,j)}$ represents $f^{(i,j)} = \{f^{(i)}, f^{(j)}\}$. Note that $\mathcal{M}^{(60)}$ can be affected by $2^{|\mathcal{K}_{60}|+2} - 1 = 127$ combinations of sensor faults, however the diagnosis set $\Upsilon^{(60)}$ narrows down the combinations to 13.

Table 4.6: The sensor fault signature matrix of the agent $\mathcal{M}^{(60)}$

	f^s	$f^{(60)}$	$f^{(55)}$	$f^{(57)}$	$f^{(58)}$	$f^{(59)}$	$f^{(83)}$	$f^{(60,57,58,83)}$
$\mathcal{E}^s$	1	*	*	*	*	*	*	*
$\mathcal{E}^{(60)}$	*	1	*	*	*	*	*	1
$\mathcal{E}^{(55)}$	*	*	1	0	0	0	*	*
$\mathcal{E}^{(57)}$	*	*	0	1	*	0	0	1
$\mathcal{E}^{(58)}$	*	*	0	*	1	*	*	1
$\mathcal{E}^{(59)}$	*	*	0	0	*	1	*	*
$\mathcal{E}^{(83)}$	*	*	*	0	*	*	1	1

Fig. 8.3 presents the reference points y^s_{ref}, $y^{(j)}_{ref}$ (black dashed line), the sensor measurements y^s, $y^{(j)}$ (green solid line), the actual temperatures T_{st}, T_{z_j} (red dashed-doted line) and the estimations $\hat{T}_{st}$, $\hat{T}_{z_j}$ (blue dotted line) of the subsystems Σ^s, $\Sigma^{(j)}$, $j \in M$, respectively. It is noted that for those subsystems that the sensor fault occurs locally (e.g., $f^{(1)}$ is the local sensor fault of $\Sigma^{(1)}$) the actual temperature (red dashed-dotted line) deviates from their corresponding reference point (black dashed line). Furthermore, it can be observed that also some zones with healthy local sensor are affected by sensor faults occurring in sensors of neighboring subsystems. For example, the temperature in subsystems $\Sigma^{(17)}$, $\Sigma^{(43)}$ and $\Sigma^{(59)}$ deviate from their corresponding reference point although there is no local sensor fault. This is due to the distributed control scheme that is implemented, where each controller aggregates local and neighboring sensor measurements in order to obtain the local control input, thus the temperature of a zone can be affected also by neighboring sensor faults. Also it is worth mentioning that the corresponding neighboring monitoring agents of the affected subsystems (i.e., $\Sigma^{(17)}$, $\Sigma^{(43)}$, $\Sigma^{(59)}$) as illustrated in Fig. 4.6 do not detect the sensor faults occurred in their neighboring subsystems (i.e., Σ^s, $\Sigma^{(j)}$, $j \in M$). This is due to the fact that the ARR of each distributed sensor fault diagnosis agent is more sensitive to the occurrence of the local sensor fault and less sensitive to the occurrence of a propagated sensor fault. Further, we can observe that even if the actual temperatures of $\Sigma^{(17)}$, $\Sigma^{(43)}$, $\Sigma^{(59)}$ are affected by neighboring faults (i.e., do not track their corresponding reference temperature), both the estimation and measurements of the temperatures are close to the actual temperature. We may infer that the residuals of the neighboring agents are not severely affected from propagated sensor faults, and thus it is more possible to detect a local sensor fault that to detect a sensor fault occurred in a neighboring subsystem. To conclude, the design of the proposed methodology allows to detect and isolate sensor faults even if the use of a distributed control scheme is affected by the

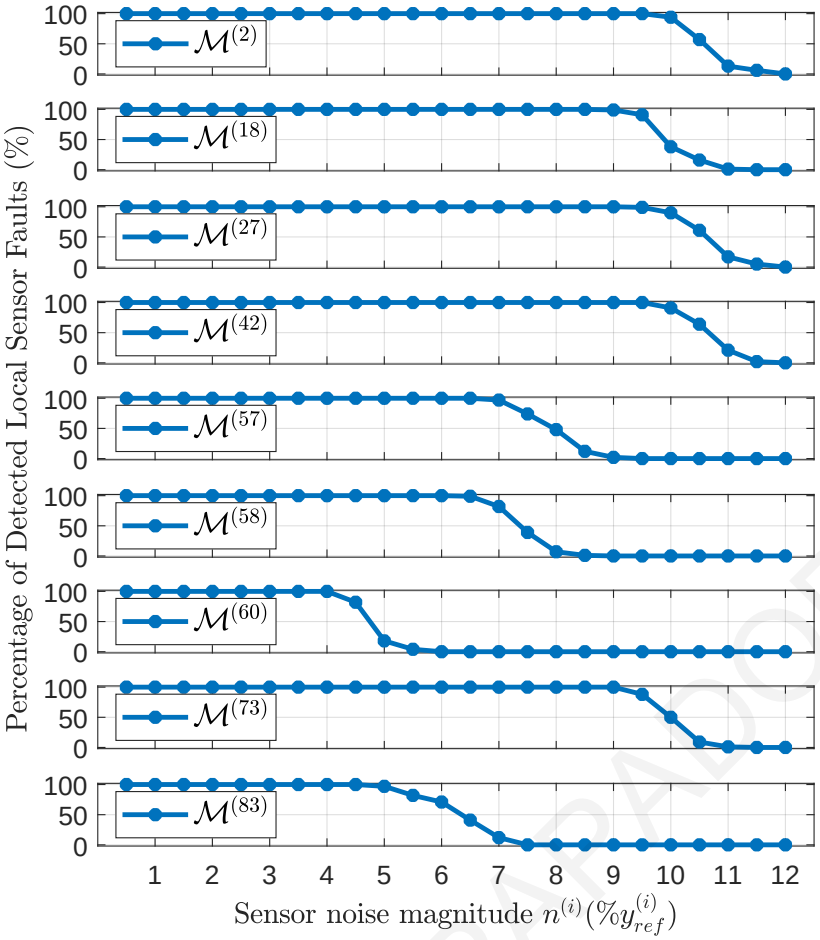

Figure 4.8: Sensitivity analysis of the FDI algorithm with respect to sensor noise variance: Percentage of detected local sensor faults with respect to local sensor noise variance $n^{(i)}(t)$. Each blue dot corresponds to the times that the corresponding diagnosis agent detected the presence of the local sensor fault from the 100 simulations obtained for each sensor noise variance $n^{(i)}(t)$. Note that the percentage of sensor noise variance is the same for all sensors in the building.

propagation a sensor fault.

In order to investigate the effectiveness of the proposed sensor fault diagnosis method, we implemented numerous simulation scenarios modifying the range of noise corrupting the sensor measurements; i.e. $n^{(i)}(t)$ satisfies Assumption 2 with $[0.5\%y^{(i)}_{ref}\ 12\%y^{(i)}_{ref}]$ for all $i \in \{1,\ldots,83\}$. For the multiple sensor fault scenario denoted with the red squared boxes in Figure 5, we run 100 times the same simulation while keeping the sensor noise magnitude of all 83 air temperature sensors the same. The simulated sensor faults occur at $t^{(j)}_f = 0.5$ hours with $f^{(j)} = 15\%y^{(j)}_{ref}$ for $j \in \{2, 18, 27, 42, 57, 58, 60, 73, 83\}$ and the simulation time is 1 hour. Figure 8 shows the percentage of detected local sensor faults (%), given by

$$P^{(i)}_D = \frac{\text{No. of Detected Local Sensor Faults}}{\text{No. of Total Generated Local Sensor Faults}} \times 100\% \tag{4.63}$$

for each agent with respect to the local sensor noise variance $n^{(i)}(t)$. Specifically, each blue dot in Figure 8 corresponds to the instances (from the 100 simulations obtained for each sensor noise variance $n^{(i)}(t)$) that the corresponding sensor fault diagnosis agent detected the presence of the local sensor

fault. As illustrated, the percentage of detected local sensor faults of the sensor fault diagnosis agents is decreasing as the variance of sensor noise is increasing. Note that detection decision of each agent is not only affected by the noise from its local sensor but it is also affected by sensor noise from its neighbouring subsystems (see (4.9)–(4.13) and (4.36)). Therefore, the agents that monitor zones that have the same number of neighbouring zones (i.e., same $|\mathcal{K}_i|$) and same design properties (see Table 4.5) may have a similar percentage of detected local sensor faults (see $\mathcal{M}^{(2)}$ with $\mathcal{M}^{(42)}$). However, agents that have the same $|\mathcal{K}_i|$ and same design properties, may not have a similar percentage of detected local sensor faults (see $\mathcal{M}^{(18)}$ with $\mathcal{M}^{(58)}$), since due to the distributed topology of the agents, the detection decision can be affected by sensor fault from neighbouring subsystems (i.e., $\mathcal{S}^{(57)}$ and $\mathcal{S}^{(60)}$).

4.6 Conclusions

The formulation of large-scale, complex HVAC systems as networks of interconnected subsystems allows the design of scalable distributed model-based sensor fault diagnosis methodologies. The design process of each distributed agent consists of: (i) the sensor fault detection that is based on the generation of ARRs constructed by residuals (resulted by discrepancies of the output and the estimated output of each subsystem) and thresholds that bound the residuals under healthy conditions and (ii) the sensor fault isolation that is obtained using a sensor fault signature matrix which is constructed based on the connectivity of the fault diagnosis agents and allows to eliminate the number of possible locations of the sensor faults. The distributed design of the proposed fault diagnosis method is analyzed in terms of robustness, detectability and scalability. The methodology is evaluated under a multiple sensor fault scenario for a large-scale HVAC system consists of 83 building zones. Further, the sensitivity of the proposed method is evaluated with numerous simulation scenarios modifying the sensor noise variance.

It is important to note that the proposed distributed sensor fault diagnosis algorithm can be also applied for diagnosing process or actuator faults. Specifically, the same algorithm is able to detect process and actuator faults, however, the isolation process needs to be modified or extended in order to distinguish between the different types of faults i.e., process, actuator or sensor faults. In the two forthcoming chapters (Chapters 5–6) the detection, isolation and identification of both sensor and actuators faults is studied.

Chapter 5

Distributed Fault Identification using an Adaptive Estimation Scheme

5.1 Introduction

In the previous chapters (Chapters 3 and 4), the development of a distributed detection and isolation approach for faults on sensors located in the electromechanical part and zones of a HVAC system for both non-interacting and interacting zones are presented. This goal of this chapter is to design a distributed diagnosis algorithm for sensor and actuator faults that can isolate faults (i.e., reveal their location) and identify faults (i.e., distinguish between actuator and sensor faults). The first challenge is the identification of sensor and actuator faults since the occurrence of either a sensor or an actuator fault, within the same subsystem, can lead to a same detection alarm (see Fig. 5.1). An additional challenge arises from the distributed detection architecture, since there is shared information between the neighboring distributed monitoring agents and also possibly an exchange of shared information between the distributed control agents. The isolation of sensor faults in a distributed architecture is addressed in the two previous chapters, however this chapter deals with the occurrence of both sensor and actuator faults.

The goal and the main contribution of this work is the design of a model-based distributed FD architecture for isolating bias sensor and actuator faults in a multi-zone HVAC system that is considered as a network of interconnected subsystems as presented in Section 2.4. The proposed FD scheme uses several distributed monitoring agents, where every agent combines local and neighboring information to diagnose faults in its monitored subsystem. The monitoring agent performs a sequence of diagnostic processes, including: (i) distributed fault detection for capturing the occurrence of (both sensor and actuator) faults in the monitored subsystem and its neighborhood (Section 5.3.1), (ii) local fault identification for specifying the type of local faults, i.e., actuator or sensor fault (Section 5.3.2), and (iii) distributed fault isolation for isolating multiple local faults and/or propagated sensor faults

(Section 5.3.3). The proposed FD scheme is applied to a 5-zone HVAC system, presented in Section 5.4.

5.2 Objective

The objective of this work is to design a methodology for diagnosing actuator and sensor faults that may occur in one or more building zones, assuming that there are no actuator and sensor faults in the electromechanical part of HVAC. The output of the sensor $\mathcal{S}^{(i)}$ used to measure the state (air temperature in zone i) of subsystem $\Sigma^{(i)}$ is expressed as

$$\mathcal{S}^{(i)} : y^{(i)}(t) = T_{z_i}(t) + n^{(i)}(t) + f^{(i)}(t), \tag{5.1}$$

where $y^{(i)} \in \mathbb{R}$ is the sensor output, $n^s \in \mathbb{R}$ is the measurement noise and $f^{(i)} \in \mathbb{R}$ denotes the permanent bias sensor fault (modeled as in Chapter 2.6). The input of $\Sigma^{(i)}$ is affected by actuator faults modeled as

$$u^{(i)}(t) = c^{(i)}(t) + f_a^{(i)}, \tag{5.2}$$

where $f_a^{(i)}$ is the actuator bias fault that may affect the valve regulating the flow of water in fan-coil unit of the *i-th* zone. The signals c^s in (2.23) and $c_c^{(i)}$ in (5.2) are generated using a distributed feedback linearization controller based on some (differentiable) reference signals y_{ref}^s and $y_{ref}^{(i)}$ for the states x^s and T_{z_i}, $i \in \{1, \ldots, N\}$.

5.3 Design of Distributed Diagnosis Agent

For the design of the fault diagnosis method for the multi-zone HVAC system described in the previous section we follow a distributed approach. Figure 5.1 illustrates the distributed diagnosis architecture for a simple example of two interconnected subsystems $\Sigma^{(1)}$ and $\Sigma^{(2)}$. For each subsystem, we design a monitoring agent $\mathcal{M}^{(i)}$, $i \in \{1, 2\}$. The agent $\mathcal{M}^{(i)}$ exchanges information with its neighbor, where the exchange of information is coherent with the form of the physical interconnections. The diagnosis process is executed in three steps: distributed fault detection; local fault identification; and distributed fault isolation.

5.3.1 Distributed Fault Detection

By using the local input and sensor output information, $c^{(i)}$ and $y^{(i)}$, as well as sensor information transmitted by the neighboring agents $y^{(j)}$, $j \in \mathcal{K}_i$, the agent $\mathcal{M}^{(i)}$ detects the occurrence of faults that may have affected the local actuator or sensor, or may have been propagated due to the exchange of the sensor information. The fault detection decision logic of $\mathcal{M}^{(i)}$ is based on an analytical redundancy relation (ARR) $\mathcal{E}^{(i)}$, defined as

$$\mathcal{E}^{(i)} : \quad |\varepsilon_y^{(i)}(t)| \leq \bar{\varepsilon}_y^{(i)}(t), \tag{5.3}$$

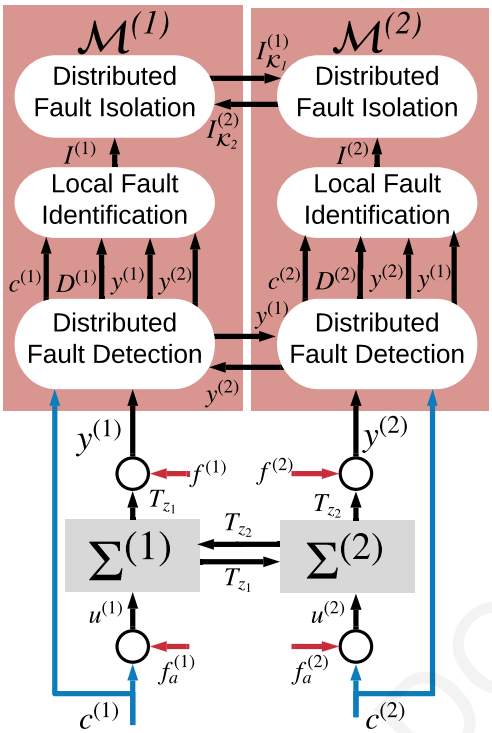

Figure 5.1: Distributed fault diagnosis architecture for two interconnected building zones.

where $\varepsilon_y^{(i)}(t)$ is the residual and $\bar{\varepsilon}_y^{(i)}(t)$ is the adaptive threshold, defined next. Under healthy conditions, i.e. when $f_a^{(i)} = 0$, $f_s^{(j)}$=0 for all $j \in \{\mathcal{K}_i \cup \{i\}\}$, $\mathcal{E}^{(i)}$ is guaranteed to be satisfied by designing the threshold $\bar{\varepsilon}_y^{(i)}(t)$ to bound the magnitude of the residual. Therefore, if there is a time instant that $\mathcal{E}^{(i)}$ is not satisfied, the agent $\mathcal{M}^{(i)}$ infers the presence of faults in its monitored subsystem $\Sigma^{(i)}$ and/or its neighbors. The output of the agent $\mathcal{M}^{(i)}$ is the boolean decision signal $D^{(i)}$, defined as

$$D^{(i)}(t) = \begin{cases} 0, & t < t_D^{(i)} \\ 1, & t \geq t_D^{(i)} \end{cases}, \tag{5.4}$$

where $t_D^{(i)} \triangleq inf\{t \geq 0 : |\varepsilon_y^{(i)}(t)| > \bar{\varepsilon}_y^{(i)}(t)\}$. When $D^{(i)}(t) = 1$, the agent $\mathcal{M}^{(i)}$ detects the occurrence of faults.

Residual Generation:

The fault detection process of the agent $\mathcal{M}^{(i)}$ is executed by monitoring the residual

$$\varepsilon_y^{(i)}(t) = y^{(i)}(t) - \hat{T}_{z_i}(t) \tag{5.5}$$

where $\hat{T}_{z_i}$ is the estimation of T_{z_i} generated by the following distributed nonlinear estimator

$$\dot{\hat{T}}_{z_i}(t) = A^{(i)}\hat{T}_{z_i}(t) + g^{(i)}(y^s(t), y^{(i)}(t))c^{(i)}(t) + \eta^{(i)}(d^{(i)}(t)) + h^{(i)}(y^{(i)}(t), y_{\mathcal{K}_i}(t)) + L^{(i)}\left(y^{(i)}(t) - \hat{T}_{z_i}(t)\right), \tag{5.6}$$

where $y_{\mathcal{K}_i}(t) = \left[y^{(j)}(t) : j \in \mathcal{K}_i\right]^\top$, $\hat{T}_{z_i}(0) = 0$ and $L^{(i)}$ is the observer gain selected such that $A_L^{(i)} = A^{(i)} - L^{(i)}$ is stable and y^s and $y^{(i)}$ are defined in (2.32) and (5.1).

Computation of Adaptive Threshold:

The adaptive threshold $\bar{\varepsilon}_y^{(i)}$ is designed to bound the corresponding residual as shown in (5.3) when $f_a^{(i)}$=0, $f_s^{(j)}$=0 for all $j \in \{\mathcal{K}_i \cup \{i\}\}$. In this case, the residual is described by

$$\varepsilon_y^{(i)}(t) = \varepsilon_x^{(i)}(t) + n^{(i)}(t), \tag{5.7}$$

where $\varepsilon_x^{(i)} = T_{z_i} - \hat{T}_{z_i}$ is the state estimation error that satisfies,

$$\begin{aligned}\dot{\varepsilon}_x^{(i)}(t) = A_L^{(i)}\varepsilon_x^{(i)}(t) + \tilde{g}^{(i)}(T_{st}(t), T_{z_i}(t), T_{st}(t), y^{(i)}(t))c^{(i)}(t) + \tilde{h}^{(i)}(T_{z_i}(t), T_{\mathcal{K}_i}(t), y^{(i)}(t), y_{\mathcal{K}_i}(t)) \\ + r^{(i)}(t) - L^{(i)}n^{(i)}(t)\end{aligned} \tag{5.8}$$

$$\tilde{g}^{(i)}(T_{st}(t), T_{z_i}(t), y^s(t), y^{(i)}(t)) = g^{(i)}(T_{st}(t), T_{z_i}(t)) - g^{(i)}(y^s(t), y^{(i)}(t)) \tag{5.9}$$

$$\tilde{h}^{(i)}(T_{z_i}(t), T_{\mathcal{K}_i}(t), y^{(i)}(t), y_{\mathcal{K}_i}(t)) = h^{(i)}(T_{z_i}(t), T_{\mathcal{K}_i}(t)) - h^{(i)}(y^{(i)}(t), y_{\mathcal{K}_i}(t)). \tag{5.10}$$

The adaptive threshold is computed by introducing the solution of (5.8) in (5.7) and bounding each term, taking into account the following assumptions:

Assumption 3. The measurement noise n^s, $n^{(i)}$ and the system disturbance $r^{(i)}$ are uniformly bounded; i.e. $|n^s(t)| \leq \bar{n}^s$, $|n^{(i)}(t)| \leq \bar{n}^{(i)}$, and $|r^{(i)}(t)| \leq \bar{r}^{(i)}$.

Assumption 4. The states T_{st}, T_{z_i} and control inputs c^s, $c^{(i)}$, for all $i \in \{1, \ldots, N\}$ remain bounded under both healthy and faulty conditions; i.e., $T_{st} \in \mathcal{X}^s$, $T_{z_i} \in \mathcal{X}^{(i)}$ and $c^s \in \mathcal{U}^s$, $c^{(i)} \in \mathcal{U}^{(i)}$, where $\mathcal{X}^s$, $\mathcal{X}^{(i)}$, $\mathcal{U}^s$ and $\mathcal{U}^{(i)}$ are compact closed sets, respectively.

Based on (2.27) and (2.28), the bounds on the functions $\tilde{g}^{(i)}$, $\tilde{h}^{(i)}$ (see (5.9), (5.10)) are computed by setting $f_s^{(i)}$=0 in (5.1); i.e.,

$$|\tilde{g}^{(i)}(T_{st}(t), T_{z_i}(t), y^s(t), y^{(i)}(t))| \leq \sigma^{(i)}\left(\bar{n}^{(i)} + \bar{n}^s\right) = \bar{g}^{(i)}(\bar{n}^{(i)}, \bar{n}^s), \tag{5.11}$$

$$\begin{aligned}|\tilde{h}^{(i)}(T_{z_i}(t), T_{\mathcal{K}_i}(t), y^{(i)}, (t)y_{\mathcal{K}_i}(t))| &\leq p^{(i)}\sum_{j\in\mathcal{K}_i} A_{d_{i,j}}\bar{\mu}^{(i)}(y^{(i)}(t), y^{(j)}(t)) + \sum_{j\in\mathcal{K}_i}\frac{a_{z_{i,j}}}{C_{z_i}}\bar{n}^{(j)} \\ &= \bar{h}^{(i)}(y^{(i)}(t), y_{\mathcal{K}_i}(t)),\end{aligned} \tag{5.12}$$

where $\bar{n}_{\mathcal{K}_i} = \left[\bar{n}^{(j)} : j \in \mathcal{K}_i\right]^\top$. The function $\bar{\mu}^{(i)}(y^{(i)}, y^{(j)})$ is computed such that

$$|\mu^{(i)}(T_{z_i}(t), T_{z_j}(t)) - \mu^{(i)}(y^{(i)}(t), y^{(j)}(t))| \leq \bar{\mu}^{(i)}(y^{(i)}(t), y^{(j)}(t)), \tag{5.13}$$

where

$$\mu^{(i)}(T_{z_i}(t), T_{z_j}(t)) = \text{sgn}(T_{z_j}(t) - T_{z_i}(t))\max(T_{z_i}(t), T_{z_j}(t))\sqrt{|T_{z_j}(t) - T_{z_i}(t)|}. \tag{5.14}$$

The detailed computation of $\bar{\mu}^{(i)}(y^{(i)}, y^{(j)})$ is presented through (4.26)-(4.30) and (4.32)-(4.34) and is designed to bound the difference $\tilde{\mu}^{(i)} = \mu^{(i)}(T_{z_i}, T_{z_j}) - \mu^{(i)}(y_H^{(i)}, y_H^{(j)})$.

The adaptive threshold $\bar{\varepsilon}_y^{(i)}(t)$ is defined as

$$\bar{\varepsilon}_y^{(i)}(t) = \rho^{(i)} e^{-\lambda^{(i)} t} \bar{x}^{(i)} + \bar{n}^{(i)} + \int_0^t \rho^{(i)} e^{-\lambda^{(i)}(t-\tau)} \Big(\left| L^{(i)} \right| \bar{n}^{(i)} + \bar{r}^{(i)} + \bar{g}^{(i)}(\bar{n}^{(i)}, \bar{n}^s) \left| c^{(i)}(t) \right| + \bar{h}^{(i)}(y^{(i)}(t), y_{\mathcal{K}_i}(t)) \Big) d\tau, \tag{5.15}$$

where $\bar{x}^{(i)}$ is a known bound such that $|T_{z_i}(t)| \leq \bar{T}_{z_i}$ for all t (see Assumption 4), and $\rho^{(i)} > 0,\ \lambda^{(i)} > 0$ are respectively selected such that $e^{A_L^{(i)} t} \leq \rho^{(i)} e^{-\lambda^{(i)} t}$, for all t. The ARR $\mathcal{E}^{(i)}$ is robust to system disturbances and noise, implying that $\mathcal{M}^{(i)}$ does not raise false alarms.

5.3.2 Local Fault Identification

The primary goal of this step is the identification of the type of the fault that may have affected the local system, i.e. actuator or sensor fault or both. This is realized using two identification modules, $\mathcal{I}_a^{(i)}$ and $\mathcal{I}_s^{(i)}$ and an aggregation module $\mathcal{A}^{(i)}$ for fault isolation. The fault identification decision logic of $\mathcal{I}_a^{(i)}$ and $\mathcal{I}_s^{(i)}$ is based on two ARRs, $\mathcal{E}_a^{(i)}$ and $\mathcal{E}_s^{(i)}$ described by

$$\mathcal{E}_a^{(i)}: \ |\varepsilon_{y_a}^{(i)}(t)| \leq \bar{\varepsilon}_{y_a}^{(i)}(t), \ \ \mathcal{E}_s^{(i)}: \ |\varepsilon_{y_s}^{(i)}(t)| \leq \bar{\varepsilon}_{y_s}^{(i)}(t), \tag{5.16}$$

where $\varepsilon_{y_a}^{(i)}(t)$, $\varepsilon_{y_s}^{(i)}(t)$ are the residuals generated by $\mathcal{I}_a^{(i)}$ and $\mathcal{I}_s^{(i)}$ respectively and $\bar{\varepsilon}_{y_a}^{(i)}(t)$, $\bar{\varepsilon}_{y_s}^{(i)}(t)$ are their corresponding adaptive thresholds. Due to the design of the adaptive thresholds, which is presented next: (i) the ARR $\mathcal{E}_a^{(i)}$ is guaranteed to be satisfied when $f_s^{(j)}$=0 for all $j \in \{\mathcal{K}_i \cup \{i\}\}$, and (ii) $\mathcal{E}_s^{(i)}$ is guaranteed to be satisfied when $f_s^{(j)}$=0 for all $j \in \mathcal{K}_i$ and $f_a^{(i)} = 0$. Therefore, as long as $\mathcal{E}_a^{(i)}$ is satisfied, $\mathcal{I}_a^{(i)}$ infers the occurrence of local actuator fault. As long as $\mathcal{E}_s^{(i)}$ is satisfied, $\mathcal{I}_s^{(i)}$ infers the occurrence of local sensor fault .

The outputs of the modules $\mathcal{I}_a^{(i)}$ and $\mathcal{I}_s^{(i)}$ are two local boolean decision functions $I_a^{(i)}$, $I_s^{(i)}$, defined as

$$I_a^{(i)}(t) = \begin{cases} 0, \ t < t_{I_a}^{(i)} \\ 1, \ t \geq t_{I_a}^{(i)} \end{cases}, \ \ I_s^{(i)}(t) = \begin{cases} 0, \ t < t_{I_s}^{(i)} \\ 1, \ t \geq t_{I_s}^{(i)} \end{cases}, \tag{5.17}$$

where $t_{I_a}^{(i)} \triangleq inf\{t \geq t_D^{(i)} : |\varepsilon_{y_a}^{(i)}(t)| > \bar{\varepsilon}_{y_a}^{(i)}(t)\}$ and $t_{I_s}^{(i)} \triangleq inf\{t \geq t_D^{(i)} : |\varepsilon_{y_s}^{(i)}(t)| > \bar{\varepsilon}_{y_s}^{(i)}(t)\}$.

Residual Generation:

The residuals associated with the modules $\mathcal{I}_a^{(i)}$ and $\mathcal{I}_s^{(i)}$ are defined as,

$$\varepsilon_{y_a}^{(i)}(t) = y^{(i)}(t) - \hat{T}_{z_i}^a(t), \tag{5.18}$$

$$\varepsilon_{y_s}^{(i)}(t) = y^{(i)}(t) - \hat{T}_{z_i}^s(t) - \hat{f}_s^{(i)}(t), \tag{5.19}$$

where $\hat{T}_{z_i}^a$ and $\hat{T}_{z_i}^s$ are both estimations of T_{z_i}, and $\hat{f}_s^{(i)}$ is the estimation of the sensor fault $f_s^{(i)}$. Assuming only local faults (i.e. $f_s^{(j)}$=0, $\forall\ j \in \mathcal{K}_i$), the state estimate $\hat{T}_{z_i}^a$ and $\hat{x}_s^{(i)}$ are computed based on the

following distributed adaptive nonlinear estimation schemes

$$\dot{\hat{T}}^{a}_{z_i}(t) = A^{(i)}\hat{T}^{a}_{z_i}(t) + g^{(i)}(y^{s}(t), y^{(i)}(t))(c^{(i)}(t) + \hat{f}^{(i)}_{a}(t)) + h^{(i)}(y^{(i)}(t), y_{\mathcal{K}_i}(t)) + \eta^{(i)}(d^{(i)}(t)) + L^{(i)}_{a}\varepsilon^{(i)}_{y_a}(t) + \Omega^{(i)}_{a}(t)\dot{\hat{f}}^{(i)}_{a}(t), \tag{5.20}$$

$$\dot{\Omega}^{(i)}_{a}(t) = A^{(i)}_{L_a}\Omega^{(i)}_{a}(t) + g^{(i)}(y^{s}(t), y^{(i)}(t)), \tag{5.21}$$

$$\dot{\hat{f}}^{(i)}_{a}(t) = \gamma^{(i)}_{a}\Omega^{(i)}_{a}(t)\mathcal{D}^{(i)}\left[\varepsilon^{(i)}_{y_a}(t)\right], \tag{5.22}$$

$$\dot{\hat{T}}^{s}_{z_i}(t) = A^{(i)}\hat{T}^{s}_{z_i}(t) + g^{(i)}(y^{s}(t), y^{(i)}(t) - \hat{f}^{(i)}(t))c^{(i)}(t) + h^{(i)}(y^{(i)}(t) - \hat{f}^{(i)}(t), y_{\mathcal{K}_i}(t)) + \eta^{(i)}(d^{(i)}(t)) + L^{(i)}_{s}\varepsilon^{(i)}_{y_s}(t) + \Omega^{(i)}_{s}(t)\dot{\hat{f}}^{(i)}(t), \tag{5.23}$$

$$\dot{\Omega}^{(i)}_{s}(t) = A^{(i)}_{L_s}\Omega^{(i)}_{s}(t) - L^{(i)}_{s} + \sigma^{(i)}c^{(i)}(t), \tag{5.24}$$

$$\dot{\hat{f}}^{(i)}(t) = \gamma^{(i)}_{s}(\Omega^{(i)}_{s}(t) + 1)\mathcal{D}^{(i)}\left[\varepsilon^{(i)}_{y_s}(t)\right], \tag{5.25}$$

where $L^{(i)}_{a}$, $L^{(i)}_{s}$ are the estimation gains, such that $A^{(i)}_{L_a} \triangleq A^{(i)} - L^{(i)}_{a}$, $A^{(i)}_{L_s} \triangleq A^{(i)} - L^{(i)}_{s}$ are stable. The term $\hat{f}^{(i)}_{a}$ and $\hat{f}^{(i)}_{s}$ are the estimation of the fault $f^{(i)}_{a}$ and $f^{(i)}_{s}$, respectively. The positive constants $\gamma^{(i)}_{a}$, $\gamma^{(i)}_{s}$ are the learning rates of the adaptive laws in (5.22) and (5.25), and $\Omega^{(i)}_{a}$, $\Omega^{(i)}_{s}$ are filtering terms necessary for ensuring the stability of the adaptive schemes. Note that $\hat{T}^{a}_{z_i}(t^{(i)}_{D}) = 0$, $\hat{T}^{s}_{z_i}(t^{(i)}_{D}) = 0$, $\hat{f}^{(i)}_{a}(t^{(i)}_{D}) = 0$ and $\hat{f}^{(i)}_{s}(t^{(i)}_{D}) = 0$, $\Omega^{(i)}_{a}(t^{(i)}_{D}) = 0$ and $\Omega^{(i)}(t^{(i)}_{D}) = 0$, where $t^{(i)}_{D}$ is the detection time. The term $\mathcal{D}^{(i)}[.]$ represents the dead-zone operator

$$\mathcal{D}^{(i)}\left[\varepsilon^{(i)}_{y_\star}(t)\right] = \begin{cases} 0, & \text{if } D^{(i)}(t) = 0 \\ \varepsilon^{(i)}_{y_\star}(t), & \text{if } D^{(i)}(t) = 1 \end{cases}, \tag{5.26}$$

where $\varepsilon^{(i)}_{y_\star}$ represents either $\varepsilon^{(i)}_{y_a}$ in (5.22) or $\varepsilon^{(i)}_{y_s}$ in (5.25) and $D^{(i)}$ is defined in (5.4).

Computation of Adaptive Thresholds:

Assuming $f^{(i)}_{s} = 0$ in (5.1), the residual in (5.18) can be expressed as,

$$\varepsilon^{(i)}_{y_a}(t) = \varepsilon^{(i)}_{x_a}(t) + n^{(i)}(t), \tag{5.27}$$

where $\varepsilon^{(i)}_{x_a}(t) = T_{z_i}(t) - \hat{T}^{a}_{z_i}(t)$ is the state estimation error. By using (2.26) and (5.20) and replacing $g^{(i)}\left(y^{s}(t), y^{(i)}(t)\right)\tilde{f}^{(i)}_{a}(t)$ with $(\dot{\Omega}^{(i)}_{a}(t) - A^{(i)}_{L}\Omega^{(i)}_{a}(t))\tilde{f}^{(i)}_{a}(t)$ (see (5.21)), and after performing some mathematical manipulations, $\varepsilon^{(i)}_{x_a}(t)$ satisfies

$$\varepsilon^{(i)}_{x_a}(t) = \Omega^{(i)}_{a}(t)\tilde{f}^{(i)}_{a}(t) + \tilde{\varepsilon}^{(i)}_{x_a}(t), \tag{5.28}$$

$$\dot{\tilde{\varepsilon}}^{(i)}_{x_a}(t) = A^{(i)}_{L_a}\tilde{\varepsilon}^{(i)}_{x_a}(t) + \tilde{g}^{(i)}(T_{st}(t), T_{z_i}(t), y^{s}(t), y^{(i)}(t))c^{(i)}(t) + \tilde{h}^{(i)}(T_{z_i}(t), T_{\mathcal{K}_i}(t), y^{(i)}(t), y_{\mathcal{K}_i}(t)) - L^{(i)}_{a}n^{(i)}(t) + r^{(i)}(t). \tag{5.29}$$

where $\tilde{f}^{(i)}_{a}(t) = f^{(i)}_{a} - \hat{f}^{(i)}_{a}(t)$ is the actuator fault estimation error and $\dot{\tilde{f}}^{(i)}_{a}(t) = -\dot{\hat{f}}^{(i)}_{a}(t)$.

The residual in (7.5) can be expressed as,

$$\varepsilon_{y_s}^{(i)}(t) = \varepsilon_{x_s}^{(i)}(t) + \tilde{f}^{(i)}(t) + n^{(i)}(t), \tag{5.30}$$

where $\varepsilon_{x_s}^{(i)}(t) = x^{(i)}(t) - \hat{x}_s^{(i)}(t)$ is the state estimation error and $\tilde{f}^{(i)}(t) = f^{(i)} - \hat{f}^{(i)}(t)$ is the sensor fault estimation error with $\dot{\tilde{f}}^{(i)}(t) = -\dot{\hat{f}}^{(i)}(t)$. Assuming that $f_a^{(i)} = 0$ in (5.2), the dynamics of $\varepsilon_{x_s}^{(i)}$ can be described by

$$\begin{aligned}\dot{\varepsilon}_{x_s}^{(i)}(t) = {} & A_{L_s}^{(i)}\varepsilon_{x_s}^{(i)} + \Omega_s^{(i)}(t)\dot{\tilde{f}}^{(i)}(t) + \sigma^{(i)}\tilde{f}^{(i)}(t)u_c^{(i)}(t) - L_s^{(i)}\tilde{f}^{(i)}(t) \\ & + p^{(i)}\sum_{j\in\mathcal{K}_i} A_{d_{i,j}}\left(\mu^{(i)}(T_{z_i}(t), T_{z_j}(t)) - \mu^{(i)}(y^{(i)}(t) - \hat{f}^{(i)}(t), y^{(j)}(t))\right) \\ & - \sum_{j\in\mathcal{K}_i}\frac{a_{z_{i,j}}}{C_{z_i}} n^{(j)}(t) + \tilde{g}^{(i)}(T_{st}(t), T_{z_i}(t), y^s(t), y^{(i)}(t))c^{(i)}(t) - L_s^{(i)}n^{(i)}(t) + r^{(i)}(t).\end{aligned} \tag{5.31}$$

Using (5.24), (5.31) can be re-written as:

$$\varepsilon_{x_s}^{(i)}(t) = \Omega_s^{(i)}\tilde{f}^{(i)}(t) + \tilde{\varepsilon}_{x_s}^{(i)}(t), \tag{5.32}$$

$$\begin{aligned}\dot{\tilde{\varepsilon}}_{x_s}^{(i)}(t) = {} & A_{L_s}^{(i)}\tilde{\varepsilon}_{x_s}^{(i)}(t) + p^{(i)}\sum_{j\in\mathcal{K}_i} A_{d_{i,j}}\left(\mu^{(i)}(T_{z_i}(t), T_{z_j}(t)) - \mu^{(i)}(y^{(i)}(t) - \hat{f}^{(i)}(t), y^{(j)}(t))\right) \\ & - \sum_{j\in\mathcal{K}_i}\frac{a_{z_{i,j}}}{C_{z_i}}\overline{n}^{(j)} + \tilde{g}^{(i)}(T_{st}(t), T_{z_i}(t), y^s(t), y^{(i)}(t))c^{(i)}(t) - L_s^{(i)}n^{(i)}(t) + r^{(i)}(t).\end{aligned} \tag{5.33}$$

Note that under the assumption of zero system disturbance and measurement noise, the errors $\tilde{\varepsilon}_{x_a}^{(i)}$ in (5.29) and $\tilde{\varepsilon}_{x_s}^{(i)}$ in (5.32) converge. If we also assume the persistence of excitation of the filters $\Omega_a^{(i)}$ and $\Omega_s^{(i)}$ in (5.21) and (5.24) respectively, then $\tilde{f}_a^{(i)}$ and $\tilde{f}^{(i)}$ converge as well.

Taking into account (5.16), the adaptive threshold $\overline{\varepsilon}_{y_a}^{(i)}(t)$ is computed by using (5.28) and the solution of (5.29) in (5.27), and the adaptive threshold and $\overline{\varepsilon}_{y_s}^{(i)}(t)$ is computed by using (5.32) and the solution of (5.33) in (5.30), and bounding each term, based on Assumptions 3 and 4 and the following assumption:

Assumption 5. The actuator and sensor faults $f_a^{(i)}$, $f^{(i)}$ are bounded; i.e. $|f_a^{(i)}(t)| \leq \overline{f}_a^{(i)}$ and $|f^{(i)}(t)| \leq \overline{f}^{(i)}$.

The adaptive thresholds $\overline{\varepsilon}_{y_a}^{(i)}(t)$ and $\overline{\varepsilon}_{y_a}^{(i)}(t)$ are defined as:

$$\begin{aligned}\overline{\varepsilon}_{y_a}^{(i)}(t) = {} & \delta_a^{(i)}e^{\left(-\xi_a^{(i)}\left(t-T_D^{(i)}\right)\right)}\overline{T}_{z_i} + \left|\Omega_a^{(i)}(t)\right|\left(\left|\tilde{f}_a^{(i)}(t)\right| + \overline{f}_a^{(i)}\right) + \overline{n}^{(i)} \\ & + \int_{T_D^{(i)}}^{t}\delta_a^{(i)}e^{\left(-\xi_a^{(i)}(t-\tau)\right)}\Bigg(\left|L_a^{(i)}\right|\overline{n}^{(i)} + \overline{r}^{(i)} + \overline{g}^{(i)}(\overline{n}^{(i)}, \overline{n}^s)\left|c^{(i)}(\tau)\right| \\ & + \overline{g}^{(i)}(\overline{n}^{(i)}, \overline{n}^s)\overline{f}_a^{(i)} + \overline{h}^{(i)}(y^{(i)}(\tau), y_{\mathcal{K}_i}(\tau))\Bigg)d\tau,\end{aligned} \tag{5.34}$$

$$\overline{\varepsilon}_{y_s}^{(i)}(t) = \delta_s^{(i)} e^{(-\xi_s^{(i)}(t-T_D^{(i)}))}\overline{T}z_i + \left(\left|\Omega_s^{(i)}(t)\right| + 1\right)\left(\left|\hat{f}^{(i)}(t)\right| + \overline{f}^{(i)}\right) + \overline{n}^{(i)}$$
$$+ \int_{T_D^{(i)}}^{t} \delta_s^{(i)} e^{(-\xi_s^{(i)}(t-\tau))} \left(\overline{g}^{(i)}(\overline{n}^s, \overline{n}^{(i)}) \left|c^{(i)}(\tau)\right| + \sum_{j\in\mathcal{K}_i} \frac{a_{z_{i,j}}}{C_{z_i}} \overline{n}^{(j)} \right.$$
$$\left. + \left|L_s^{(i)}\right| \overline{n}^{(i)} + \overline{r}^{(i)} + p^{(i)} \sum_{j\in\mathcal{K}_i} A_{d_{i,j}} \overline{\mu}_f^{(i)}(y^{(i)}(\tau) - \hat{f}^{(i)}(\tau), y^{(j)}(\tau)) \right) d\tau, \tag{5.35}$$

where $\overline{g}^{(i)}$ and $\overline{h}^{(i)}$ are defined in (5.11) and (5.12) respectively and $\delta_a^{(i)}$, $\xi_a^{(i)}$ and $\delta_s^{(i)}$, $\xi_s^{(i)}$ are selected such that $e^{(A_{La}^{(i)}t)} \leq \delta_a^{(i)} e^{(-\xi_a^{(i)}t)}$ and $e^{(A_{Ls}^{(i)}t)} \leq \delta_s^{(i)} e^{(-\xi_s^{(i)}t)}$, respectively, and $\overline{\mu}_f^{(i)}(y^{(i)} - \hat{f}^{(i)}, y^{(j)})$ is defined in 4.34 in Chapter 4.

It is noted that based on the design of $\overline{\varepsilon}_{y_a}^{(i)}$ and $\overline{\varepsilon}_{y_s}^{(i)}$, the ARRs $\mathcal{E}_a^{(i)}$ and $\mathcal{E}_s^{(i)}$ defined in (5.16) are respectively insensitive to $f_a^{(i)}$ and $f^{(i)}$.

Remark: The distributed fault detection process is applied before the local fault identification in order to reduce the computational effort of the agent $\mathcal{M}^{(i)}$ during the healthy operation of the system that may be long. Particularly, as shown in Section 5.3.1, one non-adaptive estimator is used, generating a single residual that is compared to its corresponding threshold. After the first time of fault detection, the local identification process is continuously active.

5.3.3 Distributed Fault isolation

The decisions of the two modules $\mathcal{I}_a^{(i)}$ and $\mathcal{I}_s^{(i)}$ are collected by the aggregation module $\mathcal{A}^{(i)}$ that processes them in combination. The decisions $I_a^{(i)}$, $I_s^{(i)}$ constitute the observed fault pattern defined as

$$I^{(i)}(t) = [I_a^{(i)}(t), I_s^{(i)}(t)]^\top. \tag{5.36}$$

This pattern is compared to the columns of the fault signature matrix denoted by $F^{(i)}$ shown in Table 5.1, where the term $f_{\mathcal{K}_i}$ collectively amounts for the sensor faults propagated by the neighboring agents due to the exchange of information, and $\mathcal{F}_{\mathcal{K}_i}$ represents all the combinations of local and propagated faults. The element of $F^{(i)}$ equals to 0 when the corresponding ARR has been designed to be insensitive to this fault, and equals to 1 otherwise.

Table 5.1: Fault isolation signature matrix $F^{(i)}$

	$f_a^{(i)}$	$f^{(i)}$	$\{f_a^{(i)}, f^{(i)}\}$	$f_{\mathcal{K}_i}$	$\mathcal{F}_{\mathcal{K}_i}$
$\mathcal{E}_a^{(i)}$	0	1	1	1	1
$\mathcal{E}_s^{(i)}$	1	0	1	1	1

The outcome of the comparison between the observed pattern $I^{(i)}(t)$ to the columns of $F^{(i)}$ is the diagnosis set $\Delta_I^{(i)}(t)$, including the diagnosed fault combinations that may have occurred. When

$I^{(i)}(t) = [1,1]^\top$, the diagnosis set contains more than one combinations, and the distributed fault isolation process is activated in order to decide if only local faults have occurred or also sensor faults have been propagated. Otherwise, it is inferred that a single local fault has occurred which is either actuator fault (if $I^{(i)}(t) = [0,1]^\top$), or sensor fault (if $I^{(i)}(t) = [1,0]^\top$). The decision about the propagation of sensor faults is defined as

$$I^{(i)}_{\mathcal{K}_i}(t) = \begin{cases} 0, & \text{if } \left(f^{(i)}_s \notin \Delta^{(i)}_I(t) \;\&\; f_{\mathcal{K}_i} \notin \Delta^{(i)}_I(t)\right) \text{ or } D^{(i)}(t) = 0 \\ 1, & \text{if } f^{(i)}_s \in \Delta^{(i)}_I(t) \text{ or } f_{\mathcal{K}_i} \in \Delta^{(i)}_I(t) \end{cases}.$$

When $I^{(i)}_{\mathcal{K}_i} = 1$, the agent $\mathcal{M}^{(i)}$ requests from all neighboring agents $\mathcal{M}^{(j)}$, $j \in \mathcal{K}_i$, to transmit their decisions $I^{(j)}_{\mathcal{K}_j}(t)$, creating the observed pattern of propagated sensor faults, determined as

$$I_{\mathcal{K}_i}(t) = \left[I^{(j)}_{\mathcal{K}_j}(t) : j \in \mathcal{K}_i \cup \{i\}\right]^\top. \tag{5.37}$$

This pattern is compared to the columns of a fault signature matrix denoted by $F_{\mathcal{K}_i}$ with $c = \text{card}(\mathcal{K}_i)+1$ rows and $2^c - 1$ columns. Each row corresponds to the ARR $\mathcal{E}_{\mathcal{K}_i} = \mathcal{E}^{(i)}_a \cup \mathcal{E}^{(i)}_s$ and each column corresponds to a combination of sensors faults in the set $f^{(i)} \cup f_{\mathcal{K}_i}$. The element (p,q) of $F_{\mathcal{K}_i}$, $p \in \{1,\ldots,c\}$, $q \in \{1,\ldots,2^c-1\}$ equals to 0 when the q-th ARR is structurally insensitive to the fault combination q. If the q-th fault combination includes the sensor fault $f^{(i)}$ and the p-th row corresponds to the ARR $\mathcal{E}_{\mathcal{K}_i}$, then the element (p,q) equals to 1, since $f^{(i)}_s$ is a local sensor fault for $\mathcal{E}_{\mathcal{K}_i}$. If the q-th fault combination includes only faults $f^{(j)}$, $j \in \mathcal{K}_i$ and the p-th row corresponds to the ARR $\mathcal{E}_{\mathcal{K}_i}$, then the element (p,q) is set to the symbol $*$, which represents either 1 or 0 [130]. An example of the matrix $F_{\mathcal{K}_i}$ is shown in Table 5.2 of the simulation example. The outcome of the comparison is the diagnosis set $\Delta_{\mathcal{K}_i}$ which includes the possible fault combinations of propagated sensor faults. If $f^{(j)} \notin \Delta_{\mathcal{K}_i}$ for all $j \in \mathcal{K}_i$, then the agent $\mathcal{M}^{(i)}$ infers the occurrence of local faults, while if there is at least one fault $f^{(q)} \notin \Delta_{\mathcal{K}_i}$, $q \in \mathcal{K}_i$ then the agent $\mathcal{M}^{(i)}$ infers that sensor faults may have been propagated from the agents $\mathcal{M}^{(j)}$ $j \in \{\mathcal{K}_i \setminus \{q\}\}$.

Table 5.2: Distributed fault signature matrix $F_{\mathcal{K}_1}$ ($f^{(1,2)} = \{f^{(1)}, f^{(2)}\}$, $f^{(1,3)} = \{f^{(1)}, f^{(3)}\}$, $f^{(2,3)} = \{f^{(2)}, f^{(3)}\}$, $f^{(1,2,3)} = \{f^{(1)}, f^{(2)}, f^{(3)}\}$)

	$f^{(1)}$	$f^{(2)}$	$f^{(3)}$	$f^{(1,2)}$	$f^{(1,3)}_s$	$f^{(2,3)}$	$f^{(1,2,3)}$
$\mathcal{E}_{\mathcal{K}_1}$	1	*	*	1	1	*	1
$\mathcal{E}_{\mathcal{K}_2}$	*	1	*	1	*	1	1
$\mathcal{E}_{\mathcal{K}_3}$	*	*	1	*	1	1	1

5.4 Simulation Results

In this section, we illustrate the application of the distributed diagnostic scheme, presented in Section 5.3 to a 5-zone HVAC system whose down-view is presented with solid black lines in Fig. 2.4a. Based on Fig. 2.4b, we define the following index sets $\mathcal{K}_1 = \{2,3\}$, $\mathcal{K}_2 = \{1,3,5\}$, $\mathcal{K}_3 = \{1,2,4,5\}$, $\mathcal{K}_4 = \{3,5\}$, $\mathcal{K}_5 = \{2,3,4\}$. The parameters of each subsystem are: a_{z_i}=740 KJ/h°C, $a_{z_{ij}}$=50 KJ/h°C, a_{st}=12 KJ/kg°C, a_{sz}=0.6 KJ/h°C, C_{st}=8370 kJ/°C, C_p=1.004 kJ/kgK, C_v=0.717 kJ/kgK, ρ_{air}=1.22 kg/m^3, C_{z_1}=30, C_{z_2}=58, C_{z_3}=55, C_{z_4}= C_{z_5}=27 kJ/°C, $U_{i,max}$=3700 kg/h, p=2.5, $U_{st,max}$=27.36×10^5 kg/h, ΔT_{max}=45 °C, A_{w_i}=120 m^2, h=8.29 W/m^2°C, $A_{d_{ij}}$=1.95m^2, d_1^s=$d_1^{(i)}$=$d_2^{(i)}$=10°C, d_2^s=5°C. The modeling uncertainties are modelled as r^s= 10%$d_1^s \sin(0.1t)$ (°C/h), $r^{(i)}$= 10%$d_1^{(i)} \sin(0.1t)$ (°C/h), $i \in \{1,\ldots,5\}$. The desired temperatures are selected as $y_{ref}^s = 55$°C, $y_{ref}^{(i)} = 24$°C, $\forall i$. The design parameters of the monitoring agents are: $\overline{n}^s = 3\% y_{ref}^s$, $\overline{n}^{(i)} = 3\% y_{ref}^{(i)}$, $\overline{r}^s = 10\% d_1^s$, $\overline{r}^{(i)} = 10\% d_1^{(i)}$, $L^{(i)} = 15$, $L_a^{(i)}$=4, $L_s^{(i)}$=22, $\rho^{(i)} = 1.1$, $\lambda^{(i)} = 25$, $\delta_a^{(i)}$=1.1, $\xi_a^{(i)}$=35, $\delta_s^{(i)}$=1.1, $\xi_s^{(i)}$=15, $\gamma_a^{(i)}$=5, $\gamma_s^{(i)}$=32, $\overline{f}_a^{(i)}$=1.5, $\overline{f}_s^{(i)}$=6, $\overline{x}^{(i)}$=20°C, $\forall i$.

To illustrate the decision-making process of the agents a multiple fault scenario is performed. Specifically, two consecutive faults occur in zone 1 and they have been simulated such that $f^{(1)} = 20\% y_{ref}^{(1)}$ at $t = 0.4h$ and $f_a^{(1)} = -25\% c_n^{(1)}$ at $t = 0.6h$, with $c_n^{(1)} = 0.2$ where $c_n^{(1)}$=$c^{(1)}$ in steady state and healthy conditions.

Fig. 5.2 presents the fault detection process of the agents $\mathcal{M}^{(i)}$, $i \in \{1,\ldots,5\}$. The agent $\mathcal{M}^{(1)}$ detects a fault at the time instant $t_D^{(1)} = 0.4h$. Note that, the activation of the local identification process is realized at the first time instant that the agents detect faults. On the contrary, none of the remainder agents ($\mathcal{M}^{(i)}$, $i \in \{2,\ldots,5\}$) detected any fault.

Fig. 5.3 presents the simulation results of the local identification process of $\mathcal{M}^{(1)}$. At the time instant $0.4871h$ the aggregation module $\mathcal{A}^{(1)}$ collects the decisions of the two identification modules and compares the observed pattern $I^{(1)}(0.4871) = [I_a^{(1)}(0.4871), I_s^{(1)}(0.4871)]^\top = [1,0]^\top$ to the columns of Table 5.1. The agent $\mathcal{M}^{(1)}$ decides that a single sensor fault has occurred in zone 1. The local fault identification continues being active, as well as the comparison of the observed pattern $I^{(1)}(t)$ to the columns of Table 5.1. As shown in Fig. 5.3 at the time instant $0.6551h$, the pattern $I^{(1)}$ becomes $I^{(1)}(0.6551) = [I_a^{(1)}(0.6551), I_s^{(1)}(0.6551)]^\top = [1,1]^\top$, leading to $\Delta_I^{(1)}(0.6551) = \left\{\left\{f_a^{(1)}, f^{(1)}\right\}, f_{\mathcal{K}_1}{}^{(1)}, \mathcal{F}_{\mathcal{K}_1}{}^{(1)}\right\}$ and $I_{\mathcal{K}_1}^{(1)}(0.6551) = 1$. Then, the agent $\mathcal{M}^{(1)}$ requests the transmission of the decisions $I_{\mathcal{K}_2}^{(2)}$ and $I_{\mathcal{K}_3}^{(3)}$ of the agents $\mathcal{M}^{(2)}$ and $\mathcal{M}^{(3)}$ respectively, creating the observed pattern $I_{\mathcal{K}_1}(0.6551) = [I_{\mathcal{K}_1}^{(1)}(0.6551), I_{\mathcal{K}_2}^{(2)}(0.6551), I_{\mathcal{K}_3}^{(3)}(0.6551)]^\top = [1,0,0]^\top$. This pattern is compared to the columns of the matrix shown in Table 5.2, leading to the diagnosis set $\Delta_{\mathcal{K}_1} = \{f_s^{(1)}\}$. Based on this set, the agent $\mathcal{M}^{(1)}$ excludes the propagation of sensor faults and infers the occurrence of local actuator and sensor faults.

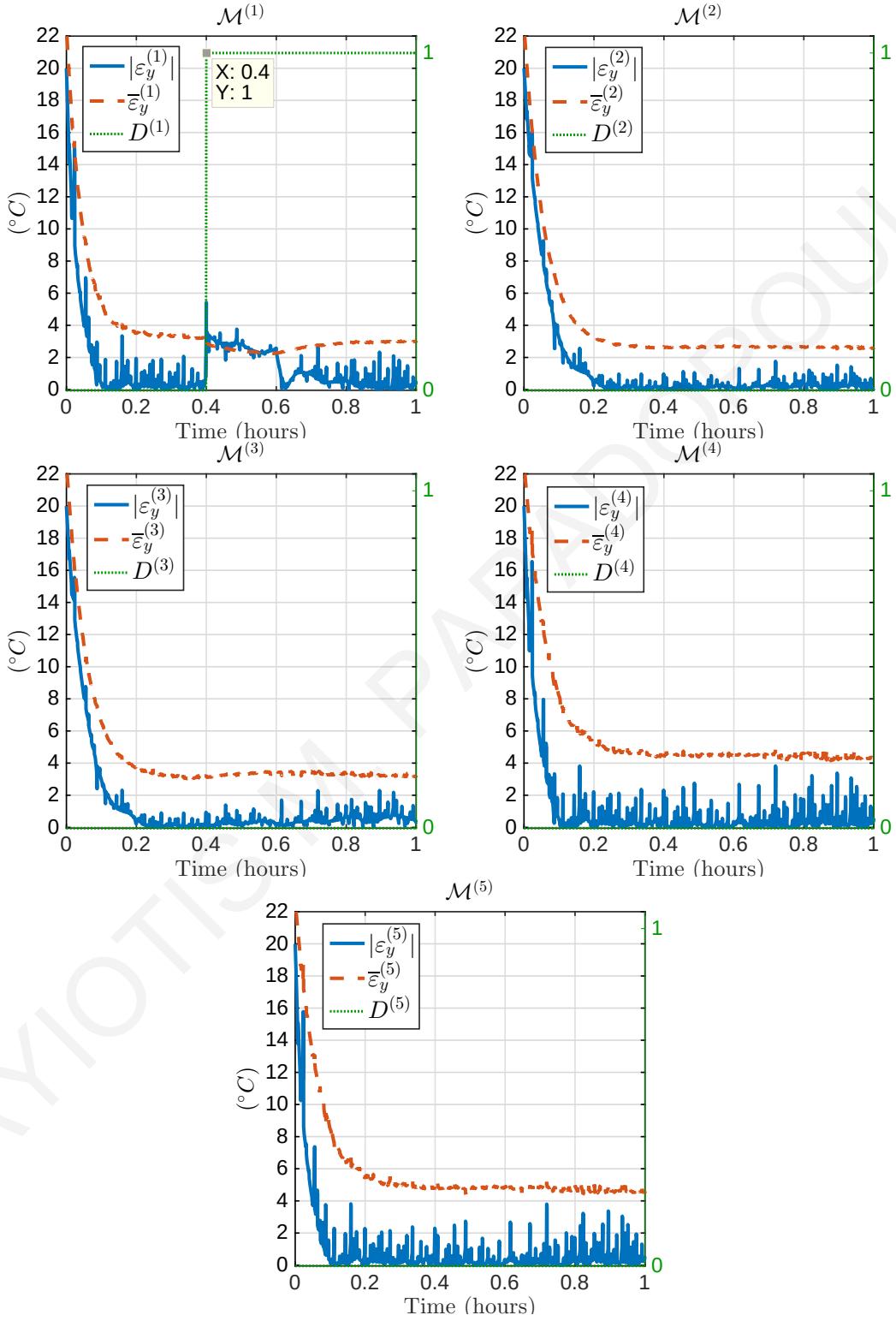

Figure 5.2: Fault detection process of agents $\mathcal{M}^{(i)}$, $i \in \{1, 2, 3, 4, 5\}$.

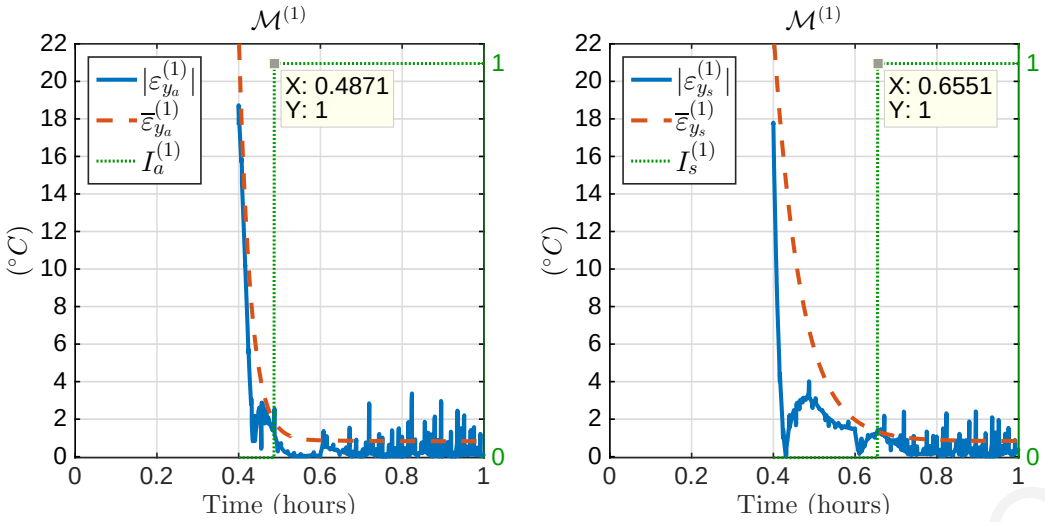

Figure 5.3: Local fault identification of of agent $\mathcal{M}^{(1)}$: $\mathcal{I}_a^{(1)}$ (left) and $\mathcal{I}_s^{(1)}$ (right).

5.5 Conclusions

In this chapter a distributed model-based fault diagnosis (FD) methodology for identifying actuator and sensor faults in a multi-zone HVAC system is presented. The proposed architecture relies on the deployment of a number distributed monitoring agents, one for each zone, which are allowed to exchange information. Every agent is designed to detect the presence of faults, identify the type and infer the number and location (local or propagated faults). Specifically, each agent consists an observer-based distrubuted fault detection module, that is able to detect the presence of faults (i.e., both sensor and actuator faults). Since the detection module detects a fault, then, with in the same agent, the local fault identification module is activated, that consists two observer-based adaptive estimation schemes. The one is designed to estimate/approximate the magnitude of a local actuator fault, while the other is designed to estimate/approximate the magnitude of a local sensor fault. In the same sense, a couple of ARRs is obtained such that in the presence of local sensor fault the one ARR will be violated while in the presence of an actuator fault the other ARR can be violated. The identification decision signal is passed to the distributed fault isolation module and by combining the identification signals of the neighboring agents, a binary logic is used to identify the type and infer the number and location (local or propagated faults).

Chapter 6

Distributed Fault Identification using a Dedicated Observer Scheme

6.1 Introduction

This chapter deals with the detection and isolation of sensor and actuator faults in large-scale buildings, of which climate is regulated by Air Handling Units (AHUs) (see Chapter 2.5). In the previous chapter (Chapter 5), a distributed methodology to detect, identify and isolate both actuator and sensor faults in FCU HVAC systems using adaptive estimation schemes is presented. However, the performance of the fault identification methods in the aforesaid study relies on the assumption that sensor and actuator faults are distinguishable by the proposed ARRs. Moreover, the aforementioned algorithm was evaluated by simulating the HVAC system using the model of the system, while in this work the proposed algorithm is evaluated using a realistic model provided by the *EnergyPlus* software, that performs a whole building energy simulation used to model energy consumption for HVAC, lighting, plug and process loads.

The main contribution of this work is the design of a distributed fault diagnosis algorithm that can detect, isolate and identify faults that can affect the actuators of the air handling units (AHUs) (i.e., water flow valves) or the sensor devices (measuring the zone air temperature, supply air temperature, heating and cooling coil's water temperature), that are used to regulate the thermal conditions in large-scale, multi-zone buildings. The presence of actuator and sensor faults can result to a similar behavior, making it challenging to comprehend the type and location of either single or multiple faults. Moreover, in the case of novel distributed control designs [53, 91, 92, 111, 169, 177], in the sense that a local controller can also use sensor measurements from its neighboring subsystems, sensor faults may result to propagation of their effect making it even more difficult to pinpoint the location of a fault.

Modeling the temperature dynamics of each component (i.e., mixing box, fan, cooling coil and heating coil) within each local AHU and its underlying zone with respect to its neighboring zones

as presented in Chapter 2.5, a local monitoring agent $\mathcal{M}^{(i)}$ is designed. Each local monitoring agent $\mathcal{M}^{(i)}$ utilizes local control inputs and both local and neighboring measurements to detect faults and identify their type and location, considering bounded modeling uncertainty and measurement noise. Each local diagnosis agent consists a number of modules that can estimate on-line: (i) the temperature of the air in the underlying zone, (ii) the temperature of the supplied air to the zone from the AHU, (iii) the temperature of the water in the cooling coil and (iv) the temperature of the water in the heating coil. For every estimation, a residual is developed, that is calculated as the difference between the measured and estimated value at each time step. Under healthy conditions, in the absence of any of the possible faults, the residual is bounded by its corresponding adaptive threshold that is also calculated at each time step, taking into account the bounds on modeling uncertainties and measurement noise, in order to avoid any false alarms. Each pair of residual and adaptive threshold forms an analytical redundancy relation (ARR). The violation of any of the ARRs indicates the detection of a fault. Exploiting the dependency of each (actuator and sensor) fault with every ARR, a decision logic is obtained, that can reveal the location and type of the fault during the operation of the system. The proposed distributed fault diagnosis algorithm is evaluated through a simulation example using a prototype primary school building model with 25 thermal zones, offered in the suite of ASHRAE Standard 90.1 prototype buildings.

6.2 Objective

The objective is to design a distributed model-based fault diagnosis (FD) algorithm that can effectively detect, isolate and identify both actuator and sensor faults in multi-zone AHU HVAC systems. The proposed distributed FD algorithm consists of number of FD Agents, dedicated for each zone-AHU, considering that each zone is served by a single AHU. Each FD agent can collect control inputs and sensor measurements from the AHU, its underlying zone and their neighboring zones. Using the available building and electro-mechanical system parameters, such as dimensions, material coefficients, coil efficiencies, etc, and moreover taking into account modeling uncertainties as a result of internal heat gains and measurement noise, the distributed FD algorithm can trigger alarms in the presence of faults, both in sensors and actuators and it can derive the possible location(s) of fault(s).

Each FD agent is designed for each zone-AHU and consists of four modules ($\mathcal{M}_{\mathrm{z}}^{(i)}$,$\mathcal{M}_{\mathrm{sa}}^{(i)}$, $\mathcal{M}_{\mathrm{sh}}^{(i)}$ and $\mathcal{M}_{\mathrm{sc}}^{(i)}$ as illustrated in Fig. 6.1b) that monitor the zone air temperature T_{z_i}, the supply air temperature T_{sa_i} and the water temperature that pass through the cooling coil T_{cc_i} and heating coil T_{hc_i}, respectively. The architecture of the modules inside the agent $\mathcal{M}^{(i)}$ is based on the partitioning of the subsystem $\Sigma^{(i)}$ presented in Fig. 6.1a. The available sensor measurements for each AHU that are given in (2.61), (2.62)(2.63) (2.64) where f_{z_i}, f_{sa_i} f_{cc_i}, f_{hc_i} are the possible sensor faults. Moreover, faults can occurred in the actuation devices of the AHU, that are the mechanical valves used to regulate the water mass

flow rate of the cold/hot water that pass through the cooling and heating coils, respectively as it is illustrated in (2.66) and (2.65) where $f^m_{\text{cc}_i}$, $f^m_{\text{hc}_i}$ are the possible actuator faults.

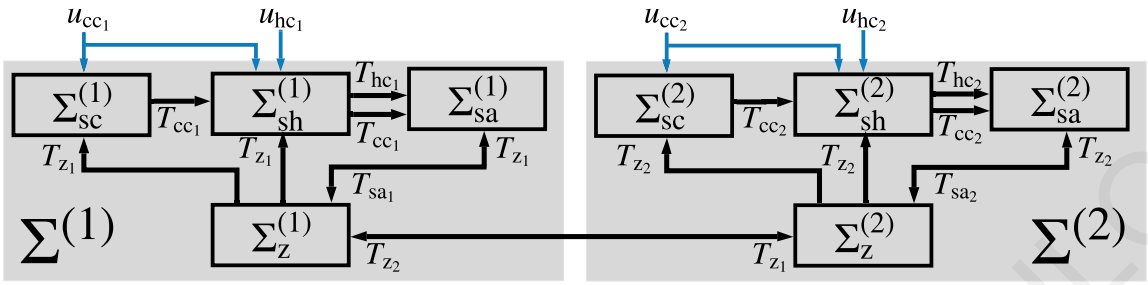

(a) Subsystems of the AHU HVAC system

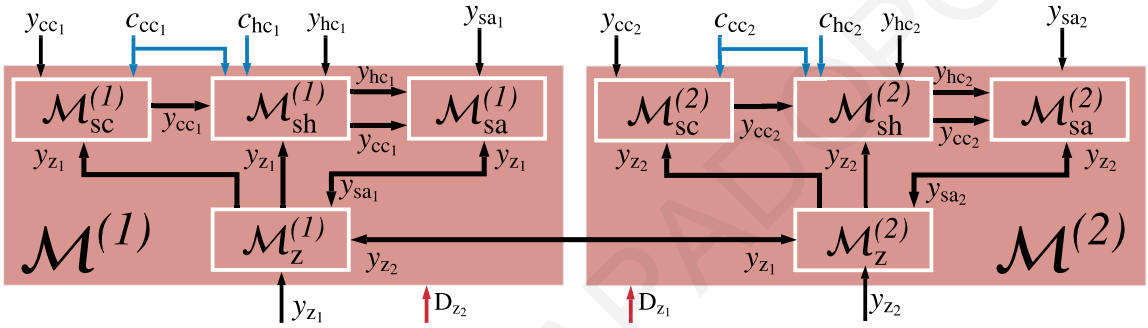

(b) Agents of the AHU HVAC system

Figure 6.1: Distributed Fault Diagnosis Architecture for AHU HVAC systems.

Note that for the purposes of this work the measurements of heated and chilled water temperature in the storage tank T^{h}_{st} and T^{c}_{st}, respectively and ambient air temperature T_{amb} are considered known and healthy.

6.3 Design of the Distributed Fault Diagnosis Agent

This section presents the design of the proposed distributed fault diagnosis algorithm. As illustrated in Fig. 6.2, an FD Agent is designed for each zone-AHU that uses:

- the local control inputs for the water mass flow rates for the heating coil u_{hc_i} and for the cooling coil u_{hc_i} determined by the controller,
- the local measurements from the sensors installed in the local AHU i.e., zone air temperature y_{z_i}, supply air temperature y_{sa_i}, water temperature in the heating coil y_{hc_i}, water temperature in the cooling coil y_{cc_i},
- the air temperature measurements from the sensors located in the neighboring zones y_{z_j}, for all $j \in \mathcal{N}_i$, and
- the detection decision signals D_{z_j} from the $\mathcal{N}_i$ neighboring Fault Diagnosis Agents.

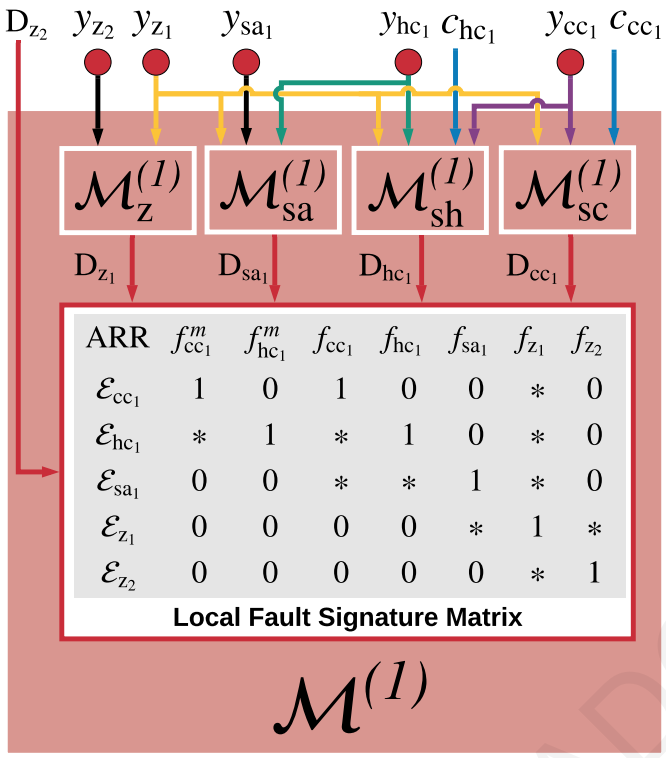

Figure 6.2: The design of the Fault Diagnosis (FD) Agent 1 of zone 1. Since zone 1 is interconnected with zone 2, the air temperature measurements of zone 2 (y_{z_2}) and the detection decision of Fault Diagnosis Agent 2 D_{z_2} are used in the fault diagnosis process of FD Agent 1.

Fig. 6.2 illustrates the architecture of the local Fault Diagnosis Agent of zone 1, where zone 1 is physically interconnected with zone 2. The diagnosis procedure of each agent consists the following on-line processes:

1. *State Estimation*. Estimation of zone air temperature by module $\mathcal{M}_z^{(i)}$, supply air temperature by module $\mathcal{M}_{sa}^{(i)}$, heating coil water temperature by module $\mathcal{M}_{sh}^{(i)}$ and cooling coil water temperature by module $\mathcal{M}_{sc}^{(i)}$.
2. *Fault Detection*. In every module, the fault detection process is based on the development of analytical redundancy relations (ARRs) for each estimated quantity. Each ARR corresponds to the comparison of a residual (i.e., the difference between the measured and each estimated quantity) with an adaptive threshold calculated considering a healthy system (i.e., absence of faults). Thus, the residual should be maintained below the adaptive threshold under healthy conditions for all time instances and the violation of the ARRs triggers an alarm and indicates the detection of a fault or faults.
3. *Distributed Fault Isolation* is responsible to reveal the location of fault. Local and neighboring detection signals form an observed decision pattern $\mathcal{D}^{(i)} = \left[D_{cc_i}, D_{hc_i}, D_{sa_j}, D_{z_i}, D_{z_j}\right]$ that is online compared with a number of theoretical decision patterns obtained by the Fault Signature Matrix illustrated in Fig. 6.2 and Table 6.2. The matrix uses binary logic and assigns "1" if a

fault pattern can directly affect an ARR, "*" if a fault pattern can indirectly (through shared measurements) affect an ARR and assigns "0" if a fault pattern can not affect an ARR. If the outcome of comparison is unique, then we can reach to a decision about the location of fault(s) or if is not unique we can reduce the number of candidate faults that trigger the alarm.

The design of the proposed distributed FD algorithm considers the following assumptions:

Assumption 6. The modeling uncertainty term $Q_i(t)$ produced by the internal heat gains, that is not available, is considered to be bounded by known bound $\overline{Q}_i$ such as $|Q_i(t)| \leq \overline{Q}_i(t)$, for all t and $i \in N$.

Assumption 7. The noise in measurements n_{z_i} n_{sa_i}, n_{hc_i} n_{cc_i} are unknown but using sensors accuracy given by manufactures' technical specifications we are able to obtain upper bounds on the measurements noise such as; $\left|n_{z_i}(t)\right| \leq \overline{n}_{z_i}$, $\left|n_{sa_i}(t)\right| \leq \overline{n}_{sa_i}$, $\left|n_{hc_i}(t)\right| \leq \overline{n}_{hc_i}$ and $\left|n_{cc_i}(t)\right| \leq \overline{n}_{cc_i}$, for all t and $i \in N$.

Using the above assumptions and the model presented in Chapter 2.5, the design of the distributed fault diagnosis algorithm is presented next.

6.3.1 Distributed Estimation Algorithm

In this section the design of the distributed estimation algorithm for each module within every FD agent $\mathcal{M}^{()i}$, for all $i \in N$, is presented.

Zone Air Temperature Estimation

This section illustrates the design of the estimator of the zone air temperature of module $\mathcal{M}_z^{(i)}$, where a dedicated Luenberger observer is designed to estimate the air temperature T_{z_i} in the ith zone as follows

$$\hat{T}_{z_i}(k+1) = A_{z_i}^{d}\hat{T}_{z_i}(k) + B_{z_i}^{d}\left(y_{sa_i}(k) + \sum_{j\in N_i}\frac{a_{i,j}}{\dot{m}_{sa_i}C_{pa}}y_{z_j}(k) + \frac{a_{z_i}}{\dot{m}_{sa_i}C_{pa}}T_{amb}(k)\right) + L_{z_i}\left(y_{z_i}(k) - \hat{T}_{z_i}(k)\right), \tag{6.1}$$

where $\hat{T}_{z_i}$ is the estimation of the ith zone air temperature with $\hat{T}_{z_i}(0) = 0$ and L_{z_i} is the observer gain selected such that $|\lambda(A_{z_i}^{d} - B_{z_i}^{d}L_{z_i})| < 1$, in order to ensure the asymptotic stability of the observer.

Then, let's define zone air temperature estimation error $\varepsilon_{z_i}(k) = T_{z_i}(k) - \hat{T}_{z_i}(k)$, where zone state-estimation error dynamics are the following:

$$\varepsilon_{z_i}(k+1) = \left(A_{z_i}^{d} - B_{z_i}^{d}L_{z_i}\right)\varepsilon_{z_i}(k) + B_{z_i}^{d}\left(-n_{sa_i}(k) - f_{sa_i}(k) + \sum_{j\in N_i}\frac{a_{ij}}{\dot{m}_{sa_i}C_{pa}}\left(-n_{z_j}(k) - f_{z_j}(k)\right)\right.$$
$$\left. + \frac{Q_i(k)}{\dot{m}_{sa_i}C_{pa}}\right) + L_{z_i}\left(n_{z_i}(k) + f_{z_i}(k)\right). \tag{6.2}$$

The solution of *i*th zone estimation error can be obtained as

$$\varepsilon_{\mathrm{z}_i}(k) = \left(A^{\mathrm{d}}_{\mathrm{z}_i} - B^{\mathrm{d}}_{\mathrm{z}_i} L_{\mathrm{z}_i}\right)^k \epsilon_{\mathrm{z}_i}(0) + B^{\mathrm{d}}_{\mathrm{z}_i} \sum_{z=1}^{k-1} \left(A^{\mathrm{d}}_{\mathrm{z}_i} - B^{\mathrm{d}}_{\mathrm{z}_i} L_{\mathrm{z}_i}\right)^{k-1-z} \Bigg(- n_{\mathrm{sa}_i}(z) - f_{\mathrm{sa}_i}(z) + \sum_{j \in N_i} \frac{a_{ij}}{\dot{m}_{\mathrm{sa_i}} C_{\mathrm{pa}}} \left(-n_{\mathrm{z}_j}(z) - f_{\mathrm{z}_j}(z)\right) + \frac{Q_i(z)}{\dot{m}_{\mathrm{sa_i}} C_{\mathrm{pa}}} \Bigg) + L_{\mathrm{z}_i} \left(n_{\mathrm{z}_i}(z) + f_{\mathrm{z}_i}(z)\right). \tag{6.3}$$

Supply Air Temperature Estimation

In order to design a proper observer that can estimate the temperature of supply air, which is produced by the AHU, A dedicated Luenberger observer is designed to estimate the supply air temperature $\mathbf{T}_{\mathrm{sa}_i}$ that is vector containing the air that passes through the cooling coil $T_{\mathrm{c,sa}_i}$ and the air that passes through the heating coil $T_{\mathrm{h,sa}_i}$ in the *i*th AHU as follows

$$\hat{\mathbf{T}}_{\mathrm{sa}_i}(k+1) = \mathbf{A}^{\mathrm{d}}_{\mathrm{sa}_i} \hat{\mathbf{T}}_{\mathrm{sa}_i}(k) + \mathbf{B}^{\mathrm{d}}_{\mathrm{sa}_i} \left(\begin{bmatrix} y_{\mathrm{cc}_i}(k) \\ y_{\mathrm{hc}_i}(k) \end{bmatrix} + \mathbf{G}_{\mathrm{f,sa}_i} + \mathbf{G}_{\mathrm{amb,sa}_i} T_{\mathrm{amb}}(k) + \mathbf{G}_{\mathrm{ma,sa}_i} y_{\mathrm{z}_i}(k) \right) + \mathbf{L}_{\mathrm{sa}_i} \left(y_{\mathrm{sa}_i}(k) - \mathbf{C} \hat{\mathbf{T}}_{\mathrm{sa}_i}(k) \right), \tag{6.4}$$

where $\hat{\mathbf{T}}_{\mathrm{sa}_i} = \begin{bmatrix} \hat{T}_{\mathrm{c,sa}_i}(k) & \hat{T}_{\mathrm{h,sa}_i}(k) \end{bmatrix}^\top$ is vector that contains the estimation of the air temperature in the cooling and heating coil with $\hat{\mathbf{T}}_{\mathrm{sa}_i}(0) = \mathbf{0}_{2\times 1}$ and $\mathbf{L}_{\mathrm{sa}_i} \in \mathbb{R}^{2\times 1}$ is a vector that consists of the observer gains selected such that $|\lambda_{\max}(\mathbf{A}^{\mathrm{d}}_{\mathrm{sa}_i} - \mathbf{L}_{\mathrm{sa}_i}\mathbf{C})| < 1$ in order to ensure the asymptotic stability of the observer. Then, let's define zone air temperature estimation error $\boldsymbol{\varepsilon}_{\mathrm{sa}_i}(k) = \mathbf{T}_{\mathrm{sa}_i}(k) - \hat{\mathbf{T}}_{\mathrm{sa}_i}(k)$, where zone state-estimation error dynamics are the following:

$$\boldsymbol{\varepsilon}_{\mathrm{sa}_i}(k+1) = \left(\mathbf{A}^{\mathrm{d}}_{\mathrm{sa}_i} - \mathbf{L}_{\mathrm{sa}_i}\mathbf{C}\right) \boldsymbol{\varepsilon}_{\mathrm{sa}_i}(k) + \mathbf{B}^{\mathrm{d}}_{\mathrm{sa}_i} \left(\begin{bmatrix} -n_{\mathrm{cc}_i}(k) - f_{\mathrm{cc}_i}(k) \\ -n_{\mathrm{hc}_i}(k) - f_{\mathrm{hc}_i}(k) \end{bmatrix} + \mathbf{G}_{\mathrm{ma,sa}_i} \left(n_{\mathrm{z}_i}(k) + f_{\mathrm{z}_i}(k)\right) \right) + \mathbf{L}_{\mathrm{sa}_i} \left(n_{\mathrm{sa}_i}(k) + f_{\mathrm{sa}_i}(k)\right) \tag{6.5}$$

The solution of supply air estimation error can be obtained as

$$\boldsymbol{\varepsilon}_{\mathrm{sa}_i}(k) = \left(\mathbf{A}^{\mathrm{d}}_{\mathrm{sa}_i} - \mathbf{L}_{\mathrm{sa}_i}\mathbf{C}\right)^k \boldsymbol{\varepsilon}_{\mathrm{sa}_i}(0) + \mathbf{B}^{\mathrm{d}}_{\mathrm{sa}_i} \sum_{z=1}^{k-1} \left(\mathbf{A}^{\mathrm{d}}_{\mathrm{sa}_i} - \mathbf{L}_{\mathrm{sa}_i}\mathbf{C}\right)^{k-1-z} \times \left(\begin{bmatrix} -n_{\mathrm{cc}_i}(z) - f_{\mathrm{cc}_i}(z) \\ -n_{\mathrm{hc}_i}(z) - f_{\mathrm{hc}_i}(z) \end{bmatrix} + \mathbf{G}_{\mathrm{ma,sa}_i} \left(n_{\mathrm{z}_i}(z) + f_{\mathrm{z}_i}(z)\right) \right) + \mathbf{L}_{\mathrm{sa}_i} \left(n_{\mathrm{sa}_i}(z) + f_{\mathrm{sa}_i}(z)\right). \tag{6.6}$$

Cooling Coil's Water Temperature Estimation

A dedicated Luenberger observer is designed to estimate the supply air temperature that pass through the cooling coil $T_{\mathrm{c,sa}_i}$ and the water temperature in the cooling coil T_{cc_i} of the ith AHU as follows

$$\hat{\mathbf{T}}_{\mathrm{sc}_i}(k+1) = \mathbf{A}^{\mathrm{d}}_{\mathrm{sc}_i}\hat{\mathbf{T}}_{\mathrm{sc}_i}(k) + \mathbf{B}^{\mathrm{d}}_{\mathrm{sc}_i}\left(\mathbf{C}^{\top}\left(T^{\mathrm{c}}_{\mathrm{st}}(k) - y_{\mathrm{cc}_i}(k)\right)c_{\mathrm{cc_i}}(k) + \mathbf{G}_{\mathrm{f,sc}_i} + \mathbf{G}_{\mathrm{amb,sc}_i}T_{\mathrm{amb}}(k) + \mathbf{G}_{\mathrm{ma,sc}_i}y_{\mathrm{z}_i}(k)\right) + \mathbf{L}_{\mathrm{sc}_i}\left(y_{\mathrm{cc}_i}(k) - \mathbf{C}\hat{\mathbf{T}}_{\mathrm{sc}_i}(k)\right), \tag{6.7}$$

where $\hat{\mathbf{T}}_{\mathrm{sc}_i} = \begin{bmatrix} \hat{T}_{\mathrm{c,sa}_i}(k) & \hat{T}_{\mathrm{cc}_i}(k) \end{bmatrix}^{\top}$ is vector that contains the estimation of the air temperature in the cooling and heating coil with $\hat{\mathbf{T}}_{\mathrm{sc}_i}(0) = \mathbf{0}_{2\times 1}$ and $\mathbf{L}_{\mathrm{sc}_i} \in \mathbb{R}^{2\times 1}$ is a vector that consists of the observer gains selected such that $|\lambda_{max}(\mathbf{A}^{\mathrm{d}}_{\mathrm{sc}_i} - \mathbf{L}_{\mathrm{sc}_i}\mathbf{C})| < 1$ in order to ensure the asymptotic stability of the observer. Then, let's define zone air temperature estimation error $\boldsymbol{\varepsilon}_{\mathrm{sc}_i}(k) = \mathbf{T}_{\mathrm{sc}_i}(k) - \hat{\mathbf{T}}_{\mathrm{sc}_i}(k)$, where zone state-estimation error dynamics are the following:

$$\begin{aligned}\boldsymbol{\varepsilon}_{\mathrm{sc}_i}(k+1) = {} & \left(\mathbf{A}^{\mathrm{d}}_{\mathrm{sc}_i} - \mathbf{L}_{\mathrm{sc}_i}\mathbf{C}\right)\boldsymbol{\varepsilon}_{\mathrm{sc}_i}(k) - \mathbf{B}^{\mathrm{d}}_{\mathrm{sc}_i}\mathbf{C}^{\top}\left(n_{\mathrm{cc}_i}(k) + f_{\mathrm{cc}_i}(k)\right)c_{\mathrm{cc}_i}(k) \\ & + \mathbf{B}^{\mathrm{d}}_{\mathrm{sc}_i}\mathbf{C}^{\top}\left(T^{\mathrm{c}}_{\mathrm{st}}(k) - T_{\mathrm{cc}_i}(k)\right)f^{m}_{\mathrm{cc}_i}(k) + \mathbf{B}^{\mathrm{d}}_{\mathrm{sc}_i}\left(\mathbf{G}_{\mathrm{ma,sc}_i}\left(n_{\mathrm{z}_i}(k) + f_{\mathrm{z}_i}(k)\right)\right) \\ & + \mathbf{L}_{\mathrm{sc}_i}\left(n_{\mathrm{cc}_i}(k) + f_{\mathrm{cc}_i}(k)\right).\end{aligned} \tag{6.8}$$

The solution of cooling coil's air and water temperature estimation error can be obtained as

$$\begin{aligned}\boldsymbol{\varepsilon}_{\mathrm{sc}_i}(k) = {} & \left(\widetilde{\mathbf{A}}_{\mathrm{sc}_i}\right)^{k}\boldsymbol{\varepsilon}_{\mathrm{sc}_i}(0) - \mathbf{B}^{\mathrm{d}}_{\mathrm{sc}_i}\sum_{z=1}^{k-1}\left(\widetilde{\mathbf{A}}_{\mathrm{sc}_i}\right)^{k-1-z}\mathbf{C}^{\top}\left(n_{\mathrm{cc}_i}(z) + f_{\mathrm{cc}_i}(k)\right)c_{\mathrm{cc}_i}(z) \\ & + \mathbf{B}^{\mathrm{d}}_{\mathrm{sc}_i}\sum_{z=1}^{k-1}\left(\widetilde{\mathbf{A}}_{\mathrm{sc}_i}\right)^{k-1-z}\mathbf{C}^{\top}\left(T^{\mathrm{c}}_{\mathrm{st}}(z) - T_{\mathrm{cc}_i}(z)\right)f^{m}_{\mathrm{cc}_i}(z) + \mathbf{B}^{\mathrm{d}}_{\mathrm{sc}_i}\sum_{z=1}^{k-1}\left(\widetilde{\mathbf{A}}_{\mathrm{sc}_i}\right)^{k-1-z}\mathbf{G}_{\mathrm{ma,sc}_i}\left(n_{\mathrm{z}_i}(z) + f_{\mathrm{z}_i}(z)\right) \\ & + \sum_{z=1}^{k-1}\left(\widetilde{\mathbf{A}}_{\mathrm{sc}_i}\right)^{k-1-z}\mathbf{L}_{\mathrm{sc}_i}\left(n_{\mathrm{cc}_i}(z) + f_{\mathrm{cc}_i}(z)\right),\end{aligned} \tag{6.9}$$

where $\widetilde{\mathbf{A}}_{\mathrm{sc}_i} = \mathbf{A}^{\mathrm{d}}_{\mathrm{sc}_i} - \mathbf{L}_{\mathrm{sc}_i}\mathbf{C}$.

Heating Coil's Water Temperature Estimation

A dedicated Luenberger observer is designed to estimate the supply air temperature that pass through the cooling coil $T_{\mathrm{h,sa}_i}$ and the water temperature in the cooling coil T_{hc_i} of the ith AHU as follows

$$\begin{aligned}\hat{\mathbf{T}}_{\mathrm{sh}_i}(k+1) = {} & \mathbf{A}^{\mathrm{d}}_{\mathrm{sh}_i}\hat{\mathbf{T}}_{\mathrm{sh}_i}(k) + \mathbf{B}^{\mathrm{d}}_{\mathrm{sh}_i}\left(\mathbf{C}^{\top}_{\mathrm{sc}}\left(T^{\mathrm{c}}_{\mathrm{st}}(k) - \mathbf{C}_{\mathrm{sc}_i}\mathbf{T}_{\mathrm{sh}_i}(k)\right)c_{\mathrm{cc_i}}(k) + \mathbf{C}^{\top}_{\mathrm{sh}}\left(T^{\mathrm{h}}_{\mathrm{st}}(k) - \mathbf{C}_{\mathrm{sh}_i}\mathbf{T}_{\mathrm{sh}_i}(k)\right)c_{\mathrm{hc_i}}(k)\right. \\ & \left. + \mathbf{G}_{\mathrm{f,sh}_i} + \mathbf{G}_{\mathrm{amb,sh}_i}T_{\mathrm{amb}}(k) + \mathbf{G}_{\mathrm{ma,sh}_i}y_{\mathrm{z}_i}(k)\right) + \mathbf{L}_{\mathrm{sh}_i}\left(y_{\mathrm{hc}_i}(k) - \mathbf{C}\hat{\mathbf{T}}_{\mathrm{sh}_i}(k)\right),\end{aligned} \tag{6.10}$$

where $\hat{\mathbf{T}}_{\mathrm{sh}_i}(k) = \begin{bmatrix} \hat{T}_{\mathrm{c,sa}_i}(k) & \hat{T}_{\mathrm{cc}_i}(k) & \hat{T}_{\mathrm{h,sa}_i}(k) & \hat{T}_{\mathrm{hc}_i}(k) \end{bmatrix}^\top$ is vector that contains the estimation of the air temperature in the cooling and heating coil with $\hat{\mathbf{T}}_{\mathrm{sh}_i}(0) = \mathbf{0}_{4\times 1}$ and $\mathbf{L}_{\mathrm{sh}_i} \in \mathbb{R}^{4\times 1}$ is a vector that consists of the observer gains selected such that $|\lambda_{\max}(\mathbf{A}^{\mathrm{d}}_{\mathrm{sh}_i} - \mathbf{L}_{\mathrm{sh}_i}\mathbf{C}_{\mathrm{sh}})| < 1$ in order to ensure the asymptotic stability of the observer. Then, let's define zone air temperature estimation error $\boldsymbol{\varepsilon}_{\mathrm{sh}_i}(k) = \mathbf{T}_{\mathrm{sh}_i}(k) - \hat{\mathbf{T}}_{\mathrm{sh}_i}(k)$, where zone state-estimation error dynamics are the following:

$$\begin{aligned}\boldsymbol{\varepsilon}_{\mathrm{sh}_i}(k+1) = {} & \left(\mathbf{A}^{\mathrm{d}}_{\mathrm{sh}_i} - \mathbf{L}_{\mathrm{sh}_i}\mathbf{C}_{\mathrm{sh}}\right)\boldsymbol{\varepsilon}_{\mathrm{sh}_i}(k) - \mathbf{B}^{\mathrm{d}}_{\mathrm{sh}_i}\mathbf{C}^{\top}_{\mathrm{sc}}\left(n_{\mathrm{cc}_i}(k) + f_{\mathrm{cc}_i}(k)\right)c_{\mathrm{cc}_i}(k) \\ & - \mathbf{B}^{\mathrm{d}}_{\mathrm{sh}_i}\mathbf{C}^{\top}_{\mathrm{sh}}\left(n_{\mathrm{hc}_i}(k) + f_{\mathrm{hc}_i}(k)\right)c_{\mathrm{hc}_i}(k) + \mathbf{B}^{\mathrm{d}}_{\mathrm{sh}_i}\mathbf{C}^{\top}_{\mathrm{sc}}\left(T^{\mathrm{c}}_{\mathrm{st}}(k) - T_{\mathrm{cc}_i}(k)\right)f^{m}_{\mathrm{cc}_i}(k) \\ & + \mathbf{B}^{\mathrm{d}}_{\mathrm{sh}_i}\mathbf{C}^{\top}_{\mathrm{sh}}\left(T^{\mathrm{h}}_{\mathrm{st}}(k) - T_{\mathrm{hc}_i}(k)\right)f^{m}_{\mathrm{hc}_i}(k) + \mathbf{B}^{\mathrm{d}}_{\mathrm{sc}_i}\mathbf{G}_{\mathrm{ma,sh}_i}\left(n_{\mathrm{z}_i}(k) + f_{\mathrm{z}_i}(k)\right) \\ & + \mathbf{L}_{\mathrm{sh}_i}\left(n_{\mathrm{hc}_i}(k) + f_{\mathrm{hc}_i}(k)\right). \end{aligned} \tag{6.11}$$

The solution of cooling coil's air and water temperature estimation error can be obtained as

$$\begin{aligned}\boldsymbol{\varepsilon}_{\mathrm{sh}_i}(k) = {} & \left(\widetilde{\mathbf{A}}_{\mathrm{sh}_i}\right)^{k}\boldsymbol{\varepsilon}_{\mathrm{sh}_i}(0) - \sum_{z=1}^{k-1}\left(\widetilde{\mathbf{A}}_{\mathrm{sh}_i}\right)^{k-1-z}\mathbf{B}^{\mathrm{d}}_{\mathrm{sh}_i}\mathbf{C}^{\top}_{\mathrm{sc}}\left(n_{\mathrm{cc}_i}(z) + f_{\mathrm{cc}_i}(k)\right)c_{\mathrm{cc}_i}(z) \\ & - \sum_{z=1}^{k-1}\left(\widetilde{\mathbf{A}}_{\mathrm{sh}_i}\right)^{k-1-z}\mathbf{B}^{\mathrm{d}}_{\mathrm{sh}_i}\mathbf{C}^{\top}_{\mathrm{sh}}\left(n_{\mathrm{hc}_i}(z) + f_{\mathrm{hc}_i}(k)\right)c_{\mathrm{hc}_i}(z) \\ & + \sum_{z=1}^{k-1}\left(\widetilde{\mathbf{A}}_{\mathrm{sh}_i}\right)^{k-1-z}\mathbf{B}^{\mathrm{d}}_{\mathrm{sh}_i}\mathbf{C}^{\top}_{\mathrm{sc}}\left(T^{\mathrm{c}}_{\mathrm{st}}(z) - T_{\mathrm{cc}_i}(z)\right)f^{m}_{\mathrm{cc}_i}(z) \\ & + \sum_{z=1}^{k-1}\left(\widetilde{\mathbf{A}}_{\mathrm{sh}_i}\right)^{k-1-z}\mathbf{B}^{\mathrm{d}}_{\mathrm{sh}_i}\mathbf{C}^{\top}_{\mathrm{sh}}\left(T^{\mathrm{h}}_{\mathrm{st}}(z) - T_{\mathrm{hc}_i}(z)\right)f^{m}_{\mathrm{hc}_i}(z) \\ & + \sum_{z=1}^{k-1}\left(\widetilde{\mathbf{A}}_{\mathrm{sh}_i}\right)^{k-1-z}\mathbf{B}^{\mathrm{d}}_{\mathrm{sc}_i}\mathbf{G}_{\mathrm{ma,sh}_i}\left(n_{\mathrm{z}_i}(z) + f_{\mathrm{z}_i}(z)\right) + \sum_{z=1}^{k-1}\left(\widetilde{\mathbf{A}}_{\mathrm{sh}_i}\right)^{k-1-z}\mathbf{L}_{\mathrm{sh}_i}\left(n_{\mathrm{hc}_i}(z) + f_{\mathrm{hc}_i}(z)\right), \end{aligned} \tag{6.12}$$

where $\widetilde{\mathbf{A}}_{\mathrm{sh}_i} = \mathbf{A}^{\mathrm{d}}_{\mathrm{sh}_i} - \mathbf{L}_{\mathrm{sh}_i}\mathbf{C}_{\mathrm{sh}}$.

6.3.2 Distributed Fault Detection Algorithm

This section presents the design of the fault detection algorithm that involves the creation of analytical redundancy relations (ARRs) comprised of residuals and adaptive thresholds assuming healthy system i.e., $f_{\mathrm{z}_i}(k)= f_{\mathrm{sa}_i}(k)= f_{\mathrm{cc}_i}(k)= f_{\mathrm{hc}_i}(k)= f^{m}_{\mathrm{cc}_i}(k)= f^{m}_{\mathrm{hc}_i}(k)=0$ for all $i \in N$. The ARRs should be valid in the absence of faults and violated in their presence. The residuals are formed as follows:

$$\epsilon_{\mathrm{z}_i}(k) = y_{\mathrm{z}_i}(k) - \hat{T}_{\mathrm{z}_i}(k), \tag{6.13}$$

$$\epsilon_{\mathrm{sa}_i}(k) = y_{\mathrm{sa}_i}(k) - \mathbf{C}\hat{\mathbf{T}}_{\mathrm{sa}_i}(k) \tag{6.14}$$

$$\epsilon_{\mathrm{cc}_i}(k) = y_{\mathrm{cc}_i}(k) - \mathbf{C}\hat{\mathbf{T}}_{\mathrm{sc}_i}(k), \tag{6.15}$$

$$\epsilon_{\mathrm{hc}_i}(k) = y_{\mathrm{hc}_i}(k) - \mathbf{C}_{\mathrm{sh}}\hat{\mathbf{T}}_{\mathrm{sh}_i}(k). \tag{6.16}$$

where the estimations $\hat{T}_{z_i}(k)$, $\hat{\mathbf{T}}_{sa_i}(k)$, $\hat{\mathbf{T}}_{sc_i}(k)$, $\hat{\mathbf{T}}_{sh_i}(k)$ are obtained by the observers given in (6.1), (6.4), (6.7) and (6.10).

Thus, the fault detection process involves the computation of an adaptive for each one the above residuals such that under healthy conditions the following ARR's must be satisfied for all $k \geq 0$;

$$\mathcal{E}_{z_i}: \quad \left|\epsilon_{z_i}(k)\right| \leq \bar{\epsilon}_{z_i}(k), \tag{6.17}$$

$$\mathcal{E}_{sa_i}: \quad \left|\epsilon_{sa_i}(k)\right| \leq \bar{\epsilon}_{sa_i}(k), \tag{6.18}$$

$$\mathcal{E}_{cc_i}: \quad \left|\epsilon_{cc_i}(k)\right| \leq \bar{\epsilon}_{cc_i}(k), \tag{6.19}$$

$$\mathcal{E}_{hc_i}: \quad \left|\epsilon_{hc_i}(k)\right| \leq \bar{\epsilon}_{hc_i}(k), \tag{6.20}$$

where $\bar{\epsilon}$ denotes the corresponding adaptive threshold. The computation of the adaptive thresholds are presented next.

Computation of Zone's Adaptive Threshold

The first step in the computation of adaptive threshold is to express the residual with respect to the corresponding estimation error. Thus, the residual $\epsilon_{z_i}(k)$ can be defined using the zone's air temperature estimation error $\varepsilon_{z_i}(k)$ given in (6.3) as follows

$$\epsilon_{z_i}(k) = y_{z_i}(k) - \hat{T}_{z_i}(k) \tag{6.21}$$

$$= \varepsilon_{z_i}(k) + n_{z_i}(k) + f_{z_i}(k). \tag{6.22}$$

From (6.3) and (6.22) can be concluded that residual $\epsilon_{z_i}(k)$ can be affected by the sensor faults f_{z_i}, f_{sa_i} and f_{z_j}, for all $j \in N_i$. Considering healthy conditions (i.e., f_{z_i}=0, f_{sa_i}=0 and f_{z_j}=0, for all $j \in N_i$), taking into account Assumptions 6 and 7 and by applying the Minkowski inequality on (6.22) we can obtained the adaptive threshold $\bar{\epsilon}_{z_i}(k)$ that corresponds to the residual $\epsilon_{z_i}(k)$, i.e.,

$$\left|\epsilon_{z_i}(k)\right| \leq \bar{\epsilon}_{z_i}(k) \tag{6.23}$$

$$= \alpha_{z_i}^k \epsilon_{z_i}^o + \bar{n}_{z_i} + B_{z_i}^d \sum_{z=1}^{k-1} (\alpha_{z_i})^{k-1-z} \left[\bar{n}_{sa_i} + \sum_{j \in N_i} \frac{a_{i,j}}{\dot{m}_{sa_i} C_{pa}} \left(\bar{n}_{z_j}\right) + L_{z_i}\left(\bar{n}_{z_i}\right) + \frac{\overline{Q}_i}{\dot{m}_{sa_i} C_{pa}} \right], \tag{6.24}$$

with $\left(A_{z_i}^d - B_{z_i}^d L_{z_i}\right) \leq \alpha_{z_i} < 1$ and $|\varepsilon_{z_i}(0)| \leq \epsilon_{z_i}^o$, where α_{z_i} and $\epsilon_{z_i}^o$ are design parameters.

Computation of Supply Air Adaptive Threshold

The residual $\epsilon_{sa_i}(k)$ can be defined using the zone's air temperature estimation error $\boldsymbol{\varepsilon}_{sa_i}(k)$ given in (6.6) as follows

$$\epsilon_{sa_i}(k) = y_{sa_i}(k) - \mathbf{C}\hat{\mathbf{T}}_{sa_i}(k) \tag{6.25}$$

$$= \mathbf{C}\boldsymbol{\varepsilon}_{sa_i}(k) + n_{sa_i}(k) + f_{sa_i}(k). \tag{6.26}$$

From (6.26) is concluded that residual $\epsilon_{\mathrm{sa}_i}(k)$ can be affected by the sensor faults f_{z_i}, f_{c_i}, f_{sa_i}. Considering now healthy conditions (i.e., f_{z_i}=0, f_{c_i}=0, f_{sa_i}=0) and by applying the Minkowski inequality on (6.6), the computation of the adaptive threshold $\bar{\epsilon}_{\mathrm{sa}_i}(k)$ on the residual $\epsilon_{\mathrm{sa}_i}(k)$ is described by

$$\begin{aligned}\left\|\epsilon_{\mathrm{sa}_i}(k)\right\| \leq \left\|\mathbf{C}\left(\tilde{\mathbf{A}}_{\mathrm{sa}_i}\right)^k \boldsymbol{\varepsilon}_{\mathrm{sa}_i}(0)\right\| + \left\|n_{\mathrm{sa}_i}(k)\right\| + \left\|\mathbf{C}\mathbf{B}^{\mathrm{d}}_{\mathrm{sa}_i}\sum_{z=1}^{k-1}\left(\tilde{\mathbf{A}}_{\mathrm{sa}_i}\right)^{k-1-z}\begin{bmatrix}-n_{\mathrm{cc}_i}(z)\\ -n_{\mathrm{hc}_i}(z)\end{bmatrix}\right\| \\ + \left\|\mathbf{C}\mathbf{B}^{\mathrm{d}}_{\mathrm{sa}_i}\sum_{z=1}^{k-1}\left(\tilde{\mathbf{A}}_{\mathrm{sa}_i}\right)^{k-1-z}\mathbf{G}_{\mathrm{ma,sa}_i}\left(n_{\mathrm{z}_i}(z)\right)\right\| + \left\|\mathbf{C}\mathbf{B}^{\mathrm{d}}_{\mathrm{sa}_i}\sum_{z=1}^{k-1}\left(\tilde{\mathbf{A}}_{\mathrm{sa}_i}\right)^{k-1-z}\mathbf{L}_{\mathrm{sa}_i}\left(n_{\mathrm{sa}_i}(z)\right)\right\|.\end{aligned} \tag{6.27}$$

where $\widetilde{\mathbf{A}}_{\mathrm{sa}_i} = \mathbf{A}^{\mathrm{d}}_{\mathrm{sa}_i} - \mathbf{L}_{\mathrm{sa}_i}\mathbf{C}$. Then, using the Assumption 6 and by applying Schwartz inequality the above equation results to the following adaptive threshold

$$\left|\epsilon_{\mathrm{sa}_i}(k)\right| \leq \bar{\epsilon}_{\mathrm{sa}_i}(k) \tag{6.28}$$

$$= \left(\alpha_{\mathrm{sa}_i}\right)^k \epsilon^o_{\mathrm{sa}_i} + \bar{n}_{\mathrm{sa}_i} + \sum_{z=1}^{k-1}\left(\alpha_{\mathrm{sa}_i}\right)^{k-1-z}\left\|\mathbf{B}^{\mathrm{d}}_{\mathrm{sa}_i}\right\|\left(\bar{n}_{\mathrm{cc}_i} + \bar{n}_{\mathrm{hc}_i}\right) + \sum_{z=1}^{k-1}\left(\alpha_{\mathrm{sa}_i}\right)^{k-1-z}\left\|\mathbf{B}^{\mathrm{d}}_{\mathrm{sa}_i}\mathbf{G}_{\mathrm{ma,sa}_i}\right\|\bar{n}_{\mathrm{z}_i} + \sum_{z=1}^{k-1}\left(\alpha_{\mathrm{sa}_i}\right)^{k-1-z}\left\|\mathbf{L}_{\mathrm{sa}_i}\right\|\bar{n}_{\mathrm{sa}_i}, \tag{6.29}$$

where $\left\|\mathbf{C}\left(\tilde{\mathbf{A}}_{\mathrm{sa}_i}\right)^k\right\| \leq \left(\alpha_{\mathrm{sa}_i}\right)^k$ and $\left\|\boldsymbol{\varepsilon}_{\mathrm{sa}_i}(0)\right\| \leq \epsilon^o_{\mathrm{sa}_i}$ for all $k \geq 0$. Note that $\alpha_{\mathrm{sa}_i} < 1$ and $\epsilon^o_{\mathrm{sa}_i}$ are design parameters.

Computation of Cooling Coil's Adaptive Threshold

The residual $\epsilon_{\mathrm{cc}_i}(k)$ can be defined using the cooling coil's air and water temperature estimation error $\boldsymbol{\varepsilon}_{\mathrm{sc}_i}(k)$ given in (6.9) as follows

$$\epsilon_{\mathrm{cc}_i}(k) = y_{\mathrm{cc}_i}(k) - \mathbf{C}\hat{\mathbf{T}}_{\mathrm{sc}_i}(k) \tag{6.30}$$

$$= \mathbf{C}\boldsymbol{\varepsilon}_{\mathrm{sc}_i}(k) + n_{\mathrm{cc}_i}(k) + f_{\mathrm{cc}_i}(k), \tag{6.31}$$

From (6.26) is concluded that residual $\epsilon_{\mathrm{sa}_i}(k)$ can be affected by the sensor faults f_{z_i} and f_{cc_i}. Considering now healthy conditions (i.e., f_{z_i}=0, f_{cc_i}=0, f_{sa_i}=0). The computation of the adaptive threshold $\bar{\epsilon}_{\mathrm{sa}_i}(k)$ on the residual $\epsilon_{\mathrm{sa}_i}(k)$ is presented in Appendix B and the result is the following

$$\left|\epsilon_{\mathrm{cc}_i}(k)\right| \leq \bar{\epsilon}_{\mathrm{cc}_i}(k) \tag{6.32}$$

$$= \left(\alpha_{\mathrm{sc}_i}\right)^k \epsilon^o_{\mathrm{sc}_i} + \bar{n}_{\mathrm{cc}_i} + \sum_{z=1}^{k-1}\left(\alpha_{\mathrm{sc}_i}\right)^{k-1-z}\left\|\mathbf{B}^{\mathrm{d}}_{\mathrm{sc}_i}\right\|\bar{n}_{\mathrm{cc}_i}\left|c_{\mathrm{cc}_i}(z)\right| + \sum_{z=1}^{k-1}\left(\alpha_{\mathrm{sc}_i}\right)^{k-1-z}\left\|\mathbf{B}^{\mathrm{d}}_{\mathrm{sc}_i}\mathbf{G}_{\mathrm{ma,sc}_i}\right\|\bar{n}_{\mathrm{z}_i} + \sum_{z=1}^{k-1}\left(\alpha_{\mathrm{sc}_i}\right)^{k-1-z}\left\|\mathbf{L}_{\mathrm{sc}_i}\right\|\bar{n}_{\mathrm{cc}_i}, \tag{6.33}$$

where $\left\|\mathbf{C}\left(\tilde{\mathbf{A}}_{\mathrm{sc}_i}\right)^k\right\| \leq \left(\alpha_{\mathrm{sc}_i}\right)^k$ and $\left\|\boldsymbol{\varepsilon}_{\mathrm{sc}_i}(0)\right\| \leq \epsilon^o_{\mathrm{sc}_i}$ for all $k \geq 0$. Note that $\alpha_{\mathrm{sc}_i} < 1$ and $\epsilon^o_{\mathrm{sc}_i}$ are design parameters.

Computation of Heating Coil's Adaptive Threshold

The residual $\epsilon_{\mathrm{hc}_i}(k)$ can be defined using the heating coil's water temperature estimation error $\varepsilon_{\mathrm{sh}_i}(k)$ given in (6.11) as follows

$$\epsilon_{\mathrm{hc}_i}(k) = y_{\mathrm{hc}_i}(k) - \mathbf{C}_{\mathrm{sh}}\hat{\mathbf{T}}_{\mathrm{sh}_i}(k) \tag{6.34}$$

$$= \mathbf{C}_{\mathrm{sh}}\boldsymbol{\varepsilon}_{\mathrm{sh}_i}(k) + n_{\mathrm{hc}_i}(k) + f_{\mathrm{hc}_i}(k), \tag{6.35}$$

From (6.35) is concluded that residual $\epsilon_{\mathrm{sh}_i}(k)$ can be affected by the sensor faults f_{z_i} and f_{hc_i}. Considering now healthy conditions (i.e., f_{z_i}=0, f_{cc_i}=0, f_{sa_i}=0). The computation of the adaptive threshold $\bar{\epsilon}_{\mathrm{sa}_i}(k)$ on the residual $\epsilon_{\mathrm{sa}_i}(k)$ is presented in Appendix B

From (6.26) is concluded that residual $\epsilon_{\mathrm{sa}_i}(k)$ can be affected by the sensor faults f_{z_i} and f_{c_i}. Considering now healthy conditions (i.e., f_{z_i}=0, f_{c_i}=0, f_{sa_i}=0).

$$\epsilon_{\mathrm{cc}_i}(k) = \mathbf{C}\left(\widetilde{\mathbf{A}}_{\mathrm{sc}_i}\right)^k \boldsymbol{\varepsilon}_{\mathrm{sc}_i}(0) + n_{\mathrm{cc}_i}(k) - \sum_{z=1}^{k-1} \mathbf{C}\left(\widetilde{\mathbf{A}}_{\mathrm{sc}_i}\right)^{k-1-z} \mathbf{B}^{\mathrm{d}}_{\mathrm{sc}_i}\left(\left(n_{\mathrm{cc}_i}(z)\right) u_{\mathrm{cc}_i}(z)\right)$$
$$+ \sum_{z=1}^{k-1} \mathbf{C}\left(\widetilde{\mathbf{A}}_{\mathrm{sc}_i}\right)^{k-1-z} \mathbf{G}_{\mathrm{ma,sc}_i}\left(n_{\mathrm{z}_i}(z)\right) + \sum_{z=1}^{k-1} \mathbf{C}\left(\widetilde{\mathbf{A}}_{\mathrm{sc}_i}\right)^{k-1-z} \mathbf{L}_{\mathrm{sc}_i}\left(n_{\mathrm{cc}_i}(z)\right), \tag{6.36}$$

By applying the Minkowski inequality on (6.36) results to

$$\left\|\epsilon_{\mathrm{cc}_i}(k)\right\| \le \left\|\mathbf{C}\left(\widetilde{\mathbf{A}}_{\mathrm{sc}_i}\right)^k \boldsymbol{\varepsilon}_{\mathrm{sc}_i}(0)\right\| + \left\|n_{\mathrm{cc}_i}(k)\right\| + \left\|\sum_{z=1}^{k-1} \mathbf{C}\left(\widetilde{\mathbf{A}}_{\mathrm{sc}_i}\right)^{k-1-z} \mathbf{B}^{\mathrm{d}}_{\mathrm{sc}_i}\left(\left(n_{\mathrm{cc}_i}(z)\right) u_{\mathrm{cc}_i}(z)\right)\right\|$$
$$+ \left\|\sum_{z=1}^{k-1} \mathbf{C}\left(\widetilde{\mathbf{A}}_{\mathrm{sc}_i}\right)^{k-1-z} \mathbf{G}_{\mathrm{ma,sc}_i} n_{\mathrm{z}_i}(z)\right\| + \left\|\sum_{z=1}^{k-1} \mathbf{C}\left(\widetilde{\mathbf{A}}_{\mathrm{sc}_i}\right)^{k-1-z} \mathbf{L}_{\mathrm{sc}_i}\left(n_{\mathrm{cc}_i}(z)\right)\right\|, \tag{6.37}$$

Then, by applying Schwartz inequality the above equation results to the adaptive threshold

$$\left\|\epsilon_{\mathrm{cc}_i}(k)\right\| \le \left\|\mathbf{C}\left(\widetilde{\mathbf{A}}_{\mathrm{sc}_i}\right)^k \boldsymbol{\varepsilon}_{\mathrm{sc}_i}(0)\right\| + \left\|n_{\mathrm{cc}_i}(k)\right\| + \sum_{z=1}^{k-1} \left\|\mathbf{C}\left(\widetilde{\mathbf{A}}_{\mathrm{sc}_i}\right)^{k-1-z} \mathbf{B}^{\mathrm{d}}_{\mathrm{sc}_i}\right\| \bar{n}_{\mathrm{cc}_i} \left|u_{\mathrm{cc}_i}(z)\right|$$
$$+ \sum_{z=1}^{k-1} \left\|\mathbf{C}\left(\widetilde{\mathbf{A}}_{\mathrm{sc}_i}\right)^{k-1-z}\right\| \left\|\mathbf{G}_{\mathrm{ma,sc}_i}\right\| \bar{n}_{\mathrm{z}_i} + \sum_{z=1}^{k-1} \left\|\mathbf{C}\left(\widetilde{\mathbf{A}}_{\mathrm{sc}_i}\right)^{k-1-z} \mathbf{L}_{\mathrm{sc}_i}\right\| \bar{n}_{\mathrm{cc}_i}, \tag{6.38}$$

$$\le (\alpha_{\mathrm{cc}_i})^k \epsilon^o_{\mathrm{cc}_i} + \bar{n}_{\mathrm{cc}_i} + \sum_{z=1}^{k-1} (\alpha_{\mathrm{cc}_i})^{k-1-z} \left\|\mathbf{B}^{\mathrm{d}}_{\mathrm{sc}_i}\right\| \bar{n}_{\mathrm{cc}_i} \left|u_{\mathrm{cc}_i}(z)\right|$$
$$+ \sum_{z=1}^{k-1} (\alpha_{\mathrm{cc}_i})^{k-1-z} \left\|\mathbf{G}_{\mathrm{ma,sc}_i}\right\| \bar{n}_{\mathrm{z}_i} + \sum_{z=1}^{k-1} (\alpha_{\mathrm{cc}_i})^{k-1-z} \left\|\mathbf{L}_{\mathrm{sc}_i}\right\| \bar{n}_{\mathrm{cc}_i}, \tag{6.39}$$

with $\left\|\mathbf{C}\left(\widetilde{\mathbf{A}}_{\mathrm{sc}_i}\right)^k\right\| \le (\alpha_{\mathrm{cc}_i})^k$ for all k and $\left\|\boldsymbol{\varepsilon}_{\mathrm{sc}_i}(0)\right\| \le \epsilon^o_{\mathrm{cc}_i}$.Note that $\alpha_{\mathrm{cc}_i} < 1$ and $\epsilon^o_{\mathrm{cc}_i}$ are design parameters.

6.3.3 Local Fault Detection Logic

The detection logic is based on a detection signal D, designed for each pair of residual and adaptive threshold as follows:

$$\mathrm{D}_{\mathrm{z}_i}(k) = \begin{cases} 1 & k \geq k^{\mathrm{D}}_{\mathrm{z}_i} \\ 0 & \text{otherwise} \end{cases}, k^{\mathrm{D}}_{\mathrm{z}_i} = \left\{k : \left|\epsilon_{\mathrm{z}_i}(k)\right| > \bar{\epsilon}_{\mathrm{z}_i}(k)\right\}, \tag{6.40}$$

$$\mathrm{D}_{\mathrm{sa}_i}(k) = \begin{cases} 1 & k \geq k^{\mathrm{D}}_{\mathrm{sa}_i} \\ 0 & \text{otherwise} \end{cases}, k^{\mathrm{D}}_{\mathrm{sa}_i} = \left\{k : \left|\epsilon_{\mathrm{sa}_i}(k)\right| > \bar{\epsilon}_{\mathrm{sa}_i}(k)\right\}, \tag{6.41}$$

$$\mathrm{D}_{\mathrm{cc}_i}(k) = \begin{cases} 1 & k \geq k^{\mathrm{D}}_{\mathrm{cc}_i} \\ 0 & \text{otherwise} \end{cases}, k^{\mathrm{D}}_{\mathrm{cc}_i} = \left\{k : \left|\epsilon_{\mathrm{cc}_i}(k)\right| > \bar{\epsilon}_{\mathrm{cc}_i}(k)\right\}, \tag{6.42}$$

$$\mathrm{D}_{\mathrm{hc}_i}(k) = \begin{cases} 1 & k \geq k^{\mathrm{D}}_{\mathrm{hc}_i} \\ 0 & \text{otherwise} \end{cases}, k^{\mathrm{D}}_{\mathrm{hc}_i} = \left\{k : \left|\epsilon_{\mathrm{hc}_i}(k)\right| > \bar{\epsilon}_{\mathrm{hc}_i}(k)\right\}. \tag{6.43}$$

where $k^{\mathrm{D}}_{\mathrm{z}_i}$, $k^{\mathrm{D}}_{\mathrm{sa}_i}$, $k^{\mathrm{D}}_{\mathrm{cc}_i}$ and $k^{\mathrm{D}}_{\mathrm{hc}_i}$ represent the detection time step of the corresponding ARR.

6.3.4 Distributed Fault Isolation Logic

The Distributed Isolation Logic is based on binary logic of ARRs given in (6.17)-(6.20). The Table 6.1 is the Incidence Matrix that summarized how each fault can affect, directly or indirectly, the ARRs using the residuals included in the fault detection algorithm of Section 6.3.2. Based on the dependency matrix the local fault signature matrix consists the logic on how all possible combinations of faults can affect the corresponding ARRs, where "1" refers to the case that the corresponding ARR is mainly affected by the corresponding fault, "*" refers to the case that the corresponding ARR is affected by the corresponding fault due to the sensor measurement exchange between the estimators and "0" denotes the case that the corresponding ARR is not affected by the corresponding fault.

Table 6.1: Incidence Matrix for i-th Fault Diagnosis Agent

	1: Direct	$*$: Indirect
$\mathcal{E}_{\mathrm{cc}_i}$	$f^m_{\mathrm{cc}_i}$, f_{cc_i}	f_{z_i}
$\mathcal{E}_{\mathrm{hc}_i}$	$f^m_{\mathrm{hc}_i}$, f_{hc_i}	$f^m_{\mathrm{cc}_i}$, f_{cc_i}, f_{z_i}
$\mathcal{E}_{\mathrm{sa}_i}$	f_{sa_i}	f_{cc_i}, f_{hc_i}, f_{z_i}
$\mathcal{E}_{\mathrm{z}_i}$	f_{z_i}	f_{sa_i}, f_{z_j}
$\mathcal{E}_{\mathrm{z}_j}$	f_{z_j}	f_{z_i}

In order to reach into a decision about the possible location of a fault in the each AHU, at each time step we can compare the observed diagnosis set $\mathcal{D}^{(i)}$ designed as

$$\mathcal{D}^{(i)}(k) = \left[\mathrm{D}_{\mathrm{cc}_i}(k), \mathrm{D}_{\mathrm{hc}_i}(k), \mathrm{D}_{\mathrm{sa}_i}(k), \mathrm{D}_{\mathrm{z}_i}(k), \mathrm{D}_{\mathrm{z}_j}(k)\right]^{\top}, \tag{6.44}$$

Table 6.2: Local Fault Signature Matrix for i-th Fault Diagnosis Agent

	$f^m_{\mathrm{cc}_i}$	$f^m_{\mathrm{hc}_i}$	f_{cc_i}	f_{hc_i}	f_{sa_i}	f_{z_i}	f_{z_j}
$\mathcal{E}_{\mathrm{cc}_i}$	1	0	1	0	0	*	0
$\mathcal{E}_{\mathrm{hc}_i}$	*	1	*	1	0	*	0
$\mathcal{E}_{\mathrm{sa}_i}$	0	0	*	*	1	*	0
$\mathcal{E}_{\mathrm{z}_i}$	0	0	0	0	*	1	*
$\mathcal{E}_{\mathrm{z}_j}$	0	0	0	0	0	*	1

with a set of theoretical patterns $\mathcal{F}^{(i)}$ obtained based on the local fault signature matrix for given in Table 6.2.

The outcome of the online comparison of the observed fault pattern $\Phi^{(i)}$ to the $N_c^{(i)}$ theoretical patterns $F_q^{(i)}$, $q \in \{1, \ldots, N_c^{(i)}\}$ is the diagnosis set $\Upsilon^{(i)}(t)$, which is determined as

$$\Upsilon^{(i)}(t) = \left\{\mathcal{F}_{c_i}^{(i)} : i \in \mathcal{I}_{\Upsilon}^{(i)}(t)\right\}, \tag{6.45}$$

with $\mathcal{I}_{\Upsilon}^{(i)}(t) = \left\{k : F_k^{(i)} = \Phi^{(i)}(t),\ k \in \{1, \ldots, N_c^{(i)}\}\right\}$. For each fault diagnosis agent, the diagnosis sets contain all the possible fault combinations. In the case the observed fault pattern has a unique match with one of the theoretical fault patterns then the isolation algorithm can accomplish to obtain the location and type of the fault, otherwise it can reduce the number of candidate fault combinations.

6.4 Simulation Analysis

In this section the application of the proposed distributed fault diagnosis scheme to a multi-zone HVAC system is presented and its performance is analyzed in the presence of sensor and actuator faults.

6.4.1 Building description

The distributed fault diagnosis algorithm is implemented in a prototype primary school building model. The building model is chosen among the ones offered in the suite of ASHRAE Standard 90.1 prototype buildings, which was developed by Pacific Northwest National Laboratory [1], which it is modified for the purposes of this work [2]. A 3D plan of the building is presented in Fig. 10.2 and corresponds to the ANSI/ASHRAE/IES Standard 90.1-2016 Primary School model, located in Denver. The building consists of 25 thermal zones that are presented in Table 6.3. The zones have different sizes, their use varies and are physically interconnected via walls and doors. Table 6.4 presents the set of indices $\mathcal{N}_i$ for all $i \in N = \{1, \ldots, 25\}$. For example, there exist several classrooms, corridors and activity areas, such as the gym or the cafeteria, which correspond to different occupancy patterns and heat loads from equipment and lighting. This implies that the temperature in each zone can be affected by various sources of heat that can not be available or modeled.

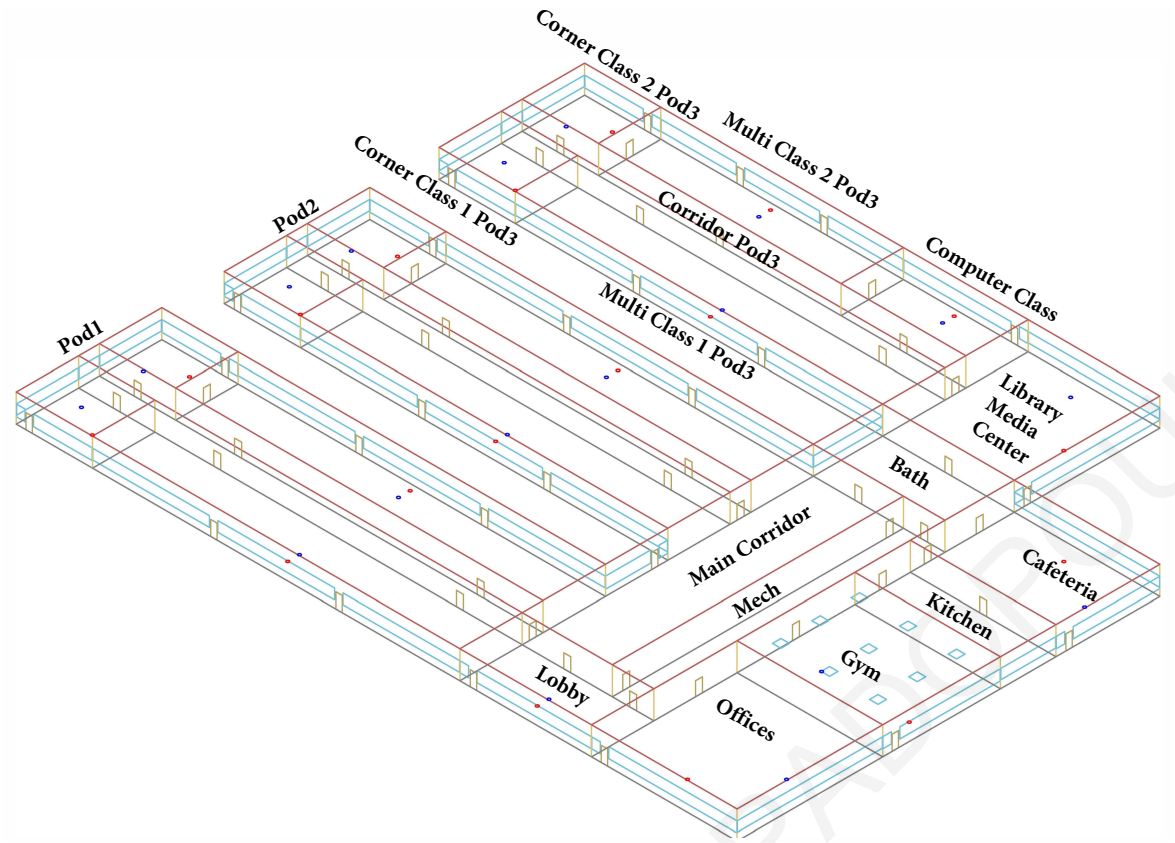

Figure 6.3: 3D plan of the ANSI/ASHRAE/IES Standard 90.1-2016 Primary School.

Each zone has an AHU to provide proper temperature regulation. The AHUs are customized to allow regulation of water mass flow rate $\dot{m}_{c_i}$ through the coil by a controller. The Energy Plus input data file (.idf) that describes the building and HVAC system is provided in the following Github link [2]. The fault diagnosis algorithm is implemented using *Matlab/Simulink*. The overall system with the *EnergyPlus* building and HVAC model and the *Matlab/Simulink* fault diagnosis scheme is co-simulated using the *Buildings Control Virtual Test Bed (BCVTB)*.

6.4.2 Simulation Details

The performance of the proposed distributed fault diagnosis algorithm of this test-bed of multi-zone HVAC system is simulated for 2 days period (1st of April to 2nd of April) using the prototype Denver weather data from *EnergyPlus*. The HVAC system is operating on weekdays, from 6am to 6pm during the winter period and from 7am to 7pm during the summer period. Occupancy schedules are specified for each zone according to its use. In addition, internal and external doors are scheduled to open and close at several times in order to capture the possible changes in the way thermal zones interact with each other. For all zones the desired temperature is selected as $T_z^{\text{ref}} = 23^o\text{C}$. All details about the building and HVAC system size are included in the aforementioned Github link. The sampling time is selected as $T_s = 60s$.

The implementation of the proposed distributed fault diagnosis algorithm requires the choice of

Table 6.3: List of building zones

No.	Zone Name	No.	Zone Name
1	Bath	14	Kitchen
2	Cafeteria	15	Library Media Center
3	Computer Class	16	Lobby
4	CornerClass 1 Pod 1	17	Main Corridor
5	CornerClass 1 Pod 2	18	Mech
6	CornerClass 1 Pod 3	19	MultiClass 1 Pod 1
7	CornerClass 2 Pod 1	20	MultiClass 1 Pod 2
8	CornerClass 2 Pod 2	21	MultiClass 1 Pod 3
9	CornerClass 2 Pod 3	22	MultiClass 2 Pod 1
10	Corridor Pod 1	23	MultiClass 2 Pod 2
11	Corridor Pod 2	24	MultiClass 2 Pod 3
12	Corridor Pod 3	25	Offices
13	Gym		

Table 6.4: List of the $\mathcal{N}_i$ set for all $i \in N$

Set	No. of Neighboring	Set	No. of Neighboring
$\mathcal{N}_1$	2,15,17,18,	$\mathcal{N}_{14}$	2,13,18
$\mathcal{N}_2$	1,14,18	$\mathcal{N}_{15}$	1,3,12,21
$\mathcal{N}_3$	12,15,24	$\mathcal{N}_{16}$	17,18,19,25
$\mathcal{N}_4$	10,19	$\mathcal{N}_{17}$	1,10,11,16,18,20,22,23
$\mathcal{N}_5$	11,20	$\mathcal{N}_{18}$	1,2,13,14,16,17,25
$\mathcal{N}_6$	12,21	$\mathcal{N}_{19}$	4,10,16,
$\mathcal{N}_7$	10,22	$\mathcal{N}_{20}$	5,11,17,
$\mathcal{N}_8$	11,23	$\mathcal{N}_{21}$	6, 12, 15
$\mathcal{N}_9$	12,24	$\mathcal{N}_{22}$	7, 10,17
$\mathcal{N}_{10}$	4,7,17,19,22	$\mathcal{N}_{23}$	8,11,17
$\mathcal{N}_{11}$	5,8,17,20,23	$\mathcal{N}_{24}$	3,9,12
$\mathcal{N}_{12}$	3,6,9,15,21,24	$\mathcal{N}_{25}$	13,16,18
$\mathcal{N}_{13}$	14,18,25		

Table 6.5: FD agents design constants.

Variable	Value
L_{z_i}	$\text{place}(A_{z_i}, 1, 0.1 \cdot \lambda(A_{z_i}))$
$\mathbf{L}_{\text{sa}_i}$	$\text{place}(\mathbf{A}_{\text{sa}_i}, \mathbf{C}, [1\times10^{-13} \;\; 2\times10^{-10}] \cdot \lambda(\mathbf{A}_{\text{sa}_i}))$
$\mathbf{L}_{\text{sc}_i}$	$\text{place}(\mathbf{A}_{\text{sc}_i}, \mathbf{C}, [0.8 \;\; 0.0087] \cdot \lambda(\mathbf{A}_{\text{sc}_i}))$
$\mathbf{L}_{\text{sh}_i}$	$\text{place}(\mathbf{A}_{\text{sh}_i}, \mathbf{C}_{\text{sh}}, [0.1 \;\; 0.2 \;\; 0.5 \;\; 0.7] \cdot \lambda(\mathbf{A}_{\text{sh}_i}))$
$\overline{Q}_i$	2 W
$\overline{n}_{z_i}, \overline{n}_{\text{sa}_i}$	0.3^oC
$\overline{n}_{\text{cc}_i}, \overline{n}_{\text{hc}_i}$	0.3^oC
$\alpha_{\text{sh}_i} < 1$	0.7
$\epsilon^o_{\text{sh}_i}$	100 ^{o}C

Table 6.6: Design parameters for fault modeling.

Faults	Model 1	Model 2	Model 3
$f_{z_i}(k)$	$(1-\gamma^k_{\text{ab}})\phi_{\text{s}}$	$(1-\gamma^k_{\text{ab}})T_{z_i}(k)$	$(1-\gamma^k_{\text{in}})\phi_{\text{s}}$
$f_{\text{sa}_i}(k)$	$(1-\gamma^k_{\text{ab}})\phi_{\text{s}}$	$(1-\gamma^k_{\text{ab}})T_{\text{sa}_i}(k)$	$(1-\gamma^k_{\text{in}})\phi_{\text{s}}$
$f_{\text{cc}_i}(k)$	$(1-\gamma^k_{\text{ab}})\phi_{\text{s}}$	$(1-\gamma^k_{\text{ab}})T_{\text{cc}_i}(k)$	$(1-\gamma^k_{\text{in}})\phi_{\text{s}}$
$f_{\text{hc}_i}(k)$	$(1-\gamma^k_{\text{ab}})\phi_{\text{s}}$	$(1-\gamma^k_{\text{ab}})T_{\text{hc}_i}(k)$	$(1-\gamma^k_{\text{in}})\phi_{\text{s}}$
$f^m_{\text{cc}_i}(k)$	$(1-\gamma^k_{\text{ab}})\phi_{\text{a}}$	$(1-\gamma^k_{\text{ab}})u_{\text{cc}_i}(k)$	$(1-\gamma^k_{\text{in}})\phi_{\text{a}}$
$f^m_{\text{hc}_i}(k)$	$(1-\gamma^k_{\text{ab}})\phi_{\text{s}}$	$(1-\gamma^k_{\text{ab}})u_{\text{hc}_i}(k)$	$(1-\gamma^k_{\text{in}})\phi_{\text{a}}$

several design parameters, such as zonal modeling uncertainty bounds, sensor noise measurement bounds and observer gains that are presented in Table 6.5. The observer gains for each observer L_{z_i}, $\mathbf{L}_{\text{sa}_i}$, $\mathbf{L}_{\text{sc}_i}$, $\mathbf{L}_{\text{sh}_i}$ are chosen to guarantee stability of the estimator for all AHUs $i \in N$. It should be noted that the observers initial condition are chosen to be equal to zero and there are reset when the HVAC system is not operate in order to avoid fault alarms during the transient behavior. The design bounds on the modeling uncertainty for each zone $\overline{Q}_i$ is selected to be 2 W and represents the maximum unknown (not modeled) heat sources. The design bounds of the sensor measurement noise can be obtained by the technical specifications of the manufacturer, while for this simulation example where selected to be 0.3^oC.

6.4.3 Simulation Results

The proposed distributed fault diagnosis algorithm is implemented in *Matlab/Simulink* and are connected to the *EnergyPlus* model using *BCVTB*. Its performance is evaluated with respect to the three

fault models that are presented in Table 6.6, where:

- *Fault Model 1* represents an abrupt additive fault with fault function ϕ_s=10 ^{o}C for the sensor faults and ϕ_a=0.1 kg/sec for the actuator (valve) faults, where γ_{ab}=1×10^{-4} determines the fault's time profile. In simulations is indicated with a red color.
- *Fault Model 2* represents an abrupt multiplicative fault that it's function is selected to be an increase of 10% on the corresponding temperature for the sensor faults and 50% increase on the control input for the actuator faults, with γ_{ab}=1×10^{-4}. In simulations is indicated with a blue color.
- *Fault Model 3* represents an incipient additive fault that has the same fault functions as Fault Model 1, where the time profile of the faults is selected such as γ_{ab}=0.97. In simulations is indicated with a green color.

For simplicity, the time of fault occurrence for all fault cases is selected as k_f=129600 sec that corresponds to day 2 of the simulation at 12:00 p.m. i.e., 01:12:00:00. To evaluate the performance of the proposed FD algorithm we run the following simulations scenarios:

- Scenario 1: Sensor fault $f_{z_{10}}$ with Fault Model 1,
- Scenario 2: Sensor faults: f_{sa_4} with Fault Model 1, f_{sa_6} with Fault Model 3,
- Scenario 3: Sensor faults: f_{cc_7} with Fault Model 1, Sensor fault f_{cc_8} with Fault Model 2,
- Scenario 3: Actuator faults: $f^m_{cc_{10}}$ with Fault Model 1, $f^m_{cc_{12}}$ with Fault Model 3.

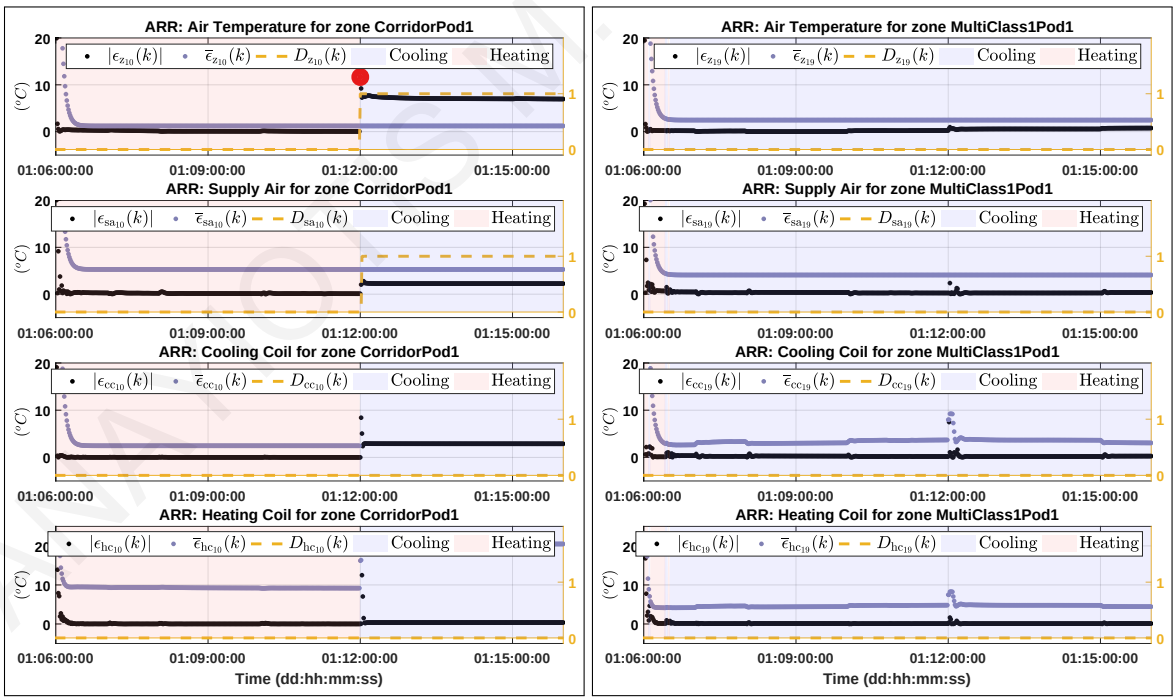

Figure 6.4: ARRs of the AHU 10 and 19 for Scenario 1.

Fig. 6.4–6.7 show the ARRs of the affected AHUs for the aforementioned fault scenarios. Specifically, in each box the absolute value of the residuals $|\epsilon_{z_i}|$, $|\epsilon_{sa_i}|$, $|\epsilon_{cc_i}|$, $|\epsilon_{hc_i}|$ that are denoted with the

black dots, their corresponding thresholds $\bar{\epsilon}_{z_i}$, $\bar{\epsilon}_{sa_i}$, $\bar{\epsilon}_{cc_i}$, $\bar{\epsilon}_{hc_i}$ that denoted with purple dots and the detection decision signals D_{z_i}, D_{sa_i}, D_{cc_i}, D_{hc_i} indicated with the yellow dashed line. The red dot represents the location of sensor fault with Model 1, the blue dot represents the location of sensor fault with Model 2, the green dot represents the location of sensor fault with Model 3. Moreover, the red star represents the location of actuator fault with Model 1, the blue star represents the location of actuator fault with Model 2 and the magenta star represents the location of actuator fault with Model 3. Note that background light blue and red color on each plot represents the cooling and heating mode, respectively, where cooling mode means that the cooling coil valve is open and cooling mode means that the heating coil valve is open.

Fig. 6.4 shows the ARRs results for AHU 10 and 19 in the fault Scenario 1. According to Table 6.4 zone 10 is connected to zone 19. The purpose of this result to show the effect of a sensor fault to the ARRs of the local FD Agent and also the effect to one of its neighboring FD Agent. Specifically, the sensor fault $f_{z_{10}}$ is applied with a Fault Model 1, which is fault of 10^oC magnitude that can be consider a large one. According to Table 6.2, $f_{z_{10}}$ can cause the violation of ARR $\mathcal{E}_{z_{10}}$ and may cause the violation of ARRs $\mathcal{E}_{sa_{10}}$, $\mathcal{E}_{hc_{10}}$, $\mathcal{E}_{cc_{10}}$ of the local FD Agent and may also cause the violation of ARRs $\mathcal{E}_{z_4}$, $\mathcal{E}_{z_7}$, $\mathcal{E}_{z_{17}}$, $\mathcal{E}_{z_{19}}$, $\mathcal{E}_{z_{22}}$ due to the exchange of the sensor information from the neighboring zones included in $\mathcal{N}_{10}$ for the estimation of the zone air temperature. From results in Fig. 6.4, the detection observed pattern is $\mathcal{D}^{(10)}(k) = [0,0,1,1,0]^\top$, $\mathcal{D}^{(19)}(k) = [0,0,0,0,0]^\top$. This means that this fault Scenario cause the ARR $\mathcal{E}_{z_{10}}$ and $\mathcal{E}_{sa_{10}}$, while the remainder ARRs involved did not violated. The outcome of the Distributed Isolation logic presented in Section 6.3.4 is that this observed pattern may caused by the following fault combinations: $\{f_{z_{10}}\}$, $\{f_{sa_{10}}\}$, or $\{f_{z_{10}}, f_{sa_{10}}\}$, based on which we can exclude the occurrence of faults $f_{hc_{10}}$, $f_{cc_{10}}$, $f^m_{hc_{10}}$, $f^m_{cc_{10}}$, f_{z_4}, f_{z_7}, $f_{z_{17}}$, $f_{z_{19}}$, $f_{z_{22}}$ and their combinations. Indicatively, we choose only the ARRs of FD Agent 19 only, but also the remainder ARRs in FD Agents 4, 7, 17 and 22 did not violated.

The Fig. 6.5 shows the ARRs results of AHU 4 and 6 caused by Scenario 2. Specifically, the sensor fault f_{sa_4} with a Fault Model 1 and the sensor fault f_{sa_6} with a Fault Model 3 are applied. According to Table 6.2, f_{sa_4} and f_{sa_6} can cause the violation of ARR $\mathcal{E}_{sa_4}$ and $\mathcal{E}_{sa_6}$, and may cause the violation of ARRs $\mathcal{E}_{z_4}$ and $\mathcal{E}_{z_6}$, respectively. From results in Fig. 6.5, the detection observed pattern is $\mathcal{D}^{(4)}(k) = [0,0,1,0,0]^\top$, $\mathcal{D}^{(6)}(k) = [0,0,1,0,0]^\top$. This means that the fault Scenario 2 cause the violation of ARR $\mathcal{E}_{sa_4}$ and $\mathcal{E}_{sa_6}$, while the remainder ARRs involved did not violated. The outcome of the Distributed Isolation logic presented in Section 6.3.4 is that this observed pattern may caused by only the following fault combination: $\{f_{sa_4}, f_{sa_6}\}$, based on which we can exclude the occurrence of the remainder fault combinations. Hence, the proposed distributed fault diagnosis algorithm is able in real-time to detect and isolate the presence of sensor fault f_{sa_4} and f_{sa_6}. Consequently, by using the proposed algorithm we can reduce the maintenance time. Note the fault $\{f_{sa_4}$ (red dot) that corresponds to an abrupt sensor fault that is detected at the occurrence time, while the $\{f_{sa_6}$ (green dot)

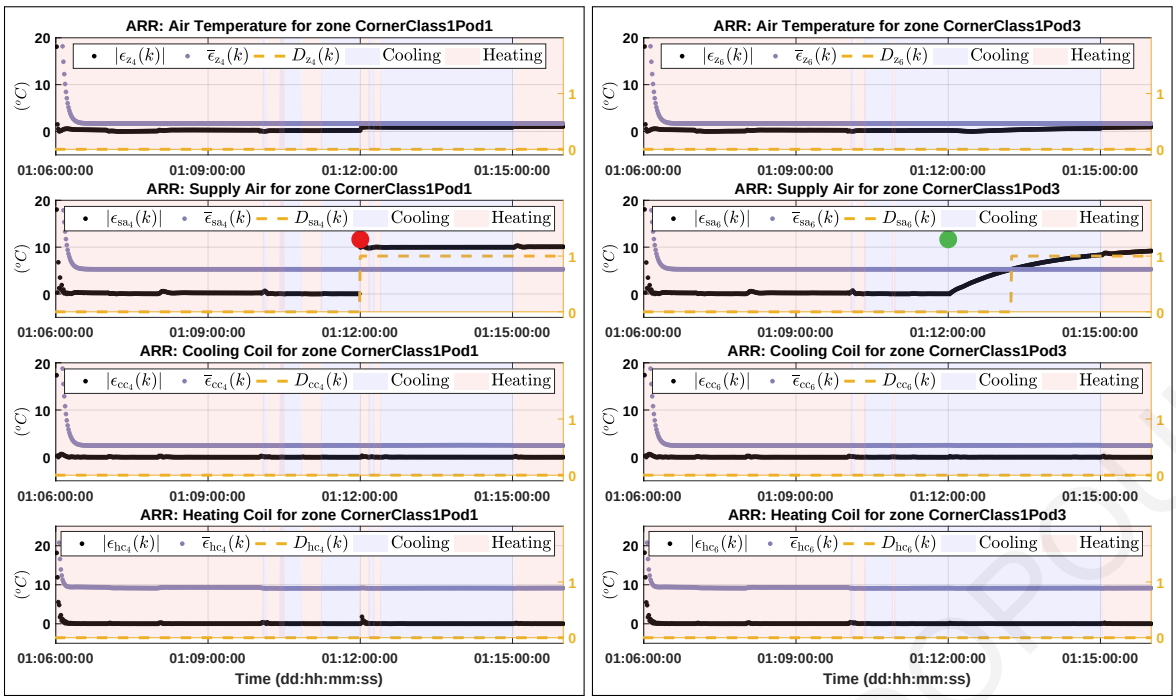

Figure 6.5: ARRs of the AHU 4 and 6 for Scenario 2.

that corresponds to an incipient sensor fault is detected approximately 1 and 15 minutes after at the occurrence time.

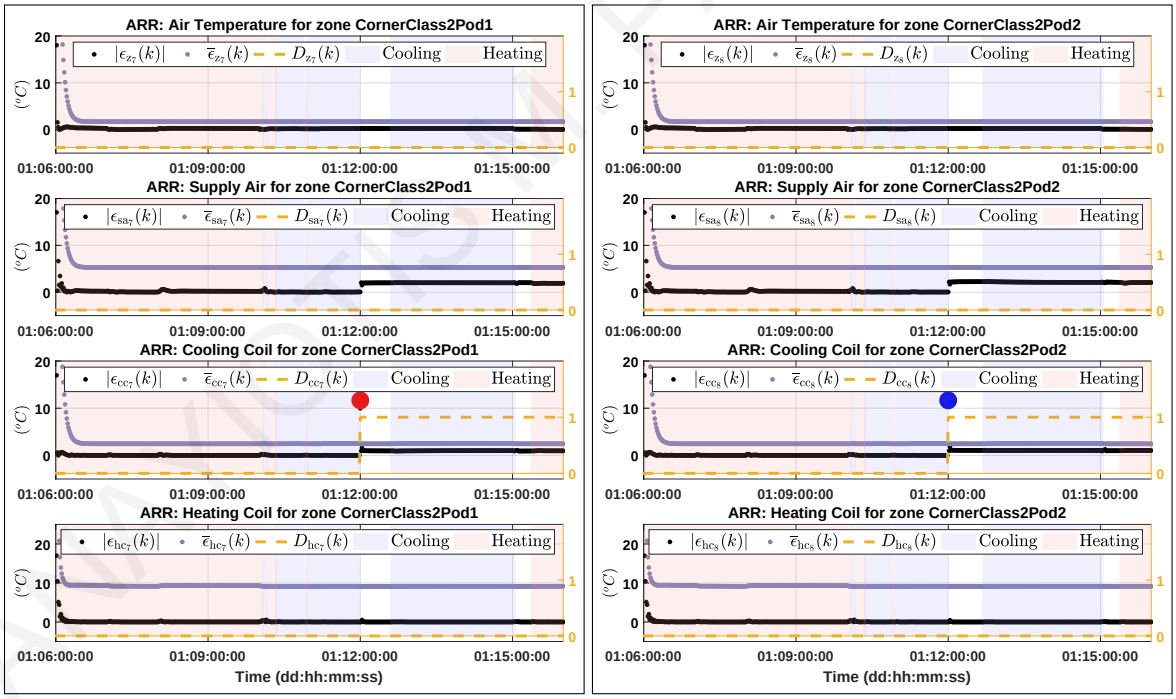

Figure 6.6: ARRs of the AHU 6 and 7 for Scenario 3.

Fig. 6.6 shows the ARRs results of AHU 7 and 8 caused by Scenario 3. Specifically, the abrupt sensor fault f_{cc_7} with a Fault Model 1 and the multiplicative sensor fault f_{cc_8} with a Fault Model 2 are applied. According to Table 6.2, f_{cc_7} and f_{cc_8} can cause the violation of ARR $\mathcal{E}_{\text{cc}_7}$ and $\mathcal{E}_{\text{cc}_8}$, and may

cause the violation of ARRs $\mathcal{E}_{\text{hc}_7}$, $\mathcal{E}_{\text{sa}_7}$ and $\mathcal{E}_{\text{hc}_8}$, $\mathcal{E}_{\text{sa}_8}$, respectively.

From results in Fig. 6.6, the detection observed pattern is $\mathcal{D}^{(7)}(k) = [1,0,0,0,0]^\top$, $\mathcal{D}^{(8)}(k) = [1,0,0,0,0]^\top$. This means that the fault Scenario 3 cause the violation of ARR $\mathcal{E}_{\text{cc}_7}$ and $\mathcal{E}_{\text{cc}_8}$, while the remainder ARRs involved did not violated. The outcome of the Distributed Isolation logic presented in Section 6.3.4 is that this observed pattern may caused by the following fault combinations:$\{f_{\text{cc}_7}\}$, $\{f^m_{\text{cc}_7}\}$, or $\{f_{\text{cc}_7}, f^m_{\text{cc}_7}\}$ for the FD Agent 7 and $\{f_{\text{cc}_8}\}$, $\{f^m_{\text{cc}_8}\}$, or $\{f_{\text{cc}_8}, f^m_{\text{cc}_8}\}$ for the FD Agent 8. Based on the above logic we can exclude the occurrence of the remainder fault combinations.

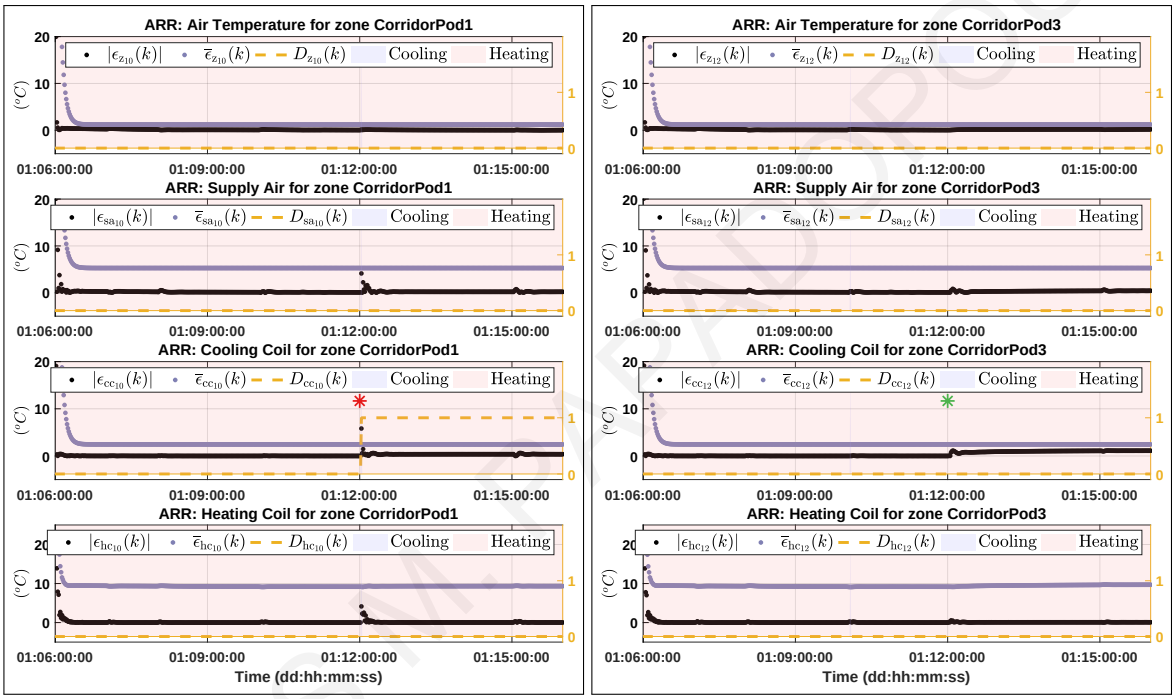

Figure 6.7: ARRs of the AHU 10 and 12 for Scenario 4.

Fig. 6.7 shows the ARRs results of AHU 10 and 12 caused by Scenario 4. Specifically, the actuator fault $f^m_{\text{cc}_{10}}$ with a Fault Model 1 and the actuator fault $f_{\text{cc}_{12}}$ with a Fault Model 3 are applied. According to Table 6.2, $f^m_{\text{cc}_{10}}$ and $f^m_{\text{cc}_{12}}$ can cause the violation of ARR $\mathcal{E}_{\text{cc}_{10}}$ and $\mathcal{E}_{\text{cc}_{12}}$, and may cause the violation of ARRs $\mathcal{E}_{\text{hc}_{10}}$ and $\mathcal{E}_{\text{hc}_{12}}$, respectively. From results in Fig. 6.7, the detection observed pattern is $\mathcal{D}^{(10)}(k) = [1,0,0,0,0]^\top$, $\mathcal{D}^{(6)}(k) = [0,0,0,0,0]^\top$. This means that the fault Scenario 3 cause the violation only of ARR $\mathcal{E}_{\text{cc}_{10}}$, while the remainder ARRs including $\mathcal{E}_{\text{cc}_{12}}$ involved did not violated. The outcome of the Distributed Isolation logic presented in Section 6.3.4 for the FD Agent 10 is that this observed pattern may caused by the following fault combinations: $\{f_{\text{cc}_{10}}\}$, $\{f^m_{\text{cc}_{10}}\}$, or $\{f_{\text{cc}_{10}}, f^m_{\text{cc}_{10}}\}$, based on which we can exclude the occurrence of the remainder fault combinations. On the other hand, the presence of the actuator fault $f_{\text{cc}_{12}}$ with a Fault Model 3 could not detected by the FD Agent 12 and this is one of the cases of missed faults.

6.5 Conclusions

In this chapter a distributed model-based fault diagnosis algorithm is presented, that in real-time, is able to detect, isolate and identify sensor and actuator faults that can affect the operation of the AHUs in large-scale, multi-zone buildings. Faults, in opposition to failures, can not be easily diagnosed from the ruled-based algorithms integrated in the existing Buildings Management Systems, causing uncomfortable thermal conditions and in some cases a huge waste of energy in a long term duration. Moreover, due to the system complexity and control closed-loop can complicate the fault diagnosis procedure of several sensors and actuators in each AHU. Modeling the thermal zones and the components of AHUs, we can design a local fault diagnosis agent for each AHU. Each fault diagnosis agent can estimate the states of measured quantities (i.e, zone air temperature, supply air temperature, cooling and heating coil's water temperature). Assuming bounded on the modeling uncertainty and sensor noise, and using the estimation of each state, we can obtain adaptive thresholds that their violation can indicate the presence of a fault or faults. By combining the local and neighboring detection signals, a binary isolation logic is designed to reveal the location and type of the fault or to decrease the number of candidate faults. Consequently, this process can reduce dramatically the maintenance time by the building's operators/staff in an abnormal operation of the HVAC system. The performance of the proposed algorithm is evaluated in a realistic simulation using a primary school building with 25 zones, offered in the ASHRAE Standard 90.1 suite.

Chapter 7

Distributed Sensor Fault Accommodation using a Virtual Sensor Scheme

7.1 Introduction

This chapter deals with the accommodation of sensor faults in FCU HVAC systems that are presented in Chapter 2.4 using a *virtual sensor* scheme. In Chapters 3-6, the development of distributed fault diagnosis schemes for multi-zone HVAC systems are presented. Using the outcome of the diagnosis process, a distributed fault accommodation scheme can be online activated to alleviate the effects of faulty measurements during the operation of the HVAC system i.e., without interrupting its operation.

In this chapter the concept of virtual sensors is employed, in the sense that instead of adapting the nominal controller to compensate the faulty measurements, an intermediate block that corresponds to the "virtual sensor" that is located between the sensor and nominal controller is implemented to alter the faulty measurements. The faulty plant, that corresponds to the plant whose measurements are faulty, together with the virtual sensor should produce, for a given input $c(t)$, the same (or approximately the same) output $y(t)$ as the nominal plant i.e., healthy system. Hence, the nominal controller "sees" the same plant and reacts in the same way as before [22]. Particularly, in this work, an adaptive estimation scheme is used to adapt the faulty sensor measurements to the nominal controller (i.e. the nominal controller remains unchanged) by estimating or learning the isolated sensor faults. The virtual sensor schemes are effective when the nominal control scheme is not available and/or can not be accessed.

7.2 Objective

The main objective of this work is the design of a distributed fault accommodation scheme for compensating the effects of sensor faults that impact the operation of a HVAC system with multiple and strongly interconnected building zones. By considering the HVAC system as a network of strongly

interconnected subsystems, several local monitoring and control agents are designed, for every subsystem. The local monitoring agent is responsible for detecting, isolating and estimating local sensor faults. The main task of each local control agent is the tracking of a corresponding desired signal under both healthy and faulty conditions. Both the local monitoring and control agents are allowed to exchange information with neighboring agents. When sensor faults are isolated by a local monitoring agent, the local and neighboring control agents are reconfigured by using the adaptive estimation of sensor faults transmitted by the neighboring monitoring agents.

7.3 Design of the Virtual Sensor Scheme

The backbone of the distributed sensor fault accommodation scheme is the design of two agents dedicated to each of the interconnected HVAC subsystems, where one agent monitors the status of the subsystem, and the other agent controls the subsystem, based on the information stemming from the monitoring agent. As illustrated in Fig. 7.1, the monitoring agents, denoted by $\mathcal{M}^s$ and $\mathcal{M}^{(i)}$, are responsible for detecting and isolating sensor faults in subsystems Σ^s and $\Sigma^{(i)}$, $i \in N$, respectively, and estimating the magnitude of the local sensor fault after been isolated. The control agents C^s and $C^{(i)}$ are responsible for tracking the reference signals for subsystems Σ^s and $\Sigma^{(i)}$ respectively, under healthy and faulty conditions using the virtual sensor measurements y_r^s and $y_r^{(i)}$, for all $i \in N$, that are constructed based on the sensor fault estimations. The monitoring and control agents are allowed to exchange information with neighboring agents.

In this work, the emphasis is on sensor faults, so we assume that there are no imperfections in the communication between the control and monitoring agents (e.g. time delays in transmission, packet dropouts), and the exchange of information is continuous and uninterrupted.

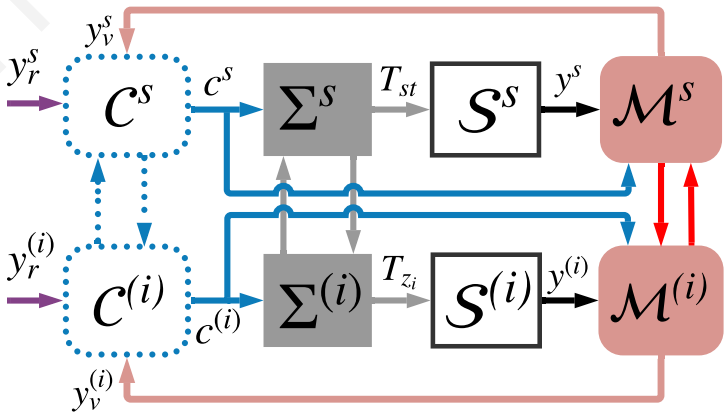

Figure 7.1: Architecture of the Distributed Virtual Sensor Scheme.

7.3.1 Distributed Adaptive Estimation Scheme

The decision of the monitoring agents $\mathcal{M}^s$ and $\mathcal{M}^{(i)}$ on the occurrence of sensor faults is obtained by checking the satisfaction of analytical redundancy relations of residuals and adaptive thresholds, as presented next.

Residual Generation

For estimating the water temperature in the storage tank a nonlinear adaptive estimation model is used by $\mathcal{M}^s$; i.e.,

$$\dot{\hat{x}}^s(t) = A^s\hat{x}^s(t) + g^s(y^s(t) - \hat{f}^s(t), d^s(t))u^s(t) + h^s(y^s(t) - \hat{f}^s(t), y(t), u(t)) + \eta^s(d^s(t)) + L^s\left(y^s(t) - \hat{x}^s(t) - \hat{f}^s(t)\right) + \Omega^s(t)\dot{\hat{f}}^s(t), \tag{7.1}$$

$$\dot{\Omega}^s(t) = A_L^s\Omega^s(t) - L^s + \frac{U_{st,max}(P_{max}-1)}{C_{st}\Delta T_{max}}u^s(t) + \frac{a_{sz}}{C_{st}}\sum_{i\in N}U_{i,max}u^{(i)}(t), \quad \Omega^s(t_I^s) = 0, \tag{7.2}$$

$$\dot{\hat{f}}^s(t) = \gamma^s(\Omega^s(t)+1)\mathcal{D}^s\left[\xi_y^s(t)\right] \tag{7.3}$$

where $\hat{f}^s(t_I^s) = 0$, $\xi_y^s(t) = y^s(t) - \hat{x}^s(t) - \hat{f}^s(t)$, $\hat{x}^s$ is the estimation of x^s, $y \triangleq \left[y^{(1)}, \ldots, y^{(N)}\right]^\top$ is a vector that collects the sensor measurements shared through monitoring agents $\mathcal{M}^{(i)}$, $i \in N$ and L^s is the estimation gain, such that $A_L^s \triangleq A^s - L^s$ is stable, $\hat{f}^s$ is the estimation of the fault f^s, Ω^s is a filtering term [44], $t_I^s \triangleq \min\{t \geq 0 : I^s(t) = 1\}$, and $\mathcal{D}^s$ a dead-zone operator such that

$$\mathcal{D}^s\left[\xi_y^s(t)\right] = \begin{cases} 0, & I^s(t) = 0 \\ \xi_y^s(t), & I^s(t) = 1 \end{cases} \tag{7.4}$$

where I^s is the isolation signal computed by the monitoring module $\mathcal{M}^s$ (see Section 7.3.4). The residual ε_y^s is defined by $\varepsilon_y^s(t) = y^s(t) - \hat{x}^s(t)$, which can be expressed as

$$\varepsilon_y^s(t) = e^{A_L^s t}\varepsilon_x^s(0) + n^s(t) + \int_0^t e^{A_L^s(t-\tau)}\Big(r^s(\tau) - L^s n^s(\tau) + \left(g^s(x^s(\tau), d^s(\tau)) - g^s(y^s(\tau), d^s(\tau))\right)u^s(\tau) + h^s(x^s(\tau), x(\tau), u(\tau)) - h^s(y^s(\tau), y(\tau), u(\tau))\Big)d\tau. \tag{7.5}$$

For estimating the air temperature in zone i, a nonlinear adaptive estimation model associated with $\mathcal{M}^{(i)}$, $i \in N$ is generated by

$$\dot{\hat{x}}^{(i)}(t) = A^{(i)}\hat{x}^{(i)}(t) + g^{(i)}(y^s(t), y^{(i)}(t) - \hat{f}^{(i)}(t))u^{(i)}(t) + h^{(i)}(y^{(i)}(t) - \hat{f}^{(i)}(t), y^{(j)}(t)) + \eta^{(i)}(d^{(i)}(t)) + L^{(i)}\left(y^{(i)}(t) - \hat{x}^{(i)}(t) - \hat{f}^{(i)}(t)\right) + \Omega^{(i)}(t)\dot{\hat{f}}^{(i)}(t), \tag{7.6}$$

$$\dot{\Omega}^{(i)}(t) = A_L^{(i)}\Omega^{(i)}(t) - L^{(i)} - \frac{U_{i,max}a_{sz}}{C_{z_i}}u^{(i)}(t), \quad \Omega^{(i)}(t_I^{(i)}) = 0, \tag{7.7}$$

$$\dot{\hat{f}}^{(i)}(t) = \gamma^{(i)}(\Omega^{(i)}(t)+1)\mathcal{D}^{(i)}\left[\xi_y^{(i)}(t)\right], \quad \hat{f}^{(i)}(t_I^{(i)}) = 0 \tag{7.8}$$

where , $\xi_y^{(i)}(t) = y^{(i)}(t) - \hat{x}^{(i)}(t) - \hat{f}^{(i)}(t)$, $\hat{x}^{(i)}$ is the estimation of $x^{(i)}$ and $L^{(i)}$ is the estimation gain, such that $A_L^{(i)} \triangleq A^{(i)} - L^{(i)}$ is stable, $\hat{f}^{(i)}$ is the estimation of the fault $f^{(i)}$, $\Omega^{(i)}$ is a filtering term, $t_I^{(i)} \triangleq \min\{t \geq 0 : I^{(i)}(t) = 1\}$ and $\mathcal{D}^{(i)}$ a dead-zone operator such that

$$\mathcal{D}^{(i)}\left[\xi_y^{(i)}(t)\right] = \begin{cases} 0, & I^{(i)}(t) = 0 \\ \xi_y^{(i)}(t), & I^{(i)}(t) = 1 \end{cases} \tag{7.9}$$

where $I^{(i)}$ is the isolation signal computed by the monitoring module $\mathcal{M}^{(i)}$ (see Section 7.3.4). The residual $\varepsilon_y^{(i)}$ is defined by $\varepsilon_y^{(i)}(t) = y^{(i)}(t) - \hat{x}^{(i)}(t)$, which can be re-written as

$$\varepsilon_y^{(i)}(t) = e^{A_L^{(i)}t}\varepsilon_x^{(i)}(0) + n^{(i)}(t) + \int_0^t e^{A_L^{(i)}(t-\tau)}\Big(r^{(i)}(\tau) - L^{(i)}n^{(i)}(\tau) + \Big(g^{(i)}(x^s(\tau), x^{(i)}(\tau)) - g^{(i)}(y^s(\tau), y^{(i)}(\tau))\Big)u^{(i)}(\tau) + h^{(i)}(x^{(i)}(\tau), x^{(j)}(\tau)) - h^{(i)}(y^{(i)}(\tau), y^{(j)}(\tau))\Big)d\tau. \tag{7.10}$$

7.3.2 Computation of Adaptive Thresholds

The adaptive thresholds bound the residual under healthy conditions taking into account the following assumption:

Assumption 8. The noise corrupting the measurements and the modeling uncertainty are unknown functions but uniformly bounded by known positive constants $\bar{n}^s$, $\bar{n}^{(i)}$, $\bar{r}^s$ and $\bar{r}^{(i)}$ such that $|n^s(t)| \leq \bar{n}^s$, $|n^{(i)}(t)| \leq \bar{n}^{(i)}$, $|r^s(t)| \leq \bar{r}^s$ and $|r^{(i)}(t)| \leq \bar{r}^{(i)}$, respectively.

The adaptive threshold $\bar{\varepsilon}_y^s$ for the monitoring module $\mathcal{M}^s$ is designed based on (7.5) and assuming healthy conditions (i.e., f^s=0, $f^{(i)}$=0 for all $i \in N$) such that $|\varepsilon^s(t)| \leq \bar{\varepsilon}^s(t)$. The adaptive threshold $\bar{\varepsilon}^s(t)$ is defined as

$$\bar{\varepsilon}_y^s(t) = \rho^s e^{-\lambda^s t}\bar{x}^s + \bar{n}^s + \int_0^t \rho^s e^{-\lambda^s(t-\tau)}\Bigg(\left|\frac{U_{st,max}(P_{max}-1)}{C_{st}\Delta T_{max}}\right|\bar{n}^s\,|u^s(\tau)| + |L^s|\,\bar{n}^s + \frac{a_{st}}{C_{st}}\sum_{i\in N} U_{i,max}\left(\bar{n}^s + \bar{n}^{(i)}\right)\left|u^{(i)}(\tau)\right| + \bar{r}^s\Bigg)d\tau, \tag{7.11}$$

where $\bar{x}^s$ is a known bound such that $|x^s(0)| \leq \bar{x}^s$ and $\rho^s > 0$, $\lambda^s > 0$ are selected such that $|e^{A_L^s t}| \leq \rho^s e^{-\lambda^s t}$ for all t.

The adaptive threshold $\bar{\varepsilon}_y^{(i)}$ for the monitoring module $\mathcal{M}^{(i)}$ is designed based on (7.10) and assuming healthy conditions (i.e., f^s=0, $f^{(i)}$=0, $f^{(j)}$=0 for all $j \in \mathcal{K}_i$) such that $|\varepsilon_y^{(i)}(t)| \leq \bar{\varepsilon}_y^{(i)}(t)$. Thus, the adaptive threshold $\bar{\varepsilon}_y^{(i)}$ is defined by

$$\bar{\varepsilon}_y^{(i)}(t) = \rho^{(i)}e^{-\lambda^{(i)}t}\bar{x}^{(i)} + \bar{n}^{(i)} + \int_0^t \rho^{(i)}e^{-\lambda^{(i)}(t-\tau)}\Bigg(\left|L^{(i)}\right|\bar{n}^{(i)} + \bar{r}^{(i)} + \frac{U_{i,max}a_{sz}}{C_{z_i}}\left(\bar{n}^{(i)} + \bar{n}^s\right)\left|u^{(i)}(\tau)\right| + \frac{1}{C_{z_i}}\sum_{j\in\mathcal{K}_i} a_{z_{ij}}\left(\bar{n}^{(i)} + \bar{n}^{(j)}\right) + \frac{\rho_{air}C_p}{C_{z_i}}\sqrt{2\left|C_p - C_v\right|}\sum_{j\in\mathcal{K}_i} A_{d_{ij}}\bar{\mu}^{(i)}(y^{(i)}(\tau), y^{(j)}(\tau))\Bigg)d\tau \tag{7.12}$$

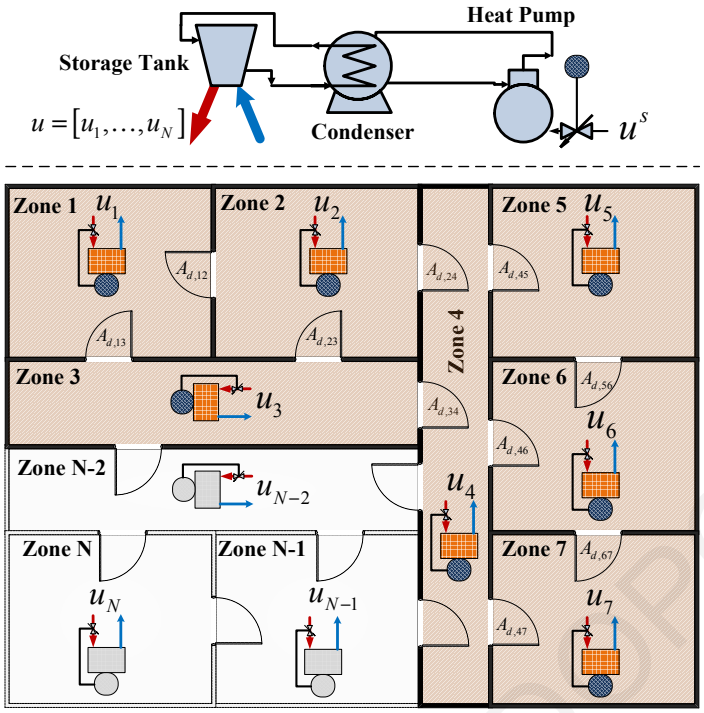

Figure 7.2: Schematic diagram of the 7-zone FCU HVAC system.

where $\bar{x}^{(i)}$ is a known bound such that $|x^{(i)}(0)| \leq \bar{x}^{(i)}$, and $\rho^{(i)} > 0$, $\lambda^{(i)} > 0$ are selected such that $|e^{A_L^{(i)}t}| \leq \rho^{(i)} e^{-\lambda^{(i)}t}$, for all t, $i \in N$. The detailed computation of $\overline{\mu}^{(i)}(y^{(i)}, y^{(j)})$ is presented through (4.26)-(4.30) and (4.32)-(4.34) and is designed to bound the difference $\widetilde{\mu}^{(i)} = \mu^{(i)}(T_{z_i}, T_{z_j}) - \mu^{(i)}(y_H^{(i)}, y_H^{(j)})$.

7.3.3 Sensor Fault Detection Decision Logic

The sensor fault detection decision logic implemented in every monitoring module relies on analytical redundancy relations (ARRs) of the residuals and adaptive thresholds. In more detail, the ARRs associated with the agents $\mathcal{M}^s$ and $\mathcal{M}^{(i)}$ are respectively determined as

$$\mathcal{E}^s: \ \left|\varepsilon_y^s(t)\right| \leq \bar{\varepsilon}_y^s(t), \quad \mathcal{E}^{(i)}: \ |\varepsilon_y^{(i)}(t)| \leq \bar{\varepsilon}_y^{(i)}(t). \tag{7.13}$$

The agent $\mathcal{M}^s$ (correspondingly for $\mathcal{M}^{(i)}$) infers the presence of sensor faults at the first time instant that $\mathcal{E}^s$ is not satisfied (correspondingly for $\mathcal{E}^{(i)}$). Note that the ARR $\mathcal{E}^s$ is sensitive to faults in sensors $\mathcal{S}^s$ and $\mathcal{S}^{(i)}$, $i \in N$, while $\mathcal{E}^{(i)}$ is sensitive to faults that may affect $\mathcal{S}^s$, $\mathcal{S}^{(i)}$ and $\mathcal{S}^{(j)}$, $j \in \mathcal{K}_i$. The outputs of the agent $\mathcal{M}^s$ and $\mathcal{M}^{(i)}$ are the boolean decision signasl D^s and $D^{(i)}$, defined as

$$D^s(t) = \begin{cases} 0, \ t < t_D^s \\ 1, \ t \geq t_D^s \end{cases}, \quad D^{(i)}(t) = \begin{cases} 0, \ t < t_D^{(i)} \\ 1, \ t \geq t_D^{(i)} \end{cases}, \tag{7.14}$$

where $t_D^s \triangleq inf\{t \geq 0 : |\varepsilon_y^s(t)| > \bar{\varepsilon}_y^s(t)\}$ and $t_D^{(i)} \triangleq inf\{t \geq 0 : |\varepsilon_y^{(i)}(t)| > \bar{\varepsilon}_y^{(i)}(t)\}$. If $\mathcal{E}^s$ and $\mathcal{E}^{(i)}$ are always satisfied, then $t_D^s \to \infty$ and $t_D^{(i)} \to \infty$.

7.3.4 Distributed Sensor Fault Isolation Decision Logic

The sensor fault isolation process of the agent $\mathcal{M}^s$ initiates the isolation process when it detects the presence of sensor faults, or when at least one of the N agents $\mathcal{M}^{(i)}$, $i \in N$ does it, while the agent $\mathcal{M}^{(i)}$ is activated when the agent itself, or at least one neighboring agents $\mathcal{M}^{(j)}$, $j \in \mathcal{K}_i$ detects the presence of sensor faults.

The distributed isolation procedure applied by a monitoring agent involves the comparison of the observed pattern of sensor faults that may affect the neighborhood of the agent to a number of theoretical patterns, represented by the columns of a sensor fault signature matrix. In the case of the agent $\mathcal{M}^s$, the observed pattern of sensor faults, denoted by $\Phi^s(t) \in [0,1]^{N+1}$, where $[0,1]^{N+1}$ denotes a binary vector of $N+1$ length, and defined as $\Phi^s(t) = [D^s, D^{(1)}, \ldots, D^{(N)}]$. Note that $D^{(i)}$ is transmitted to $\mathcal{M}^s$ by the agent $\mathcal{M}^{(i)}$ for all $i \in N$. The sensor fault signature matrix consists of $N+1$ rows, which correspond to the set of ARRs $\{\mathcal{E}^s, \mathcal{E}^{(1)}, ..., \mathcal{E}^{(N)}\}$, and $N_c = 2^{N+1} - 1$ columns that correspond to all possible sensor fault combinations that may affect the building zones and the storage tank, where the k-th combination is indicated by $\mathcal{F}^s_{c_k}$, $k \in \{1, \ldots, N_c\}$. The k-th column corresponds to the theoretical pattern, denoted by F^s_k and defined as $F^s_k = [F^s_{1k}, \ldots, F^s_{Nk}]^\top$. In the case of the agent

Table 7.1: Sensor fault signature matrix $F^{(1)}$.

	f^s	$f^{(1)}$	$f^{(2)}$	$f^{(3)}$	$f^{(4)}$	$f^{(5)}$	$f^{(6)}$	$f^{(7)}$	$\{f^s, f^{(1)}\}$
$\mathcal{E}^s$	1	*	*	*	*	*	*	*	1
$\mathcal{E}^{(1)}$	*	1	*	*	0	0	0	0	1
$\mathcal{E}^{(2)}$	*	*	1	*	*	0	0	0	*
$\mathcal{E}^{(3)}$	*	*	*	1	*	0	0	0	*

$\mathcal{M}^{(i)}$, the observed pattern of sensor faults, denoted by $\Phi^{(i)}(t) \in [0,1]^{|\mathcal{K}_i|+2}$, is a vector made up the decisions D^s, $D^{(i)}$ and $D^{(j)}$ for all $j \in \mathcal{K}_i$. The sensor fault signature matrix consists of $|\mathcal{K}_i| + 2$ rows, which correspond to the set of ARRs $\{\mathcal{E}^s, \mathcal{E}^{(i)}\} \bigcup_{j \in \mathcal{K}_i} \left\{\mathcal{E}^{(j)}\right\}$, and $N_c^{(i)} = 2^{|\mathcal{K}_i|+2} - 1$ columns that correspond to all possible sensor fault combinations that may affect the storage tank, the i-th building zone and its $|\mathcal{K}_i|$ neighboring zones. The k-th column corresponds to the theoretical pattern, denoted by $F^{(i)}_k$. For example, taking into account the 7-zone HVAC system shown in Fig. 7.2, $\mathcal{K}_1 = \{2, 3\}$, based on which the observed pattern of agent $\mathcal{M}^{(1)}$ is defined as $\Phi^{(1)}(t) = \left[D^s(t), D^{(1)}(t), D^{(2)}(t), D^{(3)}(t)\right]$. Moreover, the sensor fault signature matrix $F^{(1)}$ is comprised of 4 rows and 15 columns, while Table 7.1 illustrates a part of $F^{(1)}$ assuming the occurrence of 4 single sensor faults, and one possible combination of two simultaneous sensor faults. Hence, the assignment $F^{(1)}_{22} = 1$ implies that $f^{(1)}$ necessarily discloses its occurrence by provoking the violation of $\mathcal{E}^{(1)}$, while $F^{(1)}_{12} = *$ implies that $f^{(1)}$ may justify the violation of $\mathcal{E}^s$, but $\mathcal{E}^s$ may be satisfied in spite of its occurrence. On the other hand, $F^{(1)}_{25} = 0$, since $f^{(5)}$ is not

involved in $\mathcal{E}^{(1)}$.

The outcome of the comparison of the observed fault pattern Φ^s to the N_c theoretical fault patterns F_k^s, $k \in \{1,\dots,N_c\}$, and the observed pattern $\Phi^{(i)}$ to the $N_c^{(i)}$ theoretical patterns $F_q^{(i)}$, $q \in \{1,\dots,N_c^{(i)}\}$ is the diagnosis sets $\Upsilon^s(t)$ and $\Upsilon^{(i)}(t)$, which are determined as

$$\Upsilon^s(t) = \left\{\mathcal{F}_{c_i}^s : i \in \mathcal{I}_\Upsilon^s(t)\right\} \ , \Upsilon^{(i)}(t) = \left\{\mathcal{F}_{c_i}^{(i)} : i \in \mathcal{I}_\Upsilon^{(i)}(t)\right\}, \tag{7.15}$$

with $\mathcal{I}_\Upsilon^s(t) = \left\{k : F_k^s = \Phi^s(t),\ k \in \{1,\dots,N_c\}\right\}$ and $\mathcal{I}_\Upsilon^{(i)}(t) = \left\{k : F_k^{(i)} = \Phi^{(i)}(t),\ k \in \{1,\dots,N_c^{(i)}\}\right\}$. The isolation signals that activate the estimation of local sensor faults in (7.1)-(7.4) and (7.6)-(7.9) and its use in the distributed fault accommodation control scheme are defined as

$$I^s(t) = \begin{cases} 1, \text{ if } f^s \in \Upsilon^s(t) \\ 0, \text{ otherwise} \end{cases}, I^{(i)}(t) = \begin{cases} 1, \text{ if } f^{(i)} \in \Upsilon^{(i)}(t) \\ 0, \text{ otherwise} \end{cases}. \tag{7.16}$$

Additionally, the isolation signal related to the propagated sensor faults $f^{(i)}$, $i \in N$, which is generated by the agent $\mathcal{M}^s$ and used in the distributed fault accommodation control scheme, is defined as

$$I^{s,i}(t) = \begin{cases} 1, \text{ if } f^s \in \Upsilon^s(t) \\ 0, \text{ otherwise} \end{cases}, \tag{7.17}$$

while the isolation signal related to the propagated sensor faults f^s and $f^{(j)}$, $j \in \mathcal{K}_i$, which is generated by the agent $\mathcal{M}^{(i)}$ and used in the distributed fault accommodation control scheme, are defined as

$$I^{(i,s)}(t) = \begin{cases} 1, \text{ if } f^s \in \Upsilon^{(i)}(t) \\ 0, \text{ otherwise} \end{cases}, I^{(i,j)}(t) = \begin{cases} 1, \text{ if } f^{(j)} \in \Upsilon^{(i)}(t) \\ 0, \text{ otherwise} \end{cases}. \tag{7.18}$$

7.3.5 Distributed Fault Accommodation Control Scheme

The control agents C^s and $C^{(i)}$, $i \in N$ is not necessary to be available for the design of the proposed sensor fault accommodation scheme. However, the control agents C^s and $C^{(i)}$ should be programmed to collect the virtual sensor measurements instead of the actual measurements. Note that the virtual sensor measurements are generated by the monitoring agents based on the fault estimations according to (7.1) and (7.6), and the isolation signals I^s and $I^{(i)}$, defined in (7.16)-(7.18); i.e.,

$$C^s : u^s(t) = \chi^s(y_v^s(t), y_v(t), u(t)), \tag{7.19}$$

$$C^{(i)} : u^{(i)}(t) = \chi^{(i)}(y_v^{(i)}(t), y_v^{(i,s)}(t), y_v^{\mathcal{K}_i}(t)), \tag{7.20}$$

where

$$y_v^s(t) = y^s(t) - \mathcal{D}^s\left[\hat{f}^s(t)\right], \tag{7.21}$$

$$y_v(t) = y(t) - \left[\mathcal{D}^{s,1}\left[\hat{f}^{(1)}(t)\right], \dots, \mathcal{D}^{s,N}\left[\hat{f}^{(N)}(t)\right]\right], \tag{7.22}$$

$$y_v^{(i)}(t) = y^{(i)}(t) - \mathcal{D}^{(i)}\left[\hat{f}^{(i)}(t)\right], \tag{7.23}$$

$$y_v^{s,i}(t) = y^s(t) - \mathcal{D}^{(i,s)}\left[\hat{f}^s(t)\right], \tag{7.24}$$

and $y_v^{\mathcal{K}_i}(t)$ is a vector made up of $|\mathcal{K}_i|$ elements $y^{(j)} - \mathcal{D}^{(i,j)}\left[\hat{f}^{(j)}(t)\right]$, $j \in \mathcal{K}_i$. The terms $\mathcal{D}^s[\cdot]$ and $\mathcal{D}^{(i)}[\cdot]$ are dead-zone operators defined similarly to (7.4) and (7.9), that is $\mathcal{D}^s[\hat{f}^s(t)] = 1$ if $I^s(t) = 1$, and $\mathcal{D}^s[\hat{f}^s(t)] = 0$ otherwise (correspondingly for $\mathcal{D}^{(i)}[\cdot]$), while $\mathcal{D}^{s,i}[\cdot]$, $\mathcal{D}^{(i,s)}[\cdot]$ and $\mathcal{D}^{(i,j)}[\cdot]$ are dead-zone operators that equal to their input arguments when the associated isolation signals $I^{s,i}$, $I^{(i,s)}$ and $I^{(i,j)}$ are non-zero. Based on the design of the distributed fault accommodation scheme, *every time* that sensor faults are isolated in the neighborhood of the i-th building zone, its associated control agent $\mathcal{C}^{(i)}$, and the control agents of the neighboring subsystems, that is $\mathcal{C}^s$ and $\mathcal{C}^{(j)}$, $j \in \mathcal{K}_i$, are accommodated to the isolated sensor faults by using their estimations.

For the purposes of this paper, we assume that a local control agent can be accommodated to isolated sensor faults several times, without requiring a dwell-time between accommodation actions, or a bound on the estimations of isolated sensor faults that are transmitted by the neighboring local control agents in order to ensure subsystem's stability and good tracking performance.

7.4 Simulation Results

In this section, we illustrate the application of the distributed adaptive FTC methodology to a 7-zone HVAC system where the architectural arrangement of the 7 zones is presented by the shaded area in Figure 7.2. We consider eight subsystems $\{\Sigma^s, \Sigma^{(1)}, \ldots, \Sigma^{(7)}\}$, with the interconnections between the zones, defined by the sets $\mathcal{K}_1 = \{2,3\}$, $\mathcal{K}_2 = \{1,3,4\}$, $\mathcal{K}_3 = \{1,2,4\}$, $\mathcal{K}_4 = \{2,3,5,6,7\}$, $\mathcal{K}_5 = \{4,6\}$, $\mathcal{K}_6 = \{4,5,7\}$, $\mathcal{K}_7 = \{4,6\}$. The subsystems are described by (2.20)-(2.22) with: a_{z_i}=740, $i \in N$, $a_{z_{ij}}$=50, a_{st}=12, a_{sz} =0.6, C_{st}=837, C_p=1.004, C_v=0.717, ρ_{air}=1.22, C_{z_i}, $i \in \{1,2,3,4,5,6,7\}$ =370, $U_{i,max}$=3700, $i \in N$, $U_{st,max}$=27.36×10^4, P_{max}=3.5, ΔT_{max}=45, A_{w_i}=120, $i \in N$, h=8.29, $A_{d_{ij}}$=2.60, $i \in N$, $j \in \mathcal{K}_i$. It is assumed that the exogenous uncontrollable signals are constant, defined as follows: $T_o = 5^oC$, $T_{pl} = 10^oC$, $T_{amb} = 5^oC$, T_{i1} =10^{o}C, $i \in N$. The modeling uncertainty in each subsystem $r^s = 5\% d_1^s \sin(0.1t)$ and $r^{(i)} = 5\% d_1^{(i)} \sin(0.1t)$, $i \in N$. For simulation purposes, the noise corrupting the sensor output is defined as: $\bar{n}^s = 3\% Y^s$ and $\bar{n}^{(i)} = 3\% Y^{(i)}$, where Y^s and $Y^{(i)}$ are the steady state value of sensor measurements y^s and $y^{(i)}$, respectively, $i \in N$, under healthy conditions. The design constants for the monitoring agents are: L^s=10 and $L^{(i)}$=1, ρ^s=$\rho^{(i)}$=1.3, λ^s=30, $\lambda^{(i)}$=6, γ^s=8, $\gamma^{(i)}$=5. In this example, we simulated the following multiple sensor fault scenario: two bias abrupt faults occur affect sensors $\mathcal{S}^{(1)}$ and $\mathcal{S}^{(7)}$ at $t_f^{(1)} = t_f^{(7)} = 20$ h. The faults are modeled as $f^{(1)}(t) = -20\% Y^{(1)}(1 - e^{-10^4(t-20)})$ and $f^{(7)}(t) = -20\% Y^{(7)}(1 - e^{-10^4(t-20)})$ [127,129]. For comparison purposes, we performed simulations with and without using the proposed distributed fault accommodation control scheme described by (7.19)-(7.20). The desired values of the temperatures are set up as follows: y_{ref}^s=55 ^{o}C and $y_{ref}^{(i)}$=24 ^{o}C, $i \in N$.

Fig. 7.3 presents the response of the temperatures, controlled either by the nominal distributed control scheme (blue solid line) or by the distributed fault accommodation control scheme (red dashed

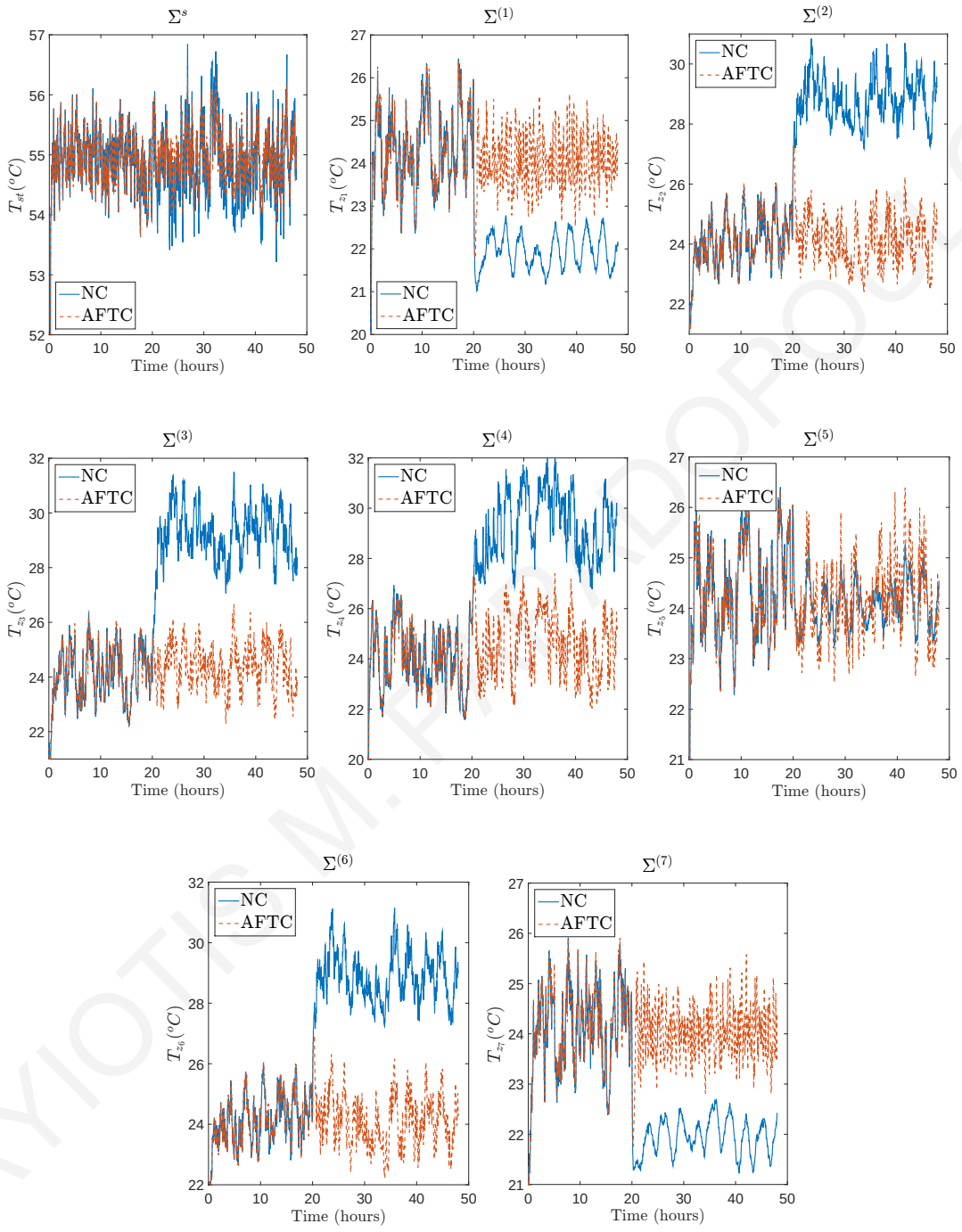

Figure 7.3: HVAC system temperature response in multiple simultaneous bias sensor fault scenario in sensors $S^{(1)}$, $S^{(7)}$: Controlled by the nominal control (NC) scheme (blue solid line) and controlled by the adaptive fault-tolerant control (AFTC) scheme (red dashed line).

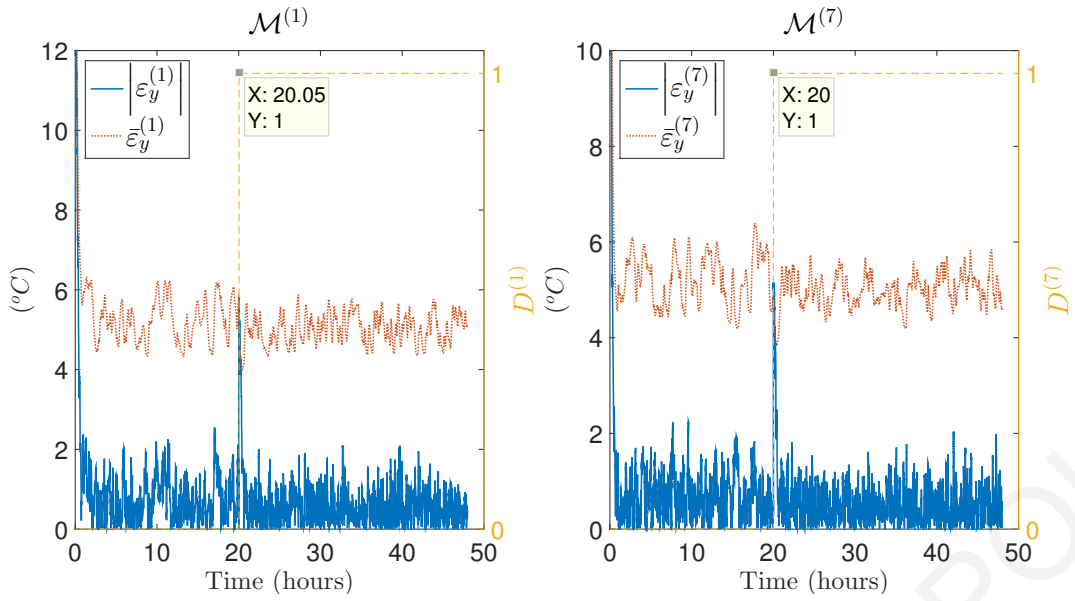

Figure 7.4: Decision-making process of the monitoring agents $\mathcal{M}^{(1)}$, $\mathcal{M}^{(7)}$: Residuals $\varepsilon^{(1)}$, $\varepsilon^{(7)}$ (blue solid line), adaptive thresholds $\bar{\varepsilon}^{(i)}$, $\bar{\varepsilon}^{(7)}$ (red dotted line) and detection signals $D^{(1)}$, $D^{(7)}$ (yellow dashed line) of the monitoring agents $\mathcal{M}^{(1)}$, $\mathcal{M}^{(7)}$.

line). The faults occur in $\mathcal{S}^{(1)}$, $\mathcal{S}^{(7)}$, significantly effect the temperature dynamics of the local subsystems $\Sigma^{(1)}$, $\Sigma^{(7)}$, respectively, as well as the dynamics of their associated neighboring subsystems $\{\Sigma^{(2)}, \Sigma^{(3)}\}$, $\{\Sigma^{(4)}, \Sigma^{(6)}\}$, while Σ^s is less affected by these faults. The use of the proposed distributed adaptive FTC scheme, contributed to the successful compensation of the sensor faults effects on the local and neighboring dynamics of subsystems $\Sigma^{(1)}$, $\Sigma^{(7)}$. Fig. 7.4 shows the residuals $\varepsilon^{(1)}$, $\varepsilon^{(7)}$ (blue solid line), adaptive thresholds $\bar{\varepsilon}^{(1)}$, $\bar{\varepsilon}^{(7)}$ (red dotted line) and the detection signals $D^{(1)}$, $D^{(7)}$ (yellow dashed line) of the monitoring agents $\mathcal{M}^{(1)}$, $\mathcal{M}^{(7)}$, while the rest of the monitoring agents $(\mathcal{M}^s, \mathcal{M}^{(2)}, \ldots, \mathcal{M}^{(6)})$ are not presented since their ARRs are not violated.

At the time instant $t_D^{(7)} = 20$ h, a fault is detected by $\mathcal{M}^{(7)}$ which initiates the isolation procedure in the monitoring agent $\mathcal{M}^{(7)}$ and its neighbouring agents $\mathcal{M}^s$, $\mathcal{M}^{(4)}$ and $\mathcal{M}^{(6)}$. In the case of $\mathcal{M}^s$, the observed pattern Φ^s equal to $\Phi^s = [0,0,0,0,0,0,0,1]$, which is compared to the theoretical patterns F_k^s for all $k \in \{1,\ldots,255\}$, leading to $\Upsilon^s = \{f^{(7)}\}$ and $I^s = I^{s,1} = \cdots = I^{s,6} = 0$ and $I^{s,7} = 1$. In the case of $\mathcal{M}^{(4)}$, $\mathcal{M}^{(6)}$, $\mathcal{M}^{(7)}$, the observed patterns are $\Phi^{(4)} = [0,0,0,1]$, $\Phi^{(6)} = [0,0,0,1]$, $\Phi^{(7)} = [0,1,0,0]$, respectively, which are compared to the theoretical patterns of $F_k^{(4)}$, $F_k^{(6)}$, $F_k^{(7)}$, for all $k \in \{1,\ldots,15\}$. The comparison leads to $\Upsilon^{(4)} = \Upsilon^{(6)} = \Upsilon^{(7)} = \{f^{(7)}\}$. Based on these diagnosis sets the non-zero isolation signals are $I^{(4,7)}$, $I^{(6,7)}$ and $I^{(7)}$. The dead-zone operator $\mathcal{D}^{(7)}[.]$ activated the estimation for the sensor fault $\hat{f}^{(7)}$ executed by agent $\mathcal{M}^{(7)}$. The local control agents that are accommodated to the isolated sensor fault $f^{(7)}$ using its estimation transmitted by the agent $\mathcal{M}^{(7)}$ are $\mathcal{C}^s$, $\mathcal{C}^{(4)}$, $\mathcal{C}^{(6)}$, and $\mathcal{C}^{(7)}$.

Similarly, at the time instant $t_D^{(1)} = 20.05$ h, a fault is detected by $\mathcal{M}^{(1)}$ which initiates the isolation procedure locally and its neighboring monitoring agents $\mathcal{M}^s$, $\mathcal{M}^{(2)}$ and $\mathcal{M}^{(3)}$. By applying the

distributed isolation process shown in Section 7.3.4, the new non-zero isolation signals are generated: $I^{s,1}$, $I^{(2,1)}$, and $I^{(3,1)}$. The dead-zone operator $\mathcal{D}^{(1)}[.]$ enables the estimation for the sensor fault $\hat{f}^{(1)}$ in $\mathcal{M}^{(1)}$, followed by the accommodation of control agents C^s, $C^{(2)}$, $C^{(3)}$, and $C^{(1)}$ to the new isolated sensor faults. Note that C^s has been accommodated twice.

7.5 Conclusions

In this chapter, the design of a distributed sensor fault accommodation scheme for HVAC systems that may be affected by multiple sensor faults is presented. Exploiting the HVAC system topology, a bank of distributed monitoring agents, that correspond to the virtual sensor, which are allowed to exchange information with neighboring agents. The virtual sensors were designed to detect, isolate and estimate the isolated sensor faults. In order to compensate the sensor fault effects, the estimation of sensor faults is used by neighboring control agents in order to compensate the effects of the faults of the isolated sensors. A simulation example illustrates the effectiveness of the proposed scheme, which is applied to a 7-zone HVAC system.

The virtual sensor schemes are effective when the nominal control scheme is not available and/or can not be accessed. This however comes at the cost of increased computational complexity since a nonlinear state estimation is required and furthermore, the stability analysis for the closed-loop system cannot be rigorously performed. In the following chapter (Chapter 8) the nominal control design is available and can be accessed, therefore the stability analysis of the closed-loop systems can be performed.

Chapter 8

Distributed Sensor Fault Accommodation using a Control Reconfiguration Scheme

8.1 Introduction

As we have seen in Chapter 7, a sensor fault accommodation algorithm based on a virtual sensor schemes can be used to adapt the faulty sensors to the nominal controller (i.e. the nominal controller remains unchanged) by estimating (learning) the isolated sensor faults. The virtual sensor schemes are effective when there is no access to and/or no available knowledge of the nominal control scheme. This however comes at the cost of increased computational complexity since nonlinear state estimation is required; as a result the stability analysis of the virtual sensor-based FTC scheme for nonlinear systems cannot be rigorously performed.

The main contribution of this work is the design of a stable distributed sensor fault accommodation scheme for multi-zone HVAC systems for maintaining the desired temperature in the building zones and the electromechanical part under both healthy and faulty conditions. For each building zone and the electromechanical part, an adaptive nonlinear controller is designed to compensate the effects of the isolated sensor faults on the local control input. The adaptive law is activated when local faults are isolated, aiming at the estimation of the local sensor fault. Due to the distributed control architecture, where sensor measurements are shared between neighboring controllers, the local fault estimation is also provided to the neighboring controllers to reduce the effects of the sensor fault propagation. The control performance of the proposed distributed sensor fault accommodation scheme is investigated based on the stability analysis, first under healthy and then under faulty conditions.

8.2 Objective

The objective of this chapter is twofold. The first objective is to design a stable distributed feedback control scheme to track the desired water temperature of the storage tank T_{st} and the desired air tem-

peratures in zones $T_{z_1}, \ldots, T_{z_N}$, taking into account modeling uncertainty and measurement noise. In the presence of a sensor fault that has been detected, the second objective is to design a distributed fault accommodation scheme to compensate the effects of sensor faults. In this chapter, we do not consider the issue of fault detection and isolation, which has been considered in previous chapters (see Chapter 3–6). Instead, we assume that a monitoring scheme has detected the presence of a fault at a particular sensor and we investigate the problem of distributed fault accommodation.

8.3 Design of the Control Reconfiguration Scheme

This section presents a distributed feedback control scheme for multi-zone HVAC systems. The distributed feedback control scheme consists of $N+1$ controllers (one controller for Σ^s and N controllers for the N zones). Each controller can exchange control input and sensor data with its neighboring controllers. First, we consider the design of the control law for the temperature in the storage tank. Taking into account the bilinear structure of the subsystem Σ^s (see (2.23)), a feedback linearization control law ϕ^s for controlling the water temperature in the storage tank is designed as

$$\begin{aligned} u_{st}^c(t) &= \phi^s(y^s(t), u(t), y(t), y_r^s(t)) \\ &= (g^s(y^s(t)))^{-1}\left[-\eta^s(T_{pl}(t)) - h^s(y^s(t), y(t), u(t)) - A^s y_r^s - (A^s + \rho^s)(y^s(t) - y_r^s(t)) + \dot{y}_r^s(t)\right], \end{aligned} \tag{8.1}$$

where u_{st}^c is the controller's output, y_r^s is the differentiable reference signal for the state T_{st}, $y = [y^{(i)} : i \in \{1, \ldots, N\}]$ is a vector comprised of the sensor signals from all zones of the HVAC system and $\rho^s > 0$ is a design constant. The reference signal y_r^s is generated by the following reference model

$$\dot{y}_r^s(t) = A^s y_r^s(t) + g^s(y_r^s(t)) u_s^{ref}(t) + h^s(y_r^s(t), y_r(t), u(t)) + \eta^s(T_{pl}(t)), \tag{8.2}$$

where u_s^{ref} is a bounded input signal for the reference model. Similarly, the feedback linearization control law $\phi^{(i)}$ for controlling air temperature of the ith zone is designed as

$$\begin{aligned} u_i^c(t) &= \phi^{(i)}(y^{(i)}(t), y^s(t), y^{\mathcal{K}_i}(t), y_r^{(i)}(t)) \\ &= \left(g^{(i)}(y^s(t), y^{(i)}(t))\right)^{-1}\left[-\eta^{(i)}(T_{i1}(t), T_{amb}(t)) - h^{(i)}(y^{(i)}(t), y^{\mathcal{K}_i}(t)) - A^{(i)} y_r^{(i)}\right. \\ &\quad \left. - \left(A^{(i)} + \rho^{(i)}\right)\left(y^{(i)}(t) - y_r^{(i)}(t)\right) + \dot{y}_r^{(i)}(t)\right] \end{aligned} \tag{8.3}$$

where u_i^c is the controller's output for the ith zone, $y_r^{(i)}$ denotes the desired (reference) temperature of ith zone and $y^{\mathcal{K}_i} = [y^{(j)} : j \in \mathcal{K}_i]$ is vector that collects the sensor signals of the $|\mathcal{K}_i|$ neighboring subsystems and $\rho^{(i)} > 0$ is a positive design constant. The reference signal $y_r^{(i)}$ is generated by:

$$\dot{y}_r^{(i)}(t) = A^{(i)} y_r^{(i)}(t) + g^{(i)}(y_r^s(t), y_r^{(i)}(t)) u_i^{ref}(t) + h^{(i)}(y_r^{(i)}(t), y_r^{\mathcal{K}_i}(t)) + \eta^{(i)}(T_{i1}(t), T_{amb}(t)), \tag{8.4}$$

where u_i^{ref} is a bounded input signal for the reference model. Note that the control laws in (8.1) and (8.3) can be designed such that $u_{st}^c(t) = [0, 1]$ and $u_i^c(t) = [0, 1]$ for all $t \geq 0$ and therefore, $u_{st}(t) = u_{st}^c(t)$ and $u_i(t) = u_i^c(t)$, for all $t \geq 0$.

By applying (8.1) on (2.23), under healthy conditions (i.e., $f^s = 0$ and $f^{(i)} = 0$, for all $i \in \{1, \ldots, N\}$), the tracking error dynamics of Σ^s are described by

$$\dot{\epsilon}^s(t) = -\rho^s \epsilon^s(t) + v^s(t), \tag{8.5}$$

where $\epsilon^s = T_{st} - y_r^s$ is the tracking error of Σ^s and v^s contains the uncertain terms (due to modeling uncertainties and measurement noise) given by

$$v^s(t) = r^s(t) - (A^s + \rho^s)\, n^s(t) + \frac{U_{st,max}\, p}{C_{st}\Delta T_{\max}} n^s(t) u_{st}(t) + \frac{a_{sz}}{C_{st}} \sum_{i \in \mathcal{N}} U_{i,max}(n^{(i)}(t) - n^s(t)) u_i(t). \tag{8.6}$$

Similarly, by applying (8.3) on (2.26), the tracking error dynamics of $\Sigma^{(i)}$ under healthy conditions are expressed by

$$\dot{\epsilon}^{(i)}(t) = -\rho^{(i)} \epsilon^{(i)}(t) + v^{(i)}(t), \tag{8.7}$$

where $\epsilon^{(i)} = T_{z_i} - y_r^{(i)}$ is the tracking error of $\Sigma^{(i)}$ and $v^{(i)}$ contains the uncertain terms indicated by

$$\begin{aligned} v^{(i)}(t) = r^{(i)}(t) - \left(A^{(i)} + \rho^{(i)}\right) n^{(i)}(t) + \sigma^{(i)}\left(n^{(i)}(t) - n^s(t)\right) u_i(t) + \sum_{j \in \mathcal{K}_i} \frac{a_{z_{i,j}}}{C_{z_i}} n^{(j)}(t) \\ + p^{(i)} \sum_{j \in \mathcal{K}_i} A_{d_{i,j}} \widetilde{\mu}^{(i)}(y^{(i)}(t), y^{(j)}(t)), \end{aligned} \tag{8.8}$$

with

$$\widetilde{\mu}^{(i)}(y^{(i)}, y^{(j)}) = \mu^{(i)}(T_{z_i}, T_{z_j}) - \mu^{(i)}(y^{(i)}, y^{(j)}). \tag{8.9}$$

In the sequel, we assume that the uncertain terms $v^s(t)$ and $v^{(i)}$ given by (8.6) and (8.8), respectively, which represent the modeling uncertainty and measurement noise, are all uniformly bounded. However, the bounds are not assumed to be known.

8.4 Distributed Sensor Fault Accommodation

In this section, we consider the design and analysis of a distributed fault accommodation scheme for a single sensor fault. The problem of designing fault detection and isolation algorithms is not considered here, since it has been investigated in previous works (for example [31, 107, 129]). At the time that a single sensor fault is isolated, a local online adaptive law is activated to estimate the sensor fault. The estimation of the sensor fault is used by the local and neighboring controllers to compensate the effects resulting from the distributed control architecture. Taking into account the controller structure of (8.1), the following reconstruction of the distributed feedback control ϕ^s is proposed, such as

$$u_{st}^c(t) = \phi^s(z^s(t), u(t), z(t), y_r^s(t)), \tag{8.10}$$

where z^s is the reconstructed sensor signal given by

$$z^s(t) = \begin{cases} y^s(t), & t < t_I^s \\ y^s(t) - \widehat{f^s}(t), & t \geq t_I^s \end{cases}, \tag{8.11}$$

where t_I^s is the isolation time of the sensor fault f^s and $\widehat{f^s}$ is the estimation of f^s. Similarly, taking into account the controller structure of (8.3), the following reconstruction of the distributed feedback control $\phi^{(i)}$ is proposed, such as

$$u_i^c(t) = \phi^{(i)}(z^{(i)}(t), z^s(t), z^{\mathcal{K}_i}(t), y_r^{(i)}(t)), \tag{8.12}$$

where $z^{\mathcal{K}_i} = [z^{(j)} : j \in \mathcal{K}_i]$ is a vector consists of the reconstructed sensor signals of the neighboring subsystems and $z^{(i)}$ denotes the reconstructed sensor signal given by

$$z^{(i)}(t) = \begin{cases} y^{(i)}(t), & t < t_I^{(i)} \\ y^{(i)}(t) - \widehat{f^{(i)}}(t), & t \geq t_I^{(i)} \end{cases}, \tag{8.13}$$

where $t_I^{(i)}$ is the isolation time of the sensor fault $f^{(i)}$ and $\widehat{f^{(i)}}$ is the estimation of $f^{(i)}$. The design of the online adaptive law that estimates the sensor fault in $\mathcal{S}^{(i)}$ is presented next. Due to page limitation the design of the online adaptive law for a single sensor fault in $\mathcal{S}^s$ is not included, but it can be obtained following the same procedure. The online adaptive law $\dot{\bar{f}}^{(i)}$ that estimates the magnitude of the local sensor fault $f^{(i)}$ is given by

$$\dot{\bar{f}}^{(i)}(t) = \mathcal{P}\left\{\gamma^{(i)}\left(\sigma^{(i)}u_i(t) - A^{(i)} - \rho^{(i)}\right)\left(\epsilon_y^{(i)}(t) - \widehat{f^{(i)}}(t)\right)\right\}, \tag{8.14}$$

with $\widehat{f^{(i)}}(t_I^{(i)}) = 0$ where $\widehat{f^{(i)}}$ is the estimation of the sensor fault $f^{(i)}$, $\epsilon_y^{(i)} = y^{(i)} - y_r^{(i)}$ is the output tracking error and $\gamma^{(i)} > 0$ is the learning rate of the online adaptive law. $\mathcal{P}\{.\}$ denotes a projection operator given in (8.15), which constrains $\widehat{f^{(i)}}$ in a bounded set such that $|\widehat{f^{(i)}}(t)| \leq \bar{f}^{(i)}$ for all $t \geq t_I^{(i)}$. Fig. 8.1 shows a schematic representation of the distributed sensor fault accommodation scheme, where with blue color is denoted the reconstructed part of the local controller.

$$\dot{\bar{f}}^{(i)} = \begin{cases} \gamma^{(i)}\left(\sigma^{(i)}u_i - A^{(i)} - \rho^{(i)}\right)\left(\epsilon_y^{(i)} - \widehat{f^{(i)}}\right), & \left\{\left|\widehat{f^{(i)}}\right| < \bar{f}^{(i)}\right\} \text{or} \left\{\left|\widehat{f^{(i)}}\right| = \bar{f}^{(i)} \right. \\ & \left. \text{and } \widehat{f^{(i)}}\gamma^{(i)}\left(\sigma^{(i)}u_i - A^{(i)} - \rho^{(i)}\right)\left(\epsilon_y^{(i)} - \widehat{f^{(i)}}\right) \leq 0\right\} \\ 0, & \left\{\left|\widehat{f^{(i)}}\right| = \bar{f}^{(i)} \right. \\ & \left. \text{and } \widehat{f^{(i)}}\gamma^{(i)}\left(\sigma^{(i)}u_i - A^{(i)} - \rho^{(i)}\right)\left(\epsilon_y^{(i)} - \widehat{f^{(i)}}\right) > 0\right\} \end{cases} \tag{8.15}$$

Given that a sensor fault $f^{(i)}$ is isolated at $t_I^{(i)}$ (there are no other faults in the remainder zones or the storage tank), the tracking error dynamics of $\epsilon^{(i)}$ in the presence of a local sensor fault $f^{(i)}$ is obtained by applying (8.3) to (2.26), i.e.,

$$\dot{\epsilon}^{(i)}(t) = -\rho^{(i)}\epsilon^{(i)}(t) + \left(\sigma^{(i)}u_i(t) - A^{(i)} - \rho^{(i)}\right)\widetilde{f^{(i)}}(t) + v_I^{(i)}(t), \tag{8.16}$$

where $\widetilde{f^{(i)}} \triangleq f^{(i)} - \widehat{f^{(i)}}$ is the fault estimation error and $v_I^{(i)}$ is defined as

$$v_I^{(i)}(t) = r^{(i)}(t) - \left(A^{(i)} + \rho^{(i)}\right) n^{(i)}(t) + \sigma^{(i)}\left(n^{(i)}(t) - n^s(t)\right) u_i(t) + \sum_{j \in \mathcal{K}_i} \frac{a_{z_{i,j}}}{C_{z_i}} n^{(j)}(t)$$
$$+ p^{(i)} \sum_{j \in \mathcal{K}_i} A_{d_{i,j}} \widetilde{\mu}^{(i)}(y^{(i)}(t) - \widehat{f^{(i)}}(t), y^{(j)}(t)), \tag{8.17}$$

with

$$\widetilde{\mu}^{(i)}(y^{(i)} - \widehat{f^{(i)}}, y^{(j)}) = \mu^{(i)}(T_{z_i}, T_{z_j}) - \mu^{(i)}(y^{(i)} - \widehat{f^{(i)}}, y^{(j)}). \tag{8.18}$$

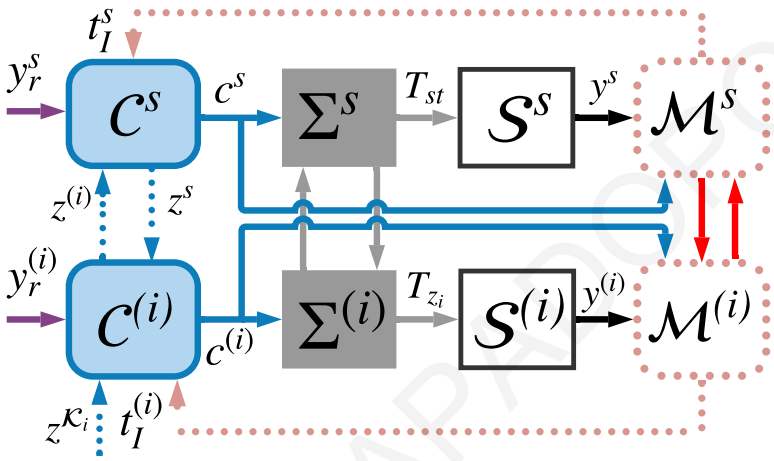

(a) Distributed Control Reconfiguration scheme

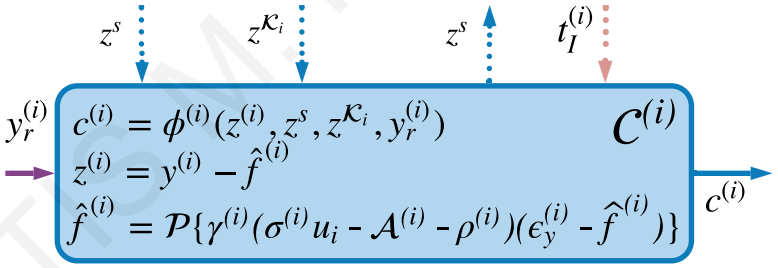

(b) Design of the local controller $C^{(i)}$.

Figure 8.1: Distributed Sensor Fault Accommodation scheme based on control reconfiguration.

8.5 Stability Analysis

The following result presents the stability properties of the proposed distributed control scheme under healthy conditions.

Theorem 1. *In the absence of any sensor fault the distributed control scheme of* (8.1)–(9.4) *guarantees that:*

1. *the tracking errors* $\epsilon^s(t)$, $\epsilon^{(i)}(t)$ *are uniformly bounded i.e.,* $\epsilon^s(t) \in L_\infty$, $\epsilon^{(i)}(t) \in L_\infty$, *for all* $i = \{1, \ldots, N\}$

2. *there exist constants* λ_1, λ_2 *such that for any* $t \geq 0$,

$$\rho^s \int_0^t |\epsilon^s(\tau)|^2 \, d\tau + \sum_{i=1}^{N} \rho^{(i)} \int_0^t \left|\epsilon^{(i)}(\tau)\right|^2 d\tau \leq \lambda_1^s + \lambda_2^s \int_0^t |v(\tau)|^2 \, d\tau, \tag{8.19}$$

where $v^2(t) = \frac{1}{2\rho^s} |v^s(t)|^2 + \frac{1}{2} \sum_{i=1}^{N} \rho^{(i)} \left|v^{(i)}(t)\right|^2$

3. *if* $v(t) \in L_2$ *(i.e.,* $v(t)$ *is square integrable) then* $\lim_{t\to\infty} \left(\rho^s |\epsilon^s(t)|^2 + \sum_{i=1}^{N} \rho^{(i)} \left|\epsilon^{(i)}(t)\right|^2\right) = 0$.

Proof. To analyze the stability properties of the overall closed-loop system under healthy conditions the following candidate Lyapunov function V is proposed, given by

$$V = \frac{1}{2} (\epsilon^s(t))^2 + \frac{1}{2} \sum_{i=1}^{N} \left(\epsilon^{(i)}(t)\right)^2. \tag{8.20}$$

The time derivative of V is given by

$$\dot{V} = \epsilon^s(t)\dot{\epsilon}^s(t) + \sum_{i=1}^{N} \epsilon^{(i)}(t)\dot{\epsilon}^{(i)}(t), \tag{8.21}$$

$$= -\rho^s (\epsilon^s(t))^2 - \sum_{i=1}^{N} \rho^{(i)} \left(\epsilon^{(i)}(t)\right)^2 + v^s(t)\epsilon^s(t) + \sum_{i=1}^{N} v^{(i)}(t)\epsilon^{(i)}(t), \tag{8.22}$$

$$= -\frac{\rho^s}{2} |\epsilon^s(t)|^2 - \sum_{i=1}^{N} \frac{\rho^{(i)}}{2} \left|\epsilon^{(i)}(t)\right|^2 - \frac{\rho^s}{2} |\epsilon^s(t)|^2 + \epsilon^s(t)v^s(t) - \sum_{i=1}^{N} \frac{\rho^{(i)}}{2} \left|\epsilon^{(i)}(t)\right|^2 + \sum_{i=1}^{N} v^{(i)}(t)\epsilon^{(i)}(t)$$

$$\leq -\frac{\rho^s}{2} |\epsilon^s(t)|^2 - \sum_{i=1}^{N} \frac{\rho^{(i)}}{2} \left|\epsilon^{(i)}(t)\right|^2 - \frac{\rho^s}{2}\left(|\epsilon^s(t)|^2 - \frac{2}{\rho^s} |\epsilon^s(t)| \, |v^s(t)|\right)$$

$$- \sum_{i=1}^{N} \frac{\rho^{(i)}}{2}\left(\left|\epsilon^{(i)}(t)\right|^2 - \frac{2}{\rho^{(i)}} \left|\epsilon^{(i)}(t)\right| \left|v^{(i)}(t)\right|\right) \tag{8.23}$$

$$\leq -\frac{\rho^s}{2} |\epsilon^s(t)|^2 - \frac{1}{2} \sum_{i=1}^{N} \rho^{(i)} \left|\epsilon^{(i)}(t)\right|^2 + \frac{1}{2\rho^s} |v^s(t)|^2 + \frac{1}{2} \sum_{i=1}^{N} \rho^{(i)} \left|v^{(i)}(t)\right|^2$$

$$\leq -\frac{\rho^s}{2} |\epsilon^s(t)|^2 - \frac{1}{2} \sum_{i=1}^{N} \rho^{(i)} \left|\epsilon^{(i)}(t)\right|^2 + v^2(t), \tag{8.24}$$

where $v^2(t) = \frac{1}{2\rho^s} |v^s(t)|^2 + \frac{1}{2} \sum_{i=1}^{N} \rho^{(i)} \left|v^{(i)}(t)\right|^2$. Based on (8.24) if

$$\frac{\rho^s}{2} |\epsilon^s(t)|^2 + \frac{1}{2} \sum_{i=1}^{N} \rho^{(i)} \left|\epsilon^{(i)}(t)\right|^2 \geq v^2(t), \tag{8.25}$$

then V will be decreasing and therefore the summation of the tracking errors i.e., $\frac{\rho^s}{2} |\epsilon^s(t)|^2 + \frac{1}{2} \sum_{i=1}^{N} \rho^{(i)} \left|\epsilon^{(i)}(t)\right|^2$ will be also decreasing. Furthermore, by integrating (8.24) from $\tau = 0$ to $\tau = t$, we obtain

$$\rho^s \int_0^t |\epsilon^s(\tau)|^2 \, d\tau + \sum_{i=1}^{N} \rho^{(i)} \int_0^t \left|\epsilon^{(i)}(\tau)\right|^2 d\tau \leq 2\,[V(0) - V(t)] + 2 \int_0^t |v(\tau)|^2 \, d\tau,$$

$$\leq \lambda_1^s + \lambda_2^s \int_0^t |v(\tau)|^2 \, d\tau. \tag{8.26}$$

where $\lambda_1 = 2\sup_{t\geq 0}[V(0) - V(t)]$ and $\lambda_2 = 2$.

Based on (8.26) if the uncertain terms $v(t)$ are uniformly bounded, then all the tracking errors ϵ^s, $\epsilon^{(i)}$ for all $i = \{1, \ldots, N\}$ will also be uniformly bounded.

Moreover, if the function $v(t)$ is square integrable i.e., $v(t) \in L_2$, then for all $t \to \infty$ (all t in the absence of any sensor fault) leads to $V(t) \in L_2$ and from (8.26) implies that

$$\rho^s |\epsilon^s(t)|^2 + \sum_{i=1}^{N} \rho^{(i)} \left|\epsilon^{(i)}(t)\right|^2 \in L_2. \tag{8.27}$$

Then, according to Barbalat's Lemma,

$$\lim_{t\to\infty}\left(\rho^s |\epsilon^s(t)|^2 + \sum_{i=1}^{N} \rho^{(i)} \left|\epsilon^{(i)}(t)\right|^2\right) = 0. \tag{8.28}$$

Since the sum of the squares of the tracking errors converges to zero, this implies that each individual tracking error will also converge to zero. □

The above result shows that the overall closed-loop system is stable and the tracking errors for each subsystems $\Sigma^s, \Sigma^{(1)}, \ldots, \Sigma^{(N)}$ is approximately of the same order as the magnitude of the corresponding uncertainty term $v(t)$. In the special case of no modeling uncertainty or measurement noise, i.e., $v(t) = 0$, implies that the tracking errors $\epsilon^s, \epsilon^{(1)}, \ldots, \epsilon^{(N)}$ will converge to zero.

The following result presents the stability properties of the proposed distributed sensor fault accommodation scheme after the isolation of the sensor fault. For simplicity purposes we analyze the stability of the corresponding subsystem that contains the faulty sensor. The Lyapunov synthesis method is used to obtain the online adaptive law of $\widehat{f^{(i)}}$ (see [44]) and moreover, the boundedness of the tracking error $\epsilon^{(i)}$ and fault estimation $\widehat{f^{(i)}}$ are examined. Note that the analysis of the tracking error $\epsilon^{(i)}$ for $t_f^{(i)} \leq t \leq t_I^{(i)}$ (i.e. after sensor fault occurrence and before the sensor fault isolation) is not included. However, if the sensor faults remain bounded i.e. $f^s < \infty$ and $f^{(i)} < \infty$ the tracking errors will remain bounded as well.

Theorem 2. *When the local sensor fault $f^{(i)}$ is isolated the distributed sensor fault accommodation scheme of (8.12)–(8.14) guarantees that:*

1. *the tracking error $\epsilon^{(i)}(t)$ is uniformly bounded i.e., $\epsilon^{(i)}(t) \in L_\infty$*
2. *there exist constants $\lambda_1^{(i)}$, $\lambda_2^{(i)}$ such that for any $t \geq t_I^{(i)}$,*

$$\int_{t_I^{(i)}}^{t} \left|\epsilon^{(i)}(\tau)\right|^2 d\tau \leq \lambda_1^{(i)} + \lambda_2^{(i)} \int_{t_I^{(i)}}^{t} \left|v_I^{(i)}(\tau)\right|^2 d\tau. \tag{8.29}$$

Proof. To examine the convergence and boundedness of the tracking error $\epsilon^{(i)}$ for $t \geq t_I^{(i)}$, the following candidate Lyapunov function is defined as

$$V^{(i)} = \frac{1}{2}\left(\epsilon^{(i)}(t)\right)^2 + \frac{1}{2\gamma^{(i)}}\left(\widetilde{f^{(i)}}(t)\right)^2, \tag{8.30}$$

such that $V^{(i)} \geq 0$ for any $\epsilon^{(i)}$ and $\widetilde{f^{(i)}}$. The time derivative of (8.30) can be computed as

$$\begin{aligned}\dot{V}^{(i)} &= \epsilon^{(i)}(t)\dot{\epsilon}^{(i)}(t) + \frac{1}{\gamma^{(i)}}\widetilde{f^{(i)}}(t)\dot{\widetilde{f}}^{(i)}(t) \\ &= -\rho^{(i)}\left|\epsilon^{(i)}(t)\right|^2 - \frac{1}{\gamma^{(i)}}\widetilde{f^{(i)}}(t)\dot{\widetilde{f}}^{(i)}(t) + \epsilon^{(i)}(t)v_I^{(i)}(t) + \left(\sigma^{(i)}u_i(t) - A^{(i)} - \rho^{(i)}\right)\widetilde{f^{(i)}}(t)\epsilon^{(i)}(t), \quad (8.31)\end{aligned}$$

where for a bias sensor fault $f^{(i)}$, the time derivative of the sensor fault gives $\dot{f}^{(i)} = 0$. Since $\epsilon^{(i)} = T_{z_i} - y_r^{(i)}$ and $\epsilon_y^{(i)} = y^{(i)} - y_r^{(i)}$, the tracking error $\epsilon^{(i)}(t)$ can be expressed as a function of $\widetilde{f^{(i)}}$, i.e.,

$$\epsilon^{(i)}(t) = \epsilon_y^{(i)}(t) - \widehat{f^{(i)}}(t) - \widetilde{f^{(i)}}(t). \quad (8.32)$$

Replacing (8.32) to (8.31), $\dot{V}^{(i)}$ is given by

$$\dot{V}^{(i)} = -\rho^{(i)}\left|\epsilon^{(i)}(t)\right|^2 + \left(\sigma^{(i)}u_i(t) - A^{(i)} - \rho^{(i)}\right)\widetilde{f^{(i)}}(t)\left(\epsilon_y^{(i)}(t) - \widehat{f^{(i)}}(t) - \widetilde{f^{(i)}}(t)\right) - \frac{1}{\gamma^{(i)}}\widetilde{f^{(i)}}(t)\dot{\widetilde{f}}^{(i)}(t) + \epsilon^{(i)}(t)v_I^{(i)}(t), \quad (8.33)$$

$$= -\rho^{(i)}\left|\epsilon^{(i)}(t)\right|^2 - \left(\sigma^{(i)}u_i(t) - A^{(i)} - \rho^{(i)}\right)\left|\widetilde{f^{(i)}}(t)\right|^2 + \epsilon^{(i)}(t)v_I^{(i)}(t) - \frac{1}{\gamma^{(i)}}\widetilde{f^{(i)}}(t)\left(\dot{\widetilde{f}}^{(i)}(t) - \gamma^{(i)}\left(\sigma^{(i)}u_i(t) - A^{(i)} - \rho^{(i)}\right)\left(\epsilon_y^{(i)}(t) - \widehat{f^{(i)}}(t)\right)\right). \quad (8.34)$$

The physical properties of the system guarantees that $A^{(i)} < 0$ and $u_i(t) \leq 1$, and since $\rho^{(i)}$ is designed $\rho^{(i)} > 0$, the first two terms of (8.34) can be negative, if

$$0 < \rho^{(i)} < \sigma^{(i)}. \quad (8.35)$$

The last term of (8.34) can be zero based on the adaptive law $\dot{\widetilde{f}}^{(i)}$ defined in (8.14). Hence, by applying the online adaptive law presented in (8.14) on (8.34), the time derivative of $V^{(i)}$ is given by

$$\dot{V}^{(i)} = -\rho^{(i)}\left|\epsilon^{(i)}(t)\right|^2 - \left(\sigma^{(i)}u_i(t) - A^{(i)} - \rho^{(i)}\right)\left|\widetilde{f^{(i)}}(t)\right|^2 + \epsilon^{(i)}(t)v_I^{(i)}(t). \quad (8.36)$$

The time derivative of $V^{(i)}$ satisfies

$$\dot{V}^{(i)} \leq -\left(\sigma^{(i)}u_i(t) - A^{(i)} - \rho^{(i)}\right)\left|\widetilde{f^{(i)}}(t)\right|^2 - \frac{\rho^{(i)}}{2}\left|\epsilon^{(i)}(t)\right|^2 - \frac{\rho^{(i)}}{2}\left(\left|\epsilon^{(i)}(t)\right|^2 - \frac{2}{\rho^{(i)}}\left|v_I^{(i)}(t)\right|\left|\epsilon^{(i)}(t)\right|\right) \quad (8.37)$$

$$\leq -\left(\sigma^{(i)}u_i(t) - A^{(i)} - \rho^{(i)}\right)\left|\widetilde{f^{(i)}}(t)\right|^2 - \frac{\rho^{(i)}}{2}\left|\epsilon^{(i)}(t)\right|^2 + \frac{1}{2\rho^{(i)}}\left|v_I^{(i)}(t)\right|^2. \quad (8.38)$$

Based on (8.38) if

$$\left|\epsilon^{(i)}\right| \geq \left|v_I^{(i)}(t)\right| / \rho^{(i)}. \quad (8.39)$$

then $V^{(i)}$ will be decreasing and therefore the tracking error $\epsilon^{(i)}$ will be decreasing as well. Furthermore, by integrating (8.38) from $\tau = t_I^{(i)}$ to $\tau = t$, we obtain

$$\begin{aligned}\int_{t_I^{(i)}}^{t} \left|\epsilon^{(i)}(\tau)\right|^2 d\tau \leq & \frac{2}{\rho^{(i)}}[V^{(i)}(t_I^{(i)}) - V^{(i)}(t)] + \frac{1}{(\rho^{(i)})^2}\int_{t_I^{(i)}}^{t} \left|v_I^{(i)}(\tau)\right|^2 d\tau, \\ \leq & \lambda_1^{(i)} + \lambda_2^{(i)} \int_{t_I^{(i)}}^{t} \left|v_I^{(i)}(\tau)\right|^2 d\tau, \end{aligned} \tag{8.40}$$

where $\lambda_1^{(i)} = \frac{2}{\rho^{(i)}} \sup_{t \geq t_I^{(i)}}[V^{(i)}(t_I^{(i)}) - V^{(i)}(t)]$ and $\lambda_2^{(i)} = \frac{1}{(\rho^{(i)})^2}$. Therefore, if $v_I^{(i)}(t)$ is uniformly bounded, based on (8.40) we establish uniform boundedness of the tracking error $\epsilon^{(i)}$ i.e., $\epsilon^{(i)} \in L_\infty$. □

8.6 Simulation Results

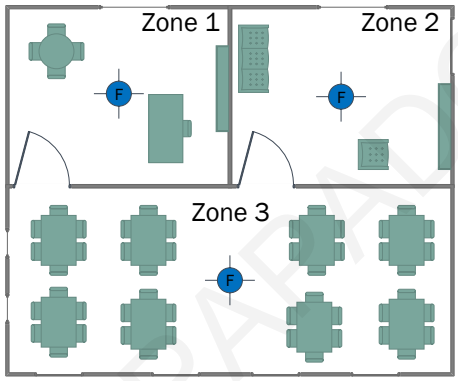

Figure 8.2: Down-view of 3 building zones that composite the 3 HVAC subsystems $\Sigma^{(i)}$, with $i \in \{1, 2, 3\}$. The blue circles represent the fan-coil units and the air temperature sensor located in each zone.

This section consist of the simulation results for a 3-zone HVAC building system consists of an electromechanical subsystem Σ^s and 3 interconnected building zones. The down-view of the 3 building zones is illustrated in Fig. 8.2, where the temperature dynamics of Zone 1, Zone 2 and Zone 3 are represented by the subsystems $\Sigma^{(1)}$, $\Sigma^{(2)}$ and $\Sigma^{(3)}$, respectively. $\Sigma^{(1)}$ and $\Sigma^{(2)}$ are thermally connected through a wall, while both $\Sigma^{(1)}$ and $\Sigma^{(2)}$ are thermally connected through doors and walls with $\Sigma^{(3)}$, such that $\mathcal{K}_1 = \{2, 3\}$, $\mathcal{K}_2 = \{1, 3\}$ and $\mathcal{K}_3 = \{1, 2\}$. The blue circle objects in Fig. 8.2 represent the fan-coil units and the temperature sensors located in each zone. The parameters of the 3-zone HVAC system are: $C_{st} = 8370$ kJ/^{o}C, $U_{i,max} = 3700$ kg/h, $a_{z_i} = 740$ kJ/h^{o}C, $a_{z_{1,2}} = a_{z_{2,3}} = 50$ kJ/h^{o}C, $A_{w_i} = 31.21$ m^2, $A_{d_{i,j}} = 1.951$ m^2, $i \in \{1, 2, 3\}$ and $C_{z_1} = C_{z_2} = 29.96$ kJ/^{o}C, $C_{z_3} = 60$ kJ/^{o}C. The remainder parameters of the 3-zone HVAC system are: $a_{st} = 12$ kJ/kg^{o}C, $a_{sz} = 0.6$ kJ/kg^{o}C, $U_{st,max} = 27.36 \times 10^5$ kJ/^{o}C, $P_{max} = 3.5$, $\Delta T_{max} = 45$ ^{o}C, $h = 8.26$ W/m^{2o}C, $T_{pl} = 20$ ^{o}C, $T_o = 5$ ^{o}C, $T_{amb} = 5$ ^{o}C and $T_{i1} = 10$ ^{o}C, $i \in \{1, 2, 3\}$. Moreover, the specific heat capacity of air at constant pressure is $C_p = 1.004$ kJ/kgK, the specific heat capacity of air at constant volume is $C_v = 0.717$ kJ/kgK, and the air density is $\rho_{air} = 1.225$ kg/m^3. The modeling uncertainty associated with each subsystem is modeled as $r^s(t) = 5\%T_{pl}\sin(0.1t)$ ^{o}C and $r^{(i)}(t) = 1\%T_{amb}\sin(0.1t)$ ^{o}C, $i \in \{1, 2, 3\}$.

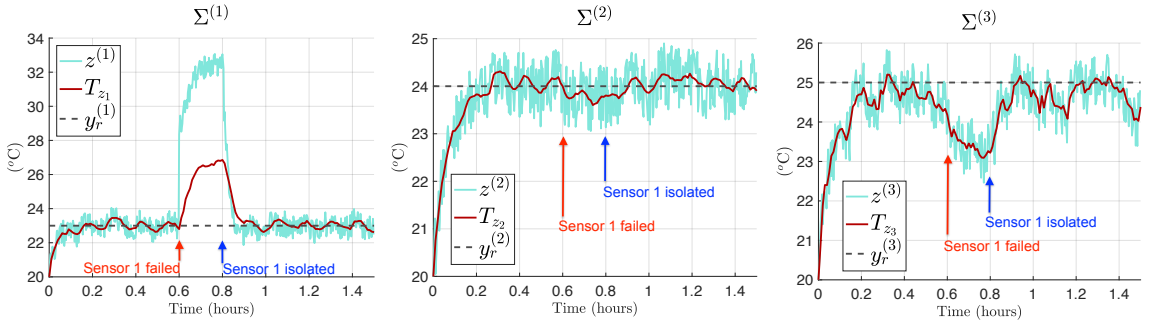

Figure 8.3: Air temperature responses of the 3-zone HVAC system represented by subsystems $\Sigma^{(1)}, \Sigma^{(2)}, \Sigma^{(3)}$.

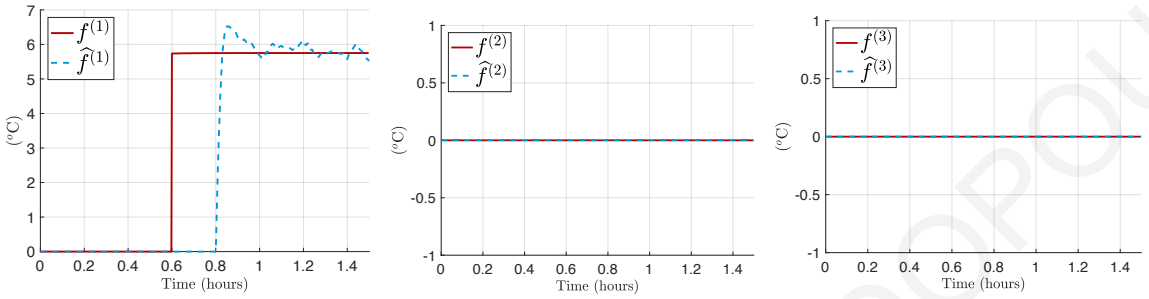

Figure 8.4: Online adaptive estimation of sensor faults $f^{(1)}$ and $f^{(2)}$.

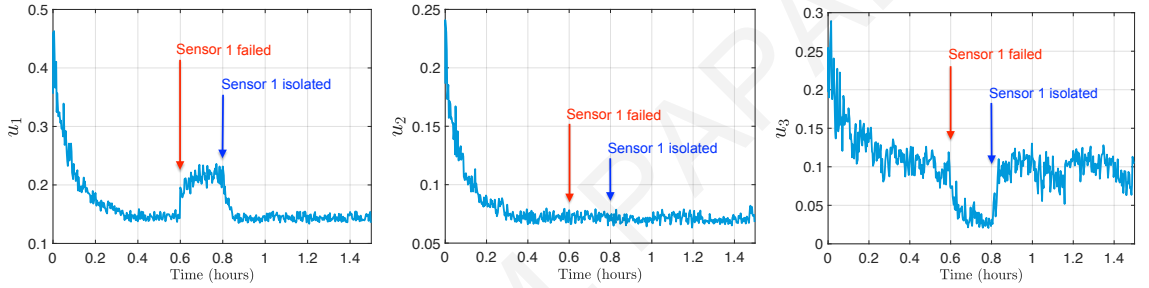

Figure 8.5: Control input responses for subsystems $\Sigma^{(1)}, \Sigma^{(2)}, \Sigma^{(3)}$.

For simulation purposes, the noise corrupting the sensors is defined as a uniform random noise with $\overline{n}^s = 3\% y_r^s$ and $\overline{n}^{(i)} = 3\% y_r^{(i)}$, where y_r^s and $y_r^{(i)}$ are the desired temperature for the water in the storage tank and the desired air temperature of the ith zone, respectively, selected as $y_r^s = 55\ ^o\text{C}$ and $y_r^{(1)} = 23\ ^o\text{C}$, $y_r^{(2)} = 24\ ^o\text{C}$ and $y_r^{(3)} = 25\ ^o\text{C}$. The 3-zone HVAC system is simulated for 1.5 hours with initial conditions $T_{st}(0) = 30\ ^o\text{C}$ and $T_{z_i}(0) = 20\ ^o\text{C}$, $i \in \{1, 2, 3\}$. The design parameters of the distributed sensor fault accommodation scheme are the controller gains and the learning rates of the online adaptive laws chosen as ρ^s=6, $\rho^{(1)}$=23.4, $\rho^{(2)}$=14, $\rho^{(1)}$=14.87 and $\gamma^{(i)}$=4, for $i \in \{1, 2, 3\}$.

A permanent bias sensor fault is simulated with constant magnitude given by $f^{(1)} = 25\% y_r^{(1)} = 5.75\ ^o\text{C}$ at $t_f^{(1)} = 0.6$ hours. Based on Fig. 8.5, we can observe that the sensor fault $f^{(1)}$ at $t_f^{(1)} = 0.6$ hours, affects both the local (i.e., $u^{(1)}$) and neighboring controllers (i.e., $u^{(2)}$, $u^{(3)}$) because of the distributed feedback control architecture. Note that the effect of $f^{(1)}$ is not distinct in $u^{(2)}$ but its effect can be slightly noticed in the temperature response T_{z_2} in Fig. 8.3. As shown in Fig. 8.3, the air temperatures T_{z_1}, T_{z_2} and T_{z_3} are affected due to the distributed feedback control loop. The effect of sensor fault propagation is more noticeable in $\Sigma^{(3)}$, since the dynamics of $\Sigma^{(3)}$ are strongly

connected with $\Sigma^{(1)}$ due to door interconnection, while the deviation of the air temperature in $\Sigma^{(2)}$ is less intensive, since the dynamics of $\Sigma^{(2)}$ are weakly connected with $\Sigma^{(1)}$ due to wall interconnection.

The preinstalled sensor fault diagnosis algorithm, isolates $f^{(1)}$ at $t_I^{(1)} = 0.8$ hours, as presented in Fig. 8.4. Immediately, at $t_I^{(1)} = 0.8$ hours, the local online adaptive law in the controller of $\Sigma^{(1)}$ is activated as denoted in (8.14), while the remainder adaptive laws in the controller of $\Sigma^{(2)}$, $\Sigma^{(3)}$ are inactive (see Fig. 8.4). Furthermore, at the same time instant, $t_I^{(1)} = 0.8$ hours, the reconstructed sensor signal $z^{(1)}$ is modified according to (8.13) by using the fault estimation $\widehat{f^{(1)}}$. Since the control laws $\phi^{(1)}$, $\phi^{(2)}$ and $\phi^{(3)}$ are reconfigured according to (8.12), the temperatures T_{z_1}, T_{z_2} and T_{z_3} begin to return close to their desired temperatures $y_r^{(1)}$, $y_r^{(2)}$ and $y_r^{(3)}$, respectively.

8.7 Conclusion

This chapter illustrates the design of a distributed methodology for control and sensor fault accommodation in multi-zone HVAC systems. The distributed feedback control scheme is designed according to the physical connectivity of the HVAC subsystems. Each local controller allows exchange of control input data and sensor information between the neighboring controllers to reduce the disturbances resulting from the physical interconnections. Perceiving the location of the sensor fault, a local online fault estimation scheme is activated. The estimation of the sensor fault is used by the local and neighboring controllers to compensate both local and propagated effects. The stability for the distributed sensor fault accommodation scheme is examined in healthy and faulty conditions, taking into account modeling uncertainty and measurement noise. The simulation of a single sensor fault in a 3-zone HVAC system illustrates the effectiveness of the proposed distributed sensor fault accommodation method.

Chapter 9

Distributed Sensor Fault-Tolerant Control for Preserving Comfortable Indoor Conditions

9.1 Introduction

In the previous Chapters, the design of fault accommodation schemes offers alleviation from the sensor fault effects that directly affect the operation of HVAC system with online learning of sensor fault characteristics i.e., unknown fault magnitude, either with virtual sensor scheme (Chapter 7) or with control reconfiguration (Chapter 8). Specifically, in Chapter 8, the tracking performance of the closed-loop HVAC system is examined in both healthy and faulty conditions. However, the delay from the fault occurrence time until the fault diagnosis and recovery, beside the impact to energy consumption can also cause violation of the indoor thermal comfort conditions. Since the impact of faults in HVAC systems to the indoor thermal comfort conditions is not investigated throughout this thesis, this chapter aims to consider this issue in the design of fault accommodation algorithms.

9.2 Objective

The contribution of this chapter is to design a distributed fault-tolerant control (FTC) scheme for preserving thermal conditions in the presence of sensor faults. The objective is to obtain the necessary conditions for the control gains not only to stabilize the local controlled subsystem but also to achieve thermal comfort for both healthy and faulty conditions. The computation of the appropriate control gains takes into consideration bounds on the measurement noise, modeling uncertainty and sensor faults. During the healthy operation of the HVAC system, the distributed sensor FTC scheme utilizes the computed control gains obtained to achieve thermal comfort. By employing a sensor fault diag-

nosis scheme (see Chapter 3–6) the distributed sensor FTC scheme is activated when a sensor fault is detected and isolated and then its local control gain is reconfigured in order to achieve thermal comfort in the presence of the sensor fault despite the possible propagation of the sensor fault effects. In previous works of the authors [108, 128], the faulty sensor outputs were reconstructed without changing the structure of the controller. Here on the other hand the goal is to change the control gain in order to compensate the effects of sensor faults.

9.3 Design of the Distributed Sensor Fault-Tolerant Control Scheme

The design of the proposed distributed FTC is realized taking into account that the occurrence of a sensor fault affecting a single zone only and the following assumptions:

Assumption 1: For all $t \geq 0$, the modeling uncertainties $r^s(t)$, $r^{(i)}(t)$ and noise measurements $n^s(t)$, $n^{(i)}(t)$ are uniformly bounded such that $|r^s(t)| \leq \bar{r}^s$, $\left|r^{(i)}(t)\right| \leq \bar{r}^{(i)}$, $|n^s(t)| \leq \bar{n}^s$, and $\left|n^{(i)}(t)\right| \leq \bar{n}^{(i)}$, $i \in \mathcal{N}$.

Assumption 2: For all $t \geq t_f^{(i)}$, where $t_f^{(i)}$ is the time instant that fault has occurred, the permanent sensor fault is bounded $f^{(i)}(t) \in [f_{\min}^{(i)}, f_{\max}^{(i)}]$, for all $i \in \mathcal{N}$.

The distributed feedback control scheme is constructed by the control agents C^s and $C^{(i)}$ that generate the control signals c^s and c^i, defined in (9.1) and (9.2). A general representation of a model-based distributed control scheme is shown in Fig. 9.1c for a 3-zone HVAC system. The control agents C^s and $C^{(i)}$ can be described by the following control laws, i.e.,

$$C^s : \left\{ \; c^s(t) = v^s(y^s(t), y(t), u(t), x_{ref}^s(t)) \quad , \right. \tag{9.1}$$

$$C^{(i)} : \left\{ \; c^{(i)}(t) = v^{(i)}(y^{(i)}(t), y^s(t), y^{\mathcal{K}_i}(t), x_{ref}^{(i)}(t)) \quad , \right. \tag{9.2}$$

where x_{ref}^s and $x_{ref}^{(i)}$ are (differentiable) reference signals for the states T_{st} and T_{z_i}, $i \in \{1, \ldots, N\}$, respectively. The controller C^s uses the sensor measurements y^s and $y = \left[y^{(i)} : i \in \{1, \ldots, N\}\right]^\top$, and the controller $C^{(i)}$ uses the sensor measurements $y^{(i)}$, y^s and $y^{\mathcal{K}_i} = \left[y^{(j)}(t) : j \in \mathcal{K}_i\right]^\top$, where $y^{\mathcal{K}_i}$ denotes a column vector of length card($\mathcal{K}_i$).

The goal of this work is to reconfigure $C^{(i)}$ only, when a sensor fault $f^{(i)}$ is diagnosed, without re-configuring the neighboring control agents C^s and $C^{(j)}$, $j \in \mathcal{K}_i$. Based on a feedback linearization approach (i.e., cancelling the nonlinearities by the combined use of feedback and change of coordinates) [44], a distributed feedback linearization control agent $C^{(i)}$ is designed as

$$\begin{aligned} c^{(i)}(t) = \left(g^{(i)}(y^s(t), y^{(i)}(t))\right)^{-1} \Big[& -\eta^{(i)}(T_{i1}(t), T_{amb}(t)) - h^{(i)}(y^{(i)}(t), y^{\mathcal{K}_i}(t)) - (A^{(i)} - K^{(i)}) x_{ref}^{(i)}(t) \\ & - K^{(i)} y^{(i)}(t) + \dot{x}_{ref}^{(i)}(t) \Big] \end{aligned} \tag{9.3}$$

where $K^{(i)}$ is selected to stabilize the term $A^{(i)} - K^{(i)}$ and $x_{ref}^{(i)}$ is generated by the following reference

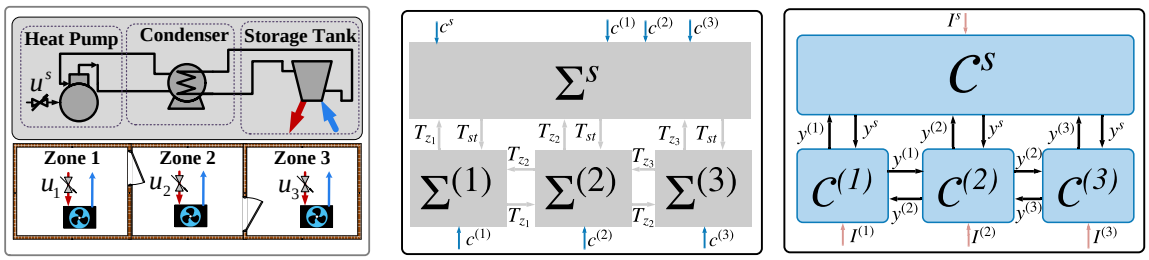

(a) (b) (c)

Figure 9.1: Configuration of the distributed FTC scheme for a 3-zone HVAC system. (a) Schematic representation of a multi-zone HVAC system that consists of the hot water unit (gray box) and the 3 building zones that are interconnected through walls and doors. The black rectangular boxes located in each zone represent the fan-coil units. (b) The subsystems configuration of the 3-zone HVAC system. The black arrows denote the shared states (temperatures) between the interconnected subsystems. (c) The distributed control agents C^s and $C^{(1)}, \ldots, C^{(3)}$. The black arrows denote the exchange of information between controllers.

model

$$\dot{x}^{(i)}_{ref}(t) = A^{(i)}x^{(i)}_{ref}(t) + g^{(i)}(x^{s}_{ref}(t), x^{(i)}_{ref}(t))u^{r}_{i}(t) + h^{(i)}(x^{(i)}_{ref}(t), x^{\mathcal{K}_i}_{ref}(t)) + \eta^{(i)}(T_{i1}(t), T_{amb}(t)), \tag{9.4}$$

where u^r_i is a bounded input to the reference system and $x^{\mathcal{K}_i}_{ref} = \left[x^{(j)}_{ref}(t) : j \in \mathcal{K}_i\right]^\top$. The following design takes into consideration that a sensor fault diagnosis scheme (e.g., [107]) monitors the subsystems $\Sigma^{(i)}$ for all $i \in \mathcal{N}$ and can provide an isolation signal $I^{(i)}$ where for $I^{(i)}(t) = 1$ the sensor fault diagnosis scheme decides that a local sensor fault has detected and isolated. Based on the isolation signal $I^{(i)}$ the controller gain $K^{(i)}$ can be reconfigured such as

$$K^{(i)}(t) = \begin{cases} K^{(i)}_H, & I^{(i)}(t) = 0 \\ K^{(i)}_F, & I^{(i)}(t) = 1 \end{cases}, \tag{9.5}$$

where $K^{(i)}_H$ is obtained in order to satisfy thermal comfort conditions under healthy measurements while $K^{(i)}_F$ is obtained to satisfy thermal comfort conditions after the occurrence of sensor fault $f^{(i)}$.

9.3.1 Tracking error satisfying comfort conditions

The tracking error of subsystem $\Sigma^{(i)}$, denoted by $\widetilde{x}^{(i)}$ is described by

$$\widetilde{x}^{(i)}(t) = T_{z_i}(t) - x^{(i)}_{ref}(t). \tag{9.6}$$

The fulfillment of the comfort conditions described by $T_{z_i}(t) \in \left[T^{\min}_{z_i}, T^{\max}_{z_i}\right]$ can be guaranteed by ensuring that the tracking error of the *i-th* zone is included in a closed interval given by

$$\widetilde{x}^{(i)}(t) \in \left[-x^{(i)}_{ref}(t) + T^{\min}_{z_i}, -x^{(i)}_{ref}(t) + T^{\max}_{z_i}\right].$$

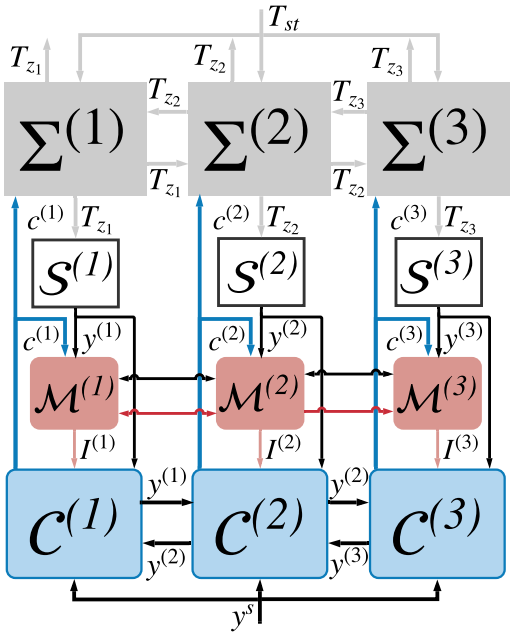

Figure 9.2: Configuration of the distributed FTC scheme for a 3-zone HVAC system. Note that this diagram do not consist the subsytem Σ^s that corresponds to the storage tank.

For all $t \geq 0$, tracking error can be expressed as

$$\widetilde{x}^{(i)}(t) = \widetilde{x}_H^{(i)}(t) + \widetilde{x}_F^{(i)}(t), \tag{9.7}$$

where $\widetilde{x}_H^{(i)}$ is the healthy (fault-free) part of the tracking error, which is associated with the bounded modeling uncertainties only, and $\widetilde{x}_F^{(i)}$ is the faulty part of the tracking error. Taking into account Assumption 1, it can be proved (see Section 9.3.2) that under healthy conditions

$$\widetilde{x}_H^{(i)}(t) \in \left[-\overline{x}_H^{(i)}(t), \overline{x}_H^{(i)}(t)\right]. \tag{9.8}$$

Then, a design requirement for selecting the controller gain $K_H^{(i)}$ is that

$$\left[-\overline{x}_H^{(i)}(t), \overline{x}_H^{(i)}(t)\right] \subseteq \left[-x_{ref}^{(i)}(t) + T_{z_i}^{\min}, -x_{ref}^{(i)}(t) + T_{z_i}^{\max}\right]. \tag{9.9}$$

Taking into account Assumption 2, it can be proved (see Section 9.3.3) that the tracking error under faulty conditions described by (9.7) satisfies

$$\widetilde{x}^{(i)}(t) \in \left[\underline{x}^{(i)}(t), \overline{x}^{(i)}(t)\right], \quad \forall t \geq T_f.$$

The controller gain $K_F^{(i)}$ is designed such that

$$\left[\underline{x}^{(i)}(t), \overline{x}^{(i)}(t)\right] \subseteq \left[-x_{ref}^{(i)}(t) + T_{z_i}^{\min}, -x_{ref}^{(i)}(t) + T_{z_i}^{\max}\right].$$

In the next section, we analyze the tracking error $\widetilde{x}^{(i)}(t)$ defined in (9.6).

In the sequel, the dependence of the signals on time (e.g. $\widetilde{x}(t)$) will be dropped for notation brevity.

9.3.2 Analysis of the tracking error

In this section the tracking error $\widetilde{x}^{(i)}$ is obtained analytically by applying the proposed distributed control scheme presented in (9.3)–(9.4) to (2.26). Hence, the dynamics of the tracking error $\widetilde{x}^{(i)}$ are computed as

$$\begin{aligned}\dot{\widetilde{x}}^{(i)} =&\dot{T}_{z_i} - \dot{x}^{(i)}_{ref}\\ =&A^{(i)}(T_{z_i} - x^{(i)}_{ref}) + g^{(i)}(T_{st}, T_{z_i})u^{(i)} - g^{(i)}(x^{s}_{ref}, x^{(i)}_{ref})u^{r}_{i} + h^{(i)}(T_{z_i}, T_{\mathcal{K}_i}) - h^{(i)}(x^{(i)}_{ref}, x^{\mathcal{K}_i}_{ref}) + r^{(i)}.\end{aligned} \tag{9.10}$$

Adding and subtracting the terms $g^{(i)}(y^s, y^{(i)})u^{(i)}$ and $h^{(i)}(y^{(i)}, y^{\mathcal{K}_i})$ on (9.10) results in

$$\begin{aligned}\dot{\widetilde{x}}^{(i)} =&A^{(i)}\widetilde{x}^{(i)} + \Big(g^{(i)}(T_{st}, T_{z_i}) - g^{(i)}(y^s, y^{(i)})\Big)u^{(i)} + r^{(i)} + h^{(i)}(T_{z_i}, T_{\mathcal{K}_i}) - h^{(i)}(y^{(i)}, y_{\mathcal{K}_i})\\ &+ g^{(i)}(y^s, y^{(i)})u^{(i)} + A^{(i)}x^{(i)}_{ref} - \dot{x}^{(i)}_{ref} + \eta^{(i)}(T_{i1}, T_{amb}) + h^{(i)}(y^{(i)}, y_{\mathcal{K}_i}).\end{aligned}$$

Assuming that $c^{(i)} \in [0, 1]$, we have $u^{(i)} = c^{(i)}$. After some mathematical manipulations and by adding and subtracting the term $K^{(i)}T_{z_i}$, the dynamics of tracking error $\widetilde{x}^{(i)}$ are computed by

$$\dot{\widetilde{x}}^{(i)} =(A^{(i)} - K^{(i)})\widetilde{x}^{(i)} + \widetilde{g}^{(i)}c^{(i)} + \widetilde{h}^{(i)} + K^{(i)}(T_{z_i} - y^{(i)}) + r^{(i)}, \tag{9.11}$$

where $\widetilde{g}^{(i)} \triangleq (g^{(i)}(T_{st}, T_{z_i}) - g^{(i)}(y^s, y^{(i)})$ and $\widetilde{h}^{(i)} \triangleq h^{(i)}(T_{z_i}, T_{\mathcal{K}_i}) - h^{(i)}(y^{(i)}, y^{\mathcal{K}_i})$ with

$$\widetilde{g}^{(i)} = \sigma^{(i)}\left(n^{(i)} - n^s + f^{(i)}\right), \tag{9.12}$$

$$\widetilde{h}^{(i)} = p^{(i)}\sum_{j\in\mathcal{K}_i} A_{d_{ij}}\left(\mu^{(i)}(T_{z_i}, T_{z_j}) - \mu^{(i)}(y^{(i)}, y^{(j)})\right) + \sum_{j\in\mathcal{K}_i}\frac{a_{z_{ij}}}{C_{z_i}}(n^{(j)} + f^{(j)}), \tag{9.13}$$

and

$$\mu^{(i)}(w_1, w_2) = \mathrm{sgn}(w_2 - w_1)\max(w_1, w_2)\sqrt{|w_2 - w_1|}.$$

9.3.3 Tracking error under healthy conditions

Assuming healthy conditions, we have $f^{(i)} = 0$, $i \in \mathcal{N}$. The healthy sensor measurements are given by

$$\begin{aligned}y^{s}_{H} =&T^{H}_{st} + n^s,\\ y^{(i)}_{H} =&T^{H}_{z_i} + n^{(i)},\\ y^{\mathcal{K}_i}_{H} =&T^{H}_{\mathcal{K}_i} + n^{\mathcal{K}_i},\end{aligned}$$

where T^{H}_{st}, $T^{H}_{z_i}$ are the water temperature and air temperature of the *i-th* zone under healthy conditions, respectively, and $T^{H}_{\mathcal{K}_i}$ is a vector collects the air temperatures of the $|\mathcal{K}_i|$ zones under healthy conditions.

Using (9.11)–(9.13) with $f^{(i)} = 0$, the dynamics of $\widetilde{x}^{(i)}_{H}$ are given by

$$\dot{\widetilde{x}}^{(i)}_{H} =\left(A^{(i)} - K^{(i)}_{H}\right)\widetilde{x}^{(i)}_{H} + \sigma^{(i)}\left(n^{(i)} - n^s\right)u^{H}_{i} + h^{(i)}(T^{H}_{z_i}, T^{H}_{\mathcal{K}_i}) - h^{(i)}(y^{(i)}_{H}, y^{\mathcal{K}_i}_{H}) + r^{(i)} - K^{(i)}_{H}n^{(i)}. \tag{9.14}$$

The bound on the tracking error is computed assuming healthy sensor measurements. The solution of (9.14) is given by

$$\begin{aligned}\widetilde{x}_H^{(i)} =& e^{\left(A^{(i)}-K_H^{(i)}\right)t}\widetilde{x}_H^{(i)}(0) + \int_0^t e^{\left(A^{(i)}-K_H^{(i)}\right)(t-\tau)}\sigma^{(i)}\left(n^{(i)}(\tau)-n^s(\tau)\right)u_H^{(i)}(\tau)d\tau \\ &+ \int_0^t e^{\left(A^{(i)}-K_H^{(i)}\right)(t-\tau)}\left(-K_H^{(i)}n^{(i)}(\tau)+r^{(i)}(\tau)\right)d\tau \\ &+ \int_0^t e^{\left(A^{(i)}-K_H^{(i)}\right)(t-\tau)}\left(h^{(i)}(T_{z_i}^H(\tau),T_{\mathcal{K}_i}^H(\tau))-h^{(i)}(y_H^{(i)}(\tau),y_H^{\mathcal{K}_i}(\tau))\right)d\tau. \end{aligned} \tag{9.15}$$

Equivalently, (9.8) can be expressed as

$$\left|\widetilde{x}_H^{(i)}\right| \leq \overline{x}_H^{(i)}. \tag{9.16}$$

Applying the triangular inequality on (9.15) and based on Assumption 1, $\overline{x}_H^{(i)}$ results in

$$\begin{aligned}\overline{x}_H^{(i)} =& e^{\left(A^{(i)}-K_H^{(i)}\right)t}\overline{x}^{(i)} - \left(1-e^{\left(A^{(i)}-K_H^{(i)}\right)t}\right)\left(A^{(i)}-K_H^{(i)}\right)^{-1}\times\left(\left|K_H^{(i)}\right|\overline{n}^{(i)} + \sum_{j\in\mathcal{K}_i}\frac{a_{z_{i,j}}}{C_{z_i}}\overline{n}^{(j)} + \overline{r}^{(i)}\right) \\ &+ \sigma^{(i)}\left(\overline{n}^s+\overline{n}^{(i)}\right)\int_0^t e^{\left(A^{(i)}-K_H^{(i)}\right)(t-\tau)}\left|u_H^{(i)}(\tau)\right|d\tau \\ &+ p^{(i)}\int_0^t e^{\left(A^{(i)}-K_H^{(i)}\right)(t-\tau)}\sum_{j\in\mathcal{K}_i}A_{d_{i,j}}\overline{\mu}^{(i)}(y_H^{(i)}(\tau),y_H^{(j)}(\tau))d\tau, \end{aligned} \tag{9.17}$$

where $|\widetilde{x}_H^{(i)}(0)| \leq \overline{x}^{(i)}$ with $\overline{x}^{(i)} = T_{z_i}(0) - x_{ref}^{(i)}(0)$ and the function $\overline{\mu}^{(i)}$ is such that

$$\left|\mu^{(i)}(T_{z_i}^H,T_{z_j}^H)-\mu^{(i)}(y_H^{(i)},y_H^{(j)})\right| \leq \overline{\mu}^{(i)}(y_H^{(i)},y_H^{(j)}),$$

whose computation is given in the Appendix of [109]. In order to sustain stability and thermal comfort in zone i under healthy conditions, $K_H^{(i)}$ should be selected such that satisfies the following conditions for all $t \geq 0$:

$$A^{(i)} - K_H^{(i)} < 0, \tag{9.18}$$

$$c^{(i)} \in [0,1] \tag{9.19}$$

$$\left[-\overline{x}_H^{(i)},\overline{x}_H^{(i)}\right] \subseteq \left[-x_{ref}^{(i)}+T_{z_i}^{\min},-x_{ref}^{(i)}+T_{z_i}^{\max}\right]. \tag{9.20}$$

9.3.4 Tracking error under local sensor faults

For the following analysis on the tracking error $\widetilde{x}^{(i)}$ a local bias sensor fault $f^{(i)}$ is considered. The remainder sensor measurements are healthy with $f^{\mathcal{K}_i} = 0$. The sensor measurements under a local fault in the sensor $\mathcal{S}^{(i)}$ are given by

$$\begin{aligned} y^s =& T_{st} + n^s, \\ y^{(i)} =& T_{z_i} + n^{(i)} + f^{(i)}, \\ y^{\mathcal{K}_i} =& T_{\mathcal{K}_i} + n^{\mathcal{K}_i} \end{aligned}$$

where the sensor fault can be written as

$$f^{(i)} = \begin{cases} 0, & t < t_f^{(i)} \\ f_o^{(i)} + \widetilde{f}^{(i)}, & t \geq t_f^{(i)} \end{cases},$$

where $f_o^{(i)}$ is the constant offset of the sensor fault $f^{(i)}$, $\widetilde{f}^{(i)}$ is the deviation of the offset $f_o^{(i)}$ from the actual fault value $f^{(i)}$ and $t_f^{(i)}$ is the time instant that fault has occurred. Based on Assumption 2, the offset $f_o^{(i)}$ can be described by

$$f_o^{(i)} = 0.5\left(f_{\min}^{(i)} + f_{\max}^{(i)}\right), \tag{9.21}$$

and the deviation $\widetilde{f}^{(i)}$ satisfies

$$\left|\widetilde{f}^{(i)}\right| \leq 0.5\left(f_{\max}^{(i)} - f_{\min}^{(i)}\right) = \overline{f}^{(i)}. \tag{9.22}$$

The dynamics of the tracking error $\widetilde{x}^{(i)}$ can be expressed as

$$\begin{aligned} \dot{\widetilde{x}}^{(i)} =& \left(A^{(i)} - K_F^{(i)}\right)\widetilde{x}^{(i)} + \left(g^{(i)}(T_{st}, T_{z_i}) - g(y^s, y^{(i)})\right)u^{(i)} + h^{(i)}(T_{z_i}, T_{\mathcal{K}_i}) - h^{(i)}(y^{(i)}, y_{\mathcal{K}_i}) \\ & - \left(g^{(i)}(T_{st}, T_{z_i}) - g(y^s, y^{(i)})\right)u^{(i)} - h^{(i)}(T_{z_i}, T_{\mathcal{K}_i}) + h^{(i)}(y^{(i)}, y^{\mathcal{K}_i}) - K_F^{(i)}\left(f^{(i)} + n^{(i)}\right) \\ & + g^{(i)}(y^s, y^{(i)})\left(u^{(i)} - c^{(i)}\right) + r^{(i)}, \end{aligned} \tag{9.23}$$

where $\widetilde{x}^{(i)}(t_f^{(i)}) = \widetilde{x}_H^{(i)}(t_f^{(i)})$. By designing the controller such that $c^{(i)} = [0, 1]$ for all $t \geq t_f^{(i)}$ the last term of (9.23) is equal to zero. Using (9.12), the dynamics of the tracking error can be described by

$$\begin{aligned} \dot{\widetilde{x}}^{(i)} =& \left(A^{(i)} - K_F^{(i)}\right)\widetilde{x}^{(i)} - K_F^{(i)} f_o^{(i)} - K_F^{(i)}\widetilde{f}^{(i)} - K_F^{(i)} n^{(i)} + \sigma^{(i)}\left(f_o^{(i)} + \widetilde{f}^{(i)}\right)u^{(i)} + \sigma^{(i)}\left(n^{(i)} - n^s\right)u^{(i)} \\ & + h^{(i)}(T_{z_i}, T_{\mathcal{K}_i}) - h^{(i)}(y^{(i)}, y^{\mathcal{K}_i}) + r^{(i)}. \end{aligned} \tag{9.24}$$

The bounds on the tracking error are computed under the scenario of a single bias sensor fault occurring locally at the subsystem $\Sigma^{(i)}$. For $\widetilde{z}_F^{(i)} = \widetilde{x}^{(i)} - \left(A^{(i)} - K_F^{(i)}\right)^{-1} K_F^{(i)} f_o^{(i)}$, (9.24) can be expressed as,

$$\begin{aligned} \dot{\widetilde{z}}_F^{(i)} =& \left(A^{(i)} - K_F^{(i)}\right)\widetilde{z}_F^{(i)} - K_F^{(i)}\widetilde{f}^{(i)} + \sigma^{(i)} f_o^{(i)} u^{(i)} + \sigma^{(i)}\widetilde{f}^{(i)} u^{(i)} - K_F^{(i)} n^{(i)} + \sigma^{(i)}\left(n^{(i)} - n^s\right)u^{(i)} \\ & + h^{(i)}(T_{z_i}, T_{\mathcal{K}_i}) - h^{(i)}(y^{(i)}, y^{\mathcal{K}_i}) + r^{(i)}. \end{aligned} \tag{9.25}$$

The solution of (9.25) is given by

$$\begin{aligned} \widetilde{z}_F^{(i)} =& e^{\left(A^{(i)} - K_F^{(i)}\right)\left(t - t_f^{(i)}\right)}\widetilde{z}_F^{(i)}(t_f^{(i)}) - K_F^{(i)}\int_{t_f^{(i)}}^{t} e^{\left(A^{(i)} - K_F^{(i)}\right)(t-\tau)}\left(\widetilde{f}(\tau) + n^{(i)}(\tau)\right)d\tau \\ & + \sigma^{(i)} f_o^{(i)}\int_{t_f^{(i)}}^{t} e^{\left(A^{(i)} - K_F^{(i)}\right)(t-\tau)}u^{(i)}(\tau)d\tau + \sigma^{(i)}\int_{t_f^{(i)}}^{t} e^{\left(A^{(i)} - K_F^{(i)}\right)(t-\tau)}\widetilde{f}^{(i)}(\tau)u^{(i)}(\tau)d\tau \\ & + \sigma^{(i)}\int_{t_f^{(i)}}^{t} e^{\left(A^{(i)} - K_F^{(i)}\right)(t-\tau)}\left(n^{(i)}(\tau) - n^s(\tau)\right)u^{(i)}(\tau)d\tau + \int_{t_f^{(i)}}^{t} e^{\left(A^{(i)} - K_F^{(i)}\right)(t-\tau)}\sum_{j\in\mathcal{K}_i}\frac{a_{z_{i,j}}}{C_{z_i}}n^{(j)}(\tau)d\tau \\ & + p^{(i)}\int_{t_f^{(i)}}^{t} e^{\left(A^{(i)} - K_F^{(i)}\right)(t-\tau)}\sum_{j\in\mathcal{K}_i} A_{d_{ij}}\left(\mu^{(i)}(T_{z_i}(\tau), T_{z_j}(\tau)) - \mu^{(i)}(y^{(i)}(\tau), y^{(j)}(\tau)) + r^{(i)}(\tau)\right)d\tau \end{aligned} \tag{9.26}$$

where $\overline{z}_F^{(i)}(t_f^{(i)}) = \overline{x}^{(i)}(t_f^{(i)}) - \left(A^{(i)} - K_F^{(i)}\right)^{-1} K^{(i)} f_o^{(i)}$. Based on Assumption 1 and 2, and by obtaining the triangle inequality on (9.26) such that $|\widetilde{z}_F^{(i)}| \leq \overline{z}_F^{(i)}$ results in

$$\begin{aligned}\overline{z}_F^{(i)} =& e^{\left(A^{(i)}-K_F^{(i)}\right)\left(t-t_f^{(i)}\right)}\overline{z}^{(i)}(t_f^{(i)}) - \left(K_F^{(i)}\left(\overline{f}^{(i)} + \overline{n}^{(i)}\right) + \overline{r}^{(i)} + \sum_{j\in\mathcal{K}_i}\frac{a_{z_{i,j}}}{C_{z_i}}\overline{n}^{(j)}\right)\left(A^{(i)} - K_F^{(i)}\right)^{-1}\left(1 - e^{\left(A^{(i)}-K_F^{(i)}\right)\left(t-t_f^{(i)}\right)}\right) \\ &+ \sigma^{(i)}\left(\left|f_o^{(i)}\right| + \overline{f}^{(i)}\right)\int_{t_f^{(i)}}^{t} e^{\left(A^{(i)}-K_F^{(i)}\right)(t-\tau)}\left|u^{(i)}(\tau)\right|d\tau + \sigma^{(i)}\left(\overline{n}^{s} + \overline{n}^{(i)}\right)\int_{t_f^{(i)}}^{t} e^{\left(A^{(i)}-K_F^{(i)}\right)(t-\tau)}\left|u^{(i)}(\tau)\right|d\tau \\ &+ p^{(i)}\int_{t_f^{(i)}}^{t} e^{\left(A^{(i)}-K_F^{(i)}\right)(t-\tau)}\sum_{j\in\mathcal{K}_i} A_{d_{ij}}\overline{\mu}^{(i)}(y^{(i)}(\tau), y^{(j)}(\tau))d\tau, \end{aligned} \tag{9.27}$$

where $\overline{z}^{(i)}(t_f^{(i)}) = \overline{x}_H^{(i)}(t_f^{(i)}) + |\left(A^{(i)} - K_F^{(i)}\right)^{-1} K_F^{(i)} f_o^{(i)}|$, since $|\widetilde{x}^{(i)}(t_f^{(i)})| \leq \overline{x}_H^{(i)}(t_f^{(i)})$. The function $\overline{\mu}^{(i)}$ is such that

$$\left|\mu^{(i)}(T_{z_i}, T_{z_j}) - \mu^{(i)}(y^{(i)}, y^{(j)})\right| \leq \overline{\mu}^{(i)}(y^{(i)}, y^{(j)}), \tag{9.28}$$

with its computation be presented in the Appendix of [109], where (9.28) is obtained with $\alpha = y^{(j)} - y^{(i)} + f_o^{(i)}$, $\beta = \overline{n}^{(j)} + \overline{n}^{(i)} + \overline{f}^{(i)}$, $w_1 = y^{(j)} + \overline{n}^{(j)}$ and $w_2 = y^{(i)} + f_o^{(i)} + \overline{n}^{(i)} + \overline{f}^{(i)}$. Hence, the tracking error $\widetilde{x}^{(i)}$ belongs to

$$\widetilde{x}^{(i)} \in \left(A^{(i)} - K_F^{(i)}\right)^{-1} K_F^{(i)} f_o^{(i)} \oplus \left[-\overline{z}_F^{(i)}, \overline{z}_F^{(i)}\right]. \tag{9.29}$$

In order to sustain stability and thermal comfort under local sensor fault $f^{(i)}$, $K_F^{(i)}$ should be selected such that (9.19) is satisfied and the following conditions are satisfied for all $t \geq t_f^{(i)}$:

$$A^{(i)} - K_F^{(i)} < 0, \tag{9.30}$$

$$\left(A^{(i)} - K_F^{(i)}\right)^{-1} K_F^{(i)} f_o^{(i)} \oplus \left[-\overline{z}_F^{(i)}, \overline{z}_F^{(i)}\right] \subseteq \left[-x_{ref}^{(i)} + T_{z_i}^{\min}, -x_{ref}^{(i)} + T_{z_i}^{\max}\right]. \tag{9.31}$$

9.4 Simulation Results

The objective of this section is to evaluate the proposed distributed FTC scheme applied to a 3-zone HVAC building. The down-view of the 3-zone HVAC building is presented in Fig. 9.1a. The parameters of the 3-zone HVAC system are given in Table 9.1, while $\mathcal{K}_1 = \{2\}$, $\mathcal{K}_2 = \{1,3\}$ and $\mathcal{K}_3 = \{2\}$. The known exogenous inputs to the 3-zone HVAC system are: $T_{pl} = 20\ ^o$C, $T_o = 5\ ^o$C, $T_{amb} = 5\ ^o$C and $T_{i1} = 10\ ^o$C, $i \in \{1,2,3\}$. The modeling uncertainty associated with each subsystem is modeled as $r^s(t) = 5\%T_{pl}\sin(0.1t)\ ^o$C and $r^{(i)}(t) = 1\%T_{amb}\sin(0.1t)\ ^o$C, $i \in \{1,2,3\}$. For simulation purposes, the noise corrupting the sensors is defined as a uniform random noise with $\overline{n}^s = 1\%x_{ref}^s$ and $\overline{n}^{(i)} = 1\%x_{ref}^{(i)}$, where x_{ref}^s and $x_{ref}^{(i)}$ are the set points of temperatures selected as $x_{ref}^s = 32\ ^o$C and $x_{ref}^{(i)} = 24\ ^o$C, $i \in \mathcal{N} = \{1,2,3\}$.

If we take into consideration that the 3-zone HVAC serves an office building in which the zone air temperature T_{z_i} can vary within a given set e.g., [18^{o}C, 30^{o}C], the *PDD* can be expressed as a function of air temperature T_{z_i} as presented in Fig. 9.3. Based on ASHRAE standard, *PPD* must be at

Table 9.1: Modeling parameters of the 3-zone HVAC system.

Parameter	Value	Parameter	Value
C_{st}	8370 kJ/^{o}C	$A_{d_{i,j}}, i \in \{1,2,3\}$	1.951 m^2
C_{z_i}	29.96 kJ/^{o}C	a_{sz}	0.6 kJ/kg^{o}C
$U_{i,max}$	3700 kg/h	$U_{st,max}$	27.36$\times$ 10^5 kJ/^{o}C
a_{st}	12 kJ/kg^{o}C	P_{max}	3.5
a_{z_i}	740 kJ/h^{o}C	ΔT_{max}	45 ^{o}C
$a_{z_{1,2}} = a_{z_{2,3}}$	50 kJ/h^{o}C	h	8.26 W/m$^2{}^o$C
$A_{w_i}, i \in \{1,2,3\}$	31.21 m^2		

most 10% in order to maintain thermal comfort. This limit is denoted with a red horizontal dotted line in Fig. 9.3. For this specific scenario the zone air temperature T_{z_i}, for all $i \in \{1,2,3\}$, is recommended to be inside the desired closed set $\mathcal{T}_i$, given by solving PPD equation with $PPD = 10$ %, i.e.,

$$T_{z_i} \in \mathcal{T}_i = \left[T_{z_i}^{\min}, T_{z_i}^{\max}\right] = [22.5^o\text{C}, 25^o\text{C}]\,. \tag{9.32}$$

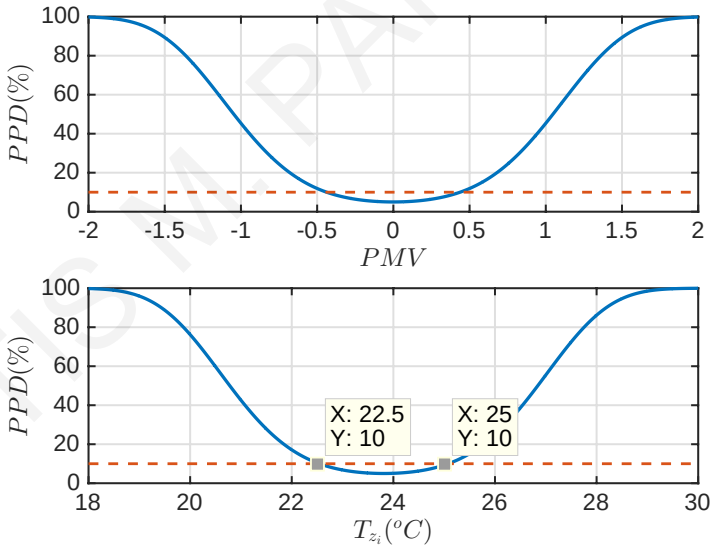

Figure 9.3: *PPD* in relation to *PMV* (top) and *PPD* in relation to zone air temperature T_{z_i} (bottom) for a particular office scenario. Red dashed lines indicate the acceptable limits for thermal comfort based on the ASHRAE standard.

The 3-zone HVAC system is simulated for 1 hour with initial conditions $T_{st}(0) = 30\ ^o$C and $T_{z_i}(0) = 20\ ^o$C, $i \in \{1,2,3\}$. A single permanent sensor fault is simulated such that $f^{(2)}(t_f^{(2)}) = -15\%x_{ref}^{(2)}$ at $t_f^{(2)} = 0.5$ hours. The limits for the sensor fault are $[f_{\min}^{(2)}, f_{\max}^{(2)}] = [-30\%x_{ref}^{(2)}, 30\%x_{ref}^{(2)}]$ and as a result $f_o^{(2)} = 0$ and $\overline{f}^{(2)} = 30\%x_{ref}^{(2)}$. The values for the control gains $\{K_H^{(1)}, K_H^{(2)}, K_H^{(3)}\} = \{105, 120, 96\}$ were calculated offline using constant values for the sensor measurements (i.e., $y^{(1)}$, $y^{(2)}$, $y^{(3)}$) in order to satisfy (9.18)–(9.20) and $\{K_F^{(1)}, K_F^{(2)}, K_F^{(3)}\} = \{24, 14, 26\}$ were calculated offline

in order to satisfy (9.19) and (9.30)–(9.31), respectively.

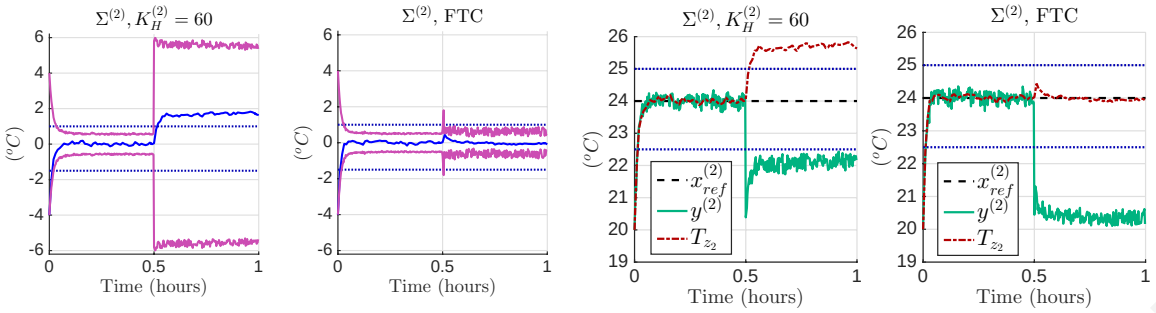

Figure 9.4: Temperature tracking in the presence of a sensor fault; with and without FTC. Subfigures (a) and (c) present the results of $\Sigma^{(2)}$ with $K_H^{(2)} = 60$, while subfigures (b) and (d) present the results with the proposed FTC scheme. Subfigures (a) and (b) illustrate the tracking error $\widetilde{x}^{(2)}$ (blue line), the bounds of the tracking error (9.29) (magenta line) and the thermal comfort bounds of (9.9) (blue dashed line). Subfigures (c) and (d) show $x_{ref}^{(2)}$, the temperature T_{z_2} and the sensor measurements $y^{(2)}$ of zone 2. In (c) and (d) the blue dashed line denotes limits the comfort set $\mathcal{T}_2$.

Figures 9.4a and 9.4c illustrate the results with $K_H^{(2)} = 60$, while Figures 3(b) and 3(d) present the results by applying the distributed sensor FTC presented in (9.5). Figures 9.4b and 9.4d show the tracking error $\widetilde{x}^{(2)}$ (blue line), the bounds on the tracking error given in (9.16)–(9.17) before sensor fault isolation and (9.29) after sensor fault isolation (magenta line) and the interval derived from the comfort bounds presented in (9.9) (blue dashed line). Figures 9.4c and 9.4d present the reference temperature $x_{ref}^{(2)}$ (black dashed line), the air temperature T_{z_2} (red dotted line), the sensor measurements $y^{(2)}$ (green line) and the thermal comfort interval $\mathcal{T}_2$ (blue dashed lines) given in (9.32).

Based on Figures 9.4a–9.4d we notice that before the fault occurrence $t \leq t_f^{(2)} = 0.5$ hours, the tracking error $\widetilde{x}^{(2)}$ and the air temperature T_{z_2} do not violate the comfort bounds (blue dotted line) after a transient period. Furthermore, the lower and upper bound of the tracking error (magenta line) converge inside the comfort bounds which indicates that the temperature will be inside the comfort bounds regardless the noise measurements of $\mathcal{S}^{(2)}$ and the modeling uncertainty of zone 2. For $t > t_f^{(2)} = 0.5$ hours, in Fig. 9.4a, the tracking error (blue line) and its lower and upper bounds (magenta lines) are outside the thermal comfort bounds (blue dashed lines) and in Fig. 9.4c, the air temperature (red dotted line) violates also the comfort bounds $\mathcal{T}_2$ (blue dashed lines) since the healthy control gain $K_H^{(2)} = 60$ is used for this simulation.

On the contrary, in Figures 9.4b and 9.4d, the FTC scheme compensates the effects of the sensor fault $f^{(2)}$, since in Fig. 9.4b the tracking error $\widetilde{x}^{(2)}$ and the lower and upper bound of the tracking error (magenta line) converge inside the interval derived from the comfort bounds (blue dashed lines), and in Fig. 9.4d the air temperature T_{z_2} (red dotted line) converges inside the thermal comfort bounds (blue dashed lines) in presence of the sensor fault.

9.5 Conclusions

This chapter presents a distributed sensor FTC control scheme for maintaining indoor thermal comfort conditions in a multi-zone HVAC system with faulty measurements. Through the analysis of the tracking error, analytical conditions are derived with respect to the controller gain for preserving stability and indoor thermal comfort, taking into account bounds on uncertainty, measurement noise and sensor faults. Based on the decision of a fault diagnosis scheme to detect and isolate the occurrence of a single sensor fault, the controller gain of the local control scheme is reconfigured to satisfy the analytical conditions. The methodology was evaluated in the presence of a single sensor fault for a 3-zone HVAC building system.

Chapter 10

Distributed Adaptive Control for Air-Handling Units HVAC systems

10.1 Introduction

According to [4] and [20], several researchers have proposed a large number of control designs to improve both tracking performance and energy efficiency. Taking into account the consecutive way that AHU components (i.e., mixing box, fan, heating coil and cooling coil) are connected as resented in Section 2.5, *cascade control* may be used. Cascade control is a specialized control architecture formed by inner and outer feedback loops. Exploiting the cascade topology of AHUs, the control design should overcome the challenges that emerge due to the large scale of buildings, and alleviate the computational complexity of traditional centralized control schemes as well as avoid single points of failure. With the recent advances in the area of Internet-of-Things (IoT), a distributed control design may not suffer from the disadvantages of centralized schemes, but instead can reduce communication requirements and improve scalability.

This chapter deals with the design of a distributed, online, adaptive control scheme which can effectively regulate temperature in multi-zone buildings while taking into account actuator dynamics and interconnections between zones and also being able to overcome parameter uncertainties and unknown disturbances. The design of the control scheme is based on the modeling of the underlying components and features a cascade scheme for each AHU and its underling zone, as well as exchange information between neighboring zones. On-line estimation of controller parameters guarantees that the system can adapt to changes as well as unknown heat gains, and distribute heat across zones in an efficient manner. We present an illustrative simulation example, where the proposed algorithm is applied to a multi-zone school building and we show how the proposed scheme may have better performance in such a dynamic environment when compared to a control scheme that considers all parameters to be known and constant. As analyzed in [119], thermal comfort may have a direct impact

on learning effectiveness in school.

10.2 Objective

The objective is to design a distributed control mechanism that is able to effectively regulate and maintain air temperature T_{z_i} in all thermal zones of the building at a desired temperature $T_{z_i}^{\text{ref}}$ that is defined by the users of each i-th zone. The proposed algorithm should assign a local controller to each heating and cooling valve that provides water to the coils of the AHU. Thus, the control input is the water mass flow rate that pass through each coil $u_{\text{cc}}^{(i)} = \dot{m}_{\text{cc}_i} \in [0, \dot{m}_{\text{cc}_{\max,i}}]$ and $u_{\text{hc}}^{(i)} = \dot{m}_{\text{hc}_i} \in [0, \dot{m}_{\text{hc}_{\max,i}}]$ for all $i \in \mathcal{N}$. In addition, the proposed control algorithm should only utilize temperature measurements and not depend on measurements of building parameters, such as dimensions, material coefficients, coil efficiencies, etc, in order to be able to overcome all uncertainties and disturbances in the system and at the same time avoid cumbersome calibrations.

Thus, each zone will have one controller for the cooling coil water valve and one for the heating coil water valve. The available measurements for each controller of zone i are zone air temperature T_{z_i}, air temperature of neighboring zones T_{z_j} $j \in N_i$, supply air temperature T_{sa_i}, temperature of water in coil T_{c_i}, water temperature in the storage tank T_{st} and ambient temperature T_{amb}.The employed temperature sensors are denoted with a red round shape in Fig. 2.5.

10.3 Distributed Control Architecture

This section demonstrates the design of a distributed adaptive control approach, where all control gains are estimated on-line to respond to parameter changes, system uncertainties and disturbances. In the first part of this section the network structure of the multi-zone HVAC system is exploited to design the structure of the proposed distributed control scheme, which is demonstrated by the diagram of Fig. 10.1. In the second part of the section on-line estimation of controller gains is introduced to make them adapt to system deviation from nominal values, in order to make the control mechanism able to handle system uncertainties and disturbances.

10.3.1 Controller Architecture

In this section the design of the distributed control scheme is presented. As it is shown in Fig. 10.1, each local controller receives sensor information from neighboring zones T_{z_j} for all $j \in \mathcal{N}_i$, in order to obtain the local control decisions $\dot{m}_{\text{cc}_i}$ and $\dot{m}_{\text{hc}_i}$ for the cooling and heating coil, respectively. The control process is designed using a cascade formulation of the underlying control laws. Specifically, the zone control C_z is based on the current values of T_{z_i}, $T_{z_i}^{\text{ref}}$, T_{z_j}, and T_{amb}, and decides the desired supply air temperature $T_{\text{sa}_i}^{\text{ref}}$. Consequently, the supply air control C_{sa} is based on the desired supply

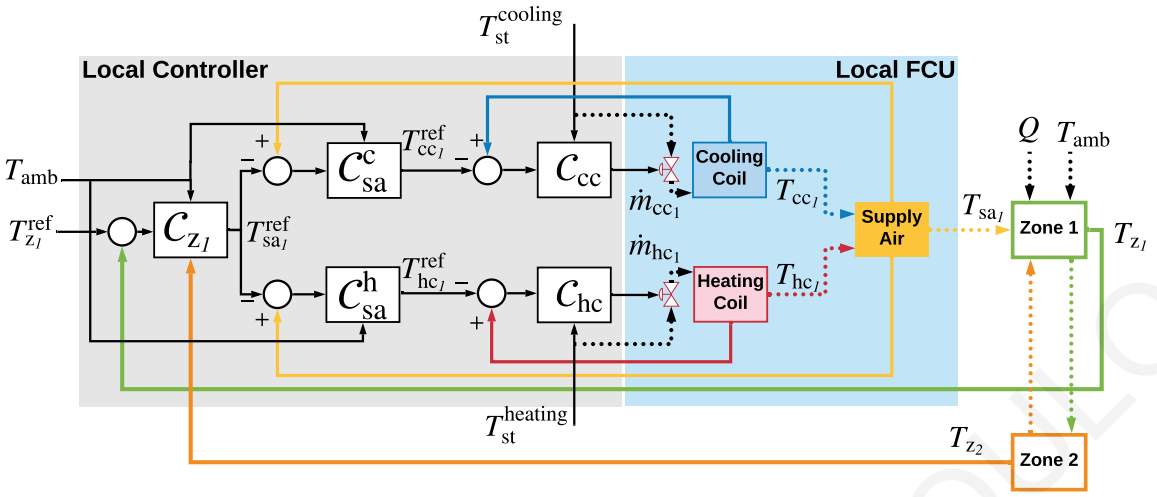

Figure 10.1: Architecture of the Distributed Control scheme for the multi-zone AHU HVAC system. The cooling and heating coil valves of each local FCU are regulated by a cascade control scheme that considers measurements from: the local states (i.e., zone's air temperature, supply air temperature, cooling and heating coil water temperature, storage tank's water temperature for both cooling and heating), neighboring states (i.e., air temperature from neighboring zones), and external disturbances (i.e., ambient air temperature).

air temperature $T^{\text{ref}}_{\text{sa}_i}$ computed online by the previous control law as well as the current values of T_{sa_i}, T_{z_i}, and T_{amb}, to determine the value of the desired coil water temperature $T^{\text{ref}}_{\text{c}_i}$, one for each mode, cooling and heating. Based on $T^{\text{ref}}_{\text{c}_i}$, T_{c_i}, T_{sa_i}, and T_{st}, the control C_{c} determines the water flow rate that passes through for each coil.

Zone control design

For the zone control design, the zone discrete time dynamic presented in (2.43) are considered. Then, by defining the zone air temperature tracking error as $e_{\text{z}_i}(k) = T_{\text{z}_i}(k) - T^{\text{ref}}_{\text{z}_i}$, where $T^{\text{ref}}_{\text{z}_i}$ represents a zone air temperature target that is defined by the users. The zone air temperature tracking error dynamics are the following:

$$e_{\text{z}_i}(k+1) = A^d_{\text{z}_i} T_{\text{z}_i}(k) + B^d_{\text{z}_i}\left[T_{\text{sa}_i}(k) + \sum_{j\in\mathcal{N}_i} \frac{a_{i,j}}{\dot{m}_{\text{sa}_i} C_{\text{pa}}} T_{\text{z}_j}(k) + \frac{a_{\text{z}_i}}{\dot{m}_{\text{sa}_i} C_{\text{pa}}} T_{\text{amb}}(k) + \frac{Q_i(k)}{\dot{m}_{\text{sa}_i} C_{\text{pa}}}\right] - T^{\text{ref}}_{\text{z}_i}. \tag{10.1}$$

Zone air temperature is regulated by using supply air temperature as the control input. However, T_{sa_i} is produced by the AHU. Thus, we can utilize (10.1) to calculate the ideal control input $T^{\text{ref}}_{\text{sa}_i}$ that would serve as an output reference for the AHU. The $T^{\text{ref}}_{\text{sa}_i}$ signal is reflecting the required heating or cooling load for zone air temperature regulation based on the zone loads and heat gains that affect its temperature. The representation of zone temperature tracking error dynamics implies the following

form for $T_{\mathrm{sa}_i}^{\mathrm{ref}}$, where the ideal zone control input that should be tracked by T_{sa_i}:

$$C_{\mathrm{z}}: \begin{cases} T_{\mathrm{sa}_i}^{\mathrm{ref}}(k) = -K_{\mathrm{z,e}_i}^{*} e_{\mathrm{z}_i}(k) - K_{\mathrm{z}_i}^{*} T_{\mathrm{z}_i}^{\mathrm{ref}}(k) - \sum_{j \in \mathcal{N}_i} K_{\mathrm{z},i,j}^{*} T_{\mathrm{z}_j}(k) - K_{\mathrm{z,amb}_i}^{*} T_{\mathrm{amb}}(k) - h_i K_i(k) \\ K_i(k) = K_i(k-1) + e_{\mathrm{z}_i}(k) \end{cases}, \tag{10.2}$$

where $\breve{A}_{\mathrm{z}_i}^{d}$ is a design constant to guarantee that zone air temperature dynamics have certain desired performance characteristics. The controller gains $K_{\mathrm{z,e}_i}^{*}$, $K_{\mathrm{z}_i}^{*}$, $K_{\mathrm{z},i,j}^{*}$, $K_{\mathrm{z,amb}_i}^{*}$ represent the nominal gains that would minimize the zone air temperature tracking error in the case of an ideal system with no uncertainties and are calculated as follows:

$$K_{\mathrm{z,e}_i}^{*} = \frac{A_{\mathrm{z}_i}^{d} - \breve{A}_{\mathrm{z}_i}^{d}}{B_{\mathrm{z}_i}^{d}}, \; K_{\mathrm{z}_i}^{*} = \frac{A_{\mathrm{z}_i}^{d} - 1}{B_{\mathrm{z}_i}^{d}}, \; K_{\mathrm{z},i,j}^{*} = \frac{a_{i,j}}{\dot{m}_{\mathrm{sa}_i} C_{\mathrm{pa}}}, \; K_{\mathrm{z,amb}_i}^{*} = \frac{a_{\mathrm{z}_i}}{\dot{m}_{\mathrm{sa}_i} C_{\mathrm{pa}}}, \tag{10.3}$$

and K_i is an accumulator with gain h_i to compensate for unknown heat gain Q_i. The approximation of Q_i as constant reflects the current occupancy, lighting and equipment operation regime.

Supply air control design

The temperature of supply air T_{sa_i}, which is produced by the AHU, should track the ideal zone control input $T_{\mathrm{sa}_i}^{\mathrm{ref}}$. In order to design a proper controller to achieve supply air temperature tracking, we re-write the supply air dynamics (2.37) in the following compact form, using the definitions of T_{m_i} and T_{f_i}, from (2.35) and (2.36) respectively:

$$\frac{\mathrm{d}T_{\mathrm{sa}_i}}{\mathrm{d}t} = A_{\mathrm{sa}_i} T_{\mathrm{sa}_i}(t) + B_{\mathrm{sa}_i} \left[T_{\mathrm{c}_i}(t) + \frac{W_{\mathrm{f}_i} f C_{\mathrm{pa}}}{(\mathrm{UA})_{\mathrm{c}_i}} + \frac{\dot{m}_{\mathrm{o}_i}}{(\mathrm{UA})_{\mathrm{c}_i}} T_{\mathrm{amb}}(t) + \frac{(\dot{m}_{\mathrm{sa}_i} - \dot{m}_{\mathrm{o}_i})}{(\mathrm{UA})_{\mathrm{c}_i}} T_{\mathrm{z}_i}(t) \right], \tag{10.4}$$

where

$$A_{\mathrm{sa}_i} = -\frac{\left((\mathrm{UA})_{\mathrm{c}_i} + \dot{m}_{\mathrm{sa}_i} C_{\mathrm{pa}}\right)}{C_{\mathrm{sa}_i}}, \; B_{\mathrm{sa}_i} = \frac{(\mathrm{UA})_{\mathrm{c}_i}}{C_{\mathrm{sa}_i}}. \tag{10.5}$$

Using sampling time T_s, we can write the discretized version of the supply air temperature dynamics as follows:

$$T_{\mathrm{sa}_i}(k+1) = A_{\mathrm{sa}_i}^{d} T_{\mathrm{sa}_i}(k) + B_{\mathrm{sa}_i}^{d} \left[T_{\mathrm{c}_i}(k) + \frac{W_{\mathrm{f}_i} f C_{\mathrm{pa}}}{(\mathrm{UA})_{\mathrm{c}_i}} + \frac{\dot{m}_{\mathrm{o}_i}}{(\mathrm{UA})_{\mathrm{c}_i}} T_{\mathrm{amb}}(k) + \frac{(\dot{m}_{\mathrm{sa}_i} - \dot{m}_{\mathrm{o}_i})}{(\mathrm{UA})_{\mathrm{c}_i}} T_{\mathrm{z}_i}(k) \right], \tag{10.6}$$

where $t = kT_s$ and

$$A_{\mathrm{sa}_i}^{d} = e^{A_{\mathrm{sa}_i} T_s}, \; B_{\mathrm{sa}_i}^{d} = \frac{A_{\mathrm{sa}_i}^{d} - 1}{A_{\mathrm{sa}_i}} B_{\mathrm{sa}_i}. \tag{10.7}$$

Then, we define the supply air temperature tracking error $e_{\mathrm{sa}_i}(k) = T_{\mathrm{sa}_i}(k) - T_{\mathrm{sa}_i}^{\mathrm{ref}}(k)$, where $T_{\mathrm{sa}_i}^{\mathrm{ref}}$ is the temperature calculated by (10.2). The supply air temperature tracking error dynamics are the following:

$$\begin{aligned} e_{\mathrm{sa}_i}(k+1) = & A_{\mathrm{sa}_i}^{d} T_{\mathrm{sa}_i}(k) + B_{\mathrm{sa}_i}^{d} \left[T_{\mathrm{c}_i}(k) + \frac{W_{\mathrm{f}_i} f C_{\mathrm{pa}}}{(\mathrm{UA})_{\mathrm{c}_i}} + \frac{\dot{m}_{\mathrm{o}_i}}{(\mathrm{UA})_{\mathrm{c}_i}} T_{\mathrm{amb}}(k) + \frac{(\dot{m}_{\mathrm{sa}_i} - \dot{m}_{\mathrm{o}_i})}{(\mathrm{UA})_{\mathrm{c}_i}} T_{\mathrm{z}_i}(k) \right] \\ & - T_{\mathrm{sa}_i}^{\mathrm{ref}}(k+1). \end{aligned} \tag{10.8}$$

Supply air temperature is regulated by using water temperature from the coil as the control input. However, T_{c_i} is regulated in the coil by properly adjusting the valve that controls the coil water flow. Thus, we can utilize (10.8) to calculate the ideal control input $T_{\mathrm{c}_i}^{\mathrm{ref}}$ that would serve as a reference for the coil. The representation of supply air temperature tracking error dynamics implies the following form for $T_{\mathrm{c}_i}^{\mathrm{ref}}$:

$$C_{\mathrm{sa}}: \left\{ T_{\mathrm{c}_i}^{\mathrm{ref}}(k) = -K_{\mathrm{sa},\mathrm{e}_i}^{*} e_{\mathrm{sa}_i}(k) - K_{\mathrm{sa}_i}^{*} T_{\mathrm{sa}_i}^{\mathrm{ref}}(k) - K_{\mathrm{sa},\mathrm{z}_i}^{*} T_{\mathrm{z}_i}(k) - K_{\mathrm{sa},\mathrm{amb}_i}^{*} T_{\mathrm{amb}}(k) - K_{\mathrm{f}_i}^{*} \right. , \tag{10.9}$$

where $\breve{A}_{\mathrm{sa}_i}^{d}$ is a design constant to provide the supply air temperature dynamics with certain desired characteristics, and $T_{\mathrm{sa}_i}^{\mathrm{ref}}(k)$ is computed by equation (10.2). The controller gains $K_{\mathrm{sa},\mathrm{e}_i}^{*}$, $K_{\mathrm{sa}_i}^{*}$, K_{i}^{*}, $K_{\mathrm{ma}_i}^{*}$, $K_{\mathrm{f}_i}^{*}$ are the nominal gains that may guarantee supply air temperature tracking in the case of an ideal AHU and are calculated as follows:

$$K_{\mathrm{sa},\mathrm{e}_i}^{*} = \frac{A_{\mathrm{sa}_i}^{d} - \breve{A}_{\mathrm{sa}_i}^{d}}{B_{\mathrm{sa}_i}^{d}}, \; K_{\mathrm{sa}_i}^{*} = \frac{A_{\mathrm{sa}_i}^{d} - 1}{B_{\mathrm{sa}_i}^{d}}, \; K_{i}^{*} = \frac{\left(\dot{m}_{\mathrm{sa}_i} - \dot{m}_{\mathrm{o}_i}\right)}{(\mathrm{UA})_{\mathrm{c}_i}}, \; K_{\mathrm{sa},\mathrm{amb}_i}^{*} = \frac{\dot{m}_{\mathrm{o}_i}}{(\mathrm{UA})_{\mathrm{c}_i}}, \; K_{\mathrm{f}_i}^{*} = \frac{W_{\mathrm{f}_i} f C_{\mathrm{pa}}}{(\mathrm{UA})_{\mathrm{c}_i}}. \tag{10.10}$$

Coil water control design

The temperature of the water that passes through the coil should track $T_{\mathrm{c}_i}^{\mathrm{ref}}$, as calculated in (10.9). To properly control coil water temperature, we re-write the coil water dynamics for both heating and cooling coil as presented in (2.38)–(2.39) as a single equation in the following compact form:

$$\frac{\mathrm{d}T_{\mathrm{c}_i}}{\mathrm{d}t} = A_{\mathrm{c}_i} T_{\mathrm{c}_i}(t) + B_{\mathrm{c}_i}\left[\dot{m}_{\mathrm{c}_i}(t)\left(T_{\mathrm{st}}(t) - T_{\mathrm{c}_i}(t)\right) + \frac{(\mathrm{UA})_{\mathrm{c}_i}}{C_{\mathrm{pw}}} T_{\mathrm{sa}_i}(t)\right], \tag{10.11}$$

where

$$A_{\mathrm{c}_i} = -\frac{(\mathrm{UA})_{\mathrm{c}_i}}{C_{\mathrm{wm}_i}}, \; B_{\mathrm{c}_i} = \frac{C_{\mathrm{pw}}}{C_{\mathrm{wm}_i}}. \tag{10.12}$$

The discrete-time version of the coil water temperature dynamics using sampling time T_s is the following:

$$T_{\mathrm{c}_i}(k+1) = A_{\mathrm{c}_i}^{d} T_{\mathrm{c}_i}(k) + B_{\mathrm{c}_i}^{d}\left[\dot{m}_{\mathrm{c}_i}(k)\left(T_{\mathrm{st}}(k) - T_{\mathrm{c}_i}(k)\right) + \frac{(\mathrm{UA})_{\mathrm{c}_i}}{C_{\mathrm{pw}}} T_{\mathrm{sa}_i}(k)\right], \tag{10.13}$$

where $t = kT_s$ and

$$A_{\mathrm{c}_i}^{d} = e^{A_{\mathrm{c}_i} T_s}, \; B_{\mathrm{c}_i}^{d} = \frac{A_{\mathrm{c}_i}^{d} - 1}{A_{\mathrm{c}_i}} B_{\mathrm{c}_i}. \tag{10.14}$$

Let's we define coil water temperature tracking error $e_{\mathrm{c}_i}(k) = T_{\mathrm{c}_i}(k) - T_{\mathrm{c}_i}^{\mathrm{ref}}(k)$, where $T_{\mathrm{c}_i}^{\mathrm{ref}}$ is the temperature calculated by (10.9). Then, coil water temperature tracking error dynamics are the following:

$$e_{\mathrm{c}_i}(k+1) = A_{\mathrm{c}_i}^{d} T_{\mathrm{c}_i}(k) + B_{\mathrm{c}_i}^{d}\left[\dot{m}_{\mathrm{c}_i}(k)\left(T_{\mathrm{st}}(k) - T_{\mathrm{c}_i}(k)\right) + \frac{(\mathrm{UA})_{\mathrm{c}_i}}{C_{\mathrm{pw}}} T_{\mathrm{sa}_i}(k)\right] - T_{\mathrm{c}_i}^{\mathrm{ref}}(k+1). \tag{10.15}$$

Coil water temperature is regulated by adjusting the valve that controls the flow of the water that passes through the coil. Thus, we can utilize (10.9) to calculate the water mass flow rate that carries

the appropriate heat load to regulate zone air temperature as desired. The representation of coil water temperature tracking error dynamics implies the following form for the control input $\dot{m}_{c_i}$:

$$C_c : \left\{ \dot{m}_{c_i}(k) = \frac{1}{T_{st}(k) - T_{c_i}(k)} \left[- K^*_{c,e_i} e_{c_i}(k) - K^*_{c_i} T^{ref}_{c_i}(k) - K^*_{c,sa_i} T_{sa_i}(k) \right] \right. , \tag{10.16}$$

where $\breve{A}^d_{c_i}$ is a design constant to modify the coil water temperature dynamics as desired. We suppose that $T_{st}(k) - T_{c_i}(k) \neq 0 \; \forall k$ when the plant is operating. When $T_{st}(k) - T_{c_i}(k) = 0$, then $\dot{m}_{c_i}(k) = \dot{m}_{c_i}(k-1)$. The controller gains K^*_{c,e_i}, $K^*_{c_i}$, K^*_{c,sa_i} are nominal gains to guarantee coil water temperature tracking in the case of ideal an coil and are calculated as follows:

$$K^*_{c,e_i} = \frac{A^d_{c_i} - \breve{A}^d_{c_i}}{B^d_{c_i}}, \quad K^*_{c_i} = \frac{A^d_{c_i} - 1}{B^d_{c_i}}, \quad K^*_{c,sa_i} = \frac{(UA)_{c_i}}{C_{pw}}. \tag{10.17}$$

Stability properties of nominal control scheme

The combination of all aforementioned controllers C_z, C_{sa} and C_c in one zone and AHU creates a cascade system, while the overall HVAC system of a building is a network of such interconnected cascade systems. The proposed control input that uses all the calculated control inputs for all units is stable and guarantees that temperature tracking error for all zones will converge to zero under some conditions for design constants $\breve{A}^d_{z_i}$, $\breve{A}^d_{sa_i}$, $\breve{A}^d_{c_i}$ and h_i, as summarized in the following theorem:

Theorem 3. *Consider the overall closed-loop system composed of N subsystems* (10.1), (10.8) *and* (10.15) *using the control scheme described by* (10.2), (10.9) *and* (10.16). *Then, for constant* Q_i *and* T_{amb}, $e_{z_i} \in l_\infty$ *and* e_{z_i} *converges to zero as* $k \to \infty$, *for all* $i \in \mathcal{N} = \{1, \ldots, N\}$, *as long as the following polynomials have all roots inside the unit circle:*

1. $z - \breve{A}^d_{c_i}$,
2. $z^2 - (A^d_{sa_i} + \breve{A}^d_{c_i})z + A^d_{sa_i} - \breve{A}^d_{sa_i} + \breve{A}^d_{sa_i}\breve{A}^d_{c_i}$,
3. $(z - A^d_{z_i})(z - A^d_{sa_i})(z - \breve{A}^d_{c_i}) + (z - A^d_{z_i})(A^d_{sa_i} - \breve{A}^d_{sa_i})(1 - \breve{A}^d_{c_i}) + (A^d_{z_i} - \breve{A}^d_{z_i})(1 - \breve{A}^d_{sa_i})(1 - \breve{A}^d_{c_i})$,
4. $(z - A^d_{z_i})(z - A^d_{sa_i})(z - \breve{A}^d_{c_i})(z - 1) + (z - A^d_{z_i})(A^d_{sa_i} - \breve{A}^d_{sa_i})(1 - \breve{A}^d_{c_i})(z - 1)$
   $+ (A^d_{z_i} - \breve{A}^d_{z_i})(1 - \breve{A}^d_{sa_i})(1 - \breve{A}^d_{c_i})(z - 1) + (1 - \breve{A}^d_{sa_i})(1 - \breve{A}^d_{c_i})B^d_{z_i} h_i z$.

Proof. First, we consider the dynamic equation of the coil water temperature (10.13) with control input (10.16). By using the definition of coil water temperature tracking error $e_{c_i}(k) = T_{c_i}(k) - T^{ref}_{c_i}(k)$, we can re-write the control input in the following equivalent form:

$$\dot{m}_{c_i}(k) = \frac{1}{T_{st}(k) - T_{c_i}(k)} \left[- K^*_{c,e_i} T_{c_i}(k) - K^*_{c,ref_i} T^{ref}_{c_i}(k) - K^*_{c,sa_i} T_{sa_i}(k) \right], \tag{10.18}$$

where $K^*_{c,ref_i} = K^*_{c_i} - K^*_{c,e_i} = \frac{\breve{A}^d_{c_i} - 1}{B^d_{c_i}}$. By applying the control input (10.18) to the coil water temperature equation (10.13) and using the z transformation, we get that coil water temperature follows its reference according to the following relation:

$$T_{c_i} = \frac{B^d_{c_i}}{z - \breve{A}^d_{c_i}} \left[-K^*_{c,ref_i} T^{ref}_{c_i} \right] = \frac{1 - \breve{A}^d_{c_i}}{z - \breve{A}^d_{c_i}} \left[T^{ref}_{c_i} \right], \tag{10.19}$$

from which we derive that the roots of $z - \check{A}^d_{\mathrm{c}_i}$ should be inside the unit circle, which means that $\check{A}^d_{\mathrm{c}_i}$ should be chosen so that $\left|\check{A}^d_{\mathrm{c}_i}\right| < 1$.

$T^{\mathrm{ref}}_{\mathrm{c}_i}$ is calculated by (10.9) as the ideal coil water temperature to regulate supply air and is the ideal control input of (10.6). Eq. (10.9) can be re-written in the following equivalent form, by using the definition of supply air temperature tracking error $e_{\mathrm{sa}_i}(k) = T_{\mathrm{sa}_i}(k) - T^{\mathrm{ref}}_{\mathrm{sa}_i}(k)$:

$$T^{\mathrm{ref}}_{\mathrm{c}_i}(k) = -K^*_{\mathrm{e,sa}_i} T_{\mathrm{sa}_i}(k) - K^*_{\mathrm{sa,ref}_i} T^{\mathrm{ref}}_{\mathrm{sa}_i}(k) - K^*_i T_{\mathrm{z}_i}(k) - K^*_{\mathrm{sa,amb}_i} T_{\mathrm{amb}}(k) - K^*_{\mathrm{f}_i}, \tag{10.20}$$

where $K^*_{\mathrm{sa,ref}_i} = K^*_{\mathrm{sa}_i} - K^*_{\mathrm{sa,e}_i} = \frac{\check{A}^d_{\mathrm{sa}_i} - 1}{B^d_{\mathrm{sa}_i}}$.

Since T_{c_i} is the actual control input of (10.6), by combining (10.6), (10.19) and (10.20) and using the z transformation, we get the following relation:

$$T_{\mathrm{sa}_i} = \frac{F_{\mathrm{sa}_i}}{R_{\mathrm{sa}_i}(z)}\left[T^{\mathrm{ref}}_{\mathrm{sa}_i}\right] + \frac{z-1}{R_{\mathrm{sa}_i}(z)}\left[B^d_{\mathrm{sa}_i}[K^*_{sa,z} T_{\mathrm{z}_i} + K^*_{\mathrm{sa,amb}_i} T_{\mathrm{amb}} + K^*_{\mathrm{f}_i}]\right], \tag{10.21}$$

where

$$F_{\mathrm{sa}_i} = (1 - \check{A}^d_{\mathrm{sa}_i})(1 - \check{A}^d_{\mathrm{c}_i}), \tag{10.22}$$

$$\begin{aligned} R_{\mathrm{sa}_i}(z) &= (z - A^d_{\mathrm{sa}_i})(z - \check{A}^d_{\mathrm{c}_i}) + (A^d_{\mathrm{sa}_i} - \check{A}^d_{\mathrm{sa}_i})(1 - \check{A}^d_{\mathrm{c}_i}), \\ &= z^2 - (A^d_{\mathrm{sa}_i} + \check{A}^d_{\mathrm{c}_i})z + A^d_{\mathrm{sa}_i} - \check{A}^d_{\mathrm{sa}_i} + \check{A}^d_{\mathrm{sa}_i}\check{A}^d_{\mathrm{c}_i}, \end{aligned} \tag{10.23}$$

from which we derive that $\check{A}^d_{\mathrm{sa}_i}$ should be chosen so that the poles of $z^2 - (A^d_{\mathrm{sa}_i} + \check{A}^d_{\mathrm{c}_i})z + A^d_{\mathrm{sa}_i} - \check{A}^d_{\mathrm{sa}_i} + \check{A}^d_{\mathrm{sa}_i}\check{A}^d_{\mathrm{c}_i}$ are inside the unit circle.

$T^{\mathrm{ref}}_{\mathrm{sa}_i}$ is calculated by (10.2) as the ideal supply air temperature to regulate zone temperature (2.43) while dealing with all uncertainties and zone heat loads. Eq. (10.2) can be re-written in the following equivalent form, by using the definition of zone air temperature tracking error $e_{\mathrm{z}_i}(k) = T_{\mathrm{z}_i}(k) - T^{\mathrm{ref}}_{\mathrm{z}_i}$:

$$T^{\mathrm{ref}}_{\mathrm{sa}_i}(k) = -K^*_{\mathrm{z,e}_i} T_{\mathrm{z}_i}(k) - K^*_{\mathrm{z,ref}_i} T^{\mathrm{ref}}_{\mathrm{z}_i} - \sum_{j \in \mathcal{N}_i} K^*_{\mathrm{z},i,j} T_{\mathrm{z}_j}(k) - K^*_{\mathrm{sa,amb}_i} T_{\mathrm{amb}}(k) - h_i K_i(k), \tag{10.24}$$

$$K_i(k) = K_i(k-1) + e_{\mathrm{z}_i}(k), \tag{10.25}$$

where $K^*_{\mathrm{z,ref}_i} = K^*_{\mathrm{z}_i} - K^*_{\mathrm{z,e}_i} = \frac{\check{A}^d_{\mathrm{z}_i} - 1}{B^d_{\mathrm{z}_i}}$. Since T_{sa_i} is the actual control input of (2.43), by combining (2.43), (10.21) and (10.24) we get the following relation:

$$\begin{aligned} T_{\mathrm{z}_i} = {} & \frac{F_{\mathrm{z}_i}}{R_{\mathrm{z}_i}(z)}\left[T^{\mathrm{ref}}_{\mathrm{z}_i}\right] + \frac{F_{\mathrm{za}_i}(z)}{R_{\mathrm{z}_i}(z)} B^d_{\mathrm{z}_i}\left[\sum_{j \in \mathcal{N}_i} K^*_{\mathrm{z},i,j} T_{\mathrm{z}_j} + K^*_{\mathrm{z,amb}_i} T_{\mathrm{amb}}\right] \\ & + \frac{(z-1)}{R_{\mathrm{z}_i}(z)} B^d_{\mathrm{z}_i} B^d_{\mathrm{sa}_i}\left[K^*_{sa,i} T_{\mathrm{z}_i} + K^*_{\mathrm{sa,amb}_i} T_{\mathrm{amb}} + K^*_{\mathrm{f}_i}\right] - \frac{F_{\mathrm{sa}_i}}{R_{\mathrm{z}_i}(z)} B^d_{\mathrm{z}_i} h_i [K_i] + \frac{R_{\mathrm{sa}_i}(z)}{R_{\mathrm{z}_i}(z)} B^d_{\mathrm{z}_i}\left[\frac{Q_i}{\dot{m}_{\mathrm{sa}_i} C_{\mathrm{pa}}}\right], \end{aligned} \tag{10.26}$$

where

$$F_{z_i} = (1 - \check{A}^d_{z_i})(1 - \check{A}^d_{sa_i})(1 - \check{A}^d_{c_i}), \tag{10.27}$$

$$R_{z_i}(z) = (z - A^d_{z_i})(z - A^d_{sa_i})(z - \check{A}^d_{c_i}) + (z - A^d_{z_i})(A^d_{sa_i} - \check{A}^d_{sa_i})(1 - \check{A}^d_{c_i}) + (A^d_{z_i} - \check{A}^d_{z_i})(1 - \check{A}^d_{sa_i})(1 - \check{A}^d_{c_i}), \tag{10.28}$$

$$F_{za_i}(z) = (z - 1)\left(z + 1 - A^d_{sa_i} - \check{A}^d_{c_i}\right). \tag{10.29}$$

From (10.26), we derive that $\check{A}^d_{z_i}$ should be chosen so that the poles of

$$R_{z_i}(z) = (z - A^d_{z_i})(z - A^d_{sa_i})(z - \check{A}^d_{c_i}) + (z - A^d_{z_i})(A^d_{sa_i} - \check{A}^d_{sa_i})(1 - \check{A}^d_{c_i}) + (A^d_{z_i} - \check{A}^d_{z_i})(1 - \check{A}^d_{sa_i})(1 - \check{A}^d_{c_i})$$

are inside the unit circle.

By using the formula of the accumulator (10.25), we can re-write (10.26) in the following form:

$$T_{z_i} = \frac{F_i(z)}{R_i(z)}\left[T^{ref}_{z_i}\right] + \frac{(z-1)F_{za_i}(z)}{R_i(z)} B^d_{z_i}\left[\sum_{j \in \mathcal{N}_i} K^*_{z,i,j} T_{z_j} + K^*_{z,amb_i} T_{amb}\right] + \frac{(z-1)^2}{R_i(z)} B^d_{z_i} B^d_{sa_i}\left[K^*_{sa,z} T_{z_i} + K^*_{sa,amb_i} T_{amb} + K^*_{f_i}\right] + \frac{(z-1)R_{sa_i}(z)}{R_i(z)} B^d_{z_i}\left[\frac{Q_i}{\dot{m}_{sa_i} C_{pa}}\right], \tag{10.30}$$

where

$$F_i(z) = F_{z_i}(z-1) + F_{sa_i} B^d_{z_i} h_i z, \tag{10.31}$$

$$R_i(z) = R_{z_i}(z)(z-1) + F_{sa_i} B^d_{z_i} h_i z. \tag{10.32}$$

From (10.30) we derive that the choice of h_i should be made so that $R_i(z)$ has all roots inside the unit circle.

Using (10.30), we can express the overall system for all N thermal zones as follows:

$$W_d(z)\,[T_z] - W_{int}(z)\,[T_z] = W_{ref}(z)\left[T^{ref}_z\right] + W_{amb}(z)\,[T_{amb}] + W_f(z)\left[K^*_f\right] + W_Q(z)\,[Q], \tag{10.33}$$

where

$$T_{\mathrm{z}} = \left[T_{\mathrm{z}_1}, T_{\mathrm{z}_2}, \ldots, T_{\mathrm{z}_N}\right]^{\top} \tag{10.34}$$

$$T_{\mathrm{z}}^{\mathrm{ref}} = \left[T_{\mathrm{z}_1}^{\mathrm{ref}}, T_{\mathrm{z}_2}^{\mathrm{ref}}, \ldots, T_{\mathrm{z}_N}^{\mathrm{ref}}\right]^{\top}, \tag{10.35}$$

$$K_{\mathrm{f}}^{*} = \left[K_{\mathrm{f}_1}^{*}, K_{\mathrm{f}_2}^{*}, \ldots, K_{\mathrm{f}_N}^{*}\right]^{\top}, \tag{10.36}$$

$$Q = \left[\frac{Q_1}{\dot{m}_{\mathrm{sa}_1} C_{\mathrm{pa}}}, \frac{Q_2}{\dot{m}_{\mathrm{sa}_2} C_{\mathrm{pa}}}, \ldots, \frac{Q_N}{\dot{m}_{\mathrm{sa}_N} C_{\mathrm{pa}}}\right]^{\top}, \tag{10.37}$$

$$W_{\mathrm{d}}(z) = \mathrm{diag}\left(\frac{F_{\mathrm{invd}_1}(z)}{R_1(z)}, \frac{F_{\mathrm{invd}_2}(z)}{R_2(z)}, \ldots, \frac{F_{\mathrm{invd}_N}(z)}{R_N(z)}\right), \tag{10.38}$$

$$W_{\mathrm{int}}(z) = \begin{bmatrix} 0 & \frac{F_{\mathrm{inv}_{1,2}}(z)}{R_1(z)} & \cdots & \frac{F_{\mathrm{inv}_{1,N}}(z)}{R_1(z)} \\ \frac{F_{\mathrm{inv}_{2,1}}(z)}{R_2(z)} & 0 & \cdots & \frac{F_{\mathrm{inv}_{2,N}}(z)}{R_2(z)} \\ \vdots & \vdots & \ddots & \vdots \\ \frac{F_{\mathrm{inv}_{N,1}}(z)}{R_N(z)} & \frac{F_{\mathrm{inv}_{N,2}}(z)}{R_N(z)} & \cdots & 0 \end{bmatrix}, \tag{10.39}$$

$$W_{\mathrm{ref}}(z) = \mathrm{diag}\left(\frac{F_1(z)}{R_1(z)}, \frac{F_2(z)}{R_2(z)}, \ldots, \frac{F_N(z)}{R_N(z)}\right), \tag{10.40}$$

$$W_{\mathrm{amb}}(z) = \begin{bmatrix} \frac{(z-1)\left(K_{\mathrm{z,amb}_1}^{*} F_{\mathrm{za}_1}(z) + (z-1) B_{\mathrm{sa}_1}^{d} K_{\mathrm{sa,amb}_1}^{*}\right) B_{\mathrm{z}_1}^{d}}{R_1(z)} \\ \frac{(z-1)\left(K_{\mathrm{z,amb}_2}^{*} F_{\mathrm{za}_2}(z) + (z-1) B_{\mathrm{sa}_2}^{d} K_{\mathrm{sa,amb}_2}^{*}\right) B_{\mathrm{z}_2}^{d}}{R_2(z)} \\ \vdots \\ \frac{(z-1)\left(K_{\mathrm{z,amb}_N}^{*} F_{\mathrm{za}_N}(z) + (z-1) B_{\mathrm{sa}_N}^{d} K_{\mathrm{sa,amb}_N}^{*}\right) B_{\mathrm{z}_N}^{d}}{R_N(z)} \end{bmatrix}, \tag{10.41}$$

$$W_{\mathrm{f}}(z) = \mathrm{diag}\left(\frac{B_{\mathrm{z}_1}^{d} B_{\mathrm{sa}_1}^{d} (z-1)}{R_1(z)}, \frac{B_{\mathrm{z}_2}^{d} B_{\mathrm{sa}_2}^{d} (z-1)}{R_2(z)}, \frac{B_{\mathrm{z}_N}^{d} B_{\mathrm{sa}_N}^{d} (z-1)}{R_N(z)}\right), \tag{10.42}$$

$$W_{\mathrm{Q}}(z) = \mathrm{diag}\left(\frac{B_{\mathrm{z}_1}^{d} (z-1) R_{\mathrm{sa}_1}(z)}{R_1(z)}, \frac{B_{\mathrm{z}_2}^{d} (z-1) R_{\mathrm{sa}_2}(z)}{R_2(z)}, \frac{B_{\mathrm{z}_N}^{d} (z-1) R_{\mathrm{sa}_N}(z)}{R_N(z)}\right), \tag{10.43}$$

and

$$F_{\mathrm{d}_i}(z) = (z-1)^2 B_{\mathrm{z}_i}^{d} B_{\mathrm{sa}_i}^{d} K_{sa,z_i}^{*}, \tag{10.44}$$

$$F_{\mathrm{invd}_i}(z) = R_i(z) - F_{\mathrm{d}_i}(z), \tag{10.45}$$

$$F_{\mathrm{inv}_{i,j}}(z) = (z-1) F_{\mathrm{za}_i}(z) B_{\mathrm{z}_i}^{d} K_{\mathrm{z},i,j}^{*}. \tag{10.46}$$

Using the final value theorem on (10.33), for constant heat gain Q_i and ambient temperature T_{amb} we have that:

$$\lim_{z \to 1} \left[(z-1)\left(W_{\mathrm{d}}(z) - W_{\mathrm{int}}(z)\right) T_{\mathrm{z}}(z)\right] = T_{\mathrm{z}}^{\mathrm{ref}}, \tag{10.47}$$

where $T_z(z)$ is the z transform of zone temperature T_z, since:

$$\lim_{z\to 1} F_i(z) = (1 - \check{A}^d_{\mathrm{sa}_i})(1 - \check{A}^d_{\mathrm{c}_i}) B^d_{\mathrm{z}_i} h_i, \tag{10.48}$$

$$\lim_{z\to 1} R_i(z) = (1 - \check{A}^d_{\mathrm{sa}_i})(1 - \check{A}^d_{\mathrm{c}_i}) B^d_{\mathrm{z}_i} h_i. \tag{10.49}$$

Thus, $\lim_{z\to 1} [(z-1)\,(W_{\mathrm{d}}(z) - W_{\mathrm{int}}(z))\,T_z(z)]$ exists. In addition, $\lim_{z\to 1} (W_{\mathrm{d}}(z) - W_{\mathrm{int}}(z))$ also exists and is non-zero and equal to:

$$\lim_{z\to 1} (W_{\mathrm{d}}(z) - W_{\mathrm{int}}(z)) = W_{\mathrm{d}_{\mathrm{lim}}} - W_{\mathrm{int}_{\mathrm{lim}}} = I_{N\times N}, \tag{10.50}$$

where $W_{\mathrm{d}_{\mathrm{lim}}} = I_{N\times N}$ and $W_{\mathrm{int}_{\mathrm{lim}}} = 0_{N\times N}$.

Therefore,

$$\lim_{z\to 1} [(z-1) T_z(z)] = T^{\mathrm{ref}}_z, \tag{10.51}$$

which implies that T_{z_i} approaches $T^{\mathrm{ref}}_{z_i}$ as $t \to \infty$, for all $i \in \mathcal{N}$. □

Theorem 3 guarantees that if design constants $\check{A}^d_{z_i}$, $\check{A}^d_{\mathrm{sa}_i}$, $\check{A}^d_{\mathrm{c}_i}$ and h_i are appropriately chosen to satisfy the aforementioned conditions 1. – 4. for each subsystem, zone air temperature will reach the desired one in each zone, overcoming unknown disturbances as well as heat exchange interactions between zones for the time period when unknown heat gains Q_i and ambient temperature remain constant. It should be noted that conditions of Theorem 3 are only local, meaning that they do not depend on the number of zones, but they should be checked for each zone individually. Thus, an increase of the building size does not increase the complexity of the conditions in order to guarantee system convergence.

10.3.2 Estimation of controller gains

In this section the adaptive laws for on-line estimation of the controller gains are introduced. HVAC systems suffer from several uncertainties or parameter changes that are caused by human activity, weather conditions, lighting, electrical equipment, material degradation, or inaccurate measurement and approximation of system parameters, such heat transfer coefficients and solar gains. Thus, controller gain adaptation is meant to accommodate for all such deviations of the system from its nominal values.

After replacing nominal (known) controller gains with their on-line estimates, each local valve controller for regulating zone air temperature is obtained by the following equations:

$$T^{\mathrm{ref}}_{\mathrm{sa}_i}(k) = -K_{\mathrm{z,e}_i}(k) e_{\mathrm{z}_i}(k) - K_{\mathrm{z}_i}(k) T^{\mathrm{ref}}_{\mathrm{z}_i}(k) - \sum_{j\in\mathcal{N}_i} K_{\mathrm{z},i,j}(k) T_{\mathrm{z}_j}(k) - K_{\mathrm{z,amb}_i}(k) T_{\mathrm{amb}}(k) - K_i(k), \tag{10.52a}$$

$$T^{\mathrm{ref}}_{\mathrm{c}_i}(k) = -K_{\mathrm{sa,e}_i}(k) e_{\mathrm{sa}_i}(k) - K_{\mathrm{sa}_i}(k) T^{\mathrm{ref}}_{\mathrm{sa}_i}(k) - K_{\mathrm{sa,z}_i}(k) T_{\mathrm{z}_i}(k) - K_{\mathrm{sa,amb}_i}(k) T_{\mathrm{amb}}(k) - K_{\mathrm{f}_i}(k), \tag{10.52b}$$

$$\dot{m}_{\mathrm{c}_i}(k) = \frac{1}{T_{\mathrm{st}}(k) - T_{\mathrm{c}_i}(k)} \left[-K_{\mathrm{c,e}_i}(k) e_{\mathrm{c}_i}(k) - K_{\mathrm{c}_i}(k) T^{\mathrm{ref}}_{\mathrm{c}_i}(k) - K_{\mathrm{c,sa}_i}(k) T_{\mathrm{sa}_i}(k) \right]. \tag{10.52c}$$

where all controller nominal gains presented in (10.2), (10.9) and (10.16) are replaced with their on-line estimates.

An adaptive algorithm based on gradient descent with projection, as presented and analyzed in [64], is used in order to generate on-line the controller adaptive gains. The algorithm is applied on every element of each cascade subsystem to calculate the corresponding on-line controller gains. Since the internal states (i.e., heating/cooling coil water temperature, supply air temperature and zone air temperature) are regulated through the cascade feedback control scheme presented in Fig. 10.1, by applying the proposed adaptive control laws of (10.52a), (10.52b), (10.52c) to control laws C_z, C_{sa}, C_c respectively, we end up with tracking error dynamics for each internal state.

In order to compute the adaptive laws we need to express each tracking error dynamics in the form of the following linear parametric model:

$$z_i(k) = \Theta_i^{*\top} \Phi_i(k), \tag{10.53}$$

where Θ_i^* are the ideal constant values to be estimated, so that the system performs as desired. $\Phi_i(k)$ and $z_i(k)$ are some know signals. $\Theta_i(k)$ corresponds to the on-line estimate of the ideal Θ_i^* and is estimated by the following algorithm:

$$\Theta_i(k) = \Theta_i(k-1) + T_s \Gamma_i \epsilon_i(k) \Phi_i(k), \tag{10.54a}$$

$$[\Theta_i(k)]_s = \begin{cases} [\Theta_i(k)]_s & \text{if } L_{i,s} \le [\Theta_i(k)]_s \le U_{i,s} \\ L_{i,s} & \text{if } [\Theta_i(k)]_s < L_{i,s} \\ U_{i,s} & \text{if } [\Theta_i(k)]_s > U_{i,s} \end{cases}, \quad \forall s \tag{10.54b}$$

$$\epsilon_i(k) = \frac{z_i(k)}{n_i^2(k)}, \tag{10.54c}$$

$$n_i^2(k) = 1 + T_s \Phi_i^\top(k) \Gamma_i \Phi_i(k), \tag{10.54d}$$

where the subscript s corresponds to the elements of $\Theta_i(k)$ for each equipment part. $\Gamma_i = \Gamma_i^\top > 0$ is a diagonal positive definite gain matrix. $U_{i,s}$ and $L_{i,s}$ are conservative bounds for the estimated parameters. $L_{0,s} > 0$ has to be strictly positive, a restriction that is imposed by the structure of all equipment dynamics and it is necessary for the stability of the overall control scheme.

The aforementioned adaptive law guarantees the following properties, as analyzed in [64], which are necessary for the stability of the overall system: (i)

1. $\Theta_i(k), \epsilon_i(k), \epsilon_i(k) n_i(k) \in l_\infty$,
2. $\epsilon_i(k) m_i(k), |\Theta_i(k) - \Theta_i(k-1)| \in l_2$,
3. $\epsilon_i(k) m_i(k), |\Theta_i(k) - \Theta_i(k-1)| \to 0$, as $k \to \infty$.

Adaptive zone control

Using (10.52a), zone air temperature tracking error dynamics of (10.1) are expressed in the following form:

$$e_{\mathrm{z}_i}(k+1) = \check{A}^d_{\mathrm{z}_i} e_{\mathrm{z}_i}(k) + B^d_{\mathrm{z}_i}\Bigg[T_{\mathrm{sa}_i}(k) + K^*_{\mathrm{z,e}_i} e_{\mathrm{z}_i}(k) + K^*_{\mathrm{z}_i} T^{\mathrm{ref}}_{\mathrm{z}_i}(k) + \sum_{j\in\mathcal{N}_i} K^*_{\mathrm{z},i,j} T_{\mathrm{z}_j}(k) + K^*_{\mathrm{z,amb}_i} T_{\mathrm{amb}}(k) + K^*_i\Bigg]. \tag{10.55}$$

For the analysis in this part, we consider the unknown heat gain Q_i to be constant, therefore $K^*_i = \frac{Q_i}{\dot{m}_{\mathrm{sa}_i} C_{\mathrm{pa}}}$.

Eq. (10.55) can be expressed as the linear parametric model given in (10.53), where:

$$z_{\mathrm{z}_i}(k) = e_{\mathrm{z}_i}(k) - \check{A}^d_{\mathrm{z}_i} e_{\mathrm{z}_i}(k-1), \tag{10.56a}$$

$$\begin{aligned}\Theta^*_{\mathrm{z}_i} &= \Big[B^d_{\mathrm{z}_i},\ B^d_{\mathrm{za}_i} K^*_{\mathrm{z,e}_i},\ B^d_{\mathrm{z}_i} K^*_{\mathrm{z}_i},\ \big[B^d_{\mathrm{z}_i} K^*_{i,j}\big]_{\forall j\in\mathcal{N}_i},\ B^d_{\mathrm{z}_i} K^*_{\mathrm{z,amb}_i}, B^d_{\mathrm{z}_i} K^*_i\Big]^\top,\\ &= \Big[\theta^*_{\mathrm{z}_{0,i}},\ \theta^*_{\mathrm{z}_{1,i}},\ \theta^*_{\mathrm{z}_{2,i}},\ \big[\theta^*_{\mathrm{z}_{3,i,j}}\big]_{\forall j\in\mathcal{N}_i},\ \theta^*_{\mathrm{z}_{4,i}},\ \theta^*_{\mathrm{z}_{5,i}}\Big]^\top,\end{aligned} \tag{10.56b}$$

$$\Phi_{\mathrm{z}_i}(k) = \Big[T_{\mathrm{sa}_i}(k-1), e_{\mathrm{z}_i}(k-1), T_{\mathrm{z}_i}{}^{\mathrm{ref}}, T_{\mathrm{z}_j}(k-1),\ T_{\mathrm{amb}}(k-1), 1\Big]^\top. \tag{10.56c}$$

Using the adaptive algorithm that is described in (10.54) on the aforementioned model, we extract the controller gains as follows:

$$K_{\mathrm{z,e}_i}(k) = \frac{\theta_{\mathrm{z}_{1,i}}(k)}{\theta_{\mathrm{z}_{0,i}}(k)},\quad K_{\mathrm{z}_i}(k) = \frac{\theta_{\mathrm{z}_{2,i}}(k)}{\theta_{\mathrm{z}_{0,i}}(k)},\quad K_{\mathrm{z},i,j}(k) = \frac{\theta_{\mathrm{z}_{3,i,j}}(k)}{\theta_{\mathrm{z}_{0,i}}(k)},\quad K_{\mathrm{z,amb}_i}(k) = \frac{\theta_{\mathrm{z}_{4,i}}(k)}{\theta_{\mathrm{z}_{0,i}}(k)},\quad K_i(k) = \frac{\theta_{\mathrm{z}_{5,i}}(k)}{\theta_{\mathrm{z}_{0,i}}(k)}. \tag{10.57}$$

Adaptive supply air control

Supply air temperature tracking error dynamics given in (10.8) can be re-written in the following form, using (10.52b):

$$e_{\mathrm{sa}_i}(k+1) + T^{\mathrm{ref}}_{\mathrm{sa}_i}(k+1) - \check{A}^d_{\mathrm{sa}_i} e_{\mathrm{sa}_i}(k) - T^{\mathrm{ref}}_{\mathrm{sa}_i}(k) = B^d_{\mathrm{sa}_i}\Bigg[T_{\mathrm{c}_i}(k) + K^*_{\mathrm{sa,e}_i} e_{\mathrm{sa}_i}(k) + K^*_{\mathrm{sa}_i} T^{\mathrm{ref}}_{\mathrm{sa}_i}(k) + K^*_{\mathrm{sa,z}_i} T_{\mathrm{z}_i}(k) + K^*_{\mathrm{sa,amb}_i} T_{\mathrm{amb}}(k) + K^*_{\mathrm{f}_i}\Bigg]. \tag{10.58}$$

Expressing (10.58) as the linear parametric model presented in (10.53), we have the following expressions:

$$z_{\mathrm{sa}_i}(k) = e_{\mathrm{sa}_i}(k) + T^{\mathrm{ref}}_{\mathrm{sa}_i}(k) - \check{A}^d_{\mathrm{sa}_i} e_{\mathrm{sa}_i}(k-1) - T^{\mathrm{ref}}_{\mathrm{sa}_i}(k-1), \tag{10.59a}$$

$$\begin{aligned}\Theta^*_{\mathrm{sa}_i} &= \Big[B^d_{\mathrm{sa}_i},\ B^d_{\mathrm{sa}_i} K^*_{\mathrm{sa,e}_i},\ B^d_{\mathrm{sa}_i} K^*_{\mathrm{sa}_i},\ B^d_{\mathrm{sa}_i} K^*_{\mathrm{sa,z}_i},\ B^d_{\mathrm{sa}_i} K^*_{\mathrm{sa,amb}_i}, B^d_{\mathrm{sa}_i} K^*_{\mathrm{f}_i}\Big]^\top,\\ &= \Big[\theta^*_{\mathrm{sa}_{0,i}},\ \theta^*_{\mathrm{sa}_{1,i}},\ \theta^*_{\mathrm{sa}_{2,i}},\ \theta^*_{\mathrm{sa}_{3,i}},\ \theta^*_{\mathrm{sa}_{4,i}},\ \theta^*_{\mathrm{sa}_{5,i}}\Big]^\top,\end{aligned} \tag{10.59b}$$

$$\Phi_{\mathrm{sa}_i}(k) = \Big[T_{\mathrm{c}_i}(k-1), e_{\mathrm{sa}_i}(k-1), T^{\mathrm{ref}}_{\mathrm{sa}_i}(k-1), T_{\mathrm{z}_i}(k-1), T_{\mathrm{amb}}(k-1), 1\Big]^\top. \tag{10.59c}$$

Using the adaptive law that is described in (10.54), we extract the controller gains as follows:

$$K_{\mathrm{sa},\mathrm{e}_i}(k) = \frac{\theta_{\mathrm{sa}_{1,i}}(k)}{\theta_{\mathrm{sa}_{0,i}}(k)}, \quad K_{\mathrm{sa}_i}(k) = \frac{\theta_{\mathrm{sa}_{2,i}}(k)}{\theta_{\mathrm{sa}_{0,i}}(k)}, \quad K_{\mathrm{sa},\mathrm{z}_i}(k) = \frac{\theta_{\mathrm{sa}_{3,i}}(k)}{\theta_{\mathrm{sa}_{0,i}}(k)},$$
$$K_{\mathrm{sa},\mathrm{amb}_i}(k) = \frac{\theta_{\mathrm{sa}_{4,i}}(k)}{\theta_{\mathrm{sa}_{0,i}}(k)}, \quad K_{\mathrm{f}_i}(k) = \frac{\theta_{\mathrm{sa}_{5,i}}(k)}{\theta_{\mathrm{sa}_{0,i}}(k)}. \tag{10.60}$$

Adaptive coil water control

We re-write coil water temperature tracking error dynamics of (10.15) using (10.52c) in the following form:

$$e_{\mathrm{c}_i}(k+1) + T^{\mathrm{ref}}_{\mathrm{c}_i}(k+1) - \check{A}^d_{\mathrm{c}_i} e_{\mathrm{c}_i}(k) - T^{\mathrm{ref}}_{\mathrm{c}_i}(k) = B^d_{\mathrm{c}_i}\left[u(k) + K^*_{\mathrm{c},\mathrm{e}_i} e_{\mathrm{c}_i}(k) + K^*_{\mathrm{c}_i} T^{\mathrm{ref}}_{\mathrm{c}_i}(k) + K^*_{\mathrm{c},\mathrm{sa}_i} T_{\mathrm{sa}_i}(k)\right]. \tag{10.61}$$

Then, we can express (10.61) as the linear parametric model given in (10.53), where:

$$z_{\mathrm{c}_i}(k) = e_{\mathrm{c}_i}(k) + T^{\mathrm{ref}}_{\mathrm{c}_i}(k) - \check{A}^d_{\mathrm{c}_i} e_{\mathrm{c}_i}(k-1) - T^{\mathrm{ref}}_{\mathrm{c}_i}(k-1), \tag{10.62a}$$

$$\begin{aligned}\Theta^*_{\mathrm{c}_i} &= \left[B^d_{\mathrm{c}_i},\ B^d_{\mathrm{c}_i} K^*_{\mathrm{c},\mathrm{e}_i},\ B^d_{\mathrm{c}_i} K^*_{\mathrm{c}_i},\ B^d_{\mathrm{c}_i} K^*_{\mathrm{c},\mathrm{sa}_i}\right]^\top, \\ &= \left[\theta^*_{\mathrm{c}_{0,i}},\ \theta^*_{\mathrm{c}_{1,i}},\ \theta^*_{\mathrm{c}_{2,i}},\ \theta^*_{\mathrm{c}_{3,i}}\right]^\top,\end{aligned} \tag{10.62b}$$

$$\Phi_{\mathrm{c}_i}(k) = \left[u(k-1), e_{\mathrm{c}_i}(k-1), T^{\mathrm{ref}}_{\mathrm{c}_i}(k-1), T_{\mathrm{sa}_i}(k-1)\right]^\top, \tag{10.62c}$$

and

$$u_{\mathrm{c}_i}(k) = \dot{m}_{\mathrm{c}_i}(k)\left(T_{\mathrm{st}}(k) - T_{\mathrm{c}_i}(k)\right). \tag{10.63}$$

By applying the adaptive algorithm that is described by eq. (10.54), we extract the controller gains as follows:

$$K_{\mathrm{c},\mathrm{e}_i}(k) = \frac{\theta_{\mathrm{c}_{1,i}}(k)}{\theta_{\mathrm{c}_{0,i}}(k)}, \quad K_{\mathrm{c}_i}(k) = \frac{\theta_{\mathrm{c}_{2,i}}(k)}{\theta_{\mathrm{c}_{0,i}}(k)}, \quad K_{\mathrm{c},\mathrm{sa}_i}(k) = \frac{\theta_{\mathrm{c}_{3,i}}(k)}{\theta_{\mathrm{c}_{0,i}}(k)}. \tag{10.64}$$

Stability properties of distributed adaptive scheme

The combination of AHU's components creates a cascade system for each thermal zone and all cascade systems form a network of cascade subsystems (see Fig. 10.1). The proposed distributed control input is formed by (10.52a), (10.52b) and (10.52c) where all controller gains are estimated using the adaptive algorithm (10.54) is stable and guarantees that air temperature tracking error for all zones will converge to zero, as summarized in the following theorem:

Theorem 4. *Consider the overall closed-loop system composed of the N subsystems* (10.1), (10.8) *and* (10.15) *using the control scheme* (10.52a), (10.52b), (10.52c) *and controller gains* (10.57), (10.60), (10.64). *For constant* Q_i, $e_{\mathrm{z}_i} \in l_\infty$ *and* e_{z_i} *converges to zero as* $t \to \infty$, *for all* $i \in \mathcal{N} = \{1, \ldots, N\}$.

Proof. Let us define the following signal that is composed of all tracking errors of the overall system:

$$\mu_f^2(k) = 1 + \sum_{i=1}^{N} \left\|(e_{z_i})_{k-1}\right\|_{2\delta}^2 + \sum_{i=1}^{N} \left\|(e_{sa_i})_{k-1}\right\|_{2\delta}^2 + \sum_{i=1}^{N} \left\|(e_{c_i})_{k-1}\right\|_{2\delta}^2, \tag{10.65}$$

where $\|(\cdot)_k\|_{2\delta}$ is the $l_{2\delta}$ norm for some $\delta \in (A_d^2, 1]$, so that $\frac{1}{\sqrt{\delta}z+A_d}$ has stable poles and $A_d = \max_{\forall i \in \mathcal{N}}(|\check{A}_{z_i}^d|, |\check{A}_{sa_i}^d|, |\check{A}_{c_i}^d|)$.

Next, we want to bound these tracking errors with respect to signal μ_f. For this, we can re-write the zone air temperature tracking error dynamics using (10.54c), (10.54d) and (10.56a) as follows:

$$e_{z_i} = \frac{z}{z - \check{A}_{z_i}^d}[\epsilon_{z_i}\mu_{z_i}^2] \tag{10.66}$$

In addition, from the definition of m_{z_i}, we derive the following inequality:

$$\mu_{z_i}^2(k) \leq 1 + T_s\lambda_{max}(\Gamma_{z_i})|\Phi_{z_i}(k)|^2 \tag{10.67}$$

and for the elements of Φ_{z_i}, as described in (10.56c), we have that for some finite $c > 0$, $T_{amb}, T_{z_i}^{ref} \in l_\infty$,

$$|T_{z_i}(k-1)| \leq |e_{z_i}(k-1)| + c, \tag{10.68}$$

$$|T_{sa_i}(k-1)| \leq |e_{sa_i}(k-1)| + |T_{sa_i}^{ref}(k-1)|, \tag{10.69}$$

and from (10.52a):

$$\begin{aligned} |T_{sa_i}^{ref}(k)| &\leq c|e_{z_i}(k)| + c|T_{z_i}(k)| + c\sum_{j\in\mathcal{N}_i}|T_{z_j}(k)| + c|T_{amb}(k)| + c, \\ &\leq c + c|e_{z_i}(k)| + c\sum_{j\in\mathcal{N}_i}|e_{z_j}(k)|, \end{aligned} \tag{10.70}$$

since the application of projection in the adaptive algorithm guarantees that $\Theta_{z_i} \in l_\infty$ and all zone controller gains in (10.57) are bounded. In addition, using Lemma A.12.33.ii of [64] and considering $H(z) = 1$, we have that $|e_i(k)| \leq \left\|e_{i_k}\right\|_{2\delta}$. Therefore,

$$|\Phi_{z_i}(k)| \leq c + \left\|(e_{z_i})_{k-1}\right\|_{2\delta}^2 + c\sum_{j\in N_i}\left\|\left(e_{z_j}\right)_{k-1}\right\|_{2\delta}^2 + \left\|(e_{sa_i})_{k-1}\right\|_{2\delta}^2, \tag{10.71}$$

That means that the signal μ_{z_i} is bounded by the signal μ_f as follows:

$$\mu_{z_i} \leq c\mu_f, \tag{10.72}$$

for some finite $c > 0$.

Applying Lemma A.12.33 from [64] and since $\frac{z}{z-\check{A}_{z_i}^d}$ is analytic in $|z| \geq \sqrt{\delta}$, equation (10.66) gives the following inequality for some finite $c > 0$:

$$\left\|(e_{z_i})_{k-1}\right\|_{2\delta} \leq c\left\|\left(\epsilon_{z_i}\mu_{z_i}^2\right)_{k-1}\right\|_{2\delta} \tag{10.73}$$

which, combined with inequality (10.72), produces the following inequality:

$$\left\|(e_{z_i})_{k-1}\right\|_{2\delta} \leq c \left\|\left(\epsilon_{z_i}\mu_{z_i}\mu_f\right)_{k-1}\right\|_{2\delta} \tag{10.74}$$

Similarly, we can re-write the supply air temperature tracking error dynamics using (10.54c), (10.54d) and (10.59a) as follows:

$$e_{sa_i} = \frac{z}{z - \check{A}^d_{sa_i}}\left[\epsilon_{sa_i}\mu^2_{sa_i}\right] - \frac{z-1}{z - \check{A}^d_{sa_i}}\left[T^{ref}_{sa_i}\right] \tag{10.75}$$

In addition, from the definition of μ_{sa_i}, we derive the following inequality:

$$\mu^2_{sa_i}(k) \leq 1 + T_s\lambda_{max}(\Gamma_{sa_i})|\Phi_{sa_i}(k)|^2 \tag{10.76}$$

and for the elements of Φ_{sa_i}, as described in (10.59c), we have that for some finite $c > 0$, $T_{amb} \in l_\infty$,

$$|T_{c_i}(k-1)| \leq |e_{c_i}(k-1)| + |T^{ref}_{c_i}(k-1)|, \tag{10.77}$$

and from (10.52b):

$$\begin{aligned} |T^{ref}_{c_i}(k)| &\leq c|e_{sa_i}(k)| + c|T_{sa_i}(k)| + c|T_{z_i}(k)| + c|T_{amb}(k)| + c \\ &\leq c|e_{sa_i}(k)| + c|T^{ref}_{sa_i}(k)| + c|e_{z_i}(k)| + c \\ &\leq c|e_{sa_i}(k)| + c|e_{z_i}(k)| + c\sum_{j\in\mathcal{N}_i}|e_{z_j}(k)| + c \end{aligned} \tag{10.78}$$

in addition to eq. (10.68) and (10.69), since the projection that is incorporated in the adaptive algorithm guarantees that $\Theta_{sa_i} \in l_\infty$ and all supply air controller gains in (10.60) are bounded.

In addition, using again Lemma A.12.33.ii of [64] with $H(z) = 1$, we have that

$$|\Phi_{sa_i}(k)| \leq c + \left\|(e_{z_i})_{k-1}\right\|^2_{2\delta} + c\sum_{j\in N_i}\left\|\left(e_{z_j}\right)_{k-1}\right\|^2_{2\delta} + c\left\|(e_{sa_i})_{k-1}\right\|^2_{2\delta} + c\left\|(e_{c_i})_{k-1}\right\|^2_{2\delta} \tag{10.79}$$

That means that the signal μ_{sa_i} is bounded by the signal μ_f as follows:

$$\mu_{sa_i} \leq c\mu_f \tag{10.80}$$

for some finite $c > 0$.

Applying Lemma A.12.33 from [64] and since $\frac{z}{z-\check{A}^d_{sa_i}}$ and $\frac{z-1}{z-\check{A}^d_{sa_i}}$ are analytic in $|z| \geq \sqrt{\delta}$, equation (10.75) gives the following inequality for some finite $c > 0$:

$$\begin{aligned} \left\|(e_{sa_i})_{k-1}\right\|_{2\delta} &\leq c\left\|\left(\epsilon_{sa_i}\mu^2_{sa_i}\right)_{k-1}\right\|_{2\delta} + c\left\|\left(T^{ref}_{sa_i}\right)_{k-1}\right\|_{2\delta} \\ &\leq c + c\left\|\left(\epsilon_{sa_i}\mu^2_{sa_i}\right)_{k-1}\right\|_{2\delta} + c\left\|(e_{z_i})_{k-1}\right\|_{2\delta} + c\sum_{j\in\mathcal{N}_i}\left\|\left(e_{z_j}\right)_{k-1}\right\|_{2\delta} \end{aligned} \tag{10.81}$$

since

$$\begin{aligned} \left\|\left(T^{ref}_{sa_i}\right)_{k-1}\right\|_{2\delta} &\leq c + c\left\|(e_{z_i})_{k-1}\right\|_{2\delta} + c\left\|(T_{z_i})_{k-1}\right\|_{2\delta} + c\sum_{j\in\mathcal{N}_i}\left\|\left(T_{z_j}\right)_{k-1}\right\|_{2\delta} + c\left\|(T_{amb})_{k-1}\right\|_{2\delta} \\ &\leq c + c\left\|(e_{z_i})_{k-1}\right\|_{2\delta} + c\sum_{j\in\mathcal{N}_i}\left\|\left(e_{z_j}\right)_{k-1}\right\|_{2\delta} \end{aligned} \tag{10.82}$$

By combining inequalities (10.80) and (10.81), the following inequality is produced:

$$\left\|(e_{\mathrm{sa}_i})_{k-1}\right\|_{2\delta} \leq c + c\left\|\left(\epsilon_{\mathrm{sa}_i}\mu_{\mathrm{sa}_i}\mu_f\right)_{k-1}\right\|_{2\delta} + c\left\|\left(\epsilon_{\mathrm{z}_i}\mu_{\mathrm{z}_i}\mu_f\right)_{k-1}\right\|_{2\delta} + c\sum_{j\in\mathcal{N}_i}\left\|\left(\epsilon_{\mathrm{z}_j}\mu_{\mathrm{z}_j}\mu_f\right)_{k-1}\right\|_{2\delta} \tag{10.83}$$

In a similar way, we re-write the coil water temperature tracking error dynamics using (10.54c), (10.54d) and (10.62a) as follows:

$$e_{\mathrm{c}_i} = \frac{z}{z-\breve{A}^d_{\mathrm{c}_i}}\left[\epsilon_{\mathrm{c}_i}m^2_{\mathrm{c}_i}\right] - \frac{z-1}{z-\breve{A}^d_{\mathrm{c}_i}}\left[T^{\mathrm{ref}}_{\mathrm{c}_i}\right] \tag{10.84}$$

In addition, from the definition of μ_{c_i}, we derive the following inequality:

$$\mu^2_{\mathrm{c}_i}(k) \leq 1 + T_{\mathrm{s}}\lambda_{max}(\Gamma_{\mathrm{c}_i})|\Phi_{\mathrm{c}_i}(k)|^2 \tag{10.85}$$

and for the elements of Φ_{c_i}, as described in (10.62c), from eq. (10.63) and (10.18), we have that for some finite $c > 0$:

$$\begin{aligned}
|u(k)| &= |\dot{m}_{\mathrm{c}_i}(k)\left(T_{\mathrm{st}}(k) - T_{\mathrm{c}_i}(k)\right)| \\
&\leq |T_{\mathrm{c}_i}(k)| + |T^{\mathrm{ref}}_{\mathrm{c}_i}(k)| + |T_{\mathrm{sa}_i}(k)| \\
&\leq c + c|e_{\mathrm{c}_i}(k)| + c|e_{\mathrm{sa}_i}(k)| + c|e_{\mathrm{z}_i}(k)| + c\sum_{j\in\mathcal{N}_i}|e_{\mathrm{z}_j}(k)|
\end{aligned} \tag{10.86}$$

in addition to the bounds from equations (10.69), (10.70) and (10.78). The projection operator of the adaptive law guarantees that $\Theta_{\mathrm{c}_i} \in l_\infty$ and, thus, all coil water controller gains in (10.64) are bounded.

In addition, using again Lemma A.12.33.ii of [64] with $H(z) = 1$, we have that

$$|\Phi_{\mathrm{c}_i}(k)| \;\leq\; c + \left\|(e_{\mathrm{z}_i})_{k-1}\right\|^2_{2\delta} + c\sum_{j\in N_i}\left\|\left(e_{\mathrm{z}_j}\right)_{k-1}\right\|^2_{2\delta} + c\left\|(e_{\mathrm{sa}_i})_{k-1}\right\|^2_{2\delta} + c\left\|(e_{\mathrm{c}_i})_{k-1}\right\|^2_{2\delta} \tag{10.87}$$

That means that the signal μ_{c_i} is bounded by the signal μ_f as follows:

$$\mu_{\mathrm{c}_i} \leq c\mu_f \tag{10.88}$$

for some finite $c > 0$.

Applying Lemma A.12.33 from [64] and since $\frac{z}{z-\breve{A}^d_{\mathrm{c}_i}}$ and $\frac{z-1}{z-\breve{A}^d_{\mathrm{c}_i}}$ are analytic in $|z| \geq \sqrt{\delta}$, equation (10.84) gives the following inequality for some finite $c > 0$:

$$\begin{aligned}
\left\|(e_{\mathrm{c}_i})_{k-1}\right\|_{2\delta} &\leq c\left\|\left(\epsilon_{\mathrm{c}_i}\mu^2_{\mathrm{c}_i}\right)_{k-1}\right\|_{2\delta} + c\left\|\left(T^{\mathrm{ref}}_{\mathrm{c}_i}\right)_{k-1}\right\|_{2\delta} \\
&\leq c + c\left\|\left(\epsilon_{\mathrm{c}_i}\mu^2_{\mathrm{c}_i}\right)_{k-1}\right\|_{2\delta} + c\left\|(e_{\mathrm{sa}_i})_{k-1}\right\|_{2\delta} + c\left\|(e_{\mathrm{z}_i})_{k-1}\right\|_{2\delta} + c\sum_{j\in\mathcal{N}_i}\left\|\left(e_{\mathrm{z}_j}\right)_{k-1}\right\|_{2\delta}
\end{aligned} \tag{10.89}$$

since

$$\begin{aligned}
\left\|\left(T^{\mathrm{ref}}_{\mathrm{c}_i}\right)_{k-1}\right\|_{2\delta} &\leq c + c\left\|(e_{\mathrm{sa}_i})_{k-1}\right\|_{2\delta} + c\left\|(T_{\mathrm{sa}_i})_{k-1}\right\|_{2\delta} + c\left\|(T_{\mathrm{z}_i})_{k-1}\right\|_{2\delta} \\
&\leq c + c\left\|(e_{\mathrm{sa}_i})_{k-1}\right\|_{2\delta} + c\left\|\left(T^{\mathrm{ref}}_{\mathrm{sa}_i}\right)_{k-1}\right\|_{2\delta} + c\left\|(e_{\mathrm{z}_i})_{k-1}\right\|_{2\delta} \\
&\leq c + c\left\|(e_{\mathrm{sa}_i})_{k-1}\right\|_{2\delta} + c\left\|(e_{\mathrm{z}_i})_{k-1}\right\|_{2\delta} + c\sum_{j\in\mathcal{N}_i}\left\|\left(e_{\mathrm{z}_j}\right)_{k-1}\right\|_{2\delta}
\end{aligned} \tag{10.90}$$

By combining inequalities (10.88) and (10.89), the following inequality is produced:

$$\begin{aligned}\left\|(e_{c_i})_{k-1}\right\|_{2\delta} \leq & c + c\left\|\left(\epsilon_{c_i}\mu_{c_i}\mu_f\right)_{k-1}\right\|_{2\delta} + c\left\|\left(\epsilon_{sa_i}\mu_{sa_i}\mu_f\right)_{k-1}\right\|_{2\delta} + c\left\|\left(\epsilon_{z_i}\mu_{z_i}\mu_f\right)_{k-1}\right\|_{2\delta} \\ & + c\sum_{j\in\mathcal{N}_i}\left\|\left(\epsilon_{z_j}\mu_{z_j}\mu_f\right)_{k-1}\right\|_{2\delta}\end{aligned} \tag{10.91}$$

Combining relations (10.65), (10.74), (10.83) and (10.91), we derive the following inequality:

$$\mu_f^2(k) \leq c + c\left\|\left(\tilde{g}\mu_f\right)_{k-1}\right\|_{2\delta}^2 \tag{10.92}$$

where

$$\tilde{g}^2 = \sum_{i=1}^{N}|\epsilon_{z_i}\mu_{z_i}|^2 + \sum_{i=1}^{N}|\epsilon_{sa_i}\mu_{sa_i}|^2 + \sum_{i=1}^{N}|\epsilon_{c_i}\mu_{c_i}|^2 \tag{10.93}$$

By applying Lemma A.12.31 from [64] on inequality (10.92) and using the fact that the geometric mean of a series is less than the arithmetic mean, for some finite $c > 0$ we obtain the following inequality:

$$\begin{aligned}\mu_f^2(k) \leq & 1 + c\sum_{p=0}^{k-1}\delta^{k-p}\tilde{g}^2(p)\mu_f^2(p) \\ & \leq 1 + c\sum_{p=0}^{k-1}\left[\delta^{k-p}\tilde{g}^2(p)\prod_{p<q<k}\left(1+\delta^{k-q}\tilde{g}^2(q)\right)\right] \\ & \leq 1 + c\sum_{p=0}^{k-1}\left[\delta^{k-p}\tilde{g}^2(p)\left(1+\frac{\sum_{q=p+1}^{k-1}\delta^{k-q}\tilde{g}^2(q)}{k-p-1}\right)^{k-p-1}\right]\end{aligned} \tag{10.94}$$

From the structure of $\tilde{g}$ it follows that $\tilde{g} \in l_2$. In addition, since $\delta < 1$ we derive the following relation:

$$\begin{aligned}\mu_f^2(k) & \leq 1 + c\sum_{p=0}^{k-1}\left[\delta^{k-p}\tilde{g}^2(p)\left(1+\frac{c}{k-p-1}\right)^{k-p-1}\right] \\ & \leq 1 + c\sum_{p=0}^{k-1}\left[\delta^{k-p}\tilde{g}^2(p)e^c\right]\end{aligned} \tag{10.95}$$

for some finite $c > 0$. Therefore, again since $\tilde{g} \in l_2$ and $\delta < 1$, we conclude that signal we defined in (10.65) is bounded, i.e., $\mu_f \in l_\infty$, since the series in the last inequality converges. Hence, all temperature tracking errors $e_i \in l_\infty$ $\forall i$ are bounded too, due to the definition of μ_f. Hence, all signals $\Phi_i(k), \mu_i \in l_\infty$ are also bounded for all $i \in \mathcal{N}$.

In addition, we have that $z_i = \epsilon_i\mu_i^2 = \epsilon_i\mu_i\mu_i$. Since $\epsilon_i\mu_i \in l_2$ and $\mu_i \in l_\infty$, then $z_i \in l_2$. Thus, ${\Theta_{z_i}^*}^\top\Phi_{z_i} \in l_2$ and ${\Theta_{z_i}^*}^\top\Phi_{z_i} \to 0$ and from

$$e_{z_i} = \frac{z}{z - \check{A}_{z_i}^d}[{\Theta_{z_i}^*}^\top\Phi_{z_i}] \tag{10.96}$$

we have that $e_{z_i} \to 0$.

We also have

$$e_{\mathrm{sa}_i} = \frac{z}{z - \check{A}^d_{\mathrm{sa}_i}} \left[{\Theta^*_{\mathrm{sa}_i}}^\top \Phi_{\mathrm{sa}_i} \right] - \frac{z-1}{z - \check{A}^d_{\mathrm{sa}_i}} \left[T^{\mathrm{ref}}_{\mathrm{sa}_i} \right] \tag{10.97}$$

with ${\Theta^*_{\mathrm{sa}_i}}^\top \Phi_{\mathrm{sa}_i} \in l_2$ and ${\Theta^*_{\mathrm{sa}_i}}^\top \Phi_{\mathrm{sa}_i} \to 0$. For constant T_{amb}, since $e_{z_i} \to 0$, we have that $T^{\mathrm{ref}}_{\mathrm{sa}_i} \to c$, where c is some constant. Thus, $e_{\mathrm{sa}_i} \to 0$.

We also have

$$e_{\mathrm{c}_i} = \frac{z}{z - \check{A}^d_{\mathrm{c}_i}} \left[{\Theta^*_{\mathrm{c}_i}}^\top \Phi_{\mathrm{c}_i} \right] - \frac{z-1}{z - \check{A}^d_{\mathrm{c}_i}} \left[T^{\mathrm{ref}}_{\mathrm{c}_i} \right] \tag{10.98}$$

with ${\Theta^*_{\mathrm{c}_i}}^\top \Phi_{\mathrm{c}_i} \in l_2$ and ${\Theta^*_{\mathrm{c}_i}}^\top \Phi_{\mathrm{c}_i} \to 0$. For constant T_{amb}, since $e_{\mathrm{sa}_i} \to 0$, we have that $T^{\mathrm{ref}}_{\mathrm{c}_i} \to c$, where c is some constant. Thus, $e_{\mathrm{c}_i} \to 0$.

Thus all tracking errors converge to 0. □

Theorem 4 guarantees that zone air temperature can be appropriately regulated for each thermal zone even in the case of system uncertainties, unknown disturbances or changes in system parameters. Heat exchange is taken into account and the control mechanism is able to adapt when zones interaction changes (i.e., opening/closing of doors). It should be noted that the stability and convergence properties of the proposed control scheme do not depend on the size of the system (i.e., number of zones or AHUs).

10.4 Simulation Analysis

In this section the application of the proposed distributed adaptive control scheme to a multi-zone HVAC system is presented and its performance is analyzed and compared to a non-adaptive (nominal control gains) scheme by considering temperature tracking and energy performance.

10.4.1 Building description

The control algorithm is implemented and used to regulate temperature in a prototype primary school building model. The building model is chosen among the ones offered in the suite of ASHRAE Standard 90.1 prototype buildings, which was developed by Pacific Northwest National Laboratory [1]. A 3D plan of the building is presented in Fig. 10.2 and corresponds to the ANSI/ASHRAE/IES Standard 90.1-2016 Primary School model, located in Denver. The building consists of 25 thermal zones that are presented in Table 6.3. The zones have different sizes, their use varies and are physically interconnected via walls and doors. For example, there exist several classrooms, corridors and activity areas, such as the gym or the cafeteria, which correspond to different occupancy patterns and heat loads from equipment and lighting. This implies that each zone may need specialized HVAC equipment to satisfy its needs.

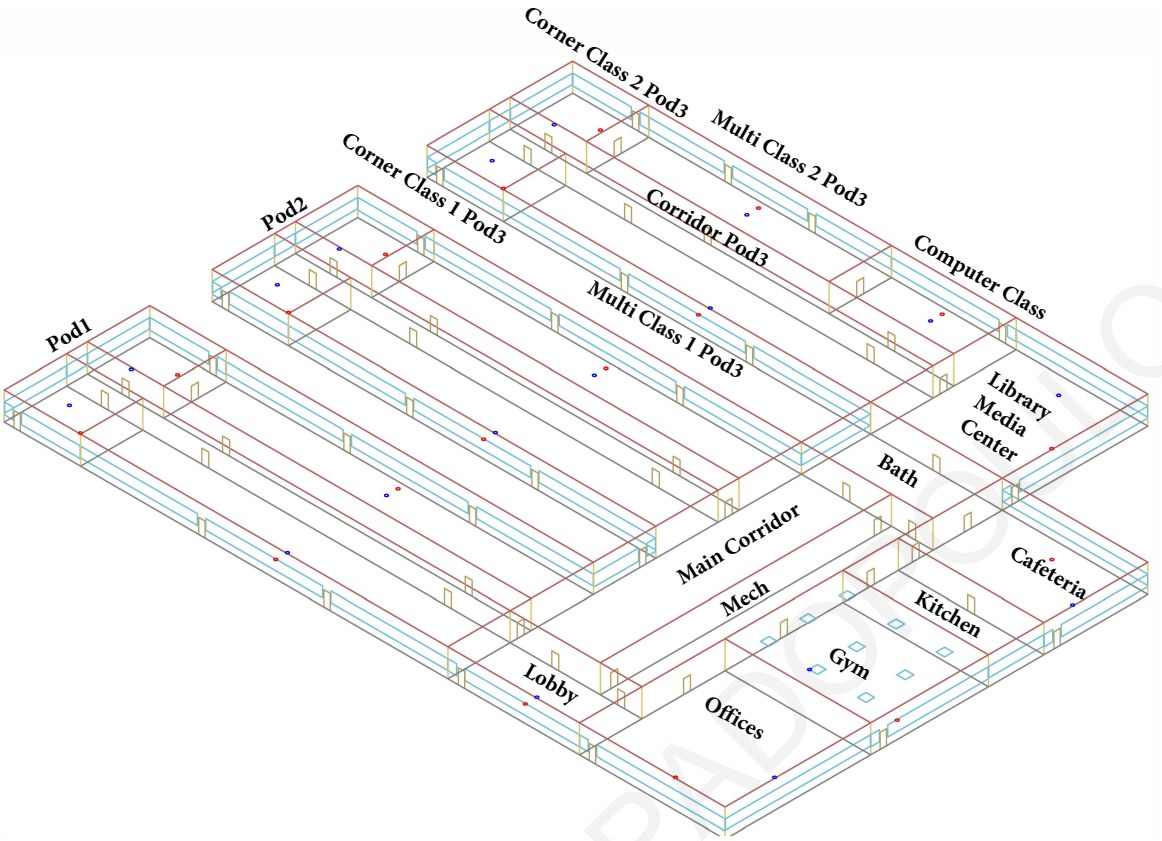

Figure 10.2: 3D plan of the ANSI/ASHRAE/IES Standard 90.1-2016 Primary School.

Each zone has an AHU to provide proper temperature regulation. The AHUs are customized to allow regulation of water mass flow rate $\dot{m}_{c_i}$ through the coil by the proposed controller. Therefore, the Energy Plus input data file (.idf) that describes the building and HVAC system is modified to included the custom AHUs and is provided in the following Github link [2]. The control algorithm is implemented using *Matlab/Simulink*. The overall system with the *EnergyPlus* building and HVAC model and the *Matlab/Simulink* control scheme is co-simulated using the *Buildings Control Virtual Test Bed (BCVTB)*.

10.4.2 Simulation Details

The performance of the HVAC system under the designed controller is simulated for 1 year period using the prototype Denver weather data from *EnergyPlus*. The HVAC system is operating on weekdays, from 6am to 6pm during the winter period and from 7am to 7pm during the summer period. Occupancy schedules are specified for each zone according to its use. In addition, internal and external doors are scheduled to open and close at several times in order to capture the possible changes in the way thermal zones interact with each other. For all zones the desired temperature is selected as $T_z^{\text{ref}} = 23^o\text{C}$. All details about the building and HVAC system size are included in the aforementioned Github link. The sampling time is selected as $T_s = 60s$.

The implementation of the proposed control scheme requires the choice of several design con-

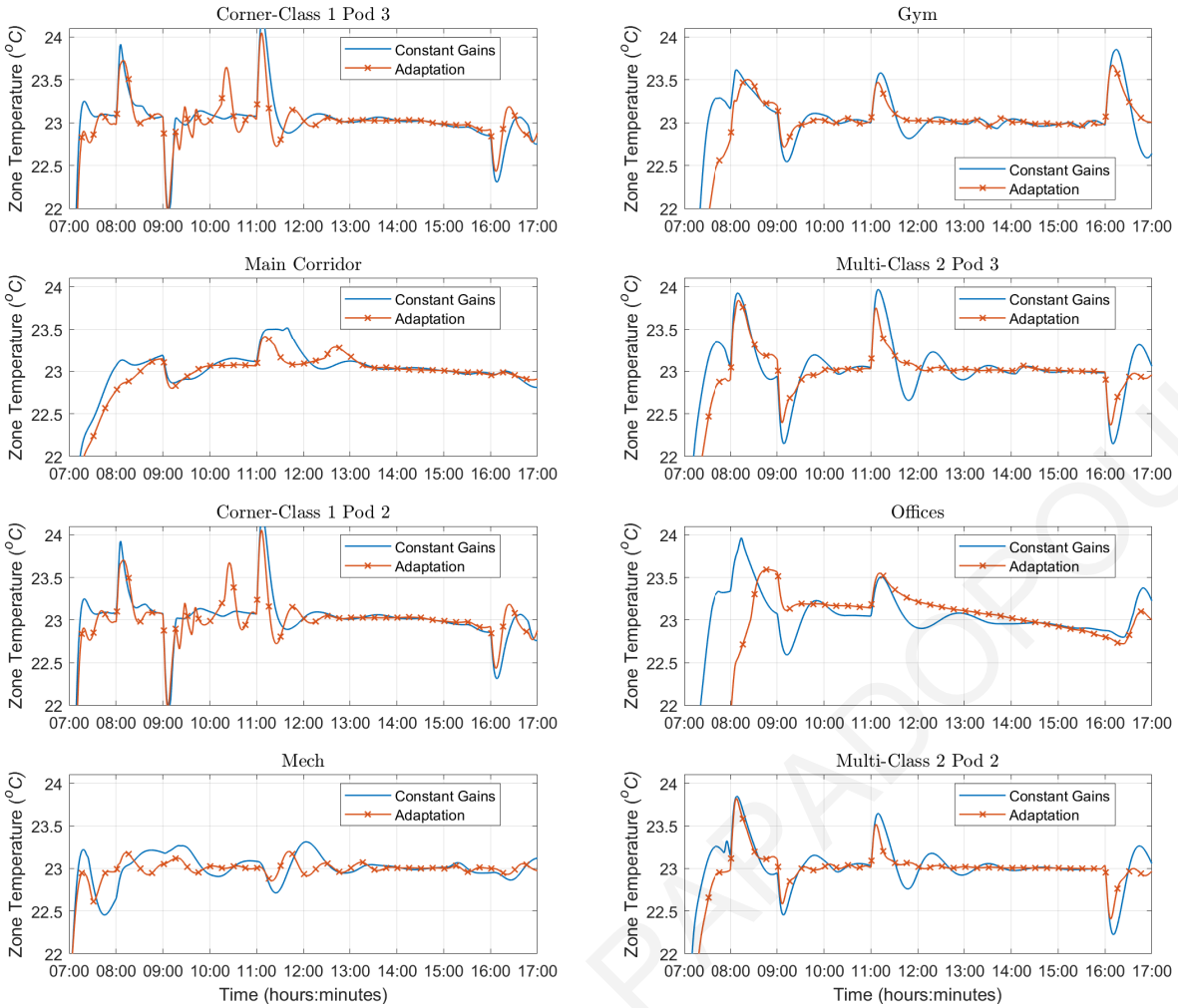

Figure 10.3: Zone air temperature in Celsius for the 1st day of the year with and without adaptation.

Table 10.1: Distributed Adaptive Control design constants.

Variable	Value	Variable	Value
$\breve{A}_{z_i}$	$0.8A_{z_i}$	h_i	0.1
$\breve{A}_{c_{C,i}}$	$1.03 \cdot A_{c_{C,i}}$	$\breve{A}_{c_{H,i}}$	$1.03 \cdot A_{c_{H,i}}$
$\breve{A}_{sa_{C,i}}$	$2.5 \cdot 10^4 \cdot A_{sa_{C,i}}$	$\breve{A}_{sa_{H,i}}$	$2.5 \cdot 10^4 \cdot A_{sa_{C,i}}$
U_{z_i}	$1 \cdot \lvert\Gamma_{z_i}\rvert$	L_{z_i}	$[0.001\ -1 \cdot \lvert\Gamma_{z_i}\rvert]$
U_{sa_i}	$1 \cdot \lvert\Gamma_{sa_i}\rvert$	L_{sa_i}	$[0.001\ -1 \cdot \lvert\Gamma_{sa_i}\rvert]$
U_{c_i}	$1 \cdot \lvert\Gamma_{c_i}\rvert$	L_{c_i}	$[0.001\ -1 \cdot \lvert\Gamma_{c_i}\rvert]$

Variable	Value
Γ_{z_i}	$\text{diag}(0.9 \cdot 10^{-7} \cdot B^d_{z_i} \cdot [1\ K^*_{z,e_i}\ K^*_{z_i}\ K^*_{z,i,j}\ K^*_{z,amb_i}\ h_i])$
Γ_{sa_i}	$\text{diag}(1 \cdot 10^{-9} \cdot B^d_{sa_i} \cdot [1\ K^*_{sa,e_i}\ K^*_{sa_i}\ K^*_i\ K^*_{sa,amb_i}\ K^*_{f_i}])$
Γ_{c_i}	$\text{diag}(1 \cdot 10^{-9} \cdot (B^d_{c_i} \cdot [1\ K^*_{c,e_i}\ K^*_{c_i}\ K^*_{c,sa_i}])$
$\Theta(0)$	Θ^* for all equipment

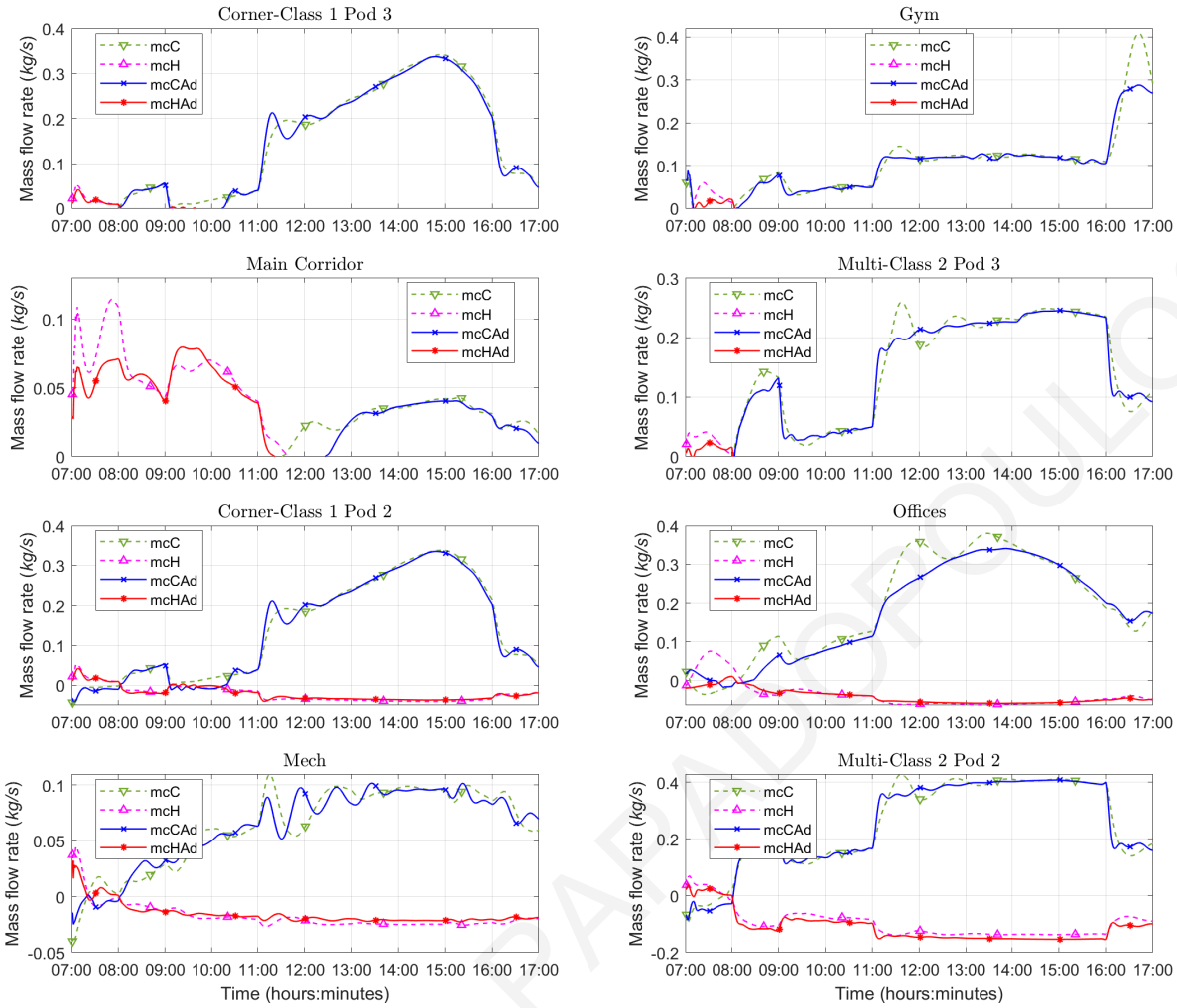

Figure 10.4: Water mass flow rate for coils for the 1st day of the year with and without adaptation.

stants, such as the closed loop poles of each AHU and the learning rates of the adaptive laws. Table 10.1 presents the choices for all design constants. The closed loop poles are chosen to guarantee stability as well as avoid undesired performance behavior, such as system oscillations. Learning rates are chosen to reflect/compensate the possible change rates of system parameters and disturbances. It should be noted that the initial values for the controller gains in the adaptive algorithm are chosen to be equal to the nominal values of such gains, in order to make use of any prior knowledge of the system. Projection bounds are chosen as conservative bounds for the gains to be estimated.

For comparison purposes, two versions of the distributed control scheme have been implemented, one with adaptation of controller gains and one without. Both are implemented in *Matlab/Simulink* and are connected to the *EnergyPlus* model using *BCVTB*.

10.4.3 Simulation Results

The proposed distributed adaptive control scheme is able to regulate temperature satisfactorily in all building zones, while overcoming changes in weather conditions, occupancy or internal heat loads as well as changes in zone interactions due to doors. The impact of adaptation is illustrated by using the

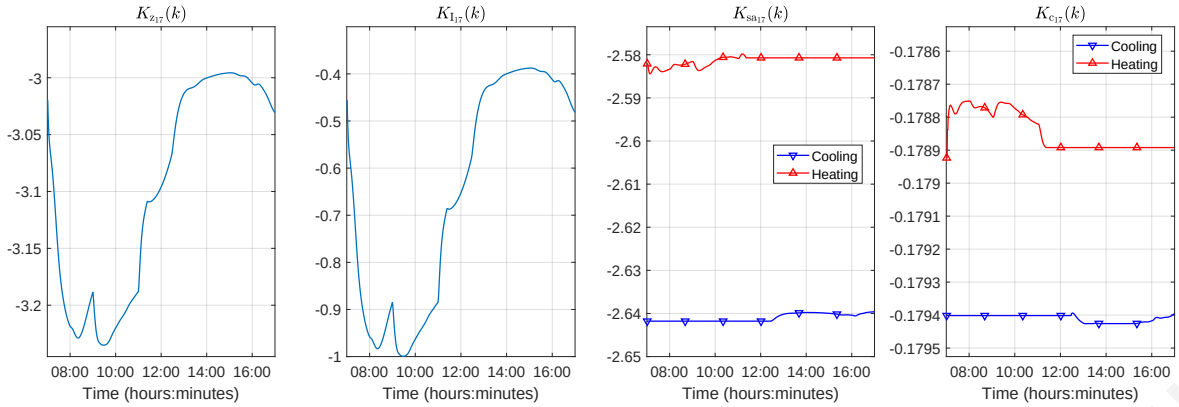

Figure 10.5: Adaptive control gains for the zone 17.

following two metrics, which correspond to the change in tracking error and consumed energy when adaptation is included:

$$\epsilon_z = \sum_{i \in N} \frac{(\sum_{k=0}^{24T_s} |\widetilde{e}_{z_i}(k)| - \sum_{k=0}^{24T_s} |e_{z_i}(k)|)}{\sum_{k=0}^{24T_s} |e_{z_i}(k)|}, \tag{10.99}$$

$$\epsilon_E = \sum_{i \in N} \frac{(\sum_{k=0}^{24T_s} |\widetilde{E}_{c_i}(k)| - \sum_{k=0}^{24T_s} |E_{c_i}(k)|)}{\sum_{k=0}^{24T_s} |E_{c_i}(k)|}, \tag{10.100}$$

where e_{z_i} denotes the zone air temperature tracking error when there exists no adaptation and E_{c_i} is the consumed energy that passes from the storage tank to the coil when there exists no adaptation. On the other hand $\widetilde{e}_{z_i}$ denotes the zone air temperature tracking error when gain adaptation is used and $\widetilde{E}_{c_i}$ is the consumed energy that passes from the storage tank to the coil when gain adaptation is used. For this particular selection of design constants the proposed distributed adaptive control scheme achieves $\epsilon_z = 9.93\%$ reduction of the overall zone air temperature tracking error and $\epsilon_E = 3\%$ improvement in overall energy usage for the 1 year period.

Fig. 10.3 shows the absolute air temperature tracking error $|e_{z_i}|$ using the nominal control gains (dark solid line) and using the adaptive control gains (gray dashed line), for all thermal zones during an indicative one day period. As it is shown in the figure, the adaptive scheme achieves satisfactory and better overall temperature tracking compared to a non-adaptive scheme, as zone air temperature approaches closer and faster the desired value even when changes or disturbances occur. The control inputs for the same day are presented in Fig. 10.4. Since the control algorithm allows communication between zones and also reacts when zones interactions or system parameters change, it is able to properly allocate heat energy through the building. The introduction of adaptation results in the valve controllers to pass less water and thus less energy to the coils, reducing energy consumption. It should be noted that since the algorithm is load-based, the AHUs switch from the operation of the cooling coil to the operation of the heating coil and vice versa automatically, as indicated by the valve controllers.

Figure 10.5 shows the adaptation of control gains $K_{z_{17}}, K_{I_{17}}, K_{sa_{17}}, K_{c_{17}}$ of the underlying controllers (zone control, supply air control and coil's water flow control) for the Main Corridor zone

(No. 17). As shown in the figure, the gains change as there are systems changes and disturbances, with gains $K_{z_{17}}$ and $K_{I_{17}}$ experiencing the bigger changes, as their values are directly connected to interconnections and external disturbances. If we compare gains $K_{sa_{17}}$, $K_{c_{17}}$ in Fig. 10.5 with the control input of Main Corridor in Fig. 10.3, we can observe that the adaptive gains of the coil controllers are updated according to the operation of the AHU (i.e., heating or cooling).

10.5 Conclusion

This chapter proposes a distributed control scheme for Air Handling Units that are composed of Fan Coil Units in multi-zone HVAC systems. Local controllers that are designed based on the cascade structure of FCUs have proven to be able to regulate temperature satisfactorily in every thermal zone. Stability conditions for each thermal zone's controller have been derived and they depend only on the respective zone's dynamics, indicating that the performance of the proposed control methodology does not depend on the size of the building. Introducing adaptation to controller gains has shown to improve temperature tracking as well as energy consumption performance, while retaining stability properties. Simulated application of the proposed control scheme to a large school building has illustrated the satisfactory performance of the distributed cascade control architecture as well as the temperature tracking and energy consumption benefits of adaptive control to system changes and unknown heat loads.

Chapter 11

Conclusions and Future Research

11.1 Conclusions and Impact

Smart buildings utilize innovative and advance technology to create an intelligent indoor environment that improves the living conditions of occupants and increases the performance in large-scale buildings. Heating, ventilation, and air-conditioning (HVAC) systems have the primary role in indoor comfort and account the larger amount of energy use in buildings. However, due to the high complexity, large scale and variety of HVAC systems, monitoring and control them is a challenging and complicate task. Large-scale HVAC systems employ a vast number of sensing devises (measuring temperature, humidity in several points in the system) and actuating equipment (i.e., valves, fans, ducts) that may fail. Due to the complexity, strong physical interconnections and cyber-physical connectivity (due to advanced distributed control algorithms), faults effects can propagate, making it difficult to diagnosed (i.e, captured, isolated and identified) them. Moreover, the modeling uncertainty caused by the unknown disturbances (i.e., occupancy, solar gain, openings of door, etc.) and equipment performance degradation, requires advanced monitoring and control algorithms. The objective of this doctoral thesis is to propose a range of distributed monitoring and control methodologies of smart buildings in a model-based fault diagnosis and accommodation framework.

The main contribution of this thesis, with respect to the existing technology for monitoring and control of buildings, is the development of distributed, model-based fault diagnosis, accommodation and control algorithms, enhanced with (i) improved performance with respect to detectability, isolability and tracking, (ii) scalability, (iii) adaptability, (iv) robustness, and (v) reliability. All the aforementioned advantages of the proposed distributed monitoring and control methods are essential for the HVAC systems due to their profound impact on management, maintenance and operational cost of large-scale buildings and since HVAC system's operation can affect the health and productivity of occupants.

Network Configuration and Distributed Fault Detection

Firstly, the configuration of the complex HVAC system's dynamics into a network of physically interconnected subsystems, allows the design of monitoring and control algorithms in a distributed manner that feature the aforementioned advantages. The distributed monitoring algorithms involve the diagnosis (i.e., detection, isolation, identification) of sensor and actuator faults. The backbone of the distributed fault diagnosis algorithms relies on the development of distributed monitoring agents that can exchange information in real-time within their neighborhood, in order to monitor the behavior of the physical subsystems (i.e., building zones, AHUs, heating and cooling units, etc). Specifically, each fault diagnosis (FD) agent, collects input and output signals from local and neighboring subsystems to estimate on-line the temperature (i.e., state) of underlying (local) subsystem by using the nonlinear model of each monitored subsystem. The detection decision that is responsible to captures the presence of unknown faults, is based on analytical redundancy relations (ARRs), that are formed of residuals and adaptive thresholds. The residual corresponds to the difference between measured and estimated temperature (i.e., state), while the adaptive threshold is calculated to bound its corresponding residual, under healthy conditions, considering bounded modeling uncertainty and sensor noise. The violation of the ARR in each FD agent triggers the local detection signal from "0" to "1". Each local ARR can be violated from the local (sensor and/or actuator) faults and/or by sensor faults from the neighboring subsystems, due to the exchange of information between the neighboring FD agents. Hence, up to this point the algorithm can detects in the presence of a fault, but it can not infer the location, type or characteristics of the faults. The utilization of adaptive thresholds ensures the robustness of the proposed method against modeling uncertainties and measurement noise, avoiding false alarms that can distract the occupants and also be deceptive in emergency situations.

Distributed Sensor Fault Isolation

In the case of sensor faults, the isolation process that aims to reveal the location of faults is formulated as follows. In each FD agent a binary decision logic is formed by collecting the local and neighboring detection signals. The collection of local and neighboring detection signals constitutes the local observed decision signal. Each observed decision signal is compared with a set of theoretical decision patterns that are created based on a local sensor fault signature matrix. The sensor fault signature matrix is formed with local and neighboring ARRs and all possible combination of sensor faults that can affect the local ARR, where "1" means that the ARR can be violated by the corresponding sensor fault combination, "0" means that the ARR maybe can be violated by the corresponding sensor fault combination due to exchange of sensor data from the neighboring FD agents, and "0" when the ARR can not be violated. If the observed pattern agrees with a single theoretical pattern, then we can declare the location of the sensor fault. Alternatively, this isolation process can indicates the possible

location of the sensor fault or to create a smaller set of possible sensor faults. This can improve the maintenance time of the operative staff.

Distributed Fault Identification

The detection algorithm inside each FD agent can capture the presence of both local sensor and actuator faults. This thesis proposes two methodologies to identify the type of the fault (i.e., determine if the local detection signal is triggered either due to the presence of a local sensor, or due to the presence of a local actuator fault, or both). The proposed distributed fault identification methodologies are based on: (i) an adaptive estimation scheme and (ii) a dedicated observer scheme. In the former, two adaptive estimation schemes are designed within each FD agent such that the one adaptive estimation scheme is designed to estimate the magnitude of a local actuator fault, while the other adaptive estimation scheme is designed to estimate the magnitude of a local sensor fault. The latter identification method is based on a dedicated observer scheme in which a dedicated observer is designed for each one of the AHU's components; zone, supply air, cooling coil and heating coil. For each local FD agent, a set of ARRs is formulated i.e., one for each component. Following the same design procedure as in the case of sensor fault isolation logic, a local fault signature matrix is formed that can determine the type of fault(s). The aforementioned fault isolation and identification algorithms can reduce dramatically the maintenance time and consequently, this can prevent the excess waste of energy and the formation of uncomfortable conditions within the building that can be caused until the recovery from a faulty operation.

Distributed Sensor Fault Accommodation

Taking into account, the fault diagnosis decisions, a number of distributed fault accommodation methodologies are proposed in this thesis that aim to alleviate the effects of sensor faults. Specifically, three distributed fault accommodation methods are proposed using: (i) a virtual sensor (VS) scheme, (ii) control reconfiguration (CR) scheme and (iii) fault tolerant control (FTC) scheme for preserving the indoor thermal conditions. All proposed distributed fault accommodation methodologies are activated when sensor faults are isolated. The VS scheme can be applied in cases where the knowledge of or access of the nominal controller in not available, while both CR and FTC schemes are based on the design of the controller. The VS and CR scheme use the model of the underlying subsystem to reconstruct the unknown fault function, while in the case of FTC scheme the control gains of the nominal control are modified in order to keep the actual temperature in each zone to remain within the desired temperature set in both healthy and faulty sensor measurements. The aforementioned fault accommodation methodologies can provide compensation of the sensor faults effects during the operation of the system and at the same time with causing violation of occupant's thermal comfort, that can have a indirect impact to their productivity and health.

Distributed Adaptive Control

Finally, this thesis proposes a distributed adaptive control method that allows on-line update of the feedback control gains. Specifically, a cascade control algorithm is designed for each zone-AHU which allowing an exchange of sensor information with the neighboring zones. With the adaptation, each local controller can compensate the effects due to: (i) the unknown disturbances that represent heat sources produced from openings of doors, occupants and devices, and (ii) the modeling uncertainties produced from equipment degradation and model simplification.

Exploitation Requirements

The implementation of the proposed algorithms requires model calibration and algorithms tuning. The calibration of the multi-zone HVAC model involves the collection of systems parameters; i.e., zone volumes, construction materials, type of HVAC system, electromechanical equipment attributes). The algorithms tuning involves the selection of the design parameters such as (i) the modeling uncertainty bounds, (ii) the measurement noise bounds, (iii) the observer gains, and (iv) the learning rates on the adaptive laws. Furthermore, during the operation, real-time data are required such as the temperature sensor measurements form building zones and the electromechanical part of the HVAC system and control commands (e.g., valve and dumper openings, fan speed, etc.). For the distributed fault diagnosis and accommodation algorithms both outputs and inputs are required, while for the distributed adaptive control method only the outputs are needed.

11.2 Future Research

Many directions for further investigation are rising through the research outcomes of this thesis.

Modeling Uncertainty

In general, dealing with modeling uncertainty in model-based fault diagnosis approaches is a challenging task. An essential assumption in the development of the proposed distributed fault diagnosis algorithms is the uniformly bounded modeling uncertainty $\eta(t)$ by known bound $\overline{\eta}$. However, obtaining a realistic and less conservative bound on the temperature dynamics of HVAC systems can improve the performance the proposed methods and it is an interesting and substantial future research direction. Internet-of-things (IoT) devices in the building sector [97] enables the modeling of unknown heat sources produced from openings of doors or windows, occupants and devices, solar gains from glazing surfaces, etc. However, incorporate all this information it will create a complex model with several switching equations. Furthermore, a proposed model-based fault diagnosis algorithms can be combined with an online learning algorithm during the healthy operation of the HVAC system [73].

Therefore, computing the modeling uncertainty bound is an important aspect in the performance of proposed methods and it should be further examined.

Faults Modeling

As it is been stated in Chapter 1.3, faults in HVAC systems can have several types of behavior. This thesis investigates the performance of the distributed diagnosis and accommodation algorithms in the presence of abrupt and incipient faults. However, more complex fault models can be evaluated e.g. using intelligent approximation algorithms. Some preliminary results on this direction can be found in [128], where a nonlinear fault function can be approximated with linearly parameterized basis functions.

Actuator Fault Accommodation

The diagnosis of both sensor and actuator faults is extensively evaluated throughout this thesis (see Chapter 5–6). However, the fault accommodation algorithms emphasized on the alleviating the effects of sensor faults. Therefore, the development of actuator fault accommodation methods is an essential add-on for a complete monitoring and control package for large-scale buildings.

Performance of Fault Accommodation Methods

A number of sensor fault accommodation algorithms are presented in Chapter 7–9. As discussed in the conclusions, virtual sensor schemes can offer fault accommodation based on a local estimator (i.e., adaptive estimation scheme) and this is suitable when the access or the knowledge of control scheme is not feasible. On the other hand, in a control reconfiguration scheme the knowledge and access of the control scheme is required and hence the fault learning process is executed based on the control design. The comparison of the proposed methods could be made with respect to a number of performance characteristics form classical control (e.g., settling time, overshoot, etc.). The performance comparison of these fault accommodation approaches would be beneficial for the tuning or the selection between the different methodologies. Moreover, the aggregation of the proposed sensor fault accommodation algorithms could improve the fault accommodation performance in comparison to the selection of one of them.

Exploitation

A part of the proposed methods is evaluated using a realistic simulation software *EnergyPlus*, that is developed by US Department of Energy and it can perform a whole building energy simulation used to model energy consumption for HVAC, lighting, plug and process loads. In future, the performance of the proposed monitoring and control algorithms can be evaluated in an actual test-bed

(i.e., two-zone AHU system) or by creating a virtual realistic model of the HVAC building systems using computational fluid dynamics (CFD) tools. Alternatively, the evaluation can be also performed in hybrid test-bed, where a part of the systems in physical and the other part is virtual. Moreover, this direction might give an insight on how to deal with the modeling uncertainty and it can contribute in the applicability of the proposed monitoring and control methods.

Bibliography

[1] Commercial Prototype Building Models. Pacific Northwest National Laboratory operated by BATTELLE for the United States Department of Energy. Available in https://www.energycodes.gov/development/commercial/prototype_models.

[2] Github link for the Input Data Files (IDF). KIOS Research and Innovation CoE. Available in https://github.com/KIOS-Research/ACC2020.

[3] A. Afram and F. Janabi-Sharifi, "Review of modeling methods for HVAC systems," *Applied Thermal Engineering*, vol. 67, no. 1-2, pp. 507–519, 2014.

[4] A. Afram and F. Janabi-Sharifi, "Theory and applications of HVAC control systems–A review of model predictive control (MPC)," *Building and Environment*, vol. 72, pp. 343–355, 2014.

[5] Z. Afroz, G. M. Shafiullah, T. Urmee, and G. Higgins, "Modeling techniques used in building HVAC control systems: A review," pp. 64–84, 2018.

[6] Y. Al horr, M. Arif, M. Katafygiotou, A. Mazroei, A. Kaushik, and E. Elsarrag, "Impact of indoor environmental quality on occupant well-being and comfort: A review of the literature," *International Journal of Sustainable Built Environment*, vol. 5, no. 1, pp. 1–11, 2016.

[7] A. Alajmi and W. El-Amer, "Saving energy by using underfloor-air-distribution (UFAD) system in commercial buildings," *Energy Conversion and Management*, vol. 51, no. 8, pp. 1637–1642, 2010.

[8] J. Álvarez, J. Redondo, E. Camponogara, J. Normey-Rico, M. Berenguel, and P. Ortigosa, "Optimizing building comfort temperature regulation via model predictive control," *Energy and Buildings*, vol. 57, pp. 361–372, 2013.

[9] M. Anderson, M. Buehner, P. Young, D. Hittle, C. Anderson, J. Tu, and D. Hodgson, "MIMO robust control for HVAC systems," *IEEE Transactions on Control Systems Technology*, vol. 16, no. 3, pp. 475–483, 2008.

[10] B. Argüello-Serrano and M. Vélez-Reyes, "Nonlinear control of a heating, ventilating, and air conditioning system with thermal load estimation," *IEEE Transactions on Control Systems Technology*, vol. 7, no. 1, pp. 56–63, 1999.

[11] C. Arslanturk and A. F. Ozguc, "Optimization of a central-heating radiator," *Applied Energy*, vol. 83, no. 11, pp. 1190–1197, 2006.

[12] ASHRAE, "ANSI/ASHRAE Standard 62.1-2007: Ventilation for Acceptable Indoor Air Quality," pp. 1–41, 2007.

[13] S. M. Attaran, R. Yusof, and H. Selamat, "A novel optimization algorithm based on epsilon constraint-RBF neural network for tuning PID controller in decoupled HVAC system," *Applied Thermal Engineering*, vol. 99, no. 1, pp. 613–624, 2016.

[14] A. A. Badran and M. A. Hamdan, "Comparative study for under-floor heating using solar collectors or solar ponds," *Applied Energy*, vol. 77, no. 1, pp. 107–117, 2004.

[15] M. Baranski, J. Fütterer, and D. Müller, "Development of a generic model-Assisted control algorithm for building HVAC systems," *Energy Procedia*, vol. 122, no. 1, pp. 1003–1008, 2017.

[16] M. Baranski, J. Fütterer, and D. Müller, "Distributed exergy-based simulation-assisted control of HVAC supply chains," *Energy and Buildings*, vol. 175, no. 1, pp. 131–140, 2018.

[17] M. Baranski, L. Meyer, J. Fütterer, and D. Müller, "Comparative study of neighbor communication approaches for distributed model predictive control in building energy systems," *Energy*, vol. 182, no. 1, pp. 840–851, 2019.

[18] P. Bayer, D. Saner, S. Bolay, L. Rybach, and P. Blum, "Greenhouse gas emission savings of ground source heat pump systems in europe: A review," *Renewable and Sustainable Energy Reviews*, vol. 16, no. 2, pp. 1256–1267, 2012.

[19] A. Beghi, L. Cecchinato, L. Corso, M. Rampazzo, and F. Simmini, "Process history-based Fault Detection and Diagnosis for VAVAC systems," in *Proceedings of the IEEE International Conference on Control Applications*, 2013, pp. 1165–1170.

[20] F. Behrooz, N. Mariun, M. Marhaban, M. Mohd Radzi, and A. Ramli, "Review of Control Techniques for HVAC Systems—Nonlinearity Approaches Based on Fuzzy Cognitive Maps," *Energies*, vol. 11, no. 495, pp. 1–41, 2018.

[21] S. C. Bengea, P. Li, S. Sarkar, S. Vichik, V. Adetola, K. Kang, T. Lovett, F. Leonardi, and A. D. Kelman, "Fault-tolerant optimal control of a building HVAC system," *Science and Technology for the Built Environment*, vol. 21, no. 6, pp. 734–751, 2015.

[22] M. Blanke, M. Kinnaert, J. Lunze, and M. Staroswiecki, *Diagnosis and Fault-Tolerant Control*, 3rd ed. Springer Berlin Heidelberg, 2016.

[23] M. Bonvini, M. D. Sohn, J. Granderson, M. Wetter, and M. A. Piette, "Robust on-line fault detection diagnosis for HVAC components based on nonlinear state estimation techniques," *Applied Energy*, vol. 124, pp. 156 – 166, 2014.

[24] G. Boracchi, M. Michaelides, and M. Roveri, "Detecting contaminants in smart buildings by exploiting temporal and spatial correlation," in *Proceedings of the IEEE Symposium Series on Computational Intelligence*, 2015, pp. 601–608.

[25] J. E. Braun, "Intelligent building systems-past, present, and future," in *Proceedings of the American Control Conference (ACC)*. IEEE, 2007, pp. 4374–4381.

[26] A. Buonomano, U. Montanaro, A. Palombo, and S. Santini, "Temperature and humidity adaptive control in multi-enclosed thermal zones under unexpected external disturbances," *Energy and Buildings*, vol. 135, pp. 263–285, 2017.

[27] A. Capozzoli, F. Lauro, and I. Khan, "Fault detection analysis using data mining techniques for a cluster of smart office buildings," *Expert Systems with Applications*, vol. 42, no. 9, pp. 4324–4338, 2015.

[28] J. Carreira, H. Madeira, and J. G. Silva, "Assessing the effects of communication faults on parallel applications," in *Proceedings of the International Computer Performance and Dependability Symposium*. IEEE, 1995, pp. 214–223.

[29] W. Chen and J. Li, "Decentralized output-feedback neural control for systems with unknown interconnections," *IEEE Transactions on Systems, Man, and Cybernetics, Part B: Cybernetics*, vol. 38, no. 1, pp. 258–266, 2008.

[30] Y. Chen and L. Lan, "Fault detection, diagnosis and data recovery for a real building heating/cooling billing system," *Energy Conversion and Management*, vol. 51, no. 5, pp. 1015–1024, 2010.

[31] Y. Chen and L. Lan, "Fault detection, diagnosis and data recovery for a real building heating/cooling billing system," *Energy Conversion and Management*, vol. 51, no. 5, pp. 1015–1024, 2010.

[32] P. Cheng, "Heat Transfer in Geothermal Systems," *Advances in Heat Transfer*, vol. 14, pp. 1–105, 1979.

[33] H. Cheung and J. E. Braun, "Development of fault models for hybrid fault detection and diagnostics algorithm: October 1, 2014–may 5, 2015," National Renewable Energy Lab.(NREL), Golden, CO (United States), Tech. Rep., 2015.

[34] M. Cordier, P. Dague, F. Lévy, J. Montmain, M. Staroswiecki, and L. Travé-Massuyès, "Conflicts versus analytical redundancy relations: a comparative analysis of the model based diagnosis approach from the artificial intelligence and automatic control perspectives," *IEEE Transactions on Systems, Man, and Cybernetics, Part B: Cybernetics*, vol. 34, no. 5, pp. 2163–2177, 2004.

[35] T. Darure, J. J. Yame, and F. Hamelin, "Fault-adaptive Control of VAV damper stuck in a Multizone Building," in *Proceedings of the IEEE Conference on Control and Fault-Tolerant Systems (SysTol)*, 2016, pp. 170–176.

[36] L. N. De Barros, M. Lemos, V. Bernal, and J. Wainer, "Model based diagnosis for network communication faults," in *Proceedings of the International Workshop On Artificial Intelligence for Distributed Information Networking*, 1999, pp. 57–62.

[37] M. Du, J. Scott, and P. Mhaskar, "Actuator and sensor fault isolation of nonlinear process systems," *Chemical Engineering Science*, vol. 104, pp. 294–303, 2013.

[38] Z. Du and X. Jin, "Tolerant control for multiple faults of sensors in VAV systems," *Energy Conversion and Management*, vol. 48, no. 3, pp. 764–777, 2007.

[39] Z. Du, X. Jin, and Y. Yang, "Fault diagnosis for temperature, flow rate and pressure sensors in VAV systems using wavelet neural network," *Applied Energy*, vol. 86, no. 9, pp. 1624–1631, 2009.

[40] G. Eleftheriadis and M. Hamdy, "The Impact of Insulation and HVAC Degradation on Overall Building Energy Performance: A Case Study," *Buildings*, vol. 8, no. 23, pp. 1–11, 2018.

[41] Energy Efficiency Office, "Hong Kong energy end-use data," Electrical and Mechanical Services Department (EMSD), The Government of the Hong Kong Special Administrative Region, Tech. Rep., 1999.

[42] G. Evola and V. Popov, "Computational analysis of wind driven natural ventilation in buildings," *Energy and Buildings*, vol. 38, no. 5, pp. 491–501, 2006.

[43] M. Farid and W. J. Kong, "Underfloor heating with latent heat storage," *Proceedings of the Institution of Mechanical Engineers, Part A: Journal of Power and Energy*, vol. 215, no. 5, pp. 601–609, 2001.

[44] J. Farrell and M. Polycarpou, *Adaptive Approximation Based Control: Unifying Neural, Fuzzy and Traditional Adaptive Approximation Approaches*. John Wiley & Sons, 2006, vol. 48.

[45] N. Fernandez, S. Katipamula, W. Wang, Y. Xie, M. Zhao, and C. Corbin, "Impacts of Commercial Building Controls on Energy Savings and Peak Load Reduction," Pacific Northwest National Laboratory, Tech. Rep., 2017.

[46] N. Fernandez, M. R. Brambley, and S. Katipamula, "Self-correcting HVAC Controls: Algorithms for Sensors and Dampers in Air-handling Units," Pacific Northwest National Laboratory, US Department of Energy, Tech. Rep., 2009.

[47] L. Ferrarini and G. Mantovani, "Modeling and control of thermal energy of a large commercial building," in *Proceedings of the IEEE International Workshop on Intelligent Energy Systems (IWIES)*, 2013, pp. 149–154.

[48] P. M. Ferreira, S. M. Silva, A. E. Ruano, A. T. Négrier, and E. Z. Conceição, "Neural network PMV estimation for model-based predictive control of HVAC systems," in *Proceedings of the International Joint Conference on Neural Networks*, 2012, pp. 1–8.

[49] S. Fielsch, T. Grunert, M. Stursberg, and A. Kummert, "Model Predictive Control for Hydronic Heating Systems in Residential Buildings," in *Proceedings of the 20th World Congress The International Federation of Automatic Control*, 2017, pp. 4216–4221.

[50] S. Florides, Georgios & Kalogirou, "Measurements of Ground Temperature at Various Depths," in *Proceedings of the International Conference on Sustainable Energy Technologies, Nottingham, UK*, 2004.

[51] P. Frank, "Handling modelling uncertainty in fault detection and isolation systems," *Journal of Control Engineering and Applied Informatics*, vol. 4, no. 4, pp. 29–46, 2002.

[52] A. Garnier, J. Eynard, M. Caussanel, and S. Grieu, "Predictive control of multizone HVAC systems in non-residential buildings," in *Proceedings of the 19th World Congress of the International Federation of Automatic Control (IFAC)*, 2014, pp. 12 080–12 085.

[53] A. Ghofrani and M. A. Jafari, "Distributed air conditioning control in commercial buildings based on a physical-statistical approach," *Energy and Buildings*, vol. 148, pp. 106–118, 2017.

[54] V. Gunes, S. Peter, and T. Givargis, "Improving Energy Efficiency and Thermal Comfort of Smart Buildings with HVAC Systems in the Presence of Sensor Faults," in *Proceedings of the IEEE 17th International Conference on High Performance Computing and Communications, 7th International Symposium on Cyberspace Safety and Security, and 12th International Conference on Embedded Software and Systems*, 2015, pp. 945–950.

[55] C. Guo, Q. Song, and W. Cai, "A neural network assisted cascade control system for air handling unit," *IEEE Transactions on Industrial Electronics*, vol. 54, no. 1, pp. 620–628, 2007.

[56] Guo Rong Zheng, "Dynamic Modeling and Global Optimal Operation of Multizone Variable Air Volume HVAC Systems," PhD Thesis, Concordia University, Canada, 1997.

[57] F. Hajabdollahi, Z. Hajabdollahi, and H. Hajabdollahi, "Thermo-economic modeling and optimization of underfloor heating using evolutionary algorithms," *Energy and Buildings*, vol. 47, pp. 91–97, 2011.

[58] X. Hao, G. Zhang, and Y. Chen, "Fault-tolerant control and data recovery in HVAC monitoring system," *Energy and buildings*, vol. 37, no. 2, pp. 175–180, 2005.

[59] T. Hatanaka, X. Zhang, W. Shi, M. Zhu, and N. Li, "Physics-Integrated Hierarchical/Distributed HVAC Optimization for Multiple Buildings with Robustness against Time Delays," in *Proceedings of IEEE Conference on Decision and Control*, 2017, pp. 6573–6579.

[60] X. D. He and H. H. Asada, "A New Feedback Linearization Approach to Advanced Control of Multi-Unit HVAC Systems," in *Proceedings of the American Control Conference (ACC)*, 2003, pp. 2311–2316.

[61] A. Hesaraki, E. Bourdakis, A. Ploskić, and S. Holmberg, "Experimental study of energy performance in low-temperature hydronic heating systems," *Energy and Buildings*, vol. 109, pp. 108–114, 2015.

[62] J. M. House and T. F. Smith, "Optimal control of building and HVAC systems," in *Proceedings of the American Control Conference (ACC)*, 1995, pp. 4326–4330.

[63] Z. Huaguang and L. Cai, "Decentralized nonlinear adaptive control of an HVAC system," *IEEE Transactions on Systems, Man and Cybernetics Part C: Applications and Reviews*, vol. 32, no. 4, pp. 493–498, 2002.

[64] P. Ioannou and B. Fidan, *Adaptive Control Tutorial (Advances in Design and Control)*. SIAM, Society for Industrial and Applied Mathematics, 2006.

[65] R. Isermann, *Fault-diagnosis systems: An introduction from fault detection to fault tolerance*. Springer Science & Business Media, 2006.

[66] D. Ivanova, N. Valov, and M. Deyanov, "Application of the genetic algorithm for cascade control of a HVAC system," in *Proceedings of the MATEC Web of Conferences*, 2019, pp. 1–5.

[67] T. Jain, J. J. Yame, and D. Sauter, "Data-driven fault-tolerant control for energy efficiency in a multi-zone building," in *Proceedings of the IEEE International Conference on Control, Automation, Robotics and Vision (ICARCV)*, 2016, pp. 1–6.

[68] A. Jarrou, D. Sauter, and K. Alami, "Fault Diagnosis and Fault Tolerant Control Based on Model Predictive Control for Nearly Zero Energy Buildings," in *Proceedings of the Conference on Control and Fault-Tolerant Systems (SysTol)*. IEEE, 2019, pp. 219–225.

[69] L. Ji, G. Pei, T. T. Chow, W. He, A. Zhang, J. Dong, and H. Yi, "Performance of multi-functional domestic heat-pump system," *Applied Energy*, vol. 80, no. 3, pp. 307–326, 2005.

[70] X. Jin and Z. Du, "Fault tolerant control of outdoor air and AHU supply air temperature in VAV air conditioning systems using PCA method," *Applied thermal engineering*, vol. 26, no. 11, pp. 1226–1237, 2006.

[71] H. Karabay, M. Arici, and M. Sandik, "A numerical investigation of fluid flow and heat transfer inside a room for floor heating and wall heating systems," *Energy and Buildings*, vol. 67, pp. 471–478, 2013.

[72] S. Katipamula and M. R. Brambley, "Review Article: Methods for Fault Detection, Diagnostics, and Prognostics for Building Systems–A Review, Part I," *HVAC&R Research*, vol. 11, no. 1.

[73] C. Keliris, M. M. Polycarpou, and T. Parisini, "An integrated learning and filtering approach for fault diagnosis of a class of nonlinear dynamical systems," *IEEE Transactions on Neural Networks and Learning Systems*, vol. 28, no. 4, pp. 988–1004, 2017.

[74] H. K. Khalil, *Nonlinear Systems*. Prentice Hall, 2002.

[75] N. E. Klepeis, W. C. Nelson, W. R. Ott, J. P. Robinson, A. M. Tsang, P. Switzer, J. V. Behar, S. C. Hern, and W. H. Engelmann, "The National Human Activity Pattern Survey (NHAPS): A Resource for Assessing Exposure to Environmental Pollutants." *Journal of Exposure Analysis and Environmental Epidemiology*, vol. 11, no. 3, pp. 231–252, 2001.

[76] S. Klinkhieo, R. J. Patton, and C. Kambhampati, "Robust FDI for FTC coordination in a distributed network system," in *Proceedings of the 16th IFAC World Congress*, Seoul, Korea, 2008, pp. 13 551–13 556.

[77] S. Koehler and F. Borrelli, "Building temperature distributed control via explicit MPC and 'Trim and Respond' methods," in *Proceedings of the European Control Conference (ECC)*, 2013, pp. 4334–4339.

[78] S. M. Koehler, F. Chuang, Y. Ma, A. Daly, and F. Borrelli, *Distributed Model Predictive Control for Forced-Air Systems*. Springer International Publishing, 2018, pp. 167–189.

[79] M. Kumar and I. Kar, "Fault detection and diagnosis of air-conditioning systems using residuals," *Proceedings of the 10th IFAC International Symposium on Dynamics and Control of Process Systems*, pp. 607–612, 2013.

[80] A. Kusiak, M. Li, and H. Zheng, "Virtual models of indoor-air-quality sensors," *Applied Energy*, vol. 87, no. 6, pp. 2087–2094, 2010.

[81] W.-Y. Lee, J. M. House, and N.-H. Kyong, "Subsystem level fault diagnosis of a building's air-handling unit using general regression neural networks," *Applied Energy*, vol. 77, no. 2, pp. 153–170, 2004.

[82] H. Li, D. Yu, and J. E. Braun, "A review of virtual sensing technology and application in building systems," *HVAC&R Research*, vol. 17, no. 5, pp. 619–645, 2011.

[83] X. Li, Z. Shi, and S. Hu, "A novel control method of a variable volume air conditiong system for indoor thermal environment," *Proceedings of the International Conference on Computer Engineering and Technology*, vol. 2, pp. 566–570, 2010.

[84] J. Liang and R. Du, "Model-based Fault Detection and Diagnosis of HVAC systems using Support Vector Machine method," *International Journal of Refrigeration*, vol. 30, no. 6, pp. 1104–1114, 2007.

[85] J. Liang and R. Du, "Thermal comfort control based on neural network for HVAC application," in *Proceedings of the IEEE Conference on Control Applications*, 2005, pp. 819–824.

[86] O. M. Lidwell, "Air exchange through doorways. The effect of temperature difference, turbulence and ventilation flow," *Journal of Hygiene*, vol. 79, no. 1, pp. 141–154, 1977.

[87] X. F. Liu and A. Dexter, "Fault-tolerant supervisory control of VAV air-conditioning systems," *Energy and Buildings*, vol. 33, no. 4, pp. 379–389, 2001.

[88] C. Lo, P. Chan, Y. Wong, A. Rad, and K. Cheung, "Fuzzy-genetic algorithm for automatic fault detection in HVAC systems," *Applied Soft Computing*, vol. 7, no. 2, pp. 554–560, 2007.

[89] Y. Long, S. Liu, L. Xie, and K. H. Johansson, "A Hierarchical Distributed MPC for HVAC systems," in *Proceedings of the American Control Conference (ACC)*, 2016, pp. 2385–2390.

[90] G. Lymperopoulos and P. Ioannou, "Distributed Adaptive Control of Multi-Zone HVAC Systems," in *Proc. of the 27th Mediterranean Conference on Control and Automation (MED)*, 2019, pp. 553–558.

[91] G. Lymperopoulos and P. Ioannou, "Distributed Adaptive HVAC Control for Multi-Zone Buildings," in *Proceedings of the 58th Conference on Decision and Control (CDC)*. IEEE, 2019, pp. 8142–8147.

[92] G. Lymperopoulos and P. Ioannou, "Building temperature regulation in a multi-zone HVAC system using distributed adaptive control," *Energy and Buildings*, vol. 1, pp. 1–15, 2020.

[93] Y. Ma, J. Matuško, and F. Borrelli, "Stochastic Model Predictive Control for Building HVAC Systems: Complexity and Conservatism," *IEEE Transactions on Control Systems Technology*, vol. 23, no. 1, pp. 101–116, 2014.

[94] Z. Ma and S. Wang, "Online fault detection and robust control of condenser cooling water systems in building central chiller plants," *Energy and Buildings*, vol. 43, no. 1, pp. 153–165, 2011.

[95] Z. Ma and S. Wang, "Fault-tolerant supervisory control of building condenser cooling water systems for energy efficiency," *HVAC&R Research*, vol. 18, no. 1-2, pp. 126–146, 2012.

[96] T. A. Markus and E. N. Morris, *Buildings, climate and energy*. London ; Marshfield, Mass. : Pitman Pub, 1980.

[97] G. M. Milis, C. G. Panayiotou, and M. M. Polycarpou, "SEMIoTICS: Semantically Enhanced IoT-Enabled Intelligent Control Systems," *IEEE Internet of Things Journal*, no. 1, pp. 1257–1266, feb.

[98] S. A. Mona, T. Jain, and J. J. Yame, "Decentralized eMPC based fault tolerant control for energy efficiency in a multi-zone building," in *Proceedings of the Conference on Control and Fault-Tolerant Systems (SysTol)*. IEEE, 2019, pp. 238–243.

[99] A. Mona Subramaniam and T. Jain, "Fault Tolerant Economic Model Predictive Control for Energy Efficiency in a Multi-Zone Building," in *Proceedings of the IEEE Conference on Control Technology and Applications (CCTA)*, 2018, pp. 205–210.

[100] H. Moradi, M. Saffar-Avval, and F. Bakhtiari-Nejad, "Nonlinear multivariable control and performance analysis of an air-handling unit," *Energy and Buildings*, vol. 43, no. 4, pp. 805–813, 2011.

[101] L. E. Moser, P. M. Melliar-Smith, D. A. Agarwal, R. K. Budhia, and C. A. Lingley-Papadopoulos, "Totem: a fault-tolerant multicast group communication system," *Communications of the ACM*, vol. 39, no. 4, pp. 54–63, 1996.

[102] T. Mulumba, A. Afshari, K. Yan, W. Shen, and L. K. Norford, "Robust model-based fault diagnosis for air handling units," *Energy and Buildings*, vol. 86, pp. 698–707, 2015.

[103] J. A. Myhren and S. Holmberg, "Improving the thermal performance of ventilation radiators - The role of internal convection fins," *International Journal of Thermal Sciences*, vol. 50, no. 2, pp. 115–123, 2011.

[104] J. A. Myhren and S. Holmberg, "Performance evaluation of ventilation radiators," *Applied Thermal Engineering*, vol. 51, no. 1-2, pp. 315–324, 2013.

[105] S. M. Namburu, M. S. Azam, J. Luo, K. Choi, and K. R. Pattipati, "Data-driven modeling, fault diagnosis and optimal sensor selection for HVAC chillers," *IEEE Transactions on Automation Science and Engineering*, vol. 4, no. 3, pp. 469–473, 2007.

[106] M. Padilla, D. Choinière, and J. A. Candanedo, "A model-based strategy for self-correction of sensor faults in variable air volume air handling units," *Science and Technology for the Built Environment*, vol. 21, no. 7, pp. 1018–1032, 2015.

[107] P. M. Papadopoulos, V. Reppa, M. M. Polycarpou, and C. G. Panayiotou, "Distributed Adaptive Estimation Scheme for Isolation of Sensor Faults in Multi-zone HVAC Systems," in *Proceedings of the 9th IFAC Symposium on Fault Detection, Supervision and Safety for Technical Processes*, 2015, pp. 1146–1151.

[108] P. M. Papadopoulos, V. Reppa, M. M. Polycarpou, and C. G. Panayiotou, "Distributed Adaptive Sensor Fault Tolerant Control for Smart Buildings," in *Proceedings of the 54th IEEE Conference on Decision and Control*, 2015, pp. 3143–3148.

[109] P. M. Papadopoulos, V. Reppa, M. M. Polycarpou, and C. G. Panayiotou, "Distributed Diagnosis of Actuator and Sensor Faults in HVAC Systems," in *Proceedings of the 20th IFAC World Congress*, 2017, pp. 4293–4293.

[110] A. Parisio and S. P. Gutierrez, "Distributed model predictive control for building demand-side management," in *Proceedings of the European Control Conference (ECC)*, 2018, pp. 2549–2554.

[111] N. R. Patel, M. J. Risbeck, J. B. Rawlings, M. J. Wenzel, and R. D. Turney, "Distributed economic model predictive control for large-scale building temperature regulation," in *Proceedings of the IEEE American Control Conference (ACC)*, 2016, pp. 895–900.

[112] L. Pérez-Lombard, J. Ortiz, and C. Pout, "A review on buildings energy consumption information," *Energy and buildings*, vol. 40, no. 3, pp. 394–398, 2008.

[113] G. Platt, J. Li, R. Li, G. Poulton, G. James, and J. Wall, "Adaptive HVAC zone modeling for sustainable buildings," *Energy and Buildings*, no. 4, pp. 412–421.

[114] J. Ploennigs, A. Ahmed, B. Hensel, P. Stack, and K. Menzel, "Virtual sensors for estimation of energy consumption and thermal comfort in buildings with underfloor heating," *Advanced Engineering Informatics*, vol. 25, pp. 688–698, 2011.

[115] M. M. Polycarpou and A. B. Trunov, "Learning approach to nonlinear fault diagnosis: detectability analysis," *IEEE Transactions on Automatic Control*, vol. 45, no. 4, pp. 806–812, 2000.

[116] C. Price and B. P. Rasmussen, "Optimal tuning of cascaded control architectures for nonlinear HVAC systems," *Science and Technology for the Built Environment*, vol. 23, no. 8, pp. 1190–1202, 2017.

[117] M. Pătraşcu and M. Drăgoicea, "Integrating Agents and Services for Control and Monitoring: Managing Emergencies in Smart Buildings," in *Proceedings of the Service Orientation in Holonic and Multi-Agent Manufacturing and Robotics*, 2014, vol. 544, pp. 209–224.

[118] V. Puig, A. Stancu, and J. Quevedo, "Robust Fault Isolation using Nonlinear Interval Observers: The DAMADICS Benchmark Case Study," in *Proceedings of the 16th IFAC World Congress*, 2005, pp. 1850–1855.

[119] M. Puteh, M. H. Ibrahim, M. Adnan, C. N. Che'Ahmad, and N. M. Noh, "Thermal comfort in classroom: Constraints and issues," *Procedia - Social and Behavioral Sciences*, vol. 46, pp. 1834–1838, 2012.

[120] N. Radhakrishnan, S. Srinivasan, R. Su, and K. Poolla, "Learning-Based Hierarchical Distributed HVAC Scheduling With Operational Constraints," *IEEE Transactions on Control Systems Technology*, vol. 26, no. 5, pp. 1892–1900, 2018.

[121] M. Rahimi and A. Sabernaeemi, "Experimental study of radiation and free convection in an enclosure with under-floor heating system," *Energy Conversion and Management*, vol. 52, pp. 2752–2757, 2011.

[122] A. Rahmati, F. Rashidi, and M. Rashidi, "A hybrid fuzzy logic and PID controller for control of nonlinear HVAC systems," in *Proceedings of the IEEE International Conference on Systems, Man and Cybernetics*, 2003, pp. 2249–2254.

[123] M. Razmara, M. Maasoumy, M. Shahbakhti, and R. D. Robinett, "Optimal exergy control of building HVAC system," *Applied Energy*, vol. 156, no. 1, pp. 555–565, 2015.

[124] V. Reppa, M. M. Polycarpou, and C. G. Panayiotou, "A Distributed Detection and Isolation Scheme for Multiple Sensor Faults in Interconnected Nonlinear Systems," in *Proceedings of the 52nd Conference on Decision and Control (CDC)*. IEEE, 2013, pp. 4991–4996.

[125] V. Reppa, M. Polycarpou, and C. G. Panayiotou, "Distributed Sensor Fault Detection and Isolation for Nonlinear Uncertain Systems," in *Proceedings of the 8th IFAC Symposium on Fault Detection, Supervision and Safety for Technical Processes (SAFEPROCESS)*, Mexico City, Mexico, 2012, pp. 1077–1082.

[126] V. Reppa, M. Polycarpou, and C. G. Panayiotou, "Multiple Sensor Fault Detection and Isolation for Large-scale Interconnected Nonlinear Systems," in *Proceedings of the European Control Conference (ECC)*, Zurich, Switzerland, 2013, pp. 1952–1957.

[127] V. Reppa, P. Papadopoulos, M. M. Polycarpou, and C. G. Panayiotou, "Distributed Detection and Isolation of Sensor Faults in HVAC Systems," in *Proceedings of the Mediterranean Conference on Control and Automation (MED)*, 2013, pp. 401–406.

[128] V. Reppa, P. Papadopoulos, M. M. Polycarpou, and C. G. Panayiotou, "A distributed virtual sensor scheme for smart buildings based on adaptive approximation," in *Proceedings of the IEEE International Joint Conference on Neural Networks*, 2014, pp. 99–106.

[129] V. Reppa, P. Papadopoulos, M. M. Polycarpou, and C. G. Panayiotou, "A Distributed Architecture for HVAC Sensor Fault Detection and Isolation," *IEEE Transactions on Control Systems Technology*, vol. 23, no. 4, pp. 1323–1337, 2015.

[130] V. Reppa, M. M. Polycarpou, and C. G. Panayiotou, "Sensor Fault Diagnosis," *Foundations and Trends® in Systems and Control*, vol. 3, no. 1-2, pp. 1–248, 2016.

[131] J. H. Richter, *Reconfigurable Control of Nonlinear Dynamical Systems: A Fault-Hiding Approach*. Springer, 2011, vol. 408.

[132] S. Riverso, F. Boem, G. Ferrari-Trecate, and T. Parisini, "Fault Diagnosis and Control-reconfiguration in Large-scale Systems : A Plug-and-Play Approach," in *Proceedings of the IEEE Conference on Decision and Control*, 2014, pp. 4977–4982.

[133] K. W. Roth, D. Westphalen, M. Y. Feng, P. Llana, and L. Quartararo, "Energy Impact of Commercial Building Controls and Performance Diagnostics: Market Characterization, Energy Impact of Building Faults and Energy Savings Potential," U.S. Department of Energy, Tech. Rep., 2005.

[134] M. Sampath, R. Sengupta, S. Lafortune, and K. Sinnamohideen, "Failure Diagnosis Using Discrete-Event Models," *IEEE Transactions on Control Systems Technology*, vol. 4, no. 2, pp. 105–124, 1996.

[135] I. Samy, I. Postlethwaite, and D.-W. Gu, "Survey and application of sensor fault detection and isolation schemes," *Control Engineering Practice*, vol. 19, no. 7, pp. 658–674, 2011.

[136] B. Sanner, C. Karytsas, D. Mendrinos, and L. Rybach, "Current status of ground source heat pumps and underground thermal energy storage in Europe," *Geothermics*, vol. 32, no. 4, pp. 579–588, 2003.

[137] D. Sauter, J. Yame, C. Aubrun, and F. Hamelin, "Design of fault isolation filter for control reconfiguration: Application to energy efficiency control in buildings," in *Proceedings of the 23rd Mediterranean Conference on Control and Automation (MED)*. IEEE, 2015, pp. 197–202.

[138] J. Schein, S. T. Bushby, N. S. Castro, and J. M. House, "A rule-based fault detection method for air handling units," *Energy and buildings*, vol. 38, pp. 1485–1492, 2006.

[139] H. F. Scherer, M. Pasamontes, J. L. Guzmán, J. D. Álvarez, E. Camponogara, and J. E. Normey-Rico, "Efficient building energy management using distributed model predictive control," *Journal of Process Control*, vol. 24, no. 6, pp. 740–749, 2014.

[140] S. J. Self, B. V. Reddy, and M. A. Rosen, "Geothermal heat pump systems: Status review and comparison with other heating options," *Applied Energy*, vol. 101, pp. 341–348, 2013.

[141] E. Semsar, M. J. Yazdanpanah, and C. Lucas, "Nonlinear control and disturbance decoupling of an HVAC system via feedback linearization and back-stepping," in *Proceedings of the IEEE Conference on Control Applications*, vol. 1, 2003, pp. 646–650.

[142] M. M. Seron, J. A. De Dona, and J. H. Richter, "Integrated sensor and actuator fault-tolerant control," *International Journal of Control*, vol. 86, no. 4, pp. 689–708, 2013.

[143] H. Shahnazari, P. Mhaskar, J. M. House, and T. I. Salsbury, "Distributed fault diagnosis of heating, ventilation, and air conditioning systems," *American Institute of Chemical Engineers (AIChE) Journal*, vol. 65, no. 2, pp. 640–651, 2019.

[144] H. Shahnazari, P. Mhaskar, J. M. House, and T. I. Salsbury, "Modeling and fault diagnosis design for HVAC systems using recurrent neural networks," *Computers and Chemical Engineering*, vol. 126, pp. 189–203, jul 2019.

[145] J. Sun and Y. Zhang, "Towards an Energy Efficient Architecture in Smart Building," in *Proceedings of the International Conference on Computational Intelligence and Communication Networks*, 2015, pp. 1589–1592.

[146] A. Talukdar and A. Patra, "Dynamic Model-Based Fault Tolerant Control of Variable Air Volume Air Conditioning System," *HVAC&R Research*, vol. 16, no. 2, pp. 233–254, 2010.

[147] B. Tashtoush, M. Molhim, and M. Al-Rousan, "Dynamic model of an HVAC system for control analysis," *Energy*, vol. 30, no. 10, pp. 1729–1745, 2005.

[148] A. Thosar, A. Patra, and S. Bhattacharyya, "Feedback linearization based control of a variable air volume air conditioning system for cooling applications," *ISA Transactions*, vol. 47, no. 3, pp. 339–349, 2008.

[149] B. T. Thumati, M. A. Feinstein, J. W. Fonda, A. Turnbull, F. J. Weaver, M. E. Calkins, and S. Jagannathan, "An online model-based fault diagnosis scheme for HVAC systems," in *IEEE International Conference on Control Applications (CCA), 2011*, 2011, pp. 70–75.

[150] W. Turner, A. Staino, and B. Basu, "Residential HVAC fault detection using a system identification approach," *Energy and Buildings*, vol. 151, pp. 1–17, sep 2017.

[151] C. P. Underwood, "Robust control of HVAC plant I: modelling," *Building Services Engineering Research and Technology*, vol. 21, no. 1, pp. 53–61, 2000.

[152] S. Wang and Y. Chen, "Fault-tolerant control for outdoor ventilation air flow rate in buildings based on neural network," *Building and Environment*, vol. 37, no. 7, pp. 691–704, 2002.

[153] S. Wang and X. Jin, "Model-based optimal control of VAV air-conditioning system using genetic algorithm," *Building and Environment*, vol. 35, no. 6, pp. 471–487, 2000.

[154] S. Wang and Z. Ma, "Supervisory and Optimal Control of Building HVAC Systems: A Review," *HVAC&R Research*, vol. 14, no. 1, pp. 3–32, 2008.

[155] S. Wang and J. Qin, "Sensor fault detection and validation of VAV terminals in air conditioning systems," *Energy conversion and management*, vol. 46, no. 15-16, pp. 2482–2500, 2005.

[156] S. Wang and J.-B. Wang, "Robust sensor fault diagnosis and validation in HVAC systems," *Transactions of the Institute of Measurement and Control*, vol. 24, no. 3, pp. 231–262, 2002.

[157] S. Wang and F. Xiao, "AHU sensor fault diagnosis using principal component analysis method," *Energy and Buildings*, vol. 36, no. 2, pp. 147–160, 2004.

[158] S. Wang, Q. Zhou, and F. Xiao, "A system-level fault detection and diagnosis strategy for HVAC systems involving sensor faults," *Energy and buildings*, vol. 42, no. 4, pp. 477–490, 2010.

[159] Z. Wang, G. Hu, and C. J. Spanos, "Distributed model predictive control of bilinear HVAC systems using a convexification method," in *Proceedings of the 11th Asian Control Conference (ASCC)*, 2017, pp. 878–883.

[160] G. R. Watzlaf and T. E. Ackman, "Underground mine water for heating and cooling using geothermal heat pump systems," *Mine Water and the Environment*, vol. 25, no. 1, pp. 1–14, 2006.

[161] E. Witrant, S. Mocanu, and O. Sename, "A Hybrid Model and MIMO Control for Intelligent Buildings Temperature Regulation over WSN," in *Proceedings of the 8th IFAC Workshop on Time-Delay Systems*, 2009, pp. 420–425.

[162] N. E. Wu, S. Thavamani, Y. Zhang, and M. Blanke, "Sensor fault masking of a ship propulsion system," *Control Engineering Practice*, vol. 14, no. 11, pp. 1337–1345, 2006.

[163] J. J. Yame, T. Jain, and D. Sauter, "An online controller redesign based fault-tolerant strategy for thermal comfort in a multi-zone building," *Proceedings of the IEEE Conference on Control and Applications (CCA)*, pp. 1901–1906, 2015.

[164] H. Yang, P. Cui, and Z. Fang, "Vertical-borehole ground-coupled heat pumps: A review of models and systems," pp. 16–27, 2010.

[165] H. Yang, S. Cho, C.-S. Tae, and M. Zaheeruddin, "Sequential rule based algorithms for temperature sensor fault detection in air handling units," *Energy Conversion and Management*, vol. 49, no. 8, pp. 2291–2306, aug 2008.

[166] X.-B. Yang, X.-Q. Jin, Z.-M. Du, Y.-H. Zhu, and Y.-B. Guo, "A hybrid model-based fault detection strategy for air handling unit sensors," *Energy and Buildings*, vol. 57, pp. 132–143, feb 2013.

[167] J. C. M. Yiu and S. Wang, "Multiple ARMAX modeling scheme for forecasting air conditioning system performance," *Energy Conversion and Management*, vol. 48, no. 8, pp. 2276–2285, aug 2007.

[168] H. Yoshida, S. Kumar, and Y. Morita, "Online fault detection and diagnosis in VAV air handling unit by RARX modeling," *Energy and Buildings*, vol. 33, no. 4, pp. 391–401, 2001.

[169] L. Yu, D. Xie, T. Jiang, Y. Zou, and K. Wang, "Distributed Real-Time HVAC Control for Cost-Efficient Commercial Buildings Under Smart Grid Environment," *IEEE Internet of Things Journal*, vol. 5, no. 1, pp. 44–55, 2018.

[170] Y. Yu, D. Woradechjumroen, and D. Yu, "A review of fault detection and diagnosis methodologies on air-handling units," *Energy and Buildings*, vol. 82, pp. 550 – 562, 2014.

[171] S. Yuan, L. Zhang, O. Holub, and S. Baldi, "Switched Adaptive Control of Air Handling Units with Discrete and Saturated Actuators," *IEEE Control Systems Letters*, vol. 2, no. 3, pp. 417–422, 2018.

[172] M. Zaheer-Uddin, "Temperature control of multizone indoor spaces based on forecast and actual loads," *Building and Environment*, vol. 29, no. 4, pp. 485–493, 1994.

[173] M. Zaheer-Uddin and R. V. Patel, "Optimal Tracking Control of Multi-Zone Indoor Environmental Spaces," *Journal of Dynamic Systems, Measurement, and Control*, vol. 117, no. 3, pp. 292–303, 1995.

[174] M. Zaheer-Uddin, R. V. Patel, and S. A. Al-Assadi, "Design of decentralized robust controllers for multizone space heating systems," *IEEE Transactions on Control Systems Technology*, vol. 1, no. 4, pp. 246–261, 1993.

[175] M. Zaheer-Uddin and N. Tudoroiu, "Neuro-PID tracking control of a discharge air temperature system," *Energy Conversion and Management*, vol. 45, no. 1, pp. 2405–2415, 2004.

[176] R. Zhang and T. Hong, "Modeling of HVAC operational faults in building performance simulation," *Applied Energy*, vol. 202, pp. 178–188, 2017.

[177] X. Zhang, W. Shi, X. Li, B. Yan, A. Malkawi, and N. Li, "Decentralized temperature control via HVAC systems in energy efficient buildings: An approximate solution procedure," in *Proceedings of Global Conference on Signal and Information Processing*, 2016, pp. 936–940.

[178] X. Zhang, W. Shi, B. Yan, A. Malkawi, and N. Li, "Decentralized and Distributed Temperature Control via HVAC Systems in Energy Efficient Buildings," in *Proceedings of the IEEE Global Conference on Signal and Information Processing*, 2017, pp. 1–10.

[179] Y. Zhao, J. Wen, and S. Wang, "Diagnostic Bayesian networks for diagnosing air handling units faults - Part II: Faults in coils and sensors," *Applied Thermal Engineering*, vol. 90, pp. 145–157, 2015.

[180] G. Zheng and M. Zaheer-Uddin, "Optimization of thermal processes in a variable air volume HVAC system," *Energy*, vol. 21, no. 5, pp. 407–420, 1996.

[181] J. Zhuang, Y. Chen, and J. Wu, "Cascade control for supply air temperature in a variable air volume system," in *Proceedings of the IOP Conference Series: Earth and Environmental Science*, 2019, pp. 1–7.